PhD degree in Molecular Medicine (curriculum in Molecular Oncology)

European School Of Molecular Medicine (SEMM)

University of Milan and University of Naples “Federico II”

Settore disciplinare: Med/04

# KLF4 is a key determinant in the development and progression of Cerebral Cavernous Malformations

*Roberto Cuttano*

IFOM, Milan

matricola: R09867

*Supervisor*: Prof.ssa Elisabetta Dejana

IFOM, Milan

*Added Supervisor*: Noemi Rudini, PhD

IFOM, Milan

Anno Accademico: 2014-2015

*A Michela*

# TABLE OF CONTENTS

**LIST OF ABBREVIATIONS** ........ **7**

**FIGURE INDEX** ........ **13**

**TABLE INDEX** ........ **17**

**ABSTRACT** ........ **18**

**INTRODUCTION** ........ **19**

**1. VASCULAR ENDOTHELIUM** ........ 19

*1.1 Endothelial cell-to-cell junctions* ........ *19*

*1.2 Adherens junctions composition and signaling* ........ *20*

*1.3 Tight junctions composition and signaling* ........ *23*

*1.4 Endothelial heterogeneity: the example of the blood brain barrier* ........ *26*

**2. CEREBRAL CAVERNOUS MALFORMATIONS** ........ **30**

*2.1 CCM genetics* ........ *31*

*2.2 Animal models used to study CCM disease* ........ *32*

*2.3 CCM protein function and pathological implications* ........ *34*

*2.4 Future pharmacological therapies for the treatment of CCM patients* ........ *36*

**3. ENDOTHELIAL TO MESENCHYMAL TRANSITION** ........ **38**

*3.1 Definition of endothelial-to-mesenchymal transition* ........ *38*

*3.2 The TGF-β signalling pathway* ........ *39*

*3.2.1 TGF-β and BMP signalling pathway in ECs* ........ *44*

*3.3 EndMT in heart cushion formation and cardiac fibrosis* ........ *47*

*3.4 EndMT in cancer, FOP and atherosclerosis* ........ *48*

**4. THE KRÜPPEL LIKE FACTOR FAMILY OF TRANSCRIPTION FACTORS** ........ **51**

*4.1 The classification and the structure of KLFs* ........ *51*

*4.2 The characteristic of KLF4 gene and protein and its mechanisms of action* ........ *55*

*4.3 The Role of KLF4 in endothelial cell biology* ........ *58*

*4.4 The ERK5 signalling axis* ........ *60*

**5. MATERIALS AND METHODS** ........ **64**

*5.1 Antibodies* ........ *64*

*5.2 Mouse lines* ........ *64*

*5.3 Endothelial cell isolation and culture* ........ *65*

*5.4 Cell treatments* ........ *67*

*5.5 Treatment with TGFβ/BMP inhibitor in vivo* ........ *68*

*5.6 Production of Lentiviruses* ........ 68
*5.7 Cell transfection and RNA interference* ........ 69
*5.8 Western blotting* ........ 69
*5.9 qRT-PCR analysis* ........ 70
*5.10 Affymetrix* ........ 71
*5.11 Cell migration assay* ........ 71
*5.12 Cell proliferation assay* ........ 71
*5.13 Generation of 3-D endothelial spheroid assay* ........ 71
*5.14 Transcription factor binding site analysis* ........ 72
*5.15 Transcriptional reporter assay* ........ 72
*5.16 Chromatin Immunoprecipitation* ........ 74
*5. 17 Immunofluorescence and hystology* ........ 76
*5.18 Immunofluorescence analysis of the retina* ........ 78
*5. 19 Intravenous injection of tracer and tracer detection* ........ 79
*5.20 Statistics* ........ 79

**6. RESULTS ........ 80**
*6.1 Establishment of a mouse model of CCM disease* ........ 80
*6.2 CCM vascular lesions are lined by endothelial cells with a mesenchymal and stem-like phenotype* ........ 84
*6.3 Loss of Ccm1 expression induces EndMT transition in a cell-autonomous way* ........ 87
*6.4 Activation of the TGF-β signalling contributes to EndMT in CCM1 null ECs* ........ 93
*6.5 TGF-β/BMP signalling and EndMT are critical events for development and progression of CCM lesions* ........ 96
*6.6 Autocrine production of BMP6 in CCM1 null ECs induces pSMAD signalling activation and EndMT* ........ 99
*6.7 KLF4 expression is increased in murine models of CCM disease and in CCM patients.* 102
*6.8 KLF4 is a causative factor for the development and progression of CCM lesions* ........ 108
*6.9 KLF4 induces EndMT in CCM1 null ECs in vitro* ........ 116
*6.10 KLF4 induces EndMT in CCM1 null ECs in vivo in a context dependent manner* ........ 121
*6.11 KLF4 regulates BMP6-mediated signalling* ........ 129
*6.12 KLF4 directly regulates the expression of some EndMT markers* ........ 137
*6.13 KLF2 expression is dispensable for EndMT transition in CCM1 null ECs* ........ 141
*6.14 Erk5 activation mediates KLF4 upregulation and KLF4-dependent EndMT in the absence of Ccm1* ........ 143
*6.15 Mekk3-Mek5-dependent signalling cascade promotes ERK5 activation and KLF4 upregulation in CCM1 KO ECs* ........ 152

**DISCUSSION ........ 156**
*7.1 Development of a new mouse model of CCM disease* ........ 156

*7.2 Molecular mechanisms associated to CCM disease: KLF4 upregulation and KLF4-dependent EndMT ........ 157*
*7.3 MEKK3-MEK5-ERK5 signalling pathways induce KLF4 expression in Ccm null ECs . 161*
*7.4 Possible crosstalk between KLF4 and other signalling pathway involved in CCM ........ 162*
*7.5 KLF4 context-dependent functions: a possible explanation for the brain specificity of the CCM disease ........ 164*
*7.6 KLF4 constitutes a novel target for a future pharmacological therapy for the treatment of CCM ........ 165*
*7.7 KLF2 and KLF4 do not have overlapping roles in CCM ........ 167*
*7.8 Concluding remarks ........ 167*

**APPENDIX ........ 168**

**REFERENCES ........ 179**

**ACKNOWLEDGEMENTS ........ 199**

# LIST OF ABBREVIATIONS

**Aa**: Aminoacid

**ActRII**: Activin receptor type II

**AF-6**: Afadin-6

**AJ**: Adherens junction

**ALK1**: Activin-receptor Like Kinase-1

**ALK5**: Activin-receptor Like Kinase-5

**AMHRII**: AMH type II receptor

**aPKC**: Atypical PKC

α**SMA**: α Smooth Muscle Actin

**ATP:** Adenosine triphosphate

**AV**: Atrio-Ventricular

**BAD**: BCL2-Associated Agonist Of Cell Death

**BBB**: Blood Brain Barrier

**Bcl2**: B-Cell CLL/Lymphoma 2

**BMK1**: Big MAPK (BMK1)

**BMP**: Bone morphogenetic protein

**BMPRII**: BMP type II receptor

**Bp**: Base pairs

**BRE**: BMP-Responsive Elements

**C-terminus:** Carboxyl-terminus

**CAF**: Cancer-Associated Fibroblast

**CASK/lin2**: calcium/calmodulin-dependent serine protein kinase

**CBP**: cAMP response element binding protein

**CCM**: Cerebral Cavernous Malformation

**ChIP-seq**: ChIP sequencing

**ChIP:** Chromatin immunoprecipitation

**CNS**: central nervous system

**Co-SMAD**: Common SMAD

**CREB**: cAMP response element-binding protein

**CtBP**: carboxy-terminal binding proteins

**DAPI**: 4',6-diamino-2-phenylindole

**DEP-1**: Density-enhanced phosphatase-1

**EC**: Endothelial cell

**ECM**: Extracellular matrix

**Edn1**: Endothelin1

**Ednrb**: Endothelin receptor b

**EGF**: Epithelial Growth Factor

**EGFR**: Epithelial Growth Factor Receptor

**EMT**: Epithelial-to-Mesenchymal Transition

**EndMT**: Endothelial-to-mesenchymal transition

**eNOS**: endothelial Nitric Oxide Synthase

**ERK5:** Extracellular-signal-regulated kinase

**FGFR**: Fibroblast growth factor receptor

**FOP**: Fibrodysplasia Ossificans Progressiva

**FoxO1**: Forkhead-box protein-O1

**FSP1**: Fibroblast Specific Protein 1

**GAPDH**: Glyceraldehydes-3-Phosphate Dehydrogenase

**GDF**: Growth Differentiation Factor

**GF**: Growth Factor

**GLUT1**: Glucose transporter 1

**GUK**: Guanylate kinase

**HAT**: Histone acetyltransferase

**HDAC**: Histone deacetylases

**HEG**: Heart of glass

**HUVEC**: Human umbilical vein endothelial cell

**I-SMADs**: Inhibitory SMADs

**ICAM-1**: Intercellular Adhesion Molecule-1

**ID1**: Inhibitor of differentiation 1

**IFNγ**: Interferon-γ

**Ig**: Immunoglobulin

**ILβ**: Interleukin-β

**IP**: Intraperinoeal

**iPS**: Induced pluripotent stem cells

**JAM**: Junctional adhesion molecules

**KB**: Kilobase

**kDa**: Kilo Dalton

**KLF**: Krüppel-like factor

**KO**: Knock-out

**LAP**: Latent-associated peptide

**LDL**: Low Density Lipoprotein

**LPS**: Lipopolysaccharide

**MAGUK**: Membrane-Associated GUanylate Kinase homolog

**MAP2K5**: mitogen-activated protein kinase kinase

**MAPK**: Mitogen-activated protein kinase

**MAPKKK**: MAPK kinase kinase

**MEF2**: Myocyte enhancer factor 2

**MEK5**: MAPK/ERK kinase 5

**MEKK**: MEK kinase

**MH**: Mad Homology Domains

**MLC2**: Myosin light chain

**MLPA**: Multiplex ligation-dependent probe amplification

**MRI**: Magnetic resonance imaging

**MUPP-1**: Multi-PDZ domain protein

**N-cadherin**: Neuronal cadherin

**N-terminus**: Amino-terminus

**NES**: nuclear export signal

**NF-kB**: Nuclear Factor-kappa-B

**NLS**: Nuclear localization signal

**NO**: Nitric Oxide

**NVU**: neurovascular unit

**ON**: Overnight

**P**: Postnatal day

**P/CAF**: p300/CBP-associated factor

**PAF**: Paraformaldehyde

**PAF**: Platelet-activating factor

**PAI-1**: Plasminogen Activator Inhibitor-1

**PAR**: partitioning defective

**PC**: Perycite

**PCR**: Polymerase chain reaction

**PDGF**: Platelet-Derived Growth Factor

**PDGFR**: Platelet derived growth factor receptor

**PDZ:** Post synaptic density protein, Drosophila disc large tumor suppressor and Zonula occludens-1 protein

**PECAM1**: Platelet Endothelial Cell Adhesive Molecule 1

**PH**: Pulmonary hypertension

**PI3K**: Phosphatidylinositol-3 kinase

**PLVAP**: plasmalemma vesicle-associated protein

**PMN**: Polymorphonuclear neutrophil

**PmT**: Polyoma middle T

**PTGIS**: Prostaglandin I2 synthase

**PTPμ**: Protein Tyrosine Phosphatase μ

**R-SMAD**: Receptor-activated SMAD

**Rac**: Ras-related C3 botulinum toxin substrate

**Raf1**: Rapidly accelerated fibrosarcom

**Rap1**: Ras-related protein-1 small GTPase

**RNA**: Ribonucleic Acid

**ROCK**: Rho-associated protein kinase

**RT-PCR**: Reverse Transcriptase-Polymerase Chain Reaction

**RT**: Room Temperature

**Sap1a**: Serum-response factor accessory protein 1a

**SARA**: SMAD Anchor for Receptor Activation

**SBE**: SMAD-Binding Element

**Sca-1**: Stem Cell Antigen-1

**SD**: Standard Deviation

**SH**: Src Homology

**Shh**: Sonic Hedgehog

**SHP2**: Src-homology 2-containing phosphotyrosine phosphatase

**siRNA**: short interference Ribonucleic Acid

**SMAD**: Small mother against decapentaplegic

**SMC**: Smooth muscle cell

**Smurf**: SMAD ubiquitination regulatory factor

**Src**: Rous sarcoma proto-oncogene tyrosine-protein kinase

**STRIPAK**: Striatin-interacting phosphatase and kinase

**TβRI**: Transforming Growth Factor-β Receptor type I

**TβRII**: Transforming Growth Factor-β Receptor type II

**TβRs**: Transforming Growth Factor-β Receptors

**TGF-β**: Transforming growth factor-β

**Thbd**: Thrombomodulin

**Tiam**: T-Cell lymphoma invasion and metastasis

**TJ**: Tight junctions

**TNF-α**: Tumor necrosis factor-α

**Vcam-1**: Vascular cell adhesion molecule 1

**VE-cadherin**: Vascular endothelial cadherin

**VE-PTP**: Vascular Endothelial-Phosphotyrosine Phosphatase

**VEGF:** Vascular endothelial growth factor

**WB**: Western Blotting

**WT**: Wild-type

**ZO:** Zonula Occludens

**ZONAB**: ZO-1-associated nucleic acid binding protein

**ZPLD1**: Zona pellucida-like domain containing 1

# FIGURE INDEX

Figure 1 - Schematic representation of endothelial AJs. .................................................. 22

Figure 2 - Schematic representation of endothelial TJs. .................................................. 25

Figure 3 – Schematic representation of the cellular organization of the BBB. ................... 28

Figure 4 – The morphology of CCM vascular lesions ..................................................... 30

Figure 5 - Phenotypic changes that occur during the EndMT. .......................................... 39

Figure 6 – Schematic representation of TGF-β signalling pathway .................................. 43

Figure 7 - Schematic representation of the structure of KLF family members. ................ 53

Figure 8 - Schematic representation of KLF4 structure. .................................................. 56

Figure 9 – The ERK5 structure and signalling axis ......................................................... 62

Figure 10 - Representation of PGL3 basic vector backbone ............................................ 73

Figure 11 - High *Ccm1* recombination mediated by tamoxifen-induced Cre-recombinase activity in EC-CCM1 KO brains. ........................................................................ 81

Figure 12 - Endothelial *Ccm1* deletion at P1 in the mouse results in brain vascular malformations comparable to human CCM lesions. ..................................................... 82

Figure 13 - Endothelial *Ccm1* deletion at P1 in the mouse results in retinal vascular malformations comparable to human CCM lesions. ..................................................... 83

Figure 14 - *Ccm1* deletion causes EndMT *in vivo*. .......................................................... 85

Figure 15 - *Ccm1* deletion causes EndMT marker mRNA upregulation *in vivo*. ............... 86

Figure 16 - *In vitro* endothelial *Ccm1* gene ablation in lung derived ECs induces a mesenchymal and stem cell-like phenotype. ................................................................. 88

Figure 17 - Co-expression of VE-CADHERIN and representative EndMT markers in CCM1 KO ECs. ............................................................................................................. 89

Figure 18 - Endothelial *Ccm1* gene ablation induces a mesenchymal and stem cell-like phenotype in *vitro* in brain derived ECs (BMECs). ........................................................ 90

Figure 19 - Alteration of VE-CADHERIN localization in CCM1 KO BMECs. ................ 90

Figure 20 - *Ccm1* gene ablation increases cell proliferation *in vitro* and *in vivo*. .............. 91

Figure 21 - *Ccm1* null ECs shows increased cell migration *in vitro*. ................................ 92

Figure 22 - Loss of *Ccm1* induces TGF-β/BMP signalling activation in ECs. .................. 94

Figure 23 - The ALK5 inhibitor LY-364947 effectively inhibits SMAD signalling activation in CCM1 KO ECs. ......................................................................................... 94

Figure 24 - *Ccm1* deletion induces EndMT via TGF-β/BMP signalling activation. .......... 95

Figure 25 - Inhibition of TGFβ/BMP signalling decreases the proliferation rate of CCM1 KO ECs. ..................................................................................................................... 95

Figure 26 - TGF-β/BMP signalling inhibition reduces number and size of lesions and vessel leakage in CCM1 null mice. ....................................................................97
Figure 27 - TGF-β/BMP signalling inhibition reduces the mesenchymal phenotype of ECs lining CCM lesions *in vivo*. .............................................................................98
Figure 28 - *Bmp6* expression is upregulated upon loss of *Ccm1 in vitro* and *in vivo* .......100
Figure 29 - BMP6 stimulation induces SMAD phosphorylation in WT ECs. .................100
Figure 30- BMP6-mediated upregulation of mesenchymal and stem-cell makers in WT ECs. ........................................................................................................................101
Figure 31 - *Ccm1* deletion induces TGFβ/BMP signalling activation and EndMT via BMP6 upregulation. ...................................................................................................101
Figure 32 - KLF4 expression is increased in the retina of EC-CCM1 KO mice. .............103
Figure 33 - *Klf4* is upregulated at an early stage of CCM disease progression *in vivo*. ....104
Figure 34 - Endothelial-specific ablation of either *Ccm2* or *Ccm3* induces KLF4 upregulation in the brain vasculature. ....................................................................104
Figure 35 - Silencing of any of the three *Ccm* genes leads to *Klf4* upregulation *in vitro*..105
Figure 36 - KLF4 upregulation upon *Ccm1* silencing is conserved in brain ECs of human origin. .......................................................................................................................105
Figure 37 - The increase of KLF4 in ECs lining the cavernomas is observed in familial and sporadic CCM patients. ..........................................................................................106
Figure 38 - Recombination efficiency of *Ccm1* and *Klf4* in the brain vasculature of EC-CCM1 KO, EC-CCM1 KO KLF4 HET and EC-CCM1 KO KLF4 KO mice. .........109
Figure 39 - KLF4 is determinant for CCM development and progression *in vivo*. ..........110
Figure 40 - Loss of *Klf4* stringly increases survival in *Ccm1* null mice. ..........................111
Figure 41 - *Klf4* is critical for cavernoma development in the retina in the absence of *Ccm1*. ..........................................................................................................................112
Figure 42 - The vasculature of the retina is not altered in the absence of KLF4. .............114
Figure 43 - *Klf4* silencing inhibits EndMT marker expression in CCM1 KO lung derived ECs. ........................................................................................................................116
Figure 44 - Klf4 silencing decreases the proliferation rate of both lung derived WT and CCM1 KO ECs. ........................................................................................................117
Figure 45 - KLF4 silencing affects lung derived CCM1 KO ECs migration. ..................117
Figure 46 - Loss of KLF4 prevents the EndMT switch induced by the loss of *Ccm1* in BMECs. ....................................................................................................................119
Figure 47 - *Klf4* gene ablation did not restore the proper VE-CADHERIN localization at the cell-to-cell contacts. ..........................................................................................120

Figure 48 - KLF4 overexpression induces EndMT marker expression in WT ECs. ........ 120
Figure 49 - EndMT marker expression is reduced in ECs lining the cavernomas in the absence of *Klf4*. ........ 123
Figure 50 - EndMT markers gene expression analysis in freshly isolated brain ECs from mice WT or null for *Ccm1*, *Klf4* or both genes ........ 124
Figure 51 - Incomplete Klf4 gene recombination in ECs lining the vascular lesions of EC-CCM1 KO KLF4 KO mice. ........ 125
Figure 52 - KLF4 amount is higher in veins than in arteries of the retinal vasculature in both WT and EC-CCM1 KO mice. ........ 126
Figure 53 - EndMT occurs specifically in the brain vasculature of EC-CCM1 KO mice. 127
Figure 54 - Phenotype of livers in EC-CCM1 KO mice. ........ 128
Figure 55 - *Klf4* silencing decreases *Bmp6* expression in CCM1 KO lung ECs. ........ 129
Figure 56 - *Klf4* silencing decreases SMAD1 phosphorylation in CCM1 KO lung ECs. 130
Figure 57 - *Klf4* increases *Bmp6* in CCM1 KO BMECs. ........ 130
Figure 58 - Loss of endothelial *Klf4* decreases BMP6 amount *in vivo* in ECs lining the cavernomas in EC-CCM1 KO mice. ........ 131
Figure 59 - KLF4 binds *Bmp6* promoter in CCM1 null ECs. ........ 132
Figure 60 - KLF4 regulates *Bmp6* promoter activity. ........ 133
Figure 61 - KLF4 overexpression in WT ECs upregulates *Bmp6*. ........ 134
Figure 62 - KLF4 overexpression in WT ECs increases SMAD1 phosphorylation. ........ 134
Figure 63 - KLF4 binds *Bmp6* promoter in KLF4 overexpressing cells. ........ 135
Figure 64 - Knockdown efficiency of *Bmp6* in Mock and LentiKLF4 ECs transduced with a lentiviral vector expressing a shRNA directed to *Bmp6*. ........ 135
Figure 65 - Silencing of *Bmp6* in KLF4 overexpressing ECs decreases SMAD phosphorylation and EndMT marker expression. ........ 136
Figure 66 - Establishment of lung derived endothelial cell line KO for KLF4. ........ 138
Figure 67 - Loss of KLF4 does not affect SMAD1 phosphorylation upon BMP6 stimulation. ........ 138
Figure 68 - BMP6-dependent *Fsp1* and *Sca1* induction is strongly reduced in KLF4 KO lung ECs. ........ 139
Figure 69 - KLF4 directly binds to promoter regions of specific EndMT markers. ........ 139
Figure 70 - KLF4 increases promoter activity of specific EndMT markers. ........ 140
Figure 71 - Loss of *Klf4* does not affect *Klf2* expression in ECs in *vivo*. ........ 142
Figure 72 - Loss of *Ccm1* induces *Klf2* upregulation *in vitro* in BMECs. ........ 142
Figure 73 - Loss of *Ccm1* induce Erk5 phosphorylation in ECs *in vivo*. ........ 144

Figure 74 - Erk5 phosphorylation is increased upon loss of *Ccm1* in BMECs *in vitro*. ...144

Figure 75 - Erk5 activitation is responsible for KLF4 upregulation upon *Ccm1* silencing *in vitro*. ...145

Figure 76 - In the absence of *Ccm1* increased ERK5 phosphorylation is responsible for KLF4 upregulation, *Bmp6*-dependent SMAD signalling and KLF4-dependent EndMT *in vitro* in CCM1 KO ECs. ...145

Figure 77 - In the absence of *Ccm1* increased ERK5 phosphorylation is responsible for KLF4 upregulation, *Bmp6* overexpression and KLF4-dependent EndMT *in vitro* in CCM1 null BMECs. ...146

Figure 78 - Mef2A and Mef2C contribute to KLF4 upregulation in CCM1 KO ECs. ...148

Figure 79 - Combined silencing of *Mef2A*, *Mef2C* and *Mef2D* leads to partial downregulation of *Klf4* expression in CCM1 KO ECs. ...149

Figure 80 - ERK5 activation in CCM2 null ECs is responsible for KLF4 upregulation and increased EndMT marker expression. ...150

Figure 81 - ERK5 activation in CCM3 null ECs is responsible for KLF4 upregulation and increased EndMT marker expression. ...151

Figure 82 - MEKK3 activity is required for ERK5-mediated KLF4 upregulation. ...153

Figure 83 - *Mekk3* silencing inhibits KLF4 upregulation in CCM1 KO ECs. ...153

Figure 84 - MEK5 activity is required for ERK5-mediated KLF4 upregulation. ...154

Figure 85 - *Mek5* silencing decreases *Klf4* mRNA levels in CCM1 KO ECs. ...154

Figure 86 - Chemical inhibition of MEK5 activity is required for ERK5-mediated KLF4 upregulation. ...155

Figure 87 - Chemical MEK5 inhibition decreases *Klf4* mRNA levels in CCM1 KO ECs. ...155

Figure 88 - Schematic model of KLF4 activity and regulation during CCM pathogenesis. ...160

Appendix Figure 1 - Analysis of *Lrg1*, *Edn1* and *Ednrb* expression in WT, CCM1 KO and CCM1-KLF4 BMECs KO...178

# TABLE INDEX

Table 1 – List of primers used for promoter cloning ........................................................ 73
Table 2 – List of primers used in ChiP .................................................................................. 76
Appendix Table 1 – List of upregulated genes in CCM1 KO BMECs obtained by Affimetrix analysis and ranked according to the fold change……………………………174
Appendix Table 2 – List of upregulated genes in CCM1 KO BMECs obtained by Affimetrix analysis and ranked according to the fold change……………………………177

# ABSTRACT

Cerebral cavernous malformations (CCMs) are capillary-venous malformations located in the central nervous system that often lead to neurological deficits and cerebral hemorrhage. Pharmacological treatment limiting disease progression is dearly needed, as available therapy is limited to surgical lesion eradication or stereotactic radiosurgery. CCM affects up to 0.5% of the human population and can occur either in a sporadic or familial form. Loss-of-function mutations in any of three genes *CCM1*, *CCM2* and *CCM3* have been associated to familial CCM. Postnatal endothelial-specific deletion of any of the three *Ccm* genes in mice results in the development of multiple brain vascular malformations that faithfully resemble human CCM lesions. Here we describe that CCM malformations are formed by endothelial cells (ECs) undergoing endothelial-to-mesenchymal transition (EndMT), a phenotype that recapitulates most of the previously observed functional changes that are responsible for dysplasia and fragility of CCM lesions. *Ccm1* deletion leads to activation of the MEKK3-MEK5-ERK5-MEF2 signaling cascade resulting in a marked upregulation of the transcription factor Krüppel-like factor 4 (KLF4) in ECs *in vivo*. KLF4 promotes an endogenous production of bone morphogenetic protein 6 (BMP6) in ECs that, in turn, activates the transforming growth factor-β (TGF-β) and bone morphogenetic protein (BMP) signalling pathway. KLF4 transcriptional activity and KLF4-dependent TGF-β/BMP pathway activation are responsible for the EndMT switch observed in the absence of *Ccm1*. Interestingly, using both a pharmacological treatment to inhibit TGF-β/BMP pathway or a genetic approach based on endothelial-specific *Ccm1* and *Klf4* double knockout mice, we strongly reduce the development and progression of CCM lesions. Importantly loss of *Klf4* almost abolishes mouse mortality due to brain hemorrhage in endothelial *Ccm1*-ablated mice. These data indicate that KLF4, TGF-β/BMP pathway and EndMT are crucial events for CCM pathogenesis and unveil KLF4 as a key therapeutic target for CCM.

# INTRODUCTION

## 1. VASCULAR ENDOTHELIUM

### 1.1 Endothelial cell-to-cell junctions

Endothelial cells (ECs) line the internal surface of blood vessels and form a semipermeable barrier that separates blood from the tissues. The passage of fluids, molecules and cells across endothelial barrier can occur either through a transcellular [1] or a paracellular route [2]. In order to regulate paracellular permeability ECs are equipped with highly organized intercellular structures called junctions [2]. EC junctions are assembled during the first stages of development and are composed by transmembrane proteins bound to intracellular molecules that, in turn, mediate the anchorage to actin cytoskeleton thus stabilizing the entire structure [3]. Besides to have adhesive properties necessary to maintain the integrity of the endothelium, EC junctions can act as signalling units able to communicate cell position, restrain cell migration, inhibit cell growth and apoptosis, control permeability and maintain apical-basal polarity to finely promote vascular homeostasis. ECs possess two main types of cell-to-cell junctions: adherens junctions (AJs) and tight junctions (TJs) [4]. AJs and TJs are both intermingled and interconnected along the EC cleft forming a complex system with variations in depth and thickness along the submembrane plaque. To note, AJs can influence and control TJ organization both in epithelial cells [5] and ECs [6].

AJs and TJs are also differentially expressed along the several portions of the vasculature tree depending on the specific functions required. AJ are usually present in all type of vessels while TJ expression and organization is finely modulated. The brain microvasculature is enriched in TJs since a strict control of permeability is required [7,8]; on the contrary, TJs are poorly organized in post-capillary venules, where a dynamic trafficking between blood and tissue takes place [9].

## 1.2 Adherens junctions composition and signaling

Endothelial AJs are composed by members of the classical cadherin family, a family of calcium-dependent cell adhesion transmembrane molecules (Figure 1). Vascular endothelial (VE)-cadherin (also called *Cdh5*), the main component of EC AJ [10], is an endothelial-specific molecule [10] expressed during development as soon as the cell is committed to the endothelial lineage. It is characterized by five extracellular domains located at the amino (N)-terminus, a transmembrane region and a cytoplasmic tail at the carboxyl (C)-terminus. Through extracellular domains, VE-cadherin promotes $Ca^{2+}$-dependent homophilic EC adhesion by creating a pericellular zipper-like structure along the cell border through lateral interaction *in cis* and *in trans*. ECs also express neuronal (N)-cadherin (also called *Cdh2*), another member of the classical cadherin family. Despite VE- and N-cadherin show similar structure and bind the same intracellular partners, they seem to play different roles in ECs. In physiological condition N-cadherin, whose expression is not EC-specific, is excluded from cell-to-cell contacts and localizes at the cell membrane to promote the anchorage of ECs to the neighbouring cells (e.g. perycites [PCs], smooth muscle cells [SMCs] and nerve cells). However, in the absence of VE-cadherin, N-cadherin expression is increased and it localizes at cell-to-cell contacts [11,12] to mediate anti-proliferative and anti-apoptotic response to compensate for the lack of VE-cadherin. Consistently both VE- and N-cadherin knock-out (KO) mice are embryonic lethal due to severe defect in vascular remodeling [13,14], thus suggesting a partial overlapping role of the two cadherins in the endothelium.

VE-cadherin cytoplasmic tail binds many intracellular partners to promote vascular stability and control of permeability [15,16], such as the three proteins of the Armadillo family named plakoglobin, β-catenin and p120 are connected to the intracellular domain of VE-cadherin (Figure 1). Plakoglobin and β-catenin can interact with α-catenin and VE-cadherin at the same time, forming a ternary complex [17]. α-catenin, in turn, can bind actin only when it is not hired by β-catenin, thus indicating that the cadherin-catenin complex indirectly influences the actin cytoskeleton. Moreover, plakoglobin, β-catenin and p120 are also able to shuttle from the cell membrane to the nucleus and activate specific transcriptional programs. Since the transcriptional activity of β-catenin, a crucial mediator of Int/Wingless (WNT) canonical pathway, usually induces cell proliferation and differentiation, its recruitment at cell-to-cell contacts in complex with VE-cadherin and the consequent inhibition of its transcriptional activity generally promotes vascular quiescence. VE-cadherin can recruit other cytoplasmic molecules to regulate the local organization of the actin cytoskeleton. Among others, T-Cell lymphoma invasion and metastasis (Tiam) [18], a guanine nucleotide exchange factor that activates Ras-related C3 botulinum toxin substrate 1 (Rac1), is localized to the cell membrane through the Ras-related protein-1 small GTPase (Rap1) to induce the organization of peripheral actin bundles. Rap1 binds to VE-cadherin and it stabilizes the junctions by promoting the association of the Rapidly accelerated fibrosarcoma (Raf)1/Rho-associated protein kinase (ROCK) complex to VE-cadherin to regulate the phosphorylation of Myosin light chain 2 (MLC2) and the actomyosin contractility at junctions [19].

AJ can also signal intracellularly. VE-cadherin clustering is able to directly control both TJ organization and stability by inhibiting the Forkhead-box protein-O1 (FoxO1) transcriptional activity. FoxO1 acts as repressor of the main TJ component *claudin5* and, therefore, its inhibition via phosphorylation induced by VE-cadherin-phosphatidylinositol-3-OH-kinase-(PI3K)-AKT axis induces claudin5 upregulation and leads to organized TJs. On the contrary, nuclear β-catenin is able to stabilize FoxO1 on the *claudin5* promoter, thus sustaining its repressor activity [6]. Thus, VE-cadherin-dependent β-catenin engagement at junctions further limits FoxO1 activity and promotes vascular stability.

VE-cadherin can also directly modulate growth factor receptor-dependent signaling. The association of VE-cadherin with the vascular endothelial growth factor (VEGF) receptor type 2 (VEGFR2) limits its internalization and activity in the presence of the angiogenic growth factor VEGF-A [20]. Conversely, VE-cadherin binding to either TGF-β receptor complex [21], platelet derived growth factor receptor (PDGFR) [22] or fibroblast growth factor receptor-1 (FGFR-1) [12], controls endothelial proliferative signals to promote vascular quiescence.

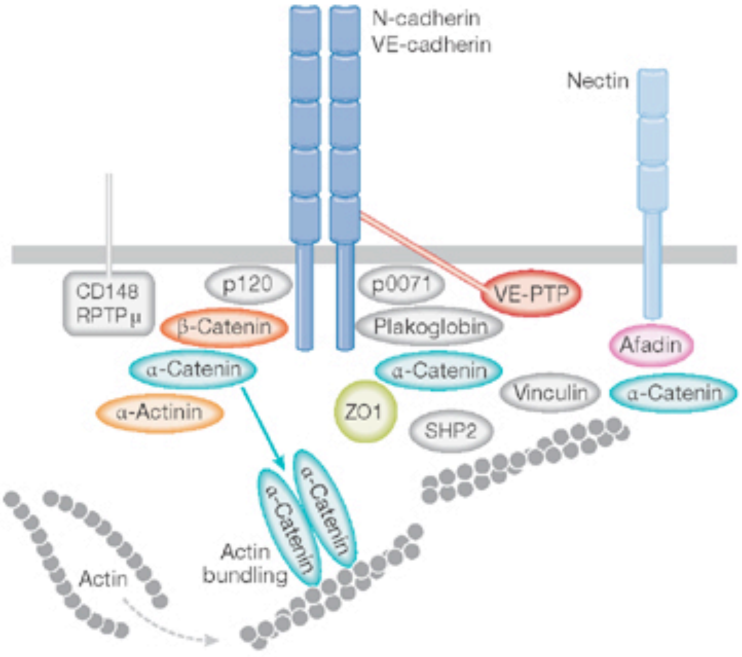
N-cadherin
VE-cadherin
Nectin
CD148
RPTPμ
p120
p0071
VE-PTP
β-Catenin
Plakoglobin
Afadin
α-Catenin
α-Catenin
Vinculin
α-Catenin
α-Actinin
ZO1
SHP2
α-Catenin
α-Catenin
Actin
bundling
Actin

**Figure 1 - Schematic representation of endothelial AJs.**

Endothelial AJs are formed by some members of the classical cadherin family such as VE-cadherin and N-cadherin. VE- cadherin is important for the interaction between neighbouring ECs while N-cadherin mediates the contact between ECs and pericytes. The cytoplasmic interactore p120, α-catenin, β-catenin and plakoglobin promote the junction stability by inducing the anchorage of the junctions to the actin cytoskeleton and they mediate the intracellular signalling. Membrane- associated phosphatases like VE-PTP, DEP-1 (or CD148) and RPTPμ regulate VE-cadherin turnover at junction *(Adapted from Nyqvist et al., 2008)*

The phosphorylation status of VE-cadherin controls vascular permeability. Tyrosine phosphorylation in the VE-cadherin cytoplasmic tail (Y658 and Y685) results in weaker junctions and impaired barrier function [23,24,25]. Permeability agents such as histamine [23], tumor necrosis factor-α (TNF-α) [26], platelet-activating factor (PAF) [27] and VEGF [24] induce tyrosine phosphorylation of VE-cadherin, β-catenin and p120 by activating the Rous sarcoma proto-oncogene tyrosine-protein kinase (Src) [16] directly associated with VE-cadherin/catenin complex. Thus, either *Src* gene deletion or the use of Src inhibitors blocks VEGF-induced VE-cadherin phosphorylation [28]. The phosphorylation status of VE-cadherin may also be modulated by AJ-associated phosphatases, such as the vascular endothelium specific protein tyrosine phosphatase (VE-PTP) [29], density-enhanced phosphatase-1 (DEP-1) [12,30], protein tyrosine phosphatase receptor type M (PTP-μ) [31] and src-homology 2 (SH2)-containing phosphotyrosine phosphatase (SHP2) [32] that bind to VE-cadherin directly on indirectly to decrease its phosphorylation status and increase the strength of the vascular barrier.

Finally, permeability can also be regulated by VE-cadherin internalization [25,33] or enzymatic proteolityc cleavage [34].

### 1.3 Tight junctions composition and signaling

TJs physically seal the plasma membrane of two adjacent cells to finely regulate the passage of cells and solutes through the paracellular space [35]. TJs are formed by members of multiple families of transmembrane signalling proteins, which include claudins, occludins and junctional adhesion molecules (JAMs) (Figure 2). These TJ transmembrane components associate to the cytoplasmic proteins like Zonula Occludens ([ZO]-1, ZO-2, ZO-3) and cingulin [36]. The high grade of junction complexity can be explained by the specific barrier properties that TJs must exert depending on the tissues in which they are located. Claudins, the major transmembrane components of TJs, are 21-28 kDa proteins and consist of four transmembrane domains, two extracellular loops and both N- and C-terminal cytoplasmic domains. The claudin family is composed by 24 members. ECs express claudin1, 3, 5 and 12 and among them only the expression of claudin5 is endothelial-specific [37]. Claudins contain the conserved aa motif GLWxxC(8-10 aa)C in the first extracellular loop and a PDZ (Post synaptic density protein, Drosophila disc large tumor suppressor and Zonula occludens-1 protein) domain-binding motif at the C-terminus, which is needed for the association with PDZ-containing TJ proteins ZO-1, ZO-2 and ZO-3 [35].

Occludin, like claudins, is a four-pass transmembrane protein with both N-terminal and C-terminal cytoplasmic domains. The C-terminal cytoplasmic region of occludin also binds to ZO-1, ZO-2 and ZO-3 [35].

JAM proteins belong to the immunoglobulin (Ig) superfamily and have two extracellular N-terminal Ig-like domains, a transmembrane region and a short cytoplasmic tail harbouring a PDZ-binding domain. At least five members are known, named JAM-A (or JAM-1 or F11R), JAM-B, JAM-C, JAM-4 and JAM-L plus a sixth molecule called ESAM that shares similarities with the JAM family. Every JAM molecule displays its own peculiar pattern of expression. JAM-A is the most widely expressed since it can be detected in both endothelial and epithelial tissues of many organs as well as in platelets, erythrocytes and leukocytes. JAM-B is expressed exclusively by ECs, while JAM-C is present both in ECs and leukocytes. Much less is known about the expression pattern of JAM-4, JAM-L and ESAM. Of note, JAM proteins are engaged in both homophilic (i.e. with identical JAM molecules) and heterophilic (i.e. with different JAMs or other unrelated proteins) interactions. JAM-A, JAM-B, JAM-C and JAM-L contain a putative dimerization loop in their N-terminal region and are able to localize at cell-to-cell contacts in close proximity with TJ strands. JAM-A interacts with many PDZ-containing molecules that mediate the anchorage to actin cytoskeleton such as ZO-1, Afadin-6 (AF-6), partitioning defective (PAR) 3/6/atypical PKC (aPKC) complex, calcium/calmodulin-dependent serine protein kinase CASK/lin2 and multi-PDZ domain protein (MUPP-1) [4, 38]. By binding PAR3/PAR6 polarity complex in association to the small GTPases Cdc42 and aPKC, JAM-A and JAM-C play a central role in the maintenance of apical-basal cell polarity [39]. Cell polarity is finally required also for a correct angiogenesis and therefore, there are evidence showing that JAM-C is involved in tumor angiogenesis and retinal neovascularization [40].

ZOs, cytoplasmic TJ components, belong to the family of the membrane-associated guanylate kinase homologs (MAGUKs) [4, 41], and consist of three PDZ domains, a Src Homology (SH)3 domain and a guanylate kinase (GUK) domain. PDZ-binding domains at the C-terminus are able to mediate the anchorage of the associated transmembrane proteins to actin cytoskeleton. When TJs are not well developed or the cells are in sparse/migrating condition, both ZO-1 and ZO-2 dissociate from the cell-to-cell contacts and migrate into the nucleus [42, 43]. ZO-1-associated nucleic acid binding protein (ZONAB), a Y-box transcription factor reported to localize both at TJs and in the nucleus, binds to the SH3 domain of ZO-1 and this interaction is required for sequestering ZONAB at the plasma membrane and restraining its nuclear localization, thus reducing cell proliferation [44, 45].

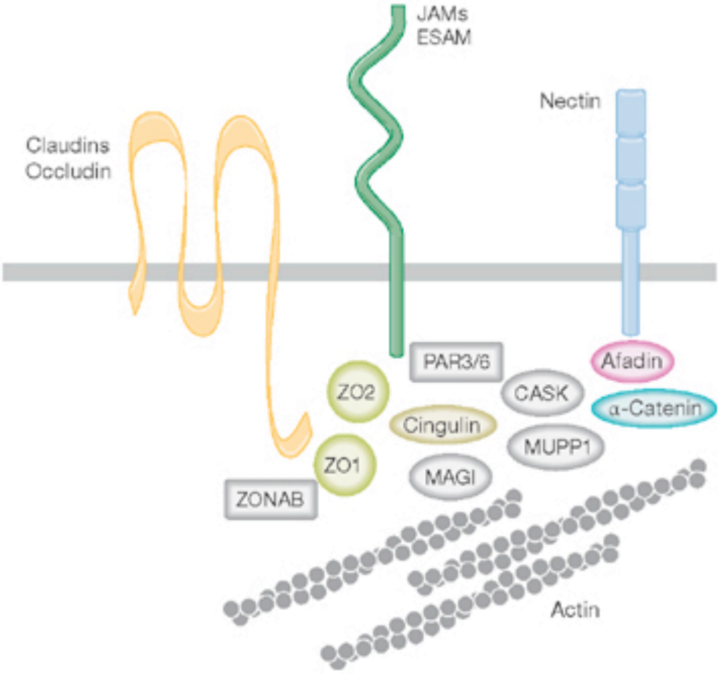

**Figure 2 - Schematic representation of endothelial TJs.**

Claudins play a central role in the formation of TJ strands between ECs with the cooperation of occludin and JAMs molecules. Many intracellular components of TJs such as ZO-1, ZO-2 and cingulin mediate junctional binding to actin cytoskeleton. (*Adapted from Nyqvist et al, 2008*)

### 1.4 Endothelial heterogeneity: the example of the blood brain barrier

The heterogeneity is an intrinsic feature of ECs. Depending on multiple factors such as tissues localization, vessel size and age, ECs can modify their phenotype in order to adapt to and support specific functions of the tissue or the organ in which they reside. Differences in terms of junction organization, cell morphology, gene expression or antigen composition and functions have been described in ECs located in different segments of the vascular tree. From a structural point of view the endothelium can be classified into three main classes: continuous non-fenestrated, continuous fenestrated and discontinuous or sinusoidal [4, 46]. Continuous non-fenestrated endothelium is peculiar of vessels inside the brain, the skin and the heart. The presence of highly organized and abundant TJs in the vasculature of these organs allows the strong sealing of cell-to-cell contacts in order to strictly control the passage of several substances. The active transcytosis of molecules across this vessel wall is mediated by caveolae, vesiculo-vacuolar organelles and specific transporters [47]. Conversely continuous fenestrated endothelium is characterized by the presence on endothelial surface of transcellular pores with a diameter of about 70 nm (the so called fenestrae) that allow the rapid exchange of molecules between the circulation and the surrounding tissue. Most of the fenestrae present a thin diaphragm that acts as a molecular filter and allows increased size selectivity [48,49]. Fenestrated endothelium is permeable to water and small solutes and, therefore, it is typical of organs involved in filtration or secretion such as exocrine and endocrine glands, renal glomeruli and the gastric-intestinal mucosa. Finally, discontinuous endothelium is similar to the fenestrated one with the exception that fenestrae are larger in diameter (100-200 nm) and lack an internal diaphragm [49].This poor restrictive endothelium is typical of certain sinusoidal vascular beds in the bone marrow and in the liver that need to allow continuous cellular trafficking [47].

Beyond structural differences, ECs express distinct patterns of cell surface markers, solute transporters and intracellular enzymes in different tissues. For instance, ultrastructural features such as the secretory organelles Weibel-Palade bodies are not found in all ECs [46], while the expression of *Glucose transporter 1* (*Glut1*) is limited to brain vascular ECs [50].

The molecular mechanisms involved in EC heterogeneity are driven by the exposure of ECs to tissue specific environmental stimuli including mechanical forces, cytokines, the contact with tissue-specific cell types, circulating immune cells, extracellular matrix (ECM) and soluble growth factors [51]. All these stimuli can activate specific receptor-mediated signalling pathways in ECs that further induce post-translational modification of proteins or modify the transcription factors-dependent gene expression. This fine regulation of the endothelial heterogeneity through the microenvironment is a biological process termed trans-differentiation [52]. In agreement with this theory, ECs cultured *in vitro* undergo a phenotypic drift because they are uncoupled from critical extracellular signals deriving from their native environment. Conversely, certain specific properties of ECs are determined by epigenetic modification (e.g. DNA methylation, histone methylation and acetylation) and can be maintained also upon EC isolation and culture since they are mitotically stable [51].

A clear example of EC heterogeneity is represented by the highly specialized endothelium of the brain microvasculature. This endothelium has to tightly control the exchange of molecules, ions and cells between the central nervous system (CNS) and the peripheral blood circulation, thus allowing proper neuronal function and the protection of the CNS from toxins and pathogens [53]. From an anatomical point of view brain ECs are supported by a basement membrane and enwrapped by PCs and astrocytic end feet processes to create a multicellular vascular structure called blood brain barrier (BBB) (Figure 3) [54, 55]. All this elements together with the contribution of neurons, microglial cells and immune cells, constitute a peculiar microenvironment known as neurovascular unit (NVU) [56]. The proper interaction between these multiple cellular components is necessary for correct formation and function of BBB [56].

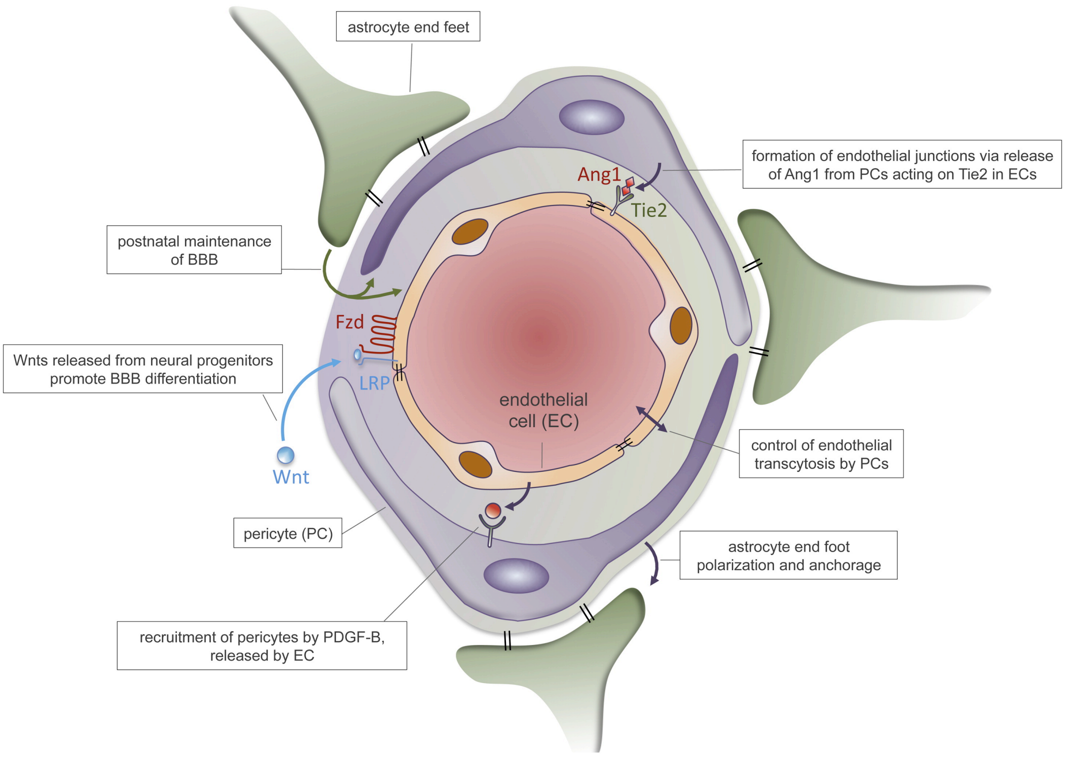
astrocyte end feet
formation of endothelial junctions via release of Ang1 from PCs acting on Tie2 in ECs
Ang1
Tie2
postnatal maintenance of BBB
Fzd
LRP
Wnts released from neural progenitors promote BBB differentiation
Wnt
endothelial cell (EC)
control of endothelial transcytosis by PCs
pericyte (PC)
astrocyte end foot polarization and anchorage
recruitment of pericytes by PDGF-B, released by EC

**Figure 3 – Schematic representation of the cellular organization of the BBB.**

ECs, covered by a basement membrane in their abluminal side, are the main components of the BBB. Pericytes partially envelope ECs and astrocytes extend their foot processes thus providing a link with the neurons. A correct crosstalk between these multiple components is required for proper barrier induction and maintenance. *(Adapted from Quaegebeur et al., 2011)*

High-throughput genomic and proteomic analyses of the molecular differences between ECs of different origins have revealed that ECs of the brain microvasculature possess unique properties. CNS ECs have highly organized TJs since *claudin5* and *occludin* expression are very enriched in the brain endothelium [57]. The importance of these TJ components is underlined by the phenotype of both claudin5 and occludin KO mice. Claudin5 deficient mice die within 10 hours after birth due to a size selective loosening of BBB against molecules smaller than 800 Da [58]. Occludin null mice develop calcifications in the CNS, thus suggesting a critical role for occludin in the regulation of calcium flux across the BBB [59]. Efflux transporters and nutrient transporters are particularly abundant in brain ECs [57]. The first are localized on the luminal cellular side and they use the hydrolysis of adenosine triphosphate (ATP) to transport small lipophilic molecules into the bloodstream [60]. In this regard is important to note that ECs of the CNS are equipped with a high amount of mitochondria in order to meet the ATP needs required by this transportation system [61]. By contrast, nutrient transporters allow the passive movement of important nutrients from the blood to CNS as well as the removal of waste products from the brain. Many of these transporters belong to the solute carrier family such as GLUT1, a transporter that allows the entry of circulating glucose into the brain [62, 63]. The transcytosis in a healthy BBB is very low as compared to peripheral ECs. In agreement, a strong upregulation of the plasmalemma vesicle-associated protein (PLVAP) is observed during BBB injury and disease [64, 65]. Finally, ECs express a very low amount of leucocyte adhesion molecules such as selectins (P-selectin and E-selectin) that are required for leukocyte adhesion and extravasation [46, 66], thus strongly limiting immune cell entry into the brain parenchyma.

Vascular heterogeneity acquires even more importance considering that some vascular diseases such as atherosclerosis [67] and rare genetic diseases including Cerebral Cavernous Malformations (CCM) [68] develop in specific types of vessels.

# 2. CEREBRAL CAVERNOUS MALFORMATIONS

Cerebral cavernous malformations (CCMs), also known as cavernous angioma or cavernoma, are vascular lesions that occur predominantly in the CNS, even if they can also be found in other anatomical districts such as liver, retina and skin in a lower percentage of the cases [69]. CCM lesions consist of mulberry-like structures composed by dilated and enlarged vessels lined by a thin layer of ECs surrounded by a thick, discontinuous basal membrane with no intervening parenchyma [70] (Figure 4). CCMs arise from the venous-capillary vascular bed and are characterized by low blood flow eventually associated with thrombosis and calcifications [69]. Ultrastructural analysis revealed that the BBB is severely compromised at the level of these lesions. Thus, TJs and AJs are strongly altered and several gaps develop between individual cells. EC surrounding PCs are reduced in number and no astrocytic foot processes are present within the lesions [70]. CCMs are often neurologically silent and it has been estimated that only approximately 60% of patients are symptomatic [71].

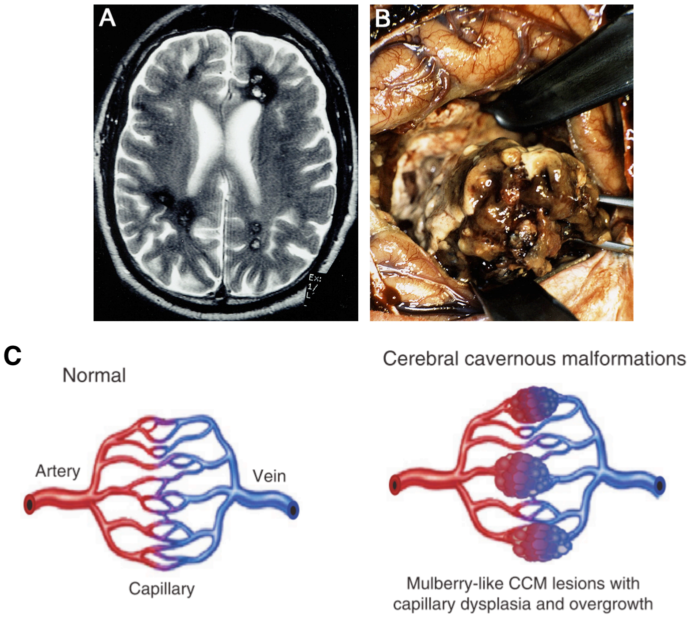
A
B
C
Normal
Artery
Vein
Capillary
Cerebral cavernous malformations
Mulberry-like CCM lesions with capillary dysplasia and overgrowth

**Figure 4 – The morphology of CCM vascular lesions**

A) Cerebral MRI showing multiple CCM lesions. B) Surgical view of a CCM lesion. C) Schematic representation of the normal vasculature (left panel) and the typical mulberry-like structure of CCM lesions (right panel). *(Adapted from Dejana et al., 2009 and Storkebaum et al., 2011)*

Clinical symptoms strongly reflect a compromised BBB and include strokes, intracranial hemorrhage, seizures and focal neurological deficits depending on the site of lesion [72].

## 2.1 CCM genetics

CCM is a rather frequent disease with a prevalence of 0.5 % in the population. It can occur both in a sporadic (80 % of cases) or familial form (20 % of cases). Sporadic patients usually develop a single lesion from the second decade of the life while familial forms are characterized by the formation of multiple lesions whose number and size usually increase with the age [71, 73]. Moreover, while sporadic cases are not inherited, familial forms are transmitted in an autosomal dominant manner with variable penetrance. 95 % of familial CCM patients harbor a heterozygous germ line mutations in one of the three different *CCM* genes known as *CCM1/KRIT1*, *CCM2/MGC4607/OSM/Malcavernin* and *CCM3/PDCD10/TFAR15* [71, 73]. Different types of *CCM* gene germline mutations have been reported (e.g. nonsense, splice-site and frameshift mutations as well as large genomic rearrangements and few missense mutations), mostly resulting in loss-of-function of the relative protein [74]. Mutations in *CCM1* gene are the most common accounting for about 56 % of familial CCM, whereas the *CCM2* and *CCM3* mutations occur in 33 % and 6 % of the familial cases respectively [74, 75]. A *CCM1* founder mutation (Q455X stop codon mutation in *CCM1*) has been identified in Hispanic Americans of Mexican descent, a population with a higher incidence for CCM [72]. Of note, no mutation in *CCM* genes has been detected in 5% of familial CCM, thus suggesting the existence of unknown additional genes implicated in CCM disease [75]. To this regard a potentially new *CCM* gene named *zona pellucida-like domain containing 1* (*ZPLD1*) has been recently identified even if its functional role in CCM pathology remains to be determined [76]. The average age of the disease onset is between the 2nd and 5th decades of life, but symptoms can start in early infancy or in older age. In comparison to CCM1 and CCM2 patients, *CCM3* mutations are associated with an earlier disease onset and more severe phenotype characterized by a higher risk for cerebral hemorrhage during childhood [77]. The standard strategy to identify mutations in CCM patients and to confirm their clinical diagnosis is the full sequencing of both the coding regions and the exonic-intronic junctions in the three *CCM* genes. If sequencing gives negative results, other approaches are currently applied in clinics including the multiplex ligation-dependent probe amplification (MLPA) analysis or the combination of microsatellite marker analysis together with quantitative real-time polymerase chain reaction (qRT-PCR) [78].

It has been hypothesized that CCM pathogenesis occur following the Knudson's two-hit mechanism. Loss of one allele in all cells (germ line mutation) might be followed by a somatic mutation in the other allele (second hit) in some ECs that, subsequently, would lead to the formation of a vascular lesion [79]. Since the detection of homozygous mutations in individual ECs inside a lesion is quite challenging, the possible cause of this "second hit" is still an open issue.

### 2.2 Animal models used to study CCM disease

Since CCM proteins are well conserved across different species [80], numerous experimental animal models have been used to study CCM pathology. Due to the availability of transgenic reporter lines expressing fluorescent proteins within the vasculature together with its transparency and amenability to genetic manipulation, the zebrafish model has been extensively used to unveil the functions of *Ccm* genes in the vascular system. Zebrafish mutants KO for either *santa* (the zebrafish orthologue of *CCM1*), *valentine* (the zebrafish orthologue of *CCM2*) or *pdcd10* (ccm3, which is duplicated in the zebrafish genome) show the so called "big heart phenotype", a severe dilation of the cardiac chambers in which the endocardium is covered by a single thin layer of myocardial cells [81-83]. The absence of heart looping and the endocardial cushion formation in these zebrafish mutants has been also reported [82]. Beyond a cardiac phenotype these mutants develop dilated thin-walled vessels without lumen [84], that are reminescent of the microvasculature observed in human CCM patients. Interestingly, the big heart phenotype of *santa, valentine* and *pdcd10* KO zebrafish is very similar to what observed in fish lacking *heart of glass* (*heg*) [85]. HEG1 is a transmembrane receptor expressed almost exclusively by vascular ECs that interacts with CCM1 and CCM2 [85]. However, since loss of HEG1 does not alter CCM lesion formation in mice and no mutations in the human orthologue *HEG1* have been identified in CCM patients [86, 87], HEG1 seems to not be directly involved in the pathogenesis of CCM disease.

Several murine models have been also developed by several groups in order to study the *in vivo* functions of CCM proteins during the vascular development. Constitutive and global deletion of any of the three *Ccm* genes in mice results in embryonic lethality due to generalized vascular defects in embryonic and extra-embryonic tissues [69, 88, 89]. Of note, mice with a systemic *Ccm3* deletion die earlier (E8.0 to E8.5) in respect to *Ccm1* and *Ccm2* KO mice (E9.5). Although *CCMs* expression is not endothelial-specific, they seem to play a specific role in the brain endothelium. Endothelial-specific deletion of either *Ccm2* or *Ccm3* strongly impairs angiogenesis and results in embryo death at mid-gestation [68, 88, 89] while conversely, neuronal-specific and smooth muscle cell-specific *Ccm2* or *Ccm3* KO mice do not show any vascular defects and survive to adulthood [88]. In order to study the role of *CCM* genes during brain angiogenesis and to clarify CCM pathophysiology, several genetic strategies have been applied to avoid the embryonic lethality of both constitutive and endothelial-specific *Ccm* KO mice. Based on the two-hits hypothesis, *Ccm* heterozygous mice, that usually do not develop cavernomas, have been crossed with error prone genetic background mice [90, 91](e.g. *p53* KO and *Msh2* KO animals). These CCM animal models, while developing lesions similar to patients, are characterized by incomplete penetrance, an increased risk of developing neoplasms and the impossibility to control the tissue specificity of the second mutation. In order to overcome these limitations endothelial specific gene ablation has been induced after birth. Postnatal day 1 (P1) deletion of any of the three *Ccm* genes in the endothelium results in the development of vascular lesions specifically in the CNS [69,92]. Interestingly postnatal *Ccm* gene ablation in other CNS cell types fails to give a pathological phenotype with the exception of the neural-specific deletion of *Ccm3*, which is characterized by diffuse enlargement of brain blood vessels and the formation of vascular lesions that recapitulate human CCM [93].

In conclusion it remains unclear the reason why *Ccm* genes ablation specifically affects the brain microvasculature and whether the role of CCMs in other cellular components of the BBB could contribute to CCM pathogenesis.

### 2.3 CCM protein function and pathological implications

CCM proteins do not share any similarity in term of sequence or structure, but they can form a cytosolic multiprotein complex, in which CCM2 is the bridge between CCM1 and CCM3 [94, 95], necessary for their proper localization at cell-to-cell contacts in ECs [96]. The existence of a unique CCM complex explains the strong similarity of the clinical manifestations observed in CCM patients and animal models upon loss-of-functions of any of the three *Ccm* genes. However, single CCM proteins can have also specific intracellular localization and they can interact with different unique partners [97]. CCMs, either as part of the same complex or as single molecular entities, exert a critical role in several ECprocesses such as cell-to-cell junctions organization, cell polarity, cytoskeletal remodeling, lumen formation and angiogenesis [97].

Enhanced vascular permeability is a hallmark of CCM lesions *in vivo*. CCM proteins control endothelial barrier function by regulating both actin cytoskeleton remodeling and endothelial junction formation and maintenance. In this regard CCMs have been described to restrain the activity of small GTPase RhoA and its kinase ROCK [88, 96]. *Ccm* gene deletion leads to RhoA activation and the following phosphorylation, mediated by ROCK, of a series of target proteins involved in stress fiber formation, motility, cell polarization and permeability. RhoA activation in response to the absence of CCM is due to reduced RhoA degradation [98] as well as to altered Striatin-interacting phosphatase and kinase (STRIPAK)-mediated activation of the RhoA inhibitor moesin [99].

CCM proteins fulfill also a crucial role in the formation and maintenance of EC junctions. Rap1 is a binding partner of CCM1, which act as a scaffold protein for a membrane-tethered complex containing VE-cadherin and β-catenin [100,101]. In the absence of *Ccm1,* Rap1 is mislocalized leading to junctional weakening and increased permeability. Lack of *Ccm2* or *Ccm3* also increases EC permeability due to AJ and TJ alterations [69, 88].

Disruption of AJs in the absence of *Ccm1* is accompanied by the loss of apical basal polarity and improper lumen formation. VE-cadherin and CCM1 form a complex that is required for the correct junctional localization and function of the members of the Par polarity complex (consisting of PAR3, PAR6 and the effector component protein kinase Cζ, PKCf) [102, 103]. Dismantling AJs by inactivation of CCM1 leads to the altered PKCζ activity and consequent abrogation of endothelial cell polarity, which might explain why CCM-mediated lesions are abnormally enlarged and present multiple lumens [103]. Consistently, also CCM3 seems to play a pivotal role in lumen formation through its interaction with GCKIII kinases [104] while for CCM2 null *ECs* no polarization defects were reported.

AJ dismantling results in increased β-catenin nuclear localization and β-catenin - dependent transcription in CCM1 [101] and CCM3 null ECs [92]. Most importantly, β-catenin signaling activation is responsible for the development and progression of vascular lesions *in vivo* in the absence of *Ccm3* [92].

*In vivo* deletion of *Ccm* genes has already revealed that CCM proteins are essential for the angiogenic phase of the cardiovascular development [69, 88, 89]. *In vitro* loss of either *Ccm1* or its interactor *Integrin Cytoplasmic Domain-Associated Protein 1* (*Icap1)* results in an excessive angiogenesis due, at least in part, to a deregulation of both the Notch pathway [105] and the integrin β1-mediated signaling [106,107]. Viceversa CCM3, that has independent and different roles in comparison to both CCM1 and CCM2 [108], has been reported to induce VEGFA-dependent signaling by stabilizing and activating VEGFR2 [89]. Thus the absence of *Ccm3* results in altered vessel growth.

Since it is evident that CCM proteins are implicated in a number of signalling pathways that seem to be crucial for EC homeostasis, it is conceivable to hypothesize that loss of *Ccm* genes could lead to a hyper-activation of specific angiogenic programs occuring in the CNS endothelium that eventually result in the formation of abnormal, fragile and irregular vascular structures. In this regards it is interesting to note that while the endothelial-specific ablation of *Ccm2* at P1 results in the formation of multiple vascular lesions in the cerebellum, gene deletion performed in adult mice rarely leads to CCM development [69]. Thus, additional stimuli such as the presence of an active angiogenesis program in the neonatal cerebellum or other context-specific factors could be necessary to promote the formation of the cavernoma. In the same line of thought, it is still unclear why CCM lesions arise predominantly in the CNS endothelium. One possible explanation is that CCM proteins could restrain improper vessel growth by promoting a correct crosstalk of ECs with other cellular components of the neurovascular unit.

### 2.4 Future pharmacological therapies for the treatment of CCM patients

The diagnosis of CCM lesions is particularly challenging since CCM lesions are not detectable by angiography [109]. Other imaging techniques are used currently for CCM diagnosis in clinics such as conventional T1- and T2- weighted MRI that allows the detection of cavernomas in a very sensitive way. The natural history of these vascular lesions is still not yet clearly understood [78]. CCM lesions are highly dynamic and they may undergo enlargement or even *de novo* formation. Moreover, depending on their location in the cerebral microvasculature, the symptoms and hemorrhage risk can be very different.

Even if a clear correlation between lesions development/growth and their relative localization within CNS has not been identified, most of the CCM lesion are supratentorial while other are more deeply located in the brainstem [110]. Once a CCM lesion is diagnosed by MRI, all these factors have to be taken in account during the clinical management of the CCM patient. To date neurosurgery is the only therapeutic approach offered in clinics and the risks associated with the microsurgical resection of the lesions are strictly related to their location. Due to this reason most of the efforts in this research field are now concentrated to identify a new pharmacological therapy able to prevent or arrest CCM lesion development. The pharmaceutical treatments proposed so far target the signaling pathways recently identified as altered in CCM. Initially Statins, well-known inhibitors of RhoA activation, have been proposed as a promising pharmacological tool to reduce the increased vascular permeability associated to CCM, but it was unable to reduce the number and the size of CCM lesions in mice [88, 111, 112]. Conversely Fasudil, a direct inhibitor of ROCK, has been reported to decrease lesion burden in CCM mouse models [113]. Recently sulindac sulfide and sulindac sulfone, two non-steroidal anti-inflammatory drugs previously used in clinics as inhibitors of β-catenin-dependent signalling, have been shown to significantly reduce the number and the size of CCM lesions *in vivo* at least in the absence of *Ccm3* [92]. Finally, by using an unbiased screening platform to repurpose previously developed drugs, Gibson and coworkers have shown that vitamin $D_3$ and TEMPOL, a scavenger of superoxide, are very effective in reducing CCM lesions at least in mouse models [112]. However the molecular mechanisms through which they act remains undefined. For this reason the major goal of this research project is the better understanding of which signalling pathways are relevant for CCM pathogenesis in order to identify new candidate targets for pharmaceutical intervention.

# 3. ENDOTHELIAL TO MESENCHYMAL TRANSITION

## 3.1 Definition of endothelial-to-mesenchymal transition

ECs are characterized by a marked plasticity and may acquire a mesenchymal phenotype through a complex biological process called EndMT (Figure 5). During this transition ECs reduce the expression of specific endothelial markers (such as VE-cadherin, claudin5 and CD31 [PECAM1]) and strongly increase the expression of mesenchymal markers such as α-Smooth Muscle Actin (αSMA) or Fibroblast Specific Protein 1 (FSP1 or S100A4) and stem cell markers like CD44, stem cell antigen 1 (SCA1) and inhibitor of differentiation1 (ID1). This process is associated with altered junction organization, loss of cell polarity, increased cell proliferation and migratory capacity [114]. EndMT has been implicated in fundamental physiological processes during embryogenesis [115-117] but, also, in pathological conditions including organ fibrosis and cancer [118-122]. EndMT has often been considered a specialized form of epithelial to mesenchymal transition (EMT), a fundamental process during embryonic development, tissue repair, and disease [123] during which a polarized epithelial cell, that normally interacts with basement membrane, acquires a mesenchymal cell phenotype with an increased invasiveness and resistance to apoptosis [124]. Both EMT and EndMT are induced by similar signaling pathways such as those mediated by transforming growth factor β (TGF-β), bone morphogenetic proteins (BMP), epidermal growth factor (EGF), fibroblast growth factor (FGF), platelet-derived growth factor (PDGF), WNT, Sonic Hedgehog (Shh), Notch, and the integrin signaling, that, in turn, induce a number of transcription factors able activate the expression of EMT/EndMT-associated genes [125].

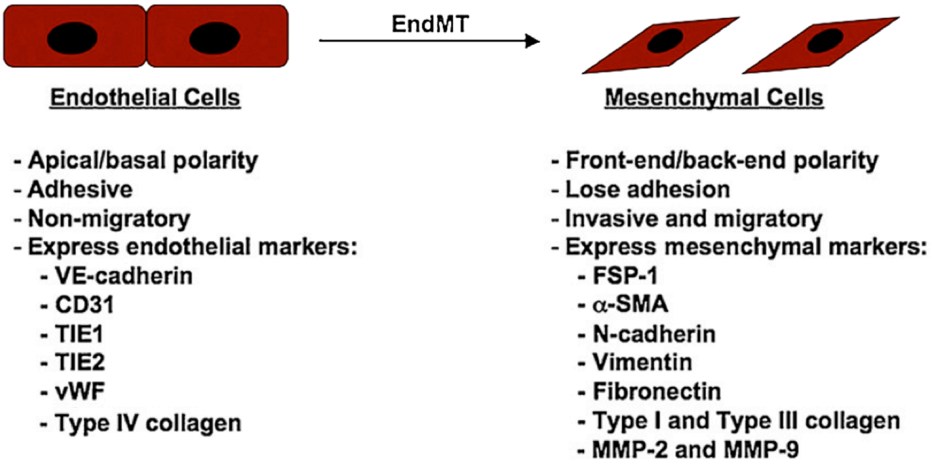
EndMT
Endothelial Cells
- Apical/basal polarity
- Adhesive
- Non-migratory
- Express endothelial markers:
- VE-cadherin
- CD31
- TIE1
- TIE2
- vWF
- Type IV collagen
Mesenchymal Cells
- Front-end/back-end polarity
- Lose adhesion
- Invasive and migratory
- Express mesenchymal markers:
- FSP-1
- α-SMA
- N-cadherin
- Vimentin
- Fibronectin
- Type I and Type III collagen
- MMP-2 and MMP-9

**Figure 5 - Phenotypic changes that occur during the EndMT**.

During EndMT ECs loose the expression of endothelial markers VE-cadherin, CD31, TIE1, TIE2, and vWF, and acquire/increase the expression of several mesenchymal markers. Distinct changes in cell polarity, cytoskeleton and ECM composition, cell-to-cell junctions and increased motility accompany the switch of the phenotype (*from Medici & Kalluri, 2012*).

## 3.2 The TGF-β signalling pathway

TGF-β signalling pathway is implicated in a large number of biological processes including cell proliferation, differentiation, migration, ECM production and apoptosis. TGF-β signaling cascade involves a family of 33 ligands, two serine/threonine kinase receptors (type I and II) and the signal transducers mother against decapentaplegic (SMADs) [126]. The ligands, which share a dimeric structure and a cysteine knot structural motif [127], include three distinct TGF-β isoforms (TGF-β1, TGF-β2 and TGF-β3), more than twenty Bone Morphogenetic Proteins (BMPs), Growth Differentiation Factors (GDFs), Mullerian Inhibitory Factors (MIFs) and Activins or Inhibins. TGF-β signalling is mediated by the binding of active ligands to an heterodimeric receptor complex composed by type I and type II serine/threonine kinase receptors [128]. A total of seven TβRI receptors, called activin receptor-like kinase (ALK1-ALK7) and five TβRII receptors, among which TGF-β type II receptor (TBRII), BMP type II receptor (BMPRII), activin receptor type IIA (ActRIIA), activin receptor type IIB (ActRIIB) and AMH type II receptor (AMHRII), have been identified. Type I (TβRI) and type II (TβRII) receptors are all composed by a cytoplasmic tail that retains kinase activity, a single transmembrane spanning region and a cysteine-rich extracellular domain. Each ligand belonging to the TGF-β superfamily can bind to different combinations of type I and type II receptors, thus mediating different signalling pathways. Commonly, BMPs and TGF-β subfamilies are synthetized as inactive monomeric pro-peptides, composed by a short N-terminal sequence, a latent-associated peptide (LAP) and a C-terminal mature domain retained in the ECM. After the synthesis, two monomeric precursors dimerize and are then processed by endoproteases of the convertase family and proteolytic enzymes, responsible for the cleavage between LAP and the release and secretion of the mature homodimer protein. This fine regulation of the protease activity is of fundamental importance since it allows the control of active TGF-β bioavailability [129].

The binding of the ligands induces the formation of the receptor complex and mediates phosphorylation of TβRI by TβRII, required to TGF-β downstream signalling. In this way TβRI can then recruit and phosphorylate the cytoplasmic mediators SMADs that, in turn, bind the common mediator SMAD4 (Co-SMAD) and translocate into the nucleus acting as TFs of specific target genes [130] (Figure 6). The TGF- β family of SMAD proteins is classified in three main groups: Receptor-associated SMADs (R-SMADs), Co-operating SMADs (Co-SMADs) and Inhibitory SMADs (I-SMADs) [131]. R-SMADs are the SMADs recruited and phosphorylated by the TβR complex. Five different R-SMADs have been identified in humans, namely SMAD1, SMAD2, SMAD3, SMAD5 and SMAD8; their structure contains two conserved Mad Homology Domains, MH1 and MH2 that are respectively responsible for the binding to DNA and for the R-SMADs oligomerization [132]. Interaction of R-SMADs with the TβRI is also promoted by the presence of auxiliary proteins, such as the SMAD Anchor for Receptor Activation (SARA), favouring the association of the TβR complex with SMAD2/3 and subsequently their phosphorylation.

ALK4, ALK5 and ALK7 mediate SMAD2 and SMAD3 phosphorylation and are usually downstream of TGF-β, activins, inhibins and nodal [133]. On the contrary, ALK1, ALK2, ALK3 and ALK6 induce pSMAD1, pSMAD5 and pSMAD8 and their activation is usually mediated by BMPs and AMH, even if it has been demonstrated in ECs that TGF-β can also interact and signal through ALK1 [134].

SMAD4 is the Co-SMAD required for the association with phospho-R-SMADs and their translocation into the nucleus, while I-SMADs, that include SMAD6 and SMAD7, mediate a negative regulation of TGF−β signaling [135]. Among the I-SMADs, SMAD7 is the main involved into the switching off of the TGF-β signalling. Indeed SMAD7 binds to activated TβRs and compete with SMAD2 and SMAD3 for the binding to ALK5, repressing its activation [136]. Moreover SMAD7 recruits the E3-ubiquitin ligases SMAD ubiquitination regulatory factor (Smurf)-1 and Smurf-2 to mediate ALK5 ubiquitination and degradation [137]. SMAD7 is also a direct target gene of TGF-β/ALK5 dependent pathway and acts in a negative feedback loop limiting the intensity and the duration of the signal [136]. In addition, SMAD6 was shown to bind BMPR-1B inhibiting SMAD1 phosphorylation, thus suggesting that also BMP signalling can be impaired by I-SMADs. In the nucleus, SMAD complex binds specific sequences on the DNA called SMAD-binding element (SBE) that contains the repeated 5’ AGCA 3’motif [138, 139]. Since the binding to SBE is relatively weak plus the fact that one of the R-SMAD (SMAD2) is not able to bind to DNA, the interaction with other TFs is strictly required to cooperate in order to mediate gene transcription. Among these, the best known are components of the FoxO family [140], members of the activating proteins-1 (Ap-1) family [141], run-related transcription factor 2 (RUNX2) [142] and nuclear factor-kappa B (NF-kB) [143].

While ALK5-induced pSMAD2/3 bind to DNA through SBE motif, ALK1-regulated SMADs preferentially bind to BMP-responsive element (BRE), a sequence enriched in guanine and cytosine (5’ GCCGNC 3’ or 5’ GRCGNC 3’). The term BRE is due to the fact that pSMAD1/5/8 are also the major downstream mediators of BMPs signaling [144, 145].

A further level of complexity in TGF-β signalling is added by the presence of the TGF-β co-receptors (TβRIII) betaglycan and endoglin, characterized by a large extracellular and a short intracellular domain lacking catalytic activity. Betaglycan interacts with TβRII playing a key role in the presentation of the TGF-β ligands to the receptor complex [146] since it is strictly required for the binding of TGF-β2 that has low affinity for TβRII [147].

Endoglin instead is a key modulator of the complex interplay between ALK1- and ALK5-dependent signalling; its inhibition *in vitro* decreases TGF-β/ALK1 pathway and indirectly enhances TGF-β/ALK5 [148], indicating that endoglin may be required for optimal TGF-β/ALK1 signalling pathway. In addition, endoglin and betaglycan were also reported to potentiate BMP signaling [149].

TGF-β superfamily can also exert its functions through a so-called non canonical non-SMAD-dependent pathway, where TGF-β/TβR complex is able to directly activate different signalling pathways including MAPK, Rho-like GTPase and PI3K/AKT thus modulating a multitude of various downstream cellular responses [150].

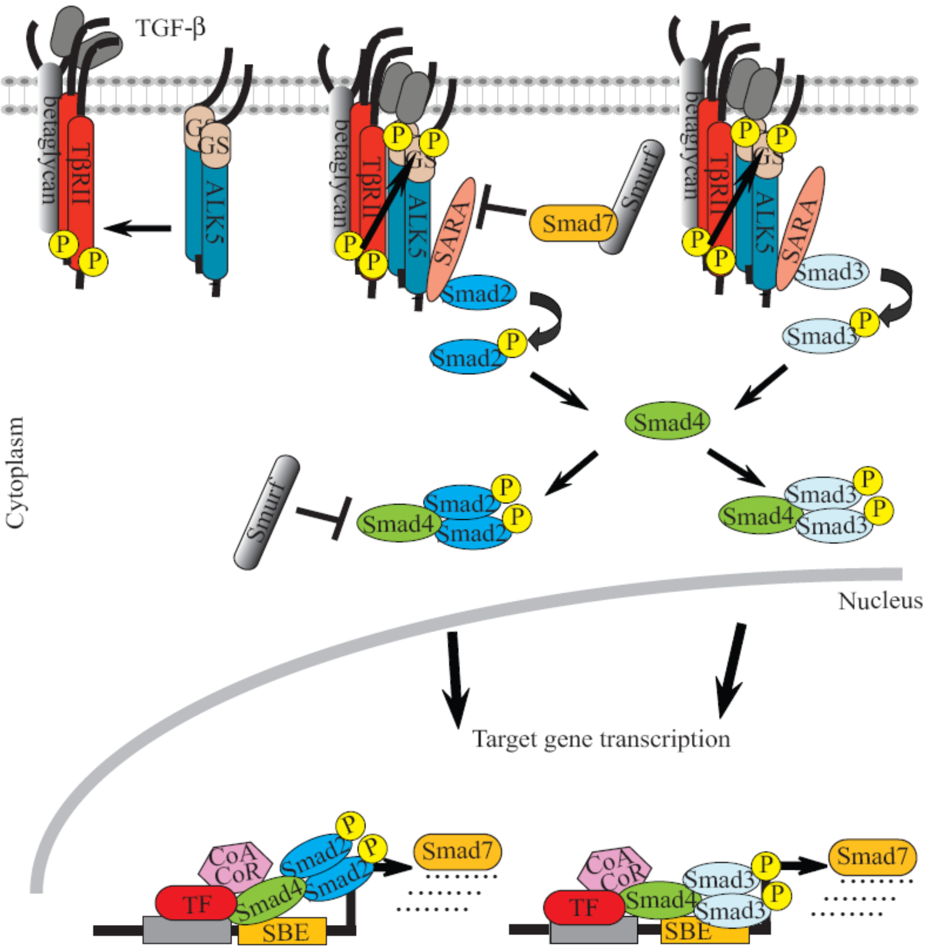
TGF-β
betaglycan
TβRII
ALK5
GS
P
SARA
Smad7
Smurf
Smad2
Smad3
Smad4
Cytoplasm
Nucleus
Target gene transcription
CoA
CoR
TF
SBE

**Figure 6 – Schematic representation of TGF-b signalling pathway**

Upon ligand binding, type II receptor can phosphorylate type I receptor that in turn phosphorylates SMAD2/3. These leads to the recruitment of Smad4 that subsequently binds to SMAD2/3 and the complex can translocate into the nucleus where it recognized specific DNA binding site to mediate the transcription of target genes. SMAD7 competes with Smad2/3 for the binding to type I receptor, attenuating the signalling. The TGF-β co-receptor endoglin assists type I and type II receptors in mediating TGF-β downstream cascade.

### 3.2.1 TGF-β and BMP signalling pathway in ECs

Mouse models and human syndromes showing either inactivation or aberrant expression of any of the components of TGF-β signalling pathway, like ligands, receptors and SMADs, all undergo embryonic lethality mainly due to cardiovascular defects [129, 151, 152], thus suggesting a critical role for TGF-β signalling during vascular morphogenesis and angiogenesis.

Moreover, in the adult, TGF-β exerts different and often divergent effects on EC homeostasis, the so-called "TGF-β paradox", and any perturbation occurring to this tuned system can lead to the onset of pathological conditions.

The effects of TGF-β signalling in ECs can be indeed finely mediated and even opposite, depending on the type I receptor involved, specifically ALK1 or ALK5 [134, 153-155]. While ALK5 is broadly expressed, ALK1 is almoust endothelium restricted. When TGF-β activates the ALK5/pSMAD2/3 axis the final outcome is the inhibition of EC migration and proliferation. The use of a specific ALK5 inhibitor, named SB-431542, has been demonstrated to facilitate EC proliferation and sheet formation in mouse embryonic stem cell-derived ECs. Furthemore SB-431542 is able to up-regulate the TJ component claudin5, thus suggesting a role for ALK5 also in the regulation of vascular permeability [156]. One of the best-known TGF-β/ALK5 molecular targets is plasminogen activator inhibitor-1 (PAI-1), an important regulator of the plasminogen activation system [134]. PAI-1 is a proteinase inhibitor that is involved in the BM formation preventing degradation of the ECM around the emerging new vessels [157]. On the contrary, the activation of ALK1/pSMAD1/5/8-endoglin axis leads to EC migration and proliferation [158]. Indeed the activation of this pathway mediates the induction of the Inhibitor of Differentiation-1 (ID1), a negative regulator of basic-helix- loop-helix (bHLH) TF, controlling multiple TGF-β-induced biological responses. In general, ID proteins are positive regulators of cell proliferation and negative regulators of cell differentiation [159] (Figure 7).

Even if ALK1 and ALK5 induce divergent outcomes in ECs, they can also interact and modulate each other. It has been shown that ECs defective for ALK5 are not able to activate ALK1 signalling cascade because its absence does not allow the correct recruitment of ALK1 to form TβR complex [158]. Conversely, ALK1 can antagonize ALK5 signalling at the level of SMADs [134, 153]. Taken together, the regulation of ALK1 and ALK5 signalling and their reciprocal interaction provide a fine regulation of EC homeostasis and function.

Evidence showed that in ECs VE-cadherin can associate with TβR complexes [21]. The proper clustering of VE-cadherin at junctions is necessary for optimal TGF-β signalling to exert anti-proliferative and anti-migratory responses. Furthemore, VE-cadherin physically interacts with all the components of the TGF-β receptor complex, including TβRII, ALK1, ALK5 and endoglin, thus enhancing TβRII/ALK1 and TβRII/ALK5 complex formation and TGF-β-dependent signaling [21].

As well as TGF-β, also BMP subfamily has a prominent role in vascular development and angiogenesis, since genetic ablation or alteration in the expression of different BMP components are embryonically lethal due to cardiovascular malformations and failure in vascular remodelling. BMP2, BMP4 and BMP6 were all reported to be able to induce angiogenesis and EC proliferation and migration [160,161]; the over-expression of these BMPs and of their target ID1 increases the ability of EC to mediate the *in vitro* assay of capillary tube formation while inhibition of ID1 expression blocks the BMP-induced migration [162]. On the contrary, BMP9 blocks either VEGF-induced angiogenesis either proliferation and migration of bovine aortic ECs (BAECs) induced by bFGF. Morevoer, BMP9 was shown to inhibit growth and migration of human dermal microvascular ECs (HDMECs). Of note, BMP9 shows different effects depending on the cellular contex and its concentration since, at low doses, BMP9 can also promote EC proliferation and promote angiogenesis in *in vitro* matrigel plug assays and *in vivo* in human pancreatic xenografts [163].

Furthermore, BMP signalling can interct with Notch signalling pathway, that fosters EC to become stalk ECs, promoting proliferation and subsequently elongation of the sprouting vessels. Data showed that inhibition of BMP downstream effector SMAD1/5 in ECs both *in vivo* and *in vitro* resulted in a decrease of Notch signalling and in reduced expression of Notch target genes, overall resulting in decreasing stalk EC activity [164, 165].

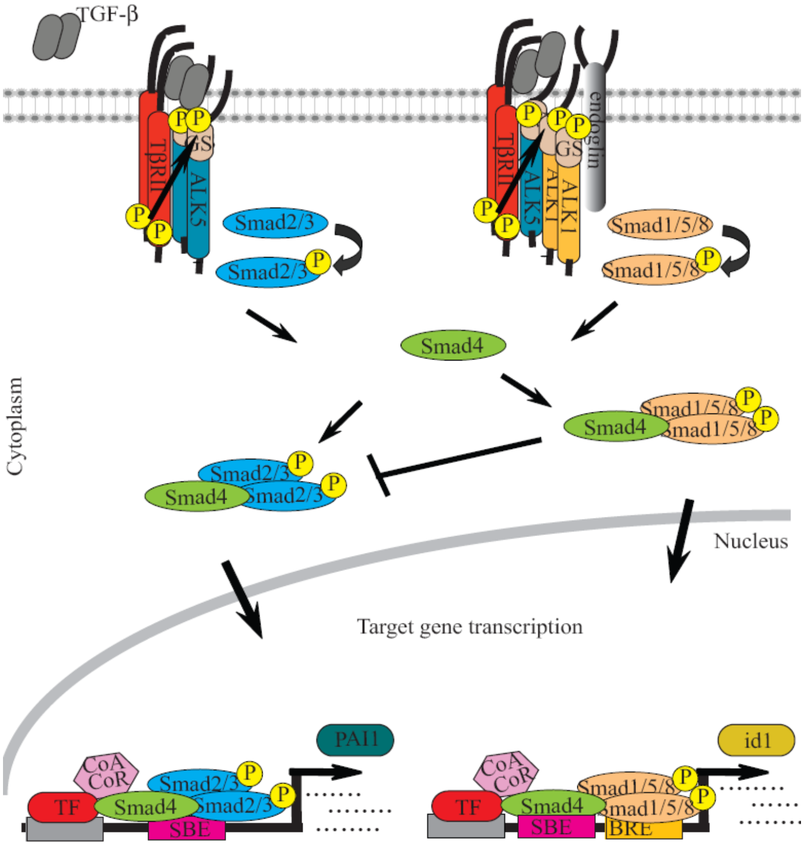
TGF-β
TβRII
ALK5
GS
P
Smad2/3
TβRII
ALK5
ALK1
GS
endoglin
Smad1/5/8
Smad4
Cytoplasm
Nucleus
Target gene transcription
CoA
CoR
TF
SBE
PAI1
id1
BRE

**Figure 7- TGF-β signalling pathway in ECs**

In ECs TGF-β can either activate ALK5/SMAD2/3 resulting in the induction of the plasminogen activator inhibitor-1 (PAI-1) or ALK1/SMAD1/5/8 that mediates ID1 expression. This latter pathway can also be initiated by BMPs that are recognized and interact with specific with type II BMP receptors (BMPRII). Smad7 and Smad6 compete respectively with SMAD2/3 and SMAD1/5/8 for the binding to ALK5 and ALK1 in order to switch off the signal, acting as negative TGF-β regulators

### 3.3 EndMT in heart cushion formation and cardiac fibrosis

EndMT was discovered in 1977 during embryonic heart development by Markwald and colleagues [115]. During heart development, the heart tube is composed by two different layers, an inner endocardium and an outer myocardium. In between the two layers there is a coat made by ECM called cardiac jelly. The endocardium is composed by ECs expressing VE-cadherin and CD31 that, during the formation of the heart cushion, receives stimuli from the outflow tract and the atrioventricular (AV) myocardium to acquire mesenchymal characteristics in order to give rise to primordial valves and membranous septa [115-117]. BMP2 released from the myocardium has been suggested to be the first initiator to induce cardiac EndMT [166] because its expression triggers an autocrine production of TGFβ from endocardial cells feeding the transition of ECs to mesenchymal ones. Also TGF-β2 plays a central role during cushion formation because it has been reported that its expression is required for the endocardial EndMT in the mouse [167] and TGF-β2 deficient mice show multiple defects in AV cushion formation [168]. Interestingly, during embryonic EndMT, TGF-β2 cooperates with β-catenin in the endocardial cells that mediate heart cushion formation. The transcriptional activity of β-catenin seems strictly required as TGF-β mediated EndMT is strongly inhibited in mice conditionally KO for β-catenin [169]. Moreover, in ECs KO for β-catenin TGF-β2-induced expression of αSMA is abolished, thus suggesting a possible interaction between TGF-β and Wnt signalling in mediating EndMT [169].

The proof of concept that EndMT mechanism was taking place during heart valve formation and could also have a causative role in cardiac fibrosis was only demonstrated many years later taking advantage from the use of *Tie1Cre;R26stoplacZ* double transgenic mice that allow to follow lineage identity of the ECs [119]. Thanks to this strategy, it has been demonstrated that fibroblasts associated to the emergence of cardiac fibrosis in a mouse model of aortic banding had an endothelial origin, as well as the cells of the AV cushion in primordial heart [119]. The key regulator of the endothelial transition during cardiac fibrosis was proven to be TGF-β1 that induced EndMT in adult coronary ECs via SMAD3 signalling pathway. On the contrary, administration of BMP7 reduced the overall fibrosis in the heart due to a reduction in the number of fibroblasts of endothelial origin, demonstrating its essential role in inhibiting EndMT-mediated cardiac fibrosis [119]. Moreover, the TFs Slug and Snail are described to be specifically required for the initiation of cardiac EndMT [170]. Slug is directly activated by Notch to mediate VE-cadherin repression to allow endocardial cells to initiate invasion in the cardiac jelly. Furthermore, Slug deficient mice showed an up-regulation of Snail expression and double KO for Snail and Slug mice reduced heart valve development, underlying the compensatory role of the Snail family members in EndMT-mediated cardiac formation.

### 3.4 EndMT in cancer, FOP and atherosclerosis

Tumors are composed by a plethora of different cell types where the malignant cancer cell clone requires a permissive environment to grow and colonize the surrounding tissues. Cells that compose the tumor stroma create this favourable condition and among them fibroblasts are key modifiers in mediating cancer progression. In particular a subpopulation of fibroblasts, the so called cancer-associated-fibroblasts (CAFs), are now recognized among the most important promoters of tumor growth and progression [171]. CAFs are defined as activated and reactive fibroblasts acquiring a modified phenotype in order to provide oncogenic signals to the transformed epithelia within the tumor [172]. CAFs form a heterogeneous population with different origins: activation and proliferation of resident tissue fibroblasts mainly contribute to CAF accumulation in tumour microenvironment, but also BM and periadventitial cells are thought to be a possible origins of activated fibroblasts [172].

Evidence showed that ECs undergoing EndMT could represent one of the CAF most important source [118]. Qualitative analysis of the fibroblasts within the tumour in a mouse model of melanoma revealed them to be double positive for the endothelial marker CD31 and the mesenchymal markers FSP1 and αSMA. Approximately 40% of FSP1 positive and 10% of αSMA positive fibroblasts were co-expressing CD31, suggesting that these CAFs were of endothelial origin. In order to prove these data and to recognize possible ECs originating CAFs that had completely lost their endothelial phenotype in favour of a mesenchymal one, Zeisberg and colleagues took advantage from the *Tie1Cre;R26stoplacZ* double transgenic mice (a similar a model already described in the previous paragraphs) where the melanoma cells were implanted to trace fate lineage of ECs. As expected, a big portion of CAFs retained the endothelial lineage tracer β-gal, proving that EndMT leading to EC transdifferentiation could be an important source of CAFs. Moreover, it was also finally demonstrated that EndMT-mediated CAF origin was strongly induced by exposure of ECs to TGF-β1, supposed to act both in an autocrine and paracrine way to promote the accumulation of activated and promoting-cancer fibroblasts in the tumor stroma [118].

Fibrodysplasia Ossificans Progressiva (FOP) is a genetic disorder causing extreme heterotopic ossification (HO) mostly in muscles and ligaments, leading to paralysis. FOP patients carry an autosomal dominant germline mutation in the ALK2 gene that results in constitutive phosphorylation of ALK2 receptor and downstream SMAD proteins [173]. Different studies were aimed at identifying the cellular lineage responsible of the ectopic bone formation that was recently suggested to be of endothelial origin. Indeed mouse model for HO induced by transgenic expression of mutant ALK2 demonstrated that ectopic bone cells expressed endothelial markers VE-cadherin, Tie1, Tie2 and vWF [174]. Comparable results were obtained in pathological samples of FOP patients [173]. Lineage tracing in reporter mice further demonstrated that most of the mesenchymal cells involved in the first phases of ectopic ossification were ECs that underwent EndMT switch.

Atherosclerosis is a multifactorial disease responsible for myocardial infarction and stroke, the largest causes of morbidity and mortality in Western Countries [175]. It occurs in large and medium-sized arteries [176] and it is characterized by the accumulation of cholesterol, a strong inflammatory reaction, increased proliferation of SMCs and fibrosis [175,177]. ECs together with leukocytes and intimal SMCs are the major players of atherosclerosis and an EndMT process in the inflamed endothelium seems to be involved in the pathogenesis of this disease [178]. Both an oscillatory blood flow and the vessel wall inflammation, two well known atherogenic stimuli, lead to the loss of FGF signaling in ECs that, in turn, results in the activation of the TGF-β signaling and in the induction of EndMT [178,179]. During atherogenesis EndMT is able to promote plaque growth by: i) increasing the deposition of fibronectin, a known proatherogenic ECM protein [180, 181]; ii) increasing endothelial expression of adhesion molecules (i.e. ICAM-1 and VCAM-1) that further recruit the circulating immune cells; iii) inducing the formation of new SMCs and fibroblasts that lead to neointima expansion and plaque growth. In line with these data, endothelial-specific disruption of FGF-dependent signaling leads to EndMT and concomintant early and increased development of atherosclerotic plaques in mice with a *Apoe*$^{-/-}$ background [178], thus suggesting that blocking EndMT could be a therapeutic strategy to halt the progression of atherosclerosis.

# 4. THE KRÜPPEL LIKE FACTOR FAMILY OF TRANSCRIPTION FACTORS

## 4.1 The classification and the structure of KLFs

Krüppel like factors (KLFs) are a family of transcriptional factors involved in a multitude of cellular processes such as proliferation, differentiation, migration and pluripotency in different cell type [182]. The name "Krüppel-like" is due to the homology with the Drosophila protein Krüppel. Drosophila Krüppel KO embryos show a lethal phenotype characterized by an altered anterior abdominal and thoracic body segmentation [183]. Due to the peculiarity of this phenotype, the protein was named "Krüppel", that is the german word for "cripple". Since the discovery of the first mammalian *Klf* gene (*Klf1*) in 1993 [184], a total amount of 18 family members have been identified and classified. The nomenclature of KLFs has been modified over the years. At the beginning, KLFs were initially named according to their expression among different tissues. Some family members are expressed ubiquitously (e.g. KLF6, 10, and 11), while other KLFs are found only in specific cell types or organs. For example *Klf1*, also named *Erythroid Krppel-like factor (Eklf)*, is expressed predominantly in red blood cells while *Klf2*, also known as *lung Krüppel-like factor (Lklf)* is abundantly expressed in the lung. Oher KLF family members were, instead, either named depending on the element they bound, such as *basic transcription element-binding protein* (*Bteb1* or *Klf9*), or depending on the physiological responses they modulated, such as the *transforming growth factor-ß-inducible early genes 1* and *2* (*Tieg1* and *Tieg2* or *Klf10* and *Klf11*, respectively) [185]. To avoid misleading connotations due to partial description of their expression and/or function, the use of a numerical nomenclature (1 to 18) based on the chronological order of discovery has been adopted [186].

KLF proteins are highly conserved across the species reflecting their ancient evolutionary history [187]. 18 genes encoding different 18 KLFs are present both in human and in mouse and are scattered all over the genome. Many of them have homologs in *Gallus gallus* (chicken), *Danio rerio* (zebrafish), and *Xenopus laevis* (frog) [182].

From a structural point of view, all members of the KLF family are characterized by three zinc-finger DNA-binding domains at the C-terminus of the protein [186, 188] that show more than 65 % of aminoacidic sequence identity among the family members [189]. Each zinc finger chelates a single zinc ion supported by two cysteine and two histidine residues. The first and second zinc fingers are composed by 25 aa, while the third contains 23 aa. The pattern of aminoacidic arrangement in a classical zinc finger is #-X-C-X(1-5)-C-X3-#-X5-#-X2-H-X(3-6)-[H/C], where C is cysteine, H is histidine and X corresponds to any aa. The symbol # marks the aa that are critical for the stable folding of the zinc finger [189]. These fingers are connected each other by the so called "Krüppel-link", a seven aa spacer TGEKP(Y/F)X highly conserved among the family members [190]. Each zinc finger recognizes three base pairs in the DNA sequence and interacts with nine base pairs in total [189]. Since the critical residues that determine the sequence specificity for the binding are largely conserved across the family, all KLF family members recognize very similar DNA sequences [186, 188]. In detail they bind to related GC- and CACCC-boxes of DNA. As nuclear localization signals (NLS) have been identified in the zinc finger domains of several KLFs [182], the C-terminal portion of these proteins is not only important for the DNA binding but it is also critical for nuclear import. The N-terminal portion of KLFs is highly divergent among the family members and typically contains either an activation or a repression domain. In addition, alternative splicing in some *Klfs* can lead to further diversification of the protein structure [191]. The divergence at the N-terminus allows the binding of different co-activators, co-repressors or other cofactors that, through specific post-translation modification (acetylation, phosphorylation, ubiquitination, and sumoylation), refine the transcriptional activity adding functional specificity to each KLF [182].

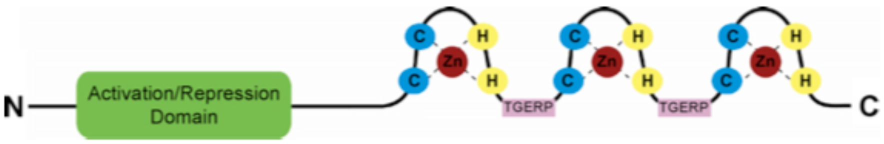

**Figure 7 - Schematic representation of the structure of KLF family members.**

KLFs are composed by a highly homologous C-terminal DNA-binding domain which contains three $C_2H_2$ zinc finger motifs connected by the “TGERP”-like spacer. Each zinc finger chelates a single zinc ion. Conversely, the N-terminus portion of the proteins is different between the family members and contains the activation and repression domains. *(Adapted from Pearson et., al, 2008)*

Taking into consideration that N-terminal sequence homology correlates with the functional similarity, it is possible to divide the KLF family members in three different groups [182]:

- Group 1 includes KLF 3, 8, and 12. These KLFs interact with the carboxy-terminal binding proteins (CtBPs) [192, 193] and act as transcriptional repressor. CtBPs repress gene transcription through the recruitment of histone deacetylases (HDACs) and histone methyltransferases to the transcriptional complexes [194]. CtBPs show also HDAC-independent mechanisms of action by inhibiting the activity of histone acetyltransferase (HAT) coactivators such as p300/CBP-associated factor (P/CAF) [194] or recruiting members of the polycomb complex [195] that promote chromatin silencing
- Group 2 comprises KLF 1, 2, 4, 5, 6, and 7. They behave predominantly as transcriptional activators since they interact with HATs, such as cAMP response element binding protein (CBP), p300 and P/CAF [182].
- Group 3 includes KLF9, 10, 11, 13, 14, and 16. These KLFs have

repressor activity since they interact at the N-terminus with the common transcriptional corepressor Sin3A [182]. Mammalian Sin3 proteins (Sin3A and Sin3B) are large multidomain proteins that bind HDAC1 and HDAC2 as well as other proteins and provide a scaffold for the assembly of multiunit complexes that modify chromatin conformation [196].

Finally, KLF15 and KLF17 are not included in this classification because they are phylogenetically distant [182] and they do not contain any defined protein interaction motifs, while KLF18 is still not properly characterized due to its recent discovery [204].

KLFs, by virtue of their ability to activate and/or repress the expression of a plethora of genes, have a key role during the development, the maintenance of homeostasis and the adaptive responses to physiological or pathobiological stimuli in mammalian tissues. The functions of the different KLF family members in any of these biological responses are in some cases overlapping and in others widely divergent [198]. Besides the homology/divergence in the structural composition, other important factors, such as differences in tissue expression, could contribute to the specificity of their relative function. Some members of the family are ubiquitously expressed, whereas others are tissue restricted. Moreover, KLF expression pattern can change dramatically during the development and thus the expression of certain KLFs may overlap at some developmental stages but not in others depending on the specific cell-context. KLF4 expression is for example altered in several types of human neoplasm and depending on tissue affected, tumor type or cancer stage, it has been reported to act either as a tumor suppressor or an oncogene [198-200]. Thus, individual KLFs show context-dependent functions that can be either exclusive or redundant.

### 4.2 The characteristic of KLF4 gene and protein and its mechanisms of action

In 1996 two different research groups cloned and characterized the murine *Klf4* gene [201, 202]. Two years later, in 1998, the human *KLF4* gene was cloned from human umbilical vein endothelial cell (HUVEC) cDNA library [202]. Since it is abundant in the intestine and in the skin, it has been initially named either *gut enriched kruppel like factor* (*GKLF*) [201] or *epithelial zinc finger* (*EZF*) [202]. Later on, as its expression has been detected also in other organs such as in lung, testis, thymus, cornea, cardiac myocytes and lymphocytes [201-205], this gene was definitely renamed as KLF4.

The human *KLF4* gene *locus* is located on chromosome 9q31, whereas mouse *Klf4* is located on chromosome 4B3. Both human and mouse *KLF4* contain five exons transcribed in a mRNA of about 3.5 kilobase (KB). Several splice variants were reported both in human and in mouse [201, 206]. The human *KLF4* gene encodes for a protein with a predicted molecular mass of 50 kDa containing 470 aa, whereas murine *Klf4* encodes for a polypeptide of 483 aa with a predicted molecular weight of 53 kDa. The human and mouse KLF4 sequences revealed a 91 % aminoacidic sequence identity. KLF4 protein can be divided in several functional domains:

- a N-terminal transcriptional activation domain (1-157 aa) rich in proline, serine, threonine and acidic aminoacid residues. Acidic residues enhance the binding of coactivators such as p300/CBP [207], HAT proteins that increase hystone acetylation at the promoter region facilitating the recruitment of other transcription factors as well as the basal transcriptional machinery.
- a repressor domain close to the N-terminal transcriptional activation domain (158-385 aa) that allows the interaction with repressors such as HDAC1 and HDAC2 [182]. Two lysine residues (K225, K229), which are acetylated by

p300/CBP, are also contained in the repressor domain [208]. The mutation of these two lysines to arginine significantly decreases the ability of KLF4 to transactivate its target genes [207], suggesting that acetylation of KLF4 is important for its function.

- a C-terminus highly conserved triple zinc finger DNA binding domain (402-483 aa). The consensus DNA binding elements for KLF4 determined by both chromatin immunoprecipitation sequencing (ChIP-seq) and base-specific mutagenesis are the following ones: [5'-GGG(C/T)G(T/G)GG-3'] [209] and [5'-(A/G)(G/A)GG(C/T)G(C/T)-3'] [210]. Notably both sequences are enriched in CpG and can be methylated. The ability to bind either unmethylated or modified DNA elements may contribute to the different KLF-mediated regulation of several biological processes via selectively recruiting different chromatin cofactors [211].

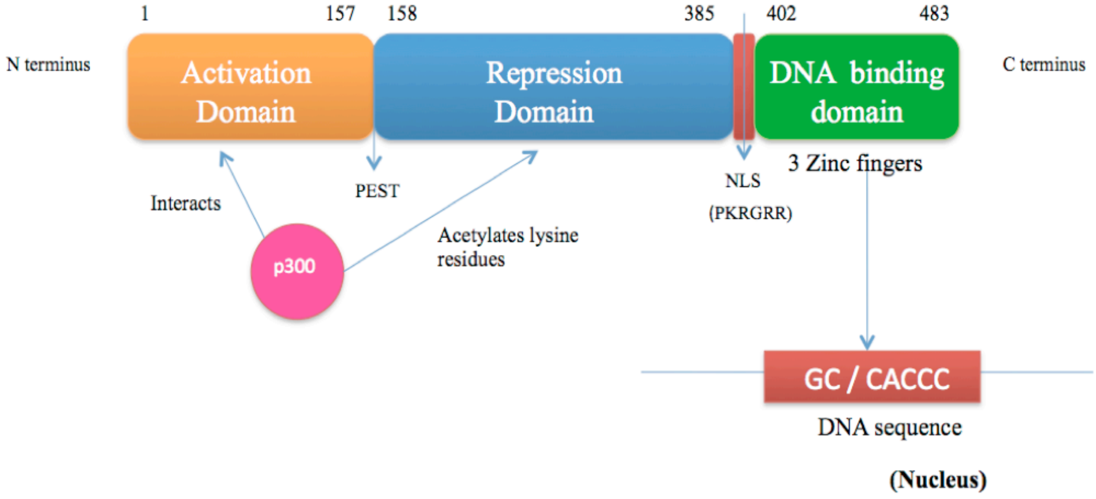
1
157
158
385
402
483
N terminus
Activation Domain
Repression Domain
DNA binding domain
C terminus
Interacts
PEST
Acetylates lysine residues
p300
NLS
(PKRGRR)
3 Zinc fingers
GC / CACCC
DNA sequence
(Nucleus)

**Figure 8 - Schematic representation of KLF4 structure.**

KLF4 is composed by three domains: an activation domain, a repression domain and a DNA binding domain. The coactivators like p300/CBP proteins are able both to interact with the activation domain and to acetylate the lysines 225 and 229 located in the repressor domain. The DNA binding domain of KLF4 located at the C-terminus is composed by three zinc fingers that bind to the GC/CACCC sequence in the promoter regions of its target genes. The transport into the nucleus is facilitated by the presence of a NLS both in the DNA binding and repression domains. *(Adapted from Vangapandu et al., 2009)*

In addition to these domains, a PEST sequence (proline [P], glutamine [G], serine [S] and threonine [T]) is reported to be located between the activation and the inhibitory domains (113-132 aa) [212], suggesting that KLF4 protein may be degraded via the ubiquitin-proteosome pathway and explaining the relative short half life of KLF4 protein (about 2 hours). Finally, KLF4 contains two discrete NLS: the first is a basic hexapeptide sequence having PKRGRR repeats just N-terminal to the three C-terminal zinc fingers, whereas the second is contained within the first two zinc fingers themselves [213].

KLF4 can function as a transcriptional repressor either by competing for the DNA binding with an activator (known as passive repression) or by the recruitment of corepressors such as HDAC to the promoter region of target genes. For instance while KLF4 inhibits SMAD3-mediated activation of *PAI-1* as well as β-catenin/TCF4-dependent transcription by directly competing for p300 binding [215], in KLF4-mediated repression of the *CD11d* gene, KLF4 directly interacts with HDAC1 and HDAC2 [216].

The presence of both activation and repressor domains might allow KLF4 to switch between its positive and negative transcriptional effects in a cell-context specific manner [212]. KLF4 is expressed in the mesenchymal cells, in the endothelium and in the epithelium by E10.5 [217]. *Klf4* KO mice were born at the expected mendelian ratio but died within 15 hours after birth secondary to dehydration due to the loss of skin barrier function [218], thus suggesting the essential role of KLF4 for skin barrier function during the development. Of note, vascular abnormalities had not been reported during the early embryonic development of *Klf4* KO mice [218]. To overcome the limitation of the peri-natal lethality, several research groups developed mice expressing Cre-recombinase under the control of specific promoters in order to study the KLF4 activity in a tissue-specific manner. Specific *Klf4* deletion in murine stomach results in increased proliferation and altered differentiation of gastric epithelial cells [219] while loss of *Klf4* in the eye leads to an abnormal corneal epithelium and the lack of goblet cells in the conjunctiva [220]. In 2006 KLF4 has been used together with Oct4, Sox2 and c-Myc to reprogramm somatic cells into pluripotent stem cells, thus being instrumental in stem cell renewal and generation of induced pluripotent stem cells (iPS cells) [221].

Since KLF4 controls multiple cellular processes in a context-dependent manner, we will focus our attention on its role in the endothelium.

### 4.3 The Role of KLF4 in endothelial cell biology

KLF2, KLF4, and KLF6 are the three members of the KLF family expressed by ECs [222]. KLF4 regulates several vascular functions such as permeability and vascular tone [223, 224], angiogenesis [225, 226], coagulation and inflammatory reactions [234, 235] thereby playing a protective role in several pathological conditions.

Limited *in vivo* studies in mice demonstrate that KLF4 depletion in lung vascular endothelium resulted in a most severe edema as well as greater lung polymorphonuclear neutrophil (PMN) sequestration in response to lipopolysaccharide (LPS) challenge thus suggesting a potential role of KLF4 in the regulation of vascular permeability [227]. In agreement with these data KLF4 has been found to regulated endothelial barrier by directly inducing the expression of both AJ and TJ components such as VE-cadherin, ZO1, occludin and claudin5 [228, 229, 230]. However further *in vivo* experiments need to be performed in order to validate and extend these observations in other patho-physiological conditions.

Endothelial KLF4 controls also the vascular tone by inducing the expression of *nitric oxide synthase 3* (*Nos3*) and *prostaglandin I2 synthase (PTGIS)*, two enzymes that catalize crucial reactions for the production of important vasodilatators such as nitric oxide (NO) and prostacyclin respectively. It also represses the expression and activity of the potent vasoconstrictor *endothelin1* (*Edn1*) and its receptor *endothelin receptor b (Ednrb)* [224]. By finely regulating the vascular tone KLF4 plays a beneficial role in pulmonary hypertension (PH), a disease characterized by an increased blood pressure in the pulmonary arteries due to the abnormal muscularization of distal pulmonary arterioles [239].

KLF4 has recently emerged as an important pro-angiogenic factor induced by hypoxia that is one of the most powerful angiogenic stimuli in physiological and pathological conditions [225, 233]. KLF4 promotes angiogenesis by inducing the expression of critical components of the VEGF signaling pathway (i.e. VEGFA and VEGFR2) [225, 234] and by inhibiting the Notch signalling pathway that usually costrains the tip cell formation [225]. In line with these data endothelial specific KLF4 overexpressing mice subcutaneously inoculated with B16F0 melanoma cells develop tumors characterized by an increase number of vessels with poor perfusion that result in reduced tumor growth, a vascular phenothype very similar to the one obtained upon Notch inhibition through DLL4 blockade [225]. Since a minor study has conversely reported that KLF4 has been able to inhibit angiogenesis in HUVECs by activating miR-15a through a transcriptional regulation [235], future studies have to be performed to clarify the role of KLF4 during different physio/pathological conditions of angiogenesis.

Finally, one of the most characterized functions of KLF4 in the endothelium is the regulation of EC responses to inflammation and shear stress. Several cytokines such as TNF-$\alpha$, interleukin-$\beta$ (IL$\beta$) and interferon-$\gamma$ (IFN$\gamma$) as well as fluid shear stress, defined as the frictional force per unit area to which ECs are subjected when exposed to blood flow [176], strongly induce *Klf4* expression [227, 228]. KLF4 upregulation, in turn, promotes multiple endothelial vasoprotective transcriptional programs in these conditions. KLF4 overexpression leads to the acquisition of a quiescient anti-inflammatory EC phenotype by both by inhibiting the expression of a diverse set of pro-inflammatory factors (including among the others *the Vascular Cell Adhesion Molecule 1* (*VCAM-1)* and the prothrombotic gene *PAI-1,* and by inducing the expression of important protective genes such as *eNOS* and *thrombomodulin* (*THBD*). Mechanistically, KLF4 switches off inflammatory gene expression by inhibiting, both alone and in combination with p300, the activity of the NF-kB subunit p65 [227-229].

In line with these roles KLF4 has been reported as a protective molecule in atherosclerosis [228]. Endothelial-specific deletion of *Klf4* in *Apoe*$^{-/-}$ mice, a genetic background prone to develop atherosclerosis when challenged with high fat diet, results in a bigger atherosclerotic burden characterized by an increased inflammatory reaction. Conversely, sustained expression of *Klf4* in the endothelium strongly reduces the area of the atherosclerotic plaque as well as the immune cell infiltration. Interestingly, the laminar flow in straights region of the arteries induces KLF expression to protect these vessel tracts from atherosclerosis [228]. ECs align in the direction of flow, express anti-inflammatory genes and show low levels of oxidative stress. Conversely when arteries divide or curve sharply, the flow becomes oscillatory, endothelial KLF4 expression is not increased and ECs acquire an activated and pro-inflammatory state characterized by increased oxidative stress and higher expression of inflammatory genes. These arterial portions exposed to oscillatory flow show a higher susceptibility to develop atherosclerosis [176]. Various signaling molecuels are involved in the perception and mediation of shear stress responses. These include the extracellular-signal-regulated kinase (ERK5), a mitogen-activated protein kinase (MAPK) able to induce KLF4 expression [226, 236].

### 4.4 The ERK5 signalling axis

The human *ERK5* gene *locus* (also termed *MAPK7)* has been cloned in 1995 by two different research groups independently [237, 238]. It is located on chromosome 17p11.2 and encodes for a protein of 816 aa with a predicted molecular mass of 102 kDa. Due to its large size in comparison to other MAPKs, ERK5 was also termed big MAPK (BMK1). The N-terminal portion of the protein contains the kinase domain and it is required for cytoplasmic targeting, oligomerisation and the interaction with the ERK5 upstream regulator MAPK/ERK kinase 5 (MEK5, also termed mitogen-activated protein kinase kinase 5 [MAP2K5]) [239, 240]. The big C-terminal region of ERK5 contains both a NLS and a nuclear export signal (NES) necessary for nuclear shuttling as well as a potent transcriptional regulation domain. The ERK5 C-terminal tail contains also two proline rich domains for the binding of proteins with a Src-homology 3 (SH3) domain and a myocyte enhancer factor 2 (MEF2)-interacting region [241-243]. Several growth factor including VEGF, EGF, FGF and PDGF as well as stress conditions (i.e. hypoxia, laminar flow or osmotic stress) are known to activate ERK5 [241-243]. Tipically these extracellular stimuli initiate the signalling cascade by activating the MAPK kinase kinases (MAPKKK) MEK kinase 2 (MEKK2) and 3 (MEKK3) that, in turn, phosphorylate MEK5 on Ser311/Thr315 [241-245]. As a consequence, phosphorylated MEK5 induce ERK5 activation by catalizing a dual phosphorylation at specific residues (Thr218/Tyr220) located in the activation loop of ERK5. In resting condition ERK5 acquires a folded conformation to mask the NLS and to expose a nuclear export signal (NES) and thereby ERK5 is retained in the cytoplasm. Upon MEK5-dependent phosphorylation, ERK5 undergoes autophosphorylation that determines a conformational change allowing ERK5 to translocate into the nucleus to regulate target gene expression [245]. Nuclear ERK5 promotes gene transcription either directly via a poorly defined transcriptional activation domain present in the C-terminal tail of the protein [246] or by increasing the activity of several transcription factors including the myocyte enhancer factors (MEF), C-myc, the cAMP response element-binding protein (CREB) and serum-response factor accessory protein 1a (Sap1a) [247, 248]. MEF2A, MEF2C and MEF2D, members of MEF family, mediate most of the ERK-5-dependent transcriptional responses. ERK5 interacts with MEF2s at the C-terminal region and it can increase their transcriptional activity by catalizing their phosphorylation [248-250].

ERK5 controls a large number of biological processes such as proliferation, migration, apoptosis and angiogenesis. In the endothelium ERK5 has a key role in the regulation of cell survival, angiogenesis and cell response to shear stress [248-250].

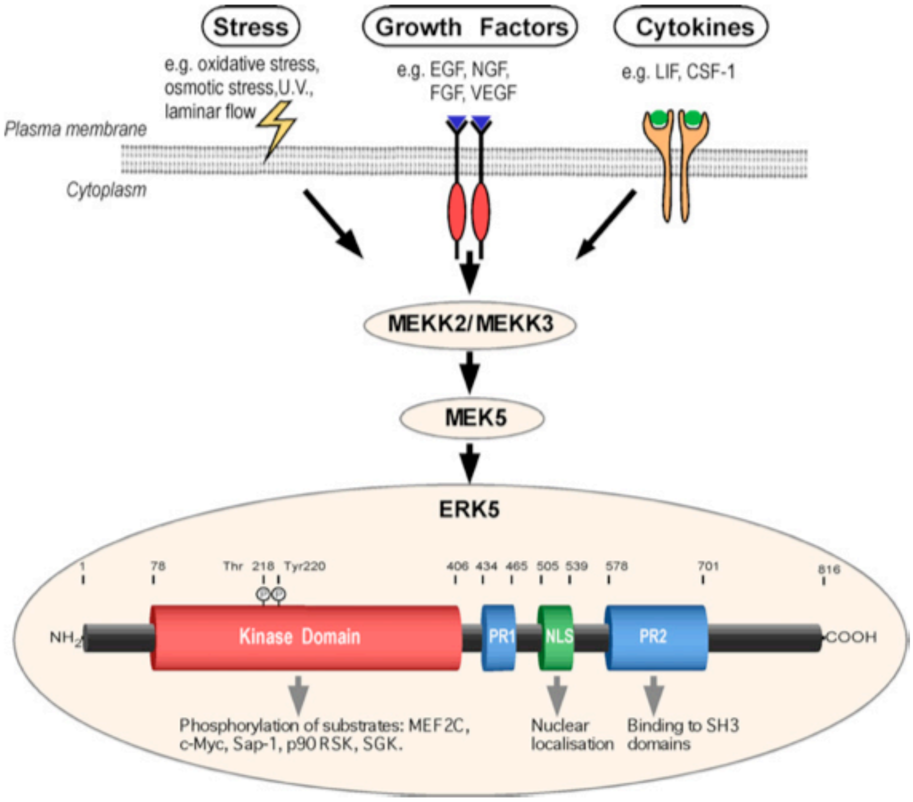
Stress
e.g. oxidative stress, osmotic stress,U.V., laminar flow
Growth Factors
e.g. EGF, NGF, FGF, VEGF
Cytokines
e.g. LIF, CSF-1
Plasma membrane
Cytoplasm
MEKK2/MEKK3
MEK5
ERK5
1
78
Thr 218 Tyr220
406 434 465 505 539
578
701
816
NH2
Kinase Domain
PR1
NLS
PR2
COOH
Phosphorylation of substrates: MEF2C, c-Myc, Sap-1, p90RSK, SGK.
Nuclear localisation
Binding to SH3 domains

**Figure 9 – The ERK5 structure and signalling axis**

Upon stress conditions (i.e. osmotic stress or laminar flow) or exposure to mitogens (growth factors and cytokines) a typical three-tiered hierarchical MAPK module is activated: the MAPKKK MEKK2/MEKK3 phosphorylate the MAPKK MEK5, which in turn activates the MAPK ERK5 by inducing the phosphorylation on Thr218 and Tyr220 residues within the kinase domain located in the C-terminus of ERK5. The kinase domain of ERK5 mediates the phosphorylation of several TF such as MEF2C, c-Myc and Sap-1. The ERK5 protein structure contains also a NLS, two proline-rich domains (PR1 and PR2) and a large C-terminal tail. *(Adopted from Nithianandarajah-Jones et. al., 2014)*

*Erk5* KO mice are lethal at embryonic day 10.5 (E10.5) due to severe cardiovascular defects. Vascular defects are due to the formation of immature and leaky blood vessels that resulted in diffuse heamorrage [249, 250]. Interestingly endothelial-specific loss of *Erk5* resulted in an altered vascular phenotype comparable to global ERK5 deletion [251], thus suggesting that ERK5 activity is essential in ECs during the vascular development. Notably, mice deficient for the two upstream activators of ERK5 such as MEKK3 and MEK5 show a similar vascular phenotype [252, 253]. Beyond its role during the development, ERK5 is important in the maintenance of vascular integrity since its deletion in adult mice is lethal within 2–3 weeks after gene ablation due to leaky blood vessels [251]. This phenotype might be attributed to the important anti-apoptotic role of ERK5 in ECs. ERK5 promotes EC survival by inducing the expression of the pro-survival protein B-Cell CLL/Lymphoma 2 (BCL-2) and by inhibiting, through phosphorylation, the activity of the pro-apoptotic protein BCL2-Associated Agonist Of Cell Death (BAD) [254].

Fluid shear stress induces MEK5-dependent ERK5 activation that results in the MEF2-dependent expression of the transcription factors KLF2 and KLF4 that, in turn, have a protective since they confer anti-thrombotic and anti-inflammatory properties to the vascular endothelium [226, 236, 255, 256]. Interestingly vasoprotective drugs such as statins have been shown to potently activate the MEK5/ERK5/KLF4 dependent gene expression in ECs, thus suggesting that some of the pleiotropic vasoprotective effects of these drugs may be elicited through activation of ERK5 [226].

ERK5 has been implicated also in the regulation of tumor angiogenesis. ERK5 is activated by the pro-angiogenic growth factors VEGF and FGF-2 in ECs [251] and its *in vivo* deletion results in a regression of tumor vasculature and concomitant growth inhibition of xenografted human tumors [257]. These evidences lead to the recent development of small-molecule inhibitors of the ERK5 signalling axis. BIX02188 and BIX02189 are two indolinone-6-carboxamides that selectively inhibit MEK5 activity [258] while XMD8-92, which derives from chemical modifications of the polo kinase inhibitor BI-2536 [259], is a highly-selective inhibitor of ERK5 activity. Notably, in contrast to the lethal phenotype due to the endothelial-specific ablation of *Erk5* in adult mice, no side effects in the vasculature were observed after XMD8-92 administration in mouse xenograft models [259], thus suggesting XMD89-2 as useful drug to target ERK5-mediated tumor growth and angiogenesis.

# 5. MATERIALS AND METHODS

## 5.1 Antibodies

For Western blotting (WB) and immunostainings the following antibodies were used: VE-CADHERIN rat (550548, BD Biosciences); VE-CADHERIN goat (sc-6458, Santa Cruz); N-CADHERIN mouse (610920, BD Biosciences); PECAM1 hamster (MAB1398Z, Millipore); PECAM1 rat (553370, BD); PECAM1 rabbit (ab28364, Abcam); mKLF4 goat (AF3158, R&D); hKLF4 goat (AF3640, R&D); FSP1 rabbit (07-2274, Millipore); ID1 rabbit (BCH-1/37-2, BIOCHECK); SCA1 rat (ab51317, Abcam); Cleaved Caspase-3 (5A1E, Cell Signaling); GFP rabbit (A-6455, Invitrogen); hCLAUDIN5 rabbit (ab53765, Abcam); pSMAD1/5 rabbit (9516, Cell Signaling); SMAD1 rabbit (9644, Cell Signaling); pSMAD3 rabbit (1880-1, Epitomics); SMAD3 rabbit (9523, Cell Signaling); Glucose transporter type 1 (GLUT1) rabbit (RB9052P1, Thermo Scientific); ERK5 rabbit (07-039, Upstate); VE-PTP rabbit (produced and purified by New England Peptide); MEKK3 rabbit (5727, Cell Signaling); MEK5 mouse (610957, BD); BMP6 sheep (LS-C150156, LS-BIO); GAPDH mouse (SC-32233, Santa Cruz); tubulin mouse (T9026, Sigma); vinculin mouse (V9264, Sigma); horseradish peroxidase (HRP)-linked anti-mouse, anti-rat and anti-rabbit (Cell Signaling); HRP-linked anti-goat (Promega). Biotin-conjugated isolectin B4 (Vector Lab) was used to identify retinal vasculature. ALEXA FLUOR 488, 555 and 647 donkey secondary antibodies were from Life Technologies.

## 5.2 Mouse lines

*Ccm1* floxed/floxed, *Ccm2* floxed/floxed and *Ccm3* floxed/floxed mouse strains were previously described [69, 92]. The *Cdh5(PAC)*-CreERT2 mouse line [260] were kindly provided by R.H. Adams. *Klf4* floxed/floxed mice [219] were kindly donated by G.K. Owens. These mice were received on a mixed background (C57BL6J/129SvJ) and subjected to MAX-BAX® Program in Charles River to perform accelerated backcross.

Mice were all bred on a C57BL/6 pure background. To obtain the EC-CCM1 KO mice, *Cdh5(PAC)*-CreERT2 animals were bred with the *Ccm1* floxed/floxed mouse strain to obtain tamoxifen-inducible endothelial-specific expression of Cre-recombinase and *Ccm1* gene recombination. To generate double EC-CCM1 KO KLF4 KO mice, *Cdh5(PAC)*-CreERT2; *Ccm1* floxed/floxed mice were crossed with *Klf4* floxed/floxed animals. Deletion of floxed exons by Cre-recombinase produces loss-of-function. Both EC-CCM2 KO and EC-CCM3 KO mice were derived as described for EC-CCM1 KO animals. EC-KLF4 KO mice were generated by crossing *Cdh5(PAC)*-CreERT2 mice with *Klf4* floxed/floxed animals. For tamoxifen-induced gene ablation, tamoxifen (T5648, Sigma) was dissolved in corn oil-10 % ethanol at 10 mg/ml and then further diluted at 2 mg/ml in corn oil. Pups were injected at P1 with an intragastric injection of 100 µg.

### 5.3 Endothelial cell isolation and culture

The cultured cell lines used in this study for *in vitro* experimental approaches were:

- WT, CCM1 KO, CCM2 KO, CCM3 KO and KLF4 KO lung derived ECs: these cells were isolated from the lung of two month old floxed mice. Lungs were removed under sterile conditions, washed two times with PBS and minced finely with scalpels. Organ disaggregation was carried out by incubating them with collagenase A (1.5 mg/ml; Roche) and DNAse (25 µg/ml; Roche) in DMEM (37 °C for 3 hours). After filtering through nylon screen, cells were collected, centrifuged at 1,200 rpm for 10 minutes and then seeded in gelatin 0.1 % coated 24 wells. Upon 48 hours ECs were washed and immortalyzed with *polyoma middle* T antigen supernatant. The purity of EC lines was analyzed by performing extensive stainings for endothelial specific molecules. *Ccm1, Ccm2* and *Klf4* floxed alleles were deleted by treating pure ECs *in vitro* with TAT-Cre recombinase using Hyclone ADCF-Mab medium (ThermoScientific) [261]. Recombination of the floxed *Ccm3* gene was induced by treating the cells at culture day 1 with the AdenoCre viral vector, as previously described [262]. All these cell lines were cultured in MCD131 (Lonza) with 20 % North American (NA) fetal bovine serum (FBS) (HyClone), glutamine (2 mM; Sigma), sodium pyruvate (1 mM; Sigma), heparin (100 µg/ml, from porcine intestinal mucosa; Sigma), and EC growth supplement (ECGS) (5 µg/ml, made in our laboratory from calf brain).

- WT, CCM1 KO and CCM1-KLF4 KO primary brain derived ECs (BMECs). Mouse brain microvascular fragments were recovered by brains of two month old mice either WT, *Ccm1* floxed/floxed or *Ccm1-Klf4* floxed/floxed mice. Brain were rolled on Whatman 3MM chromatography blotting paper to remove the meninges, triturated and digested with 0.75 % type 2 collagenase (Worthington Biochemical Corp.) 1 hour at 37 °C. The pellet was resuspended in a 25 % w/v BSA solution and centrifuged for 20 minutes at 2,600 rpm at 4 °C to obtain a microvessel enriched cell pellet. Then, further digestion was performed in 10 mg/mL collagenase/dispase (Roche) and 1 µg/ml Dnase I (Roche) for 15 minutes at 37 °C. Capillary fragments were seeded in culture medium and selected for puromycin (4 µg/ml) resistance for 2 days. Recombination of the floxed alleles was achieved by treating selected ECs with TAT-Cre recombinase *in vitro.* Culture medium was DMEM (GIBCO) with 10 % North American (NA) fetal bovine serum (FBS) (HyClone), glutamine (2 mM; Sigma), penicillin/streptomycin (100 units/l; Sigma), sodium pyruvate (1 mM; Sigma), heparin (100 µg/ml, from porcine intestinal mucosa; Sigma), and EC growth supplement (ECGS) (5 µg/ml, made in our laboratory from calf brain).
- Immortalized cerebral microvascular EC of human origin ECs (hCMEC/D3). hCMEC/D3 were provided by P.O. Couraud [263] and cultured in Rat Collagen I (Cultrex) treated plates in a complete medium composed by EBM-2 medium (Lonza) supplemented with 5 % of Fetal Bovine Serum, 1 % Penicillin/Streptomycin, 1.4 µm Hydrocortisone, 5 µg/ml Acid Ascorbic, 10 mM

HEPES, chemically defined Lipid concentrate (1/100) and FGF-2 (1 ng/ml).

- 293T packaging cells provided by IFOM Cell Culture facility and cultured in DMEM medium (GIBCO) supplemented with 10 % South American (SA) FBS (Hyclone), glutamine (2 mM) and sodium pyruvate (1 mM).
- HEK293 used to perform luciferase assay were provided by IFOM Cell Culture facility and cultured as described for 293T.

All cells were grown at 37 °C in a humidified atmosphere with 5 % $CO_2$.

For *ex-vivo* experiments, to obtain freshly isolated PECAM1+ brain derived ECs from EC-CCM1 KO, EC-CCM1 KO KLF4 KO mice and matched controls (P12), brain microvascular fragments were processed as described for BMECs. EC pellets obtained were finally resuspended in 0.1 % BSA and 2 mM EDTA in PBS pH 7.4 and incubated for 45 minutes at 4 °C with Dynabeads (Invitrogen) previously coated with rat anti-mouse PECAM1 antibody (BD). ECs were then separated using a magnet and processed without to be exposed to any culture condition. In order to obtain both lung- and spleen-derived PECAM1+ ECs from EC-CCM1 KO and matched controls, the organs were disaggregated with collagenase A plus DNAse (1.5 mg/ml and 25 μg/ml, respectively; Roche) for 2 hours at 37 °C and passed through a 70 μm cell strainer before to be incubated for 45 minutes at 4 °C with anti-mouse PECAM1 covered dynabeads. Heart-derived PECAM1+ ECs from the same animals were recovered by incubating minced hearts with type I collagenase (2 mg/ml, Sigma) for 45 minutes at 37 °C. A trituration of the heart suspension using a 30 cc syringe is required before pipetting the cell suspention through a 70 μm cell strainer and loading it on anti-mouse PECAM1 covered dynabeads.

## 5.4 Cell treatments

LY-364947 (Calbiochem), XMD8-92 (SelleckBio) and BIX-02189 (SelleckBio) were dissolved in dimethylsulphoxide (DMSO). For LY-364947 treatment, cells were grown to confluence in MCDB with 5 % FBS and daily stimulated with 40 μM LY-364947 for 1 week. For XMD8-92 and BIX-02189 treatment, confluent ECs monolayers were grown in complete media (MCDB-131 with 20 % FBS) and treated daily with either 5 μM XMD8-92 (for 72 hours), 10 μM BIX-02189 (for 48 hours) or vehicle only. For BMP6 (R&D) treatment, ECs were grown in MCDB-131 with 5 % FBS and stimulated (100 ng/ml) either for 4 hours in order to analyse SMAD1 phosphorylation or for 96 hours for EndMT marker evaluation.

### 5.5 Treatment with TGFb/BMP inhibitor *in vivo*

10 mg/kg of LY-364947 (Sigma) or 10 mg/kg of LY-364947 plus 10 mg/kg SB-431542 (SelleckBio) were intraperitoneally injected daily starting 2 days after the *Ccm1* recombination (P1). Control mice were treated with vehicle only. The animals were sacrified at P13.

### 5.6 Production of Lentiviruses

Both shRNAs against murine *Klf4* and *Bmp6* as well as control non-targeting shRNA cloned into pLKO.1 puro-based lentiviral vector were purchased from Sigma-Aldrich (St Louis, MO, USA, TRCN0000238250 and TRCN0000065652). The cDNA coding for the wild-type mouse *Klf4* was obtained by GeneCopoeia (Rockville, USA) and subcloned into the lentiviral expression vector pLenti-III-HA (provided by abm, Richmond, BC, CANADA) using XhoI and EcoRI restriction sites (Promega, Fitchburg, WI, USA). The lentiviral particles were produced in 293T cells using a four-plasmid transfection system mediated by calcium phosphate, as previously described *271*. Briefly, 24 hours before transfection $4x10^6$ cells were plated in a 158 $cm^2$ petri dish. The day after, cells were transfected with a solution composed by: 7 μg of ENV (envelop plasmid), 12.5 μg of pMDL (packaging plasmid), 6.25 μg of REV (REV-expression plasmid), 32 μg gene transfer (shCTRL, shKLF4, shBMP6, pLenti-III-HA or pLenti-III-KLF4), 156 μl $CaCl_2$

plus 0.1 X TE to a final volume of 1094 μl. 1250 μl of 2 X HBS were added to the transfection mix that then was bubbled vigorously and transferred dropwise on the cell monolayer. Lentivirus-containing supernatants were collected 48 and 72 hours after the cell transfection, passed through a 0.45 μm filter and concentrated using PEG ON at +4 °C. Two consecutive cycles of lentiviral infection were carried out in the presence of polybrene followed by a selection with 3 μg/ml puromycin for 72 hours and maintenance with 1.5 μg/ml puromycin.

### 5.7 Cell transfection and RNA interference

To perform RNA interference the following siRNA were used: Stealth RNAi directed to mouse *Bmp6* (MSS-236054, MSS-236055 and MSS-236056, Life Technologies), Stealth RNAi directed to mouse *Ccm1* (MSS294386, Life Technologies), Stealth RNAi directed to human *CCM1* (MSS234455, Life Technologies), ON-TARGET plus SMART pool directed to mouse *Ccm2* (L-057315-00-0005, Dharmacon), Stealth RNAi directed to mouse *Ccm3* (MSS249998, Life Technologies), Stealth RNAi directed to mouse *Erk5* (siERK5#1 MSS215825 and siERK5#2 MSS215827, Life Technologies), Stealth RNAi directed to mouse *Mek5* (MSS215820), Stealth RNAi directed to mouse *Mekk3* (siMEKK3#1 MSS218528 and siMEKK3#2 MSS218529), Stealth RNAi directed to mouse *Mef2A* (MSS206607), Stealth RNAi directed to mouse *Mef2C* (MSS206611), Stealth RNAi directed to mouse *Mef2D* (MSS247431), negative control siRNA Medium GC content (12935-300, Life Technologies) ON-TARGET plus siControl (D-001810-10, Dharmacon). Cells were transfected with 40 nM siRNA oligonucleotides for 5 h in Optimem using Lipofectamine 2000 (Life Technologies) in accordance with the manufacturer's instructions and as previously described [103].

### 5.8 Western blotting

For WB analysis, cells were lysed using a boiling modified Laemmli sample buffer

(2 % SDS, 20 % glycerol, and 125 mM Tris-HCl, pH 6.8). After 10 minutes incubation at 100 °C, lysates were spinned for 1 minute at 13,000 rpm to discard cell debris. Protein concentration of the collected supernatant was estimated using the BCA Protein Assay Kit (Pierce). Equal amounts of proteins were separated by SDS–PAGE on acrylamide/bis-acrylamide gels at different concentrations and transferred to a Protran nitrocellulose membrane 0.2 μm pores (Whatman). The membranes were then blocked for 1 hour at room temperature (RT) and, then, incubated with primary antibody (overnight [ON] at 4 °C) and HRP-linked secondary antibodies (1 hour at RT) in Tris-Buffered Saline-Tween (TBST) containing 5 % BSA. After three washing steps, membranes were incubated with Amersham ECL WB detection reagents (GE Healthcare) for 1 minute and specific signals were detected by chemi-luminescence system (GE Healthcare) using ChemiDoc™ MP System (Biorad).

### 5.9 qRT-PCR analysis

Total RNA was isolated by extraction with the RNeasy mini kit (Qiagen). Isolation of RNA from freshly isolated PECAM1+ brain derived ECs was performed using RNeasy micro kit (Qiagen). 1 μg RNA was reverse transcribed with random hexamers (High Capacity cDNA Archive kit; Applied Biosystems). cDNA (5 ng) was amplified in triplicate with the TaqMan Gene Expression assay (Applied Biosystems) and an ABI/Prism 7900 HT thermocycler. For any sample the expression level normalized to the housekeeping genes encoding *18S*, hypoxanthine phosphoribosyltransferase 1 (*Hprt1)* or *Glucuronidase beta (Gusb)* was determined by the comparative threshold cycle ($C_t$) method as described previously [265]. mRNA levels of the several transcripts of interest obtained by freshly isolated tissue derived ECs were normalized for endothelial cell content using *Pecam1* amount.

### 5.10 Affymetrix

RNA was extracted from WT and CCM1 KO BMECs upon 7 days of culture and analyzed using Affymetrix GeneChip arrays Gene ST 1.0 containing probes for 29,000 murine genes. For each condition, total RNA from three distinct preparations was used to measure biological variability. In order to identify the modulated genes, an initial filter was applied to select transcripts regulated with a statistical p-value below 0.05.

### 5.11 Cell migration assay

Wound healing assay was used to measure cell migration. Confluent EC monolayers were starved ON and then manually wounded with a pipette tip. Cells were then washed with Phosphate-Buffered Saline (PBS) and incubated at 37 °C for the 6 hours in complete media. Cell migration was examined by crystal violet staining (0.5 % crystal violet in 20 % methanol) and phase contrast microscopy. Quantification of migration was performed by ImageJ software.

### 5.12 Cell proliferation assay

Cell proliferation assay was performed as previously described [12]. Briefly, cells were plated at density of 4,000 cells/well in 96 well plates and analyzed at the indicated time points by crystal violet staining (0.1 % crystal violet in 20 % methanol). The optical density of the dye was measured using a Victor Microplate reader at the wavelenght of 590 nm. Where indicated, cell proliferation were evaluated by measuring the percentage of Ki-67 positive cells.

### 5.13 Generation of 3-D endothelial spheroid assay

EC spheroids were generated by seeding in non adherent round-bottom 96 well plates (Greiner) a number of 500 WT and CCM1 KO ECs in culture medium containing 0.25 % (w/v) carboxymethylcellulose. Suspended cells formed single EC spheroid within

24 hours. Then, cell spheroids were embedded into collagen gels as described [266] in a cell culture medium containing both 10 ng/ml VEGF-A (PeproTech) and 10 ng/ml FGF-2 (PeproTech) was added. After 24 hours of incubation EC spheroids were fixed in 4 % paraformaldehyde (PAF). Actin staining (TRITC-Phalloidin, Sigma) was performed in order to evaluate cell sprouting and migration. The cumulative length of sprouts that originate was from quantified with ImageJ software. At least 10 spheroids per experimental group were analysed in each experiment.

### 5.14 Transcription factor binding site analysis

The identification of putative KLF4 binding sequences on genomic DNA was performed using the software MatInspector [267], which predicts the transcription factor binding sites (TFBS) by using a large library of weight matrices. Using the RSAT software (http://rsat.sb-roscoff.fr/) we retrieved a sequence spanning from 5000 bp upstream and 1000 bp downstream the transcription start site (tss) of *Fsp1*, *Sca1*, *Id1*, *Bmp6* genes.

### 5.15 Transcriptional reporter assay

Genomic DNA isolated from lung derived murine WT ECs was used to amplify promoter regions, identifed as enriched in KLF4 binding sites by chromatin immunoprecipitation (ChIP), of either *Fsp1 (1.8 KB)*, *Sca1 (2.1 KB)* or *Bmp6 (2.3 KB)*. As depicted in Table 2, we designed for each promoter sequence both forward and reverse primers modified at their estremity in order to contain restriction sites for specific restriction enzymes (XhoI and KpnI for both *Fsp1* and *Sca1* promoters; XhoI and BglII for *Bmp6).* The three promoter sequences were amplified using 200 ng of DNA, 10 mM dNTPs, 10 µM forward and revers primers, 1µl DMSO, 10µl Phusion HF buffer 5X and 0.5 µl high fidelity DNA polymerase Phusion (NEB). The following thermal cycle programs were applied:

*Fsp1*- 98 °C 30 sec, 98 °C 10 sec, 65 °C 25 sec, 72 °C 54 sec, 72 °C 10 min

*Sca1*- 98 °C 30 sec, 98 °C 10 sec, 65 °C 25 sec, 72 °C 70 sec, 72 °C 10 min

*Bmp6*- 98 °C 30 sec, 98 °C 10 sec, 67 °C  25 sec, 72 °C 70 sec, 72 °C 10 min

Upon the enzimatic restiction we cloned these DNA fragments into the polinker of PGL3-basic vector (Promega) upstream the luciferase cDNA.

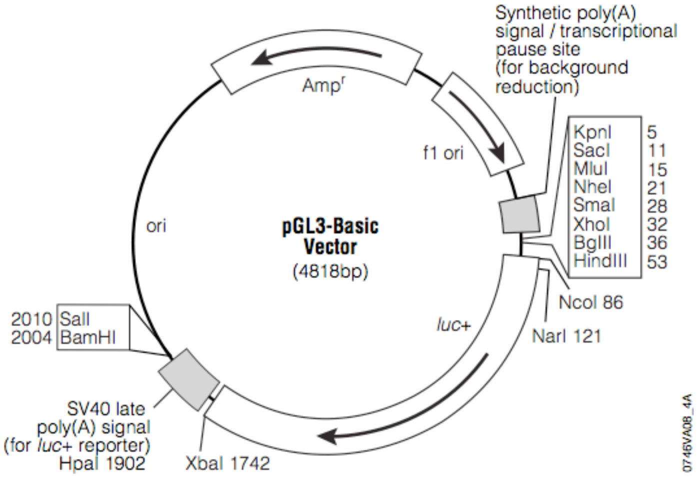
Synthetic poly(A) signal / transcriptional pause site (for background reduction)
Amp^r
f1 ori
ori
pGL3-Basic Vector
(4818bp)
KpnI 5
SacI 11
MluI 15
NheI 21
SmaI 28
XhoI 32
BglII 36
HindIII 53
NcoI 86
NarI 121
luc+
2010 SalI
2004 BamHI
SV40 late poly(A) signal (for luc+ reporter)
HpaI 1902
XbaI 1742
0746VA08_4A

**Figure 10 - Representation of PGL3 basic vector backbone**

| Gene | Forward | Reverse |
|---|---|---|
| BMP6 | 5′-ACCGCTCGAGCAAGAGGATGGGGAAGGCT-3′ | 5′-GGAAGATCTTCCAGCTCCTCCCATTGC-3′ |
| FSP1 | 5′-CGGGGTACCCACTGCCACCCTAACTCCA-3′ | 5′-ACCGCTCGAGTGCCATGGTAACCGTTGAG-3′ |
| SCA1 | 5′-CGGGGTACCTGATGGCCCCGTTGTCAT-3′ | 5′-ACCGCTCGAGACTGAGCTCCACGTGTCC-3′ |

**Table 1 – List of primers used for promoter cloning**

To perform the transcriptional reporter assay, HEK-293 cells were plated in 24 well plates and transfected for 5 hours in Optimem using Lipofectamine 2000 (Life Technologies) with the reporter plasmids expressing the luciferase cDNA under the control of a promoter portion of either *Fsp1*, *Sca1* or *Bmp6*. pCDNA3 expression vectors containing either full length KLF4 or a mutant KLF4 lacking the DNA-binding zinc finger domain (KLF4 ΔZnF) (kind gifts of Mukesh Jain) [214] were co-transfected where indicated.

Renilla expressing plasmid was used as an internal control to correct for transfection efficiency. DualLuciferase® Reporter Assay System (Promega) was used to measure firefly and renilla luciferase activities 30 hours upon transfection with a GloMax® luminometer (Promega).

### 5.16 Chromatin Immunoprecipitation

ChIP assays were performed as described elsewhere [268]. Briefly, cells were starved ON and cross-linked with 1 % formaldehyde for 10 minutes at RT. 125 mM glycine for 5 minutes at RT was then added in order to inactivate formaldehyde. After two washes with ice-cold PBS ECs were lysed by scraping in ice-cold SDS buffer (NaCl 100 mM, Tris HCl pH 8.1 50 mM, EDTA 5mM, NaN3 0.2 %, SDS 0.5 %). The lysate was collected and then centrifuged at 1,300 rpm for 5 minutes at 4 °C. After removal of the supernatant, the pellet was resuspended in Immunoprecipitation buffer (1 volume of SDS Buffer + 0.5 volume of Triton Dilution Buffer [NaCl 100 mM, Tris HCl pH 8.6 100 mM, EDTA 5 mM, NaN3 0.2 %, Triton X-100 5 %]). Sample sonication in microTUBE (COVARIS) was performed after 10 minutes of incubation using a COVARIS S220 according to the following conditions: Peak Incident Power 175.0 Watt, Duty Factor 10 %, 200 Cycles/Burst. An aliquot of chromatin was then digested with Proteinase K (1 ug/ul) for 30 minutes at 55 °C, incubated at 65 °C for 3 hours to revert the cross-linking and then purified using the QIAquick Gel extraction Kit (QIAGEN). The purified chromatin was loaded on 1 % agarose gel to evaluate the size of the sonicated chromatin fragments. 1 mg of DNA fragments with an average size of 500 base pairs (bp) were incubated with either 10 µg of KLF4 directed antibody or IgG control ON at 4 °C in the presence of protein G covered magnetic beads (Life Technologies). The following day, beads were recovered and washed twice with Mixed Micelle Washing Buffer (NaCl 150 mM, TrisHCl pH 8.1 20 mM, EDTA 5 mM, Sucrose 5.2 % w/v, $NaN_3$ 0.02%, Triton X-100 1 %, 0.2 % SDS), 500 Buffer (Deoxycholic acid 0.1 % w/v, NaCl 500 mM, HEPES pH 7.5 25 mM, EDTA 1 mM, $NaN_3$

0.02 %, Triton X-100 1 %), LiCl Detergent Washing Buffer (Deoxycholic acid 0.5 % w/v, LiCl 250 mM, EDTA 1 mM, NP-40 0.5 % v/v, $NaN_3$ 0.02 %, Tris HCl pH 8.0 10 mM). Proteins/DNA complexes were detached from beads by heating the samples at 65 °C for 10 minutes. De-crosslinking was performed at 65 °C ON. DNA was purified using Wizard SV Gel and PCR Clean-Up System (Promega) and amplified by qRT-PCR using oligonucleotides flanking the assayed promoter regions (listed below). Primers were always tested to avoid "auto- amplification" due to self-complementarity. qRT-PCR reactions were carried out by diluting DNA in the presence of specific primers (0.4 μM each) to a final volume of 25 μl in SYBR Green Reaction Mix (Perkin Elmer). S.D.S 2.2.1 software was used to convert qRT-PCR curves in $C_t$ values. For each region the mean of the $C_t$s of the inputs was calculated and subtracted to the $C_t$ values of the immune samples (ΔCt). Then, the % of enrichment of input for the immune samples was obtained as 2^-ΔCt and multiplied by the % of input taken during the experiment. The same calculation was performed for the non-immune (IgG control) immunoprecipitated samples. To remove unspecific signal, the non-immune values were subtracted from the immune samples.

| Gene | Position | Forward | Reverse |
|---|---|---|---|
| BMP6 | -5.0 KB | 5′-TTTCTTTCTGGCCTCTGCAT-3′ | 5′-CCCTGAAGAGGTTGGTTCTG-3′ |
| | -3.4 KB | 5′-CACATCTGGCTTCTTGACGA-3′ | 5′-AGGTCTGCCTCCAGAGTTCA-3′ |
| | -3.0 KB | 5′-CCCCGAGTTTCACTTGACAT-3′ | 5′-GTGCACTCTCAACCTGGACA-3′ |
| | -1.9 KB | 5′-TGTTTCAGACCCCATAAACCA-3′ | 5′-GCTCAAATGGCCACTCATCT-3′ |
| | -1.3 KB | 5′-AACTCAAATGCAGCCCAAAC-3′ | 5′-TGGAATGTAGGCGTTTAGCA-3′ |
| | -1.1 KB | 5′-ACTCCTGATGCCTCCAAGAA-3′ | 5′-CAGCCAATGGAGAGGTGACT-3′ |
| | +0.3 KB | 5′-AATGACGACGAAGAGGATGG-3′ | 5′-AGACTCTTGCGGTTCAAGGA-3′ |
| | +0.6 KB | 5′-AGGATTTTGGGGGTAGCATC-3′ | 5′-GTGTTCCAGCTCCTCCCATT-3′ |
| FSP1 | -3.6KB | 5′-TCTTCAAGCCCTGTGCTTCT-3′ | 5′-AATGGGGCTGAAGTGTCAAG-3′ |
| | -3.1 KB | 5′-CCAGCTATGCTTCTGGGGTA-3′ | 5′-GCGCCACTTCAGTTGCTATT-3′ |
| | -2.2 KB | 5′-CAGGTCTCCAAAAGGCAGAG-3′ | 5′-TCTACCACCTTCACCCCAAC-3′ |
| | -2.0 KB | 5′-GTTGGGGTGAAGGTGGTAGA-3′ | 5′-CTCCGACTGGCAGATCTTGT -3′ |
| | -1.4 KB | 5′-CCCAGTAGCCTCTGATCCAA-3′ | 5′-GGTGGGGTTAGCACATCAAG-3′ |
| | -0.9 KB | 5′-GGTGTCAGGCCCTGTAGAAA-3′ | 5′-ACTCTCCTTGCAGCATCTGG-3′ |
| | +0.1 KB | 5′-ACTGCTAGCGGCATTAGAGG-3′ | 5′-CTCCGGGAGCTCAGATGTAG-3′ |
| | +0.7 KB | 5′-GCAGGCATTCGTGTTTGTAG-3′ | 5′-AAAAACCCCAGCTGCCTAAT-3′ |
| SCA1 | -3.9 KB | 5′-TGAGGGCCTTCATACCTCTG-3′ | 5′-GGTGAAGATGCCTGACTGCT-3′ |
| | -3.3 KB | 5′-GCATGACAGTGGTGAGATGG-3′ | 5′-CCCCCAAGAAAACAGACAGA-3′ |
| | -1.4 KB | 5′-GAAGGGAGGACTGTCACCTG-3′ | 5′-CACGGAGTCCCTCTTTCAGT-3′ |
| | -0.9 KB | 5′-ACCACTGTGCTGGGTTATGC-3′ | 5′- ACCCCACTTAAGCAGGGAAG-3′ |
| | -0.4 KB | 5′-GCCACTGCAAACCATACCTT -3′ | 5′-CTGGCTCCAACACACAGCTA-3′ |
| | -0.1 KB | 5′-AACATGATGGCCTGGAAAAG-3′ | 5′-GCACAGTGGCAAGTTCTGTC-3′ |
| | +0.4 KB | 5′-CCCTTCTCTGAGGATGGACA-3′ | 5′-AGGTGTACCCACAACCCTGA-3′ |
| ID1 | -4.9 KB | 5′-AGAACTCTCCAGGAAGTGATGG-3′ | 5′-TCGAGACAGGGTTTCTCTGTG-3′ |
| | -4.6 KB | 5′-TCTTGCTGTTTCTAGGGCATC-3′ | 5′-CGGAAACAGCCTCAACATCT-3′ |
| | -3.8 KB | 5′-CACATACCCACCCTTCTGCT-3′ | 5′-AGCTTCATGTAGCCCATGCT-3′ |
| | -3.5 KB | 5′-CCTCTTGAAACAGCACAGCA-3′ | 5′-CAAGCCTGATGATTGACACC-3′ |
| | -3.0 KB | 5′-GCTCTGGATGTCCTGGAACT-3′ | 5′-AAAGGACTGGAGAGGCACTG-3′ |
| | -2.0 KB | 5′-AGAATGCTCCAGCCCAGTTT-3′ | 5′-GTTGGGGTGTGTGTTGAGG-3′ |
| | -1.0 KB | 5′-AGAATGCTCCAGCCCAGTTT-3′ | 5′-GGGCTGGTCTGTGTCAGC-3′ |
| | +0.1 KB | 5′-TCCCACACTCTGTTCTCAGC-3′ | 5′-TCCCACACTCTGTTCTCAGC-3′ |
| | +0.5 KB | 5′-TGAGGTCCGAGGCAGAGTAT-3′ | 5′-GAGACCCACTGGAAAGGACA-3′ |

**Table 2 – List of primers used in ChiP**

## 5. 17 Immunofluorescence and hystology

For immunofluorescence stainings perfomed *in vitro*, ECs were plated in 15 µ-slides (Ibidi) and, at confluency, fixed for 10 minutes in 4 % PAF at RT or for 3 minutes in ice-cold Methanol. Cells fixed in PAF were subjected to a permeabilization step with PBS plus 0.05 % TritonX-100 for 5 minutes. A PBS solution containing 5 % Donkey Serum and 2 % BSA was used to perform the blocking the samples for 1 hour at RT. After the blocking ECs were incubated for 1 hour at RT with primary antibodies diluted in blocking solution. Appropriate fluorofore-conjugated secondary antibodies (Molecular Probes) were used on cells for 2 hours at RT. After several washing steps, sections were post-fixed with 2 % PAF for 5 minutes and then mounted with Vectashield containing DAPI (Vector Laboratories).

For tissue immunostaining, mouse brains were dissected, embedded in Tissue-Tek OCT (Sakura) and snap frozen. 10 µm-thick sections were fixed either in 4 % PAF for 20 minutes or ice-cold methanol for 5 minutes. PAF-fixed samples were permeabilized with PBS containing 0.5 % Triton X-100 for 5 minutes at RT. Slides were then blocked for 3 hours at RT with PBS containing 2 % BSA, 5 % Donkey Serum and 0.05 % TritonX-100 (blocking solution). Incubation with primary antibodies (ON at 4 °C) and secondary (3 hours at RT) antibodies was carried out in blocking solution. After several washing steps, section were counterstained with DAPI, post-fixed with 2 % PAF for 5 minutes and then mounted with Vectashield (Vector Laboratories). Analysis of the staining was performed with a Leica TCS AOBS confocal microscope using several objectives: 20x (HC PL FLUOTAR NA=0.5, dry), 40x (HCX PL APO NA=1.25, oil) or 63x (HCX PL APO lbd.BL NA=1.4, oil). Images were acquired with Leica Confocal Software and then adjusted with Adobe Photoshop. The adjustments used in the preparation of the figures were for brightness, contrast and background noise (blur filter).

For lesion quantifications brains were fixed in 4 % PAF ON at 4 °C and then embedded in 4 % low-melting-point agarose. Serial sagittal sections (150 µm) of the cerebellum were obtained using a vibratome (1000 Plus, The Vibratome Company, St. Louis, MO, US). Each section was stained for *Glucose transporter 1 (Glut1)* for vessel detection and examined under confocal microscopy (10× and 20× objectives). Analysis of the number/size of the CCM cavernae was performed using Image J software. Three different groups of caverns were defined according to their size (area in µm$^2$) [69].

For immunochemistry on human samples, 3 µm paraffin sections were stained with hematoxylin and eosin (H&E) to assess the histological features. Immunohistochemical analysis for CLAUDIN5 and KLF4 was performed on serial sections. Paraffin was removed with xylene and the sections were rehydrated in graded alcohol. Antigen retrieval was carried out using preheated sodium citrate solution for 50 minutes. Tissue sections were blocked with 5 % FBS in PBS for 60 minutes and incubated ON with primary antibodies. HRP-Polymer Kit (Biocare Medical, Pike Lane Concord, CA, USA) was used for the detection of antigens followed by a diaminobenzidine chromogen reaction (Peroxidase substrate kit, DAB, SK-4100; Vector Lab). All sections were counterstained with Mayer's hematoxylin. Images were acquired using an upright microscope (Olimpus BX51) using a 20x objective (UPlanFL N 20x NA=0.5). NIS-elements software was used for image analysis. BMP6 and PECAM1 immunohistochemistry on murine brain samples were performed as described above for CLAUDIN5 and KLF4. Antigen retrieval was carried out using sodium citrate for BMP6 and EDTA for PECAM1.

### 5.18 Immunofluorescence analysis of the retina

Retina immunostaining was carried out with littermates processed simultaneously under the same conditions. The retinas were dissected from fixed eyes in 2 % PFA for 2 hours at 4 °C. After blocking/permeabilization in 1 % BSA, 5 % donkey serum and 0.5 % Triton-X100 in PBS ON, the retinas were washed in Pblec Buffer (1 % Triton X-100, 1 mM $CaCl_2$, 1 mM $MgCl_2$ and 0.1 mM $MnCl_2$ in PBS, pH 6.8) and incubated ON at 4 °C in Pblec buffer containing biotinylated isolectin B4 (IB4) and the primary antibodies. Then, the retinas were incubated with both fluorophore-conjugated secondary antibodies and with Alexa Fluor 488/555/647 streptavidin (Life Technologies) and mounted with ProLong Gold (Life Technologies). Confocal analysis was performed using a Leica TCS AOBS or a Leica TCS SP5 confocal microscope using the following objectives: 40x (HCX PL APO NA=1.25, oil) or 10x (HC PL FLUOTAR NA=0.3, dry). Leica Confocal Software was used for the acquisition. The figures were prepared as described in “Immunofluorescence and histology” section. The vessel front density and vascular progression in the retinae were measured as previously described [269]. All image analyses were carried out using the ImageJ software. Quantification of the nuclear pixel intensity was obtained by using the co-localization highlighter plug-in of ImageJ software. Mean intensity of co-localizing pixel per field has been calculated through ImageJ and normalized on the number of endothelial nuclei.

### 5. 19 Intravenous injection of tracer and tracer detection

Cadaverine conjugated to Alexa Fluor-555 (Invitrogen) was injected IP at the dose of 12.5 μg/g 2 hours before mice sacrifice (P13). Animals were then anesthezitazed with an intraperitoneal injection of Avertin (20 μl/g) in order to perform a 5 minutes perfusion with PBS. Brains were dissected and fixed in 4 % PAF ON at 4 °C. Cadaverine leakage in the brain was measured by evaluating mean fluorescence of brain images acquired under a stereomicroscope equipped with HBO 100 lamp and a Filter Set Lumar 43 HE. ImageJ software was used to calculate cadaverine mean fluorescence.

### 5.20 Statistics

Data are expressed as mean ± standard deviation (SD). Student’s two-tailed non-paired *t*-tests were used to determine the statistical significance of the *in vitro, ex-vivo* and *in vivo* analyses. The significance level was set at $P<0.05$. For survival experiment, Kaplan-Meier curves were analyzed with the Mantel-Cox test.

# 6. RESULTS

## 6.1 Establishment of a mouse model of CCM disease

Over the past years numerous studies have provided new insights into CCM protein functions *in vitro*. However, a clear understanding of which signalling pathways are relevant *in vivo* to the etiology of the CCM disease is still lacking.

To investigate the role of CCM1 *in vivo* in mice and circumvent the embryonic lethality of ubiquitous inactivation of the gene [270] we generated endothelial specific and inducible *Ccm1* loss-of-function mice (EC-CCM1 KO mice) by crossing tamoxifen-inducible *Cdh5(PAC)*-CreERT2 and *Ccm1* floxed/floxed transgenic mice [260]. *Cdh5(PAC)*-CreERT2-*Ccm1*-floxed/floxed mice were then bred with *Rosa 26-Enhanced Green Fluorescent Protein* (*EYFP*) mice [271] to monitor tamoxifen-induced Cre/Lox recombination through the expression of EYFP. Animals were tamoxifen-injected at P1 and analyzed between P3 and P15. High gene recombination efficiency was verified by qRT-PCR in freshly isolated PECAM+ brain derived ECs, since *Ccm1* transcript was reduced by more than 80% in EC-CCM1 KO pups analyzed at P12 in comparison to vehicle treated WT mice (Figure 11). *Ccm1* deletion resulted in the development of several vascular lesions within the central nervous system and in the retina in all *Ccm1*-ablated mice (Figure 12 A and Figure 13). Cavernomas started to develop three days after treatment with tamoxifen and they progressively increased in number and size with time. The lesions were mostly concentrated in the cerebellum and presented comparable features to human CCM lesions. Indeed histology and immunofluorescence analysis showed that lesions were composed of dilated vessels (Figure 12 A, B) that, with time, formed multiple caverns with signs of vascular leakage and chronic accumulation of haemosiderin (Figure 12 B). At late stages of lesion development (>P12) we also observed a marked inflammatory and immune reaction around the vascular lesions previously reported in CCM patients [272], characterized by infiltration of macrophages Cd11b positive (Figure 12 C) and lymphocytes CD3 positive (Figure 12 D) that increased with lesion size (Figure 12 E). 5% of familial CCM patients present vascular lesions also in the retina [273]. Consistenlty we observed that EC-CCM1 KO animals presented CCM vascular malformations of retinal vascular plexus in

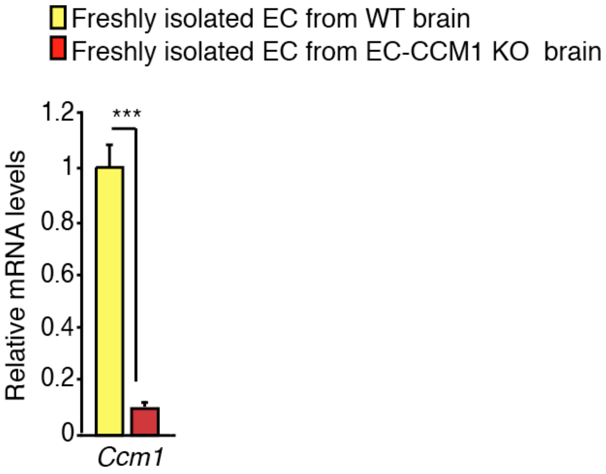

**Figure 11 - High *Ccm1* recombination mediated by tamoxifen-induced Cre-recombinase activity in EC-CCM1 KO brains.**

qRT-PCR analysis of *Ccm1* in freshly isolated brain PECAM+ ECs from wild-type and EC-CCM1 KO mice. Data are mean ± SD from three independent observations. ***P< 0.001.

in both eyes (Figure 13 A, B). EYFP staining of the retina of EC-CCM1 KO mice confirmed also in this context the high recombination efficiency after tamoxifen treatment [69, 274, 275] (Figure 13 B). Consistent with what was observed in human retinal CCM lesion by angiography [73], CCM lesions were restricted to the venous-capillary bed that can be easily distinguished by morphological analysis of EC-CCM1 KO retinas (Figure 13 A). Furthermore, using the same gene targeting strategy (*Ccm2* or *Ccm3* floxed/floxed animals crossed with *Cdh5(PAC)*-CreERT2 mice), tamoxifen-induced endothelial specific deletion of either *Ccm2* or *Ccm3* at P1 resulted in CCM malformations in the CNS and in the retina [69, 92]. As in patients, the morphology of the cavernomas was indistinguishable in the absence of any of the three *Ccm* genes, with *Ccm3* endothelial deficiency showing the most severe phenotype [69].

Overall these data demonstrate that this mouse model reproduced to a large extent human CCM features with a complete penetrance and high reproducibility, thus being suitable both for deciphering the molecular mechanisms involved in the different phases of development and progression of the disease and for the evaluation of future therapeutic agents.

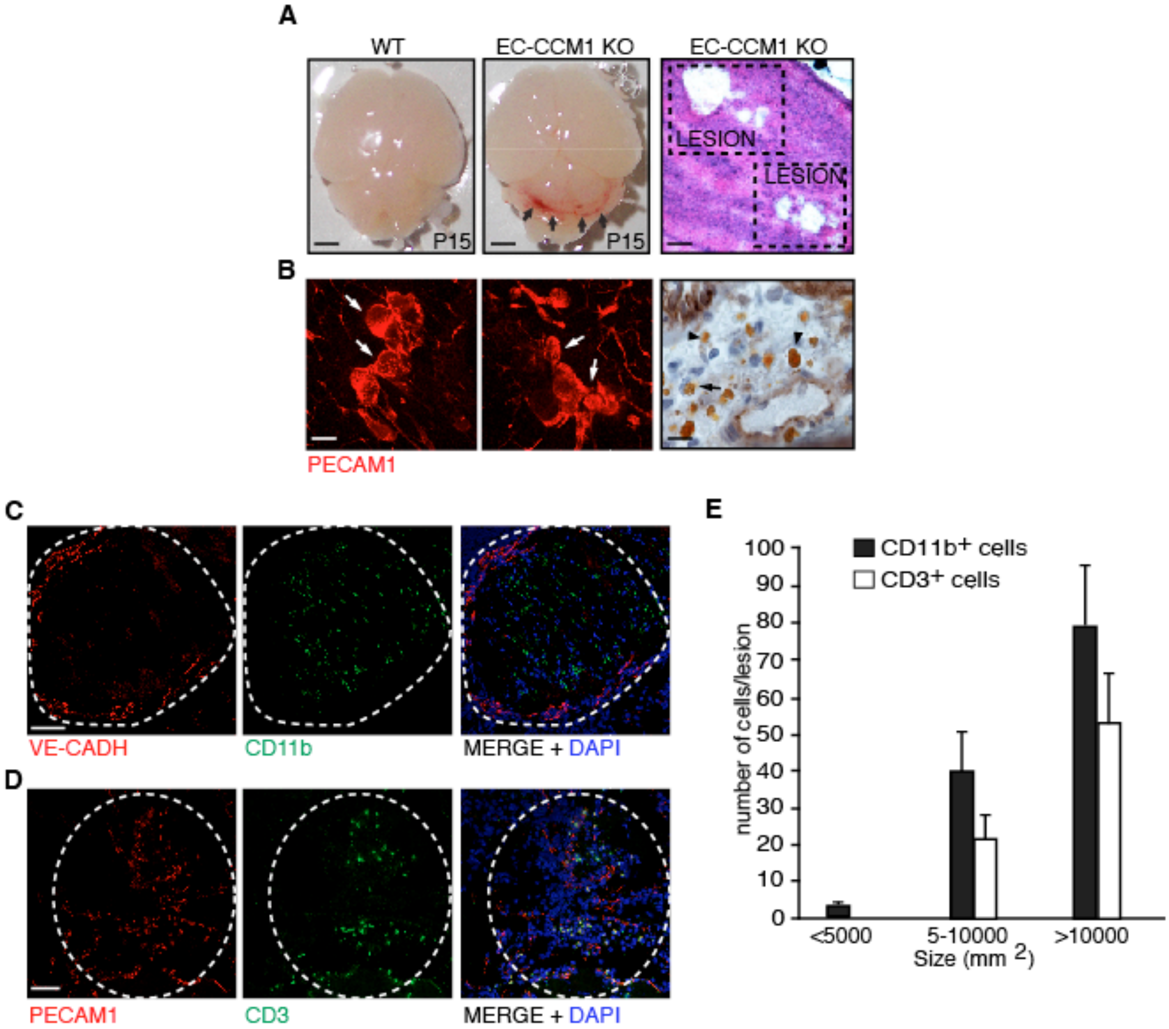
A
WT
EC-CCM1 KO
EC-CCM1 KO
P15
P15
LESION
LESION
B
PECAM1
C
VE-CADH
CD11b
MERGE + DAPI
D
PECAM1
CD3
MERGE + DAPI
E
CD11b+ cells
CD3+ cells
number of cells/lesion
0
10
20
30
40
50
60
70
80
90
100
<5000
5-10000
>10000
Size (mm 2)

**Figure 12 - Endothelial *Ccm1* deletion at P1 in the mouse results in brain vascular malformations comparable to human CCM lesions.**

A) Representative images of WT and EC-CCM1 KO mouse brains after dissection at P12. EC-CCM1 KO mice show cerebellar vascular lesions (black arrows). Right panel: cavernomas visualised by H&E staining. B) Left and middle panels: mulberry–shaped lesions (white arrows); PECAM1 (red) is used to identify blood vessels. Right panel: histology showing accumulation of haemosiderin (black arrowheads) in CCM. C-D) Immune cells infiltration in CCM lesions: immunofluorescence showing accumulation of CD11b-positive macrophages (green) and CD3-positive T-lymphocytes (green) in cavernomas of EC-CCM1 KO mice.

PECAM1 marks ECs. Cell nuclei are visualised with DAPI. E) Quantification of leukocyte infiltration in CCM lesions (classified in three groups based on their size) in a total of 8 EC-CCM1 KO mice. Scale bar: 500 μm (A, left and middle panels), 100 μm (A, right panel), 60 μm (B-D).

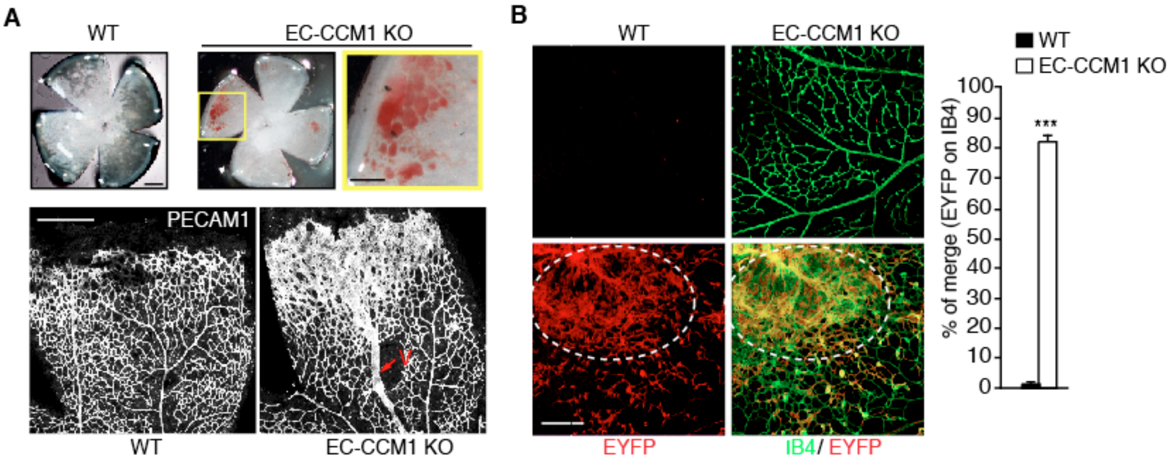
A
WT
EC-CCM1 KO
PECAM1
V
WT
EC-CCM1 KO
B
WT
EC-CCM1 KO
EYFP
IB4/ EYFP
■ WT
□ EC-CCM1 KO
% of merge (EYFP on IB4)
100
90
80
70
60
50
40
30
20
10
0
***

**Figure 13 - Endothelial *Ccm1* deletion at P1 in the mouse results in retinal vascular malformations comparable to human CCM lesions.**

A) Upper panels: representative images of WT and EC-CCM1 KO mouse retinas upon dissection at P15; Lower panels: PECAM1 staining of WT and EC-CCM1 KO mouse retinas. V= vein. B) Analysis and quantification of *Ccm1* recombination in retinal endothelium of WT and EC-CCM1 KO mice at P15 by EYFP staining (red). Isolectin B4 (IB4) (green) marks the endothelium. Dotted line indicates the lesion area. Data are representative of 3 independent observations (n = 5 for genotype from 2 different litters). Scale bars: 500 μm (A, left and middle); 200 μm (I, upper panels); 100 μm (A, right; I, lower panels; J); 60 μm (B-G);

### 6.2 CCM vascular lesions are lined by endothelial cells with a mesenchymal and stem-like phenotype

Since CCM proteins interact with critical components of adherens junction (AJ), to investigate the phenotype of ECs lining the vascular lesions we first analyzed the expression and the organization of junctional proteins. The key AJ protein VE-cadherin expressed presented a disorganized distribution outside cell-to-cell contacts in the ECs forming the lesion (Figure 14 A, left and middle panels) as compared with ECs lining the pseudo-normal vessels surrounding the lesion where it appeared to be perfectly localized at intercellular cleft (Figure 14 A, right panel). Conversely N-cadherin, a pro-migratory cadherin that was previously reported to be weakly expressed at cell-to-cell junctions in normal quiescent vessels [12], was remarkably upregulated in the CCM lesion (Figure 14 B). Cadherin switch (downregulation of VE- and upregulation of N-cadherin) has been previously associated to EndMT [276, 277]. During this transition ECs lose progressively the expression and proper localization of endothelial specific molecules and acquire the expression of mesenchymal and stem-like markers as well as a higher proliferative and migratory capability. To further prove the hypothesis that EndMT occurred in *Ccm1* null ECs, we evaluated the expression of a number of mesenchymal markers, such as SLUG (also known as SNAI2), ID1 and αSMA [122, 278, 279]. Interestingly we found that these proteins were absent in pseudo-normal peri-lesion vessels, whereas they were strongly upregulated in the ECs forming the vascular malformation (Figure 14 C-E). In addition, SCA1 and CD44, which are widely accepted stem cell-markers in normal and tumor tissues [280, 281] were also highly expressed in ECs lining the lesions in comparison to ECs of the surrounding normal vessels (Figure 14 F, G). Importantly, KLF4, a zinc finger transcription factor involved in the regulation of many endothelial biological processes such as proliferation, differentiation, development, inflammation and apoptosis [222-228], was the only EndMT related marker analyzed whose expression was increased both in the lesion and the normal vasculature of EC-CCM1 KO mice (Figure 14 H), while it was poorly expressed in brain vessels of WT mice (Figure 14 I). Interestingly, the upregulation of mesenchymal and stem-cell markers in the absence of *Ccm1* was confirmed in freshly isolated PECAM+ brain EC isolated by EC-CCM1 KO mice (Figure 15).

Thus, our results showed that *Ccm1*-ablation *in vivo* causes a general modification of the endothelial phenotype conferring mesenchymal and stem-like traits to these cells.

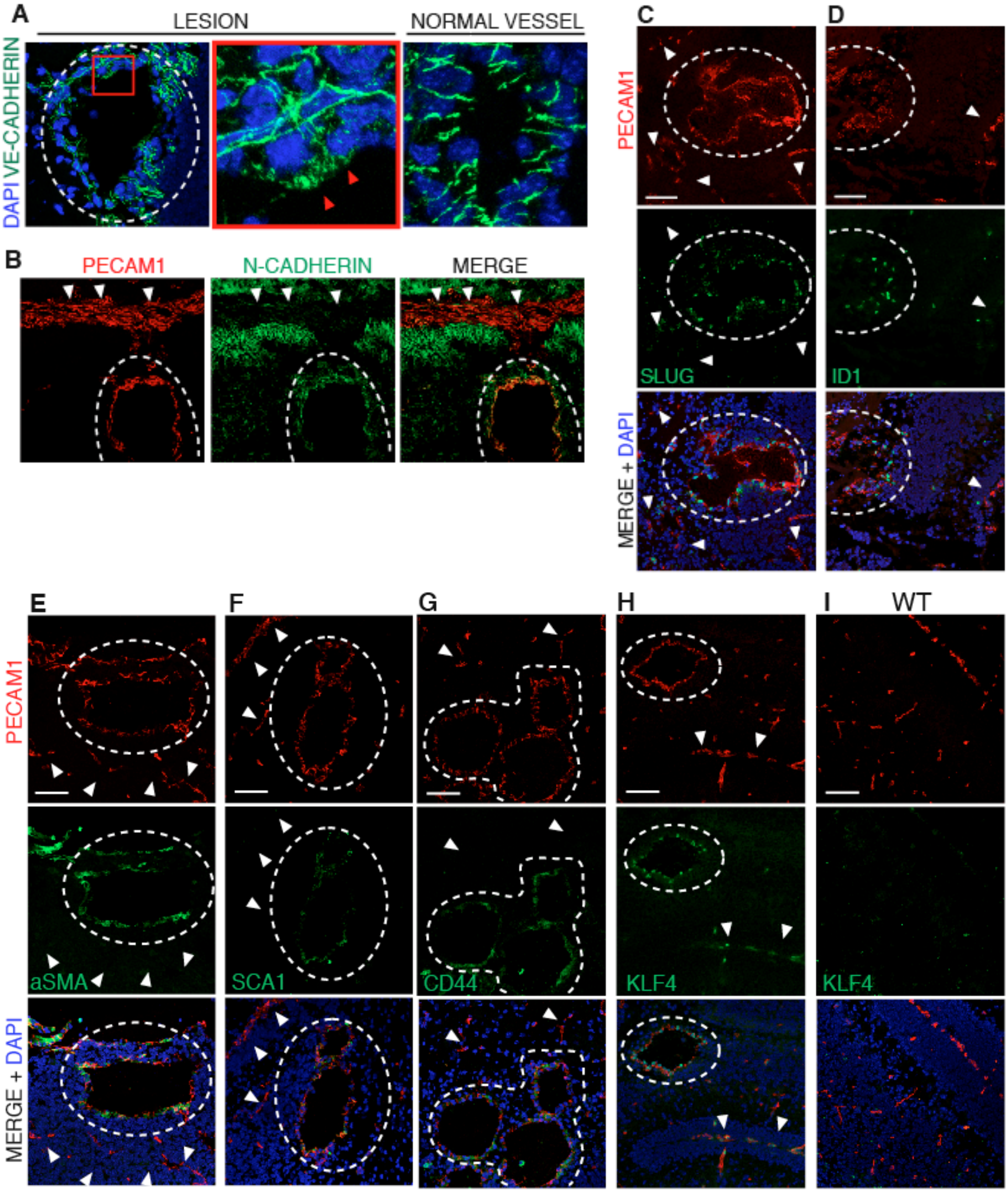
A
LESION
NORMAL VESSEL
DAPI VE-CADHERIN
B
PECAM1
N-CADHERIN
MERGE
C
D
PECAM1
SLUG
ID1
MERGE + DAPI
E
F
G
H
I
WT
PECAM1
aSMA
SCA1
CD44
KLF4
KLF4
MERGE + DAPI

**Figure 14 - *Ccm1* deletion causes EndMT *in vivo*.**

A) VE-cadherin expression (green) in normal vessels and vascular lesions (indicated by dotted area) of EC-CCM1 KO mouse brains. DAPI visualizes cell nuclei. Red arrowheads denote VE-cadherin out of the junctions. Central and right panels show higher magnification. B) N-cadherin staining (green) in lesion and in normal peri-lesion vessels (PECAM1, red) of EC-CCM1 mouse brains. PECAM1 staining identifies ECs. C-H) Mesenchymal and stem-cell markers (green) in the vascular lesions (PECAM1, red) of EC-CCM1 KO mouse brains. PECAM1 marks ECs. DAPI visualizes cell nuclei. I) KLF4 expression (green) in WT mouse brain. Data are representative of three independent observations (n= 5 for each genotype from two different litters). White arrowheads highlight normal peri-lesion vessels; dotted areas denote vascular lesions. Scale bars: 50 μm (A, left); 60 μm (B-I); 8 μm (A, middle and right).

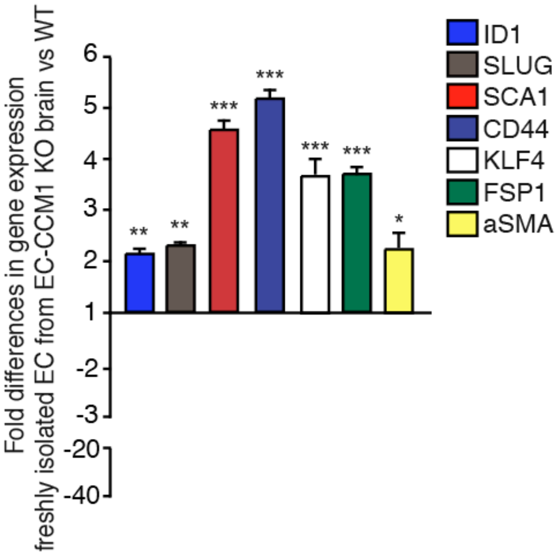

**Figure 15 - *Ccm1* deletion causes EndMT marker mRNA upregulation *in vivo*.**

qRT-PCR of EndMT markers in freshly isolated PECAM+ brain ECs (fold difference in gene expression in EC-CCM1 KO- versus WT-derived ECs). Data are mean ± SD from three independent observations. *P<0.05; **P<0.01; ***P<0.001.

### 6.3 Loss of *Ccm1* expression induces EndMT transition in a cell-autonomous way

To directly investigate whether EndMT induction in EC-CCM1 KO mouse lesions is a cell-autonomous process, ECs were isolated from lungs of *Ccm1* floxed/floxed mice, immortalized with PmT antigen and then treated with TAT-Cre to induce gene recombination. TAT-Cre treatment resulted in the complete loss of *Ccm1* at both mRNA and protein level *in vitro* (Figure 16 A). The absence of CCM1 caused a switch in phenotype of cultured ECs, which recapitulated, to a large extent, the phenotype observed *in vivo* in EC-CCM1 KO mice. In *Ccm1* null ECs both VE-CADHERIN and the tight junctions protein CLAUDIN-5 were significantly reduced while a large number of representative mesenchymal markers such as ID1, FSP1, VIMENTIN, FIBROBECTIN, L1, MMP14 were strongly increased [114, 282] (Figure 16 B, C). Interestingly, we also observed an increased expression of stem cell markers CD44, SCA1, KLF4 in CCM1 KO ECs (Figure 16 B, C).

To exclude the contribution of any culture contaminant to the increased expression of EndMT markers observed in the absence of *Ccm1*, we performed a co-staining analysis of a representative set of EndMT markers together with a specific endothelial molecule in WT and CCM1 KO ECs. As depicted in Figure 17 (A-C), endothelial cultures were 100% pure and the increased expression of either FSP1 (Figure 17 A), SCA1 (Figure 17 B) or KLF4 (Figure 17 C) was always observed in VE-CADHERIN positive CCM1 KO ECs, thus proving that cells that acquired a mesenchymal phenotype had an endothelial origin.

Since CCM is a disease that affects specifically brain microvasculature, we moved to confirm our findings in a more physiological cellular model such as cultured primary brain derived ECs (BMECs). ECs isolated from the brain of both WT or *Ccm1* floxed/floxed mice were seeded in culture and then treated with TAT-cre recombinase to induce recombination of floxed alleles *in vitro*. As depicted in Figure 18 A, a good but not complete reduction of CCM1 protein levels was obtained. Inhibition of CCM1 expression in BMECs recapitulated the data observed in lung derived CCM1 KO ECs since several mesenchymal and stem-cell markers were strongly increased (Figure 18 A, B) while VE-CADHERIN organization at cell-to-cell junctions was dismantled in CCM1 KO compared to WT BMECs (Figure 19). However, due to limitations in both the supply of primary ECs from the brain and their extremely limited mitotic index, most of the analyses were performed in lung derived cell lines to understand the molecular alteration occurring in *Ccm1* null ECs and finally validated in BMECs.

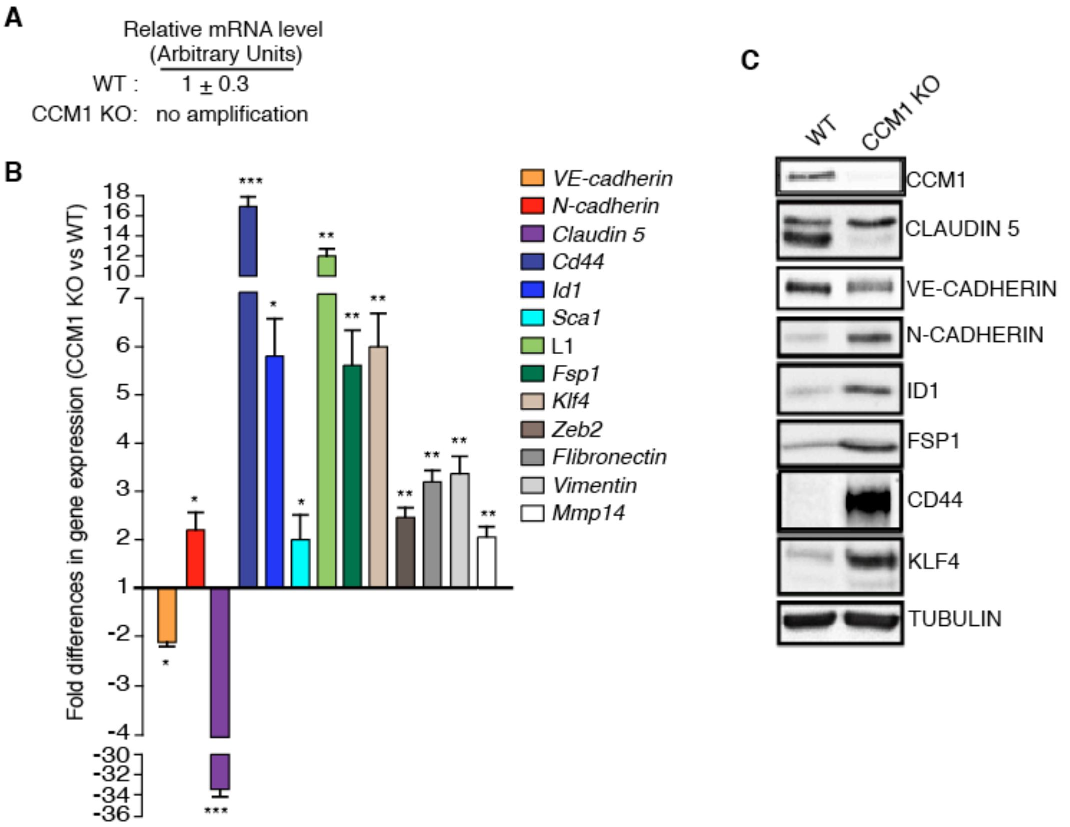

**Figure 16 - *In vitro* endothelial *Ccm1* gene ablation in lung derived ECs induces a mesenchymal and stem cell-like phenotype.**

A) qRT-PCR of *Ccm1* in lung derived WT and CCM1 KO ECs recombinated *in vitro*. B-C) qRT-PCR (B) and WB (C) analysis of EndMT-realted marker expression in WT and CCM1 KO ECs. qRT-PCR data are means ± SD from three independent experiments.*P<0.05; **P<0.01; ***P<0.001. WB results are representative of three independent observation.

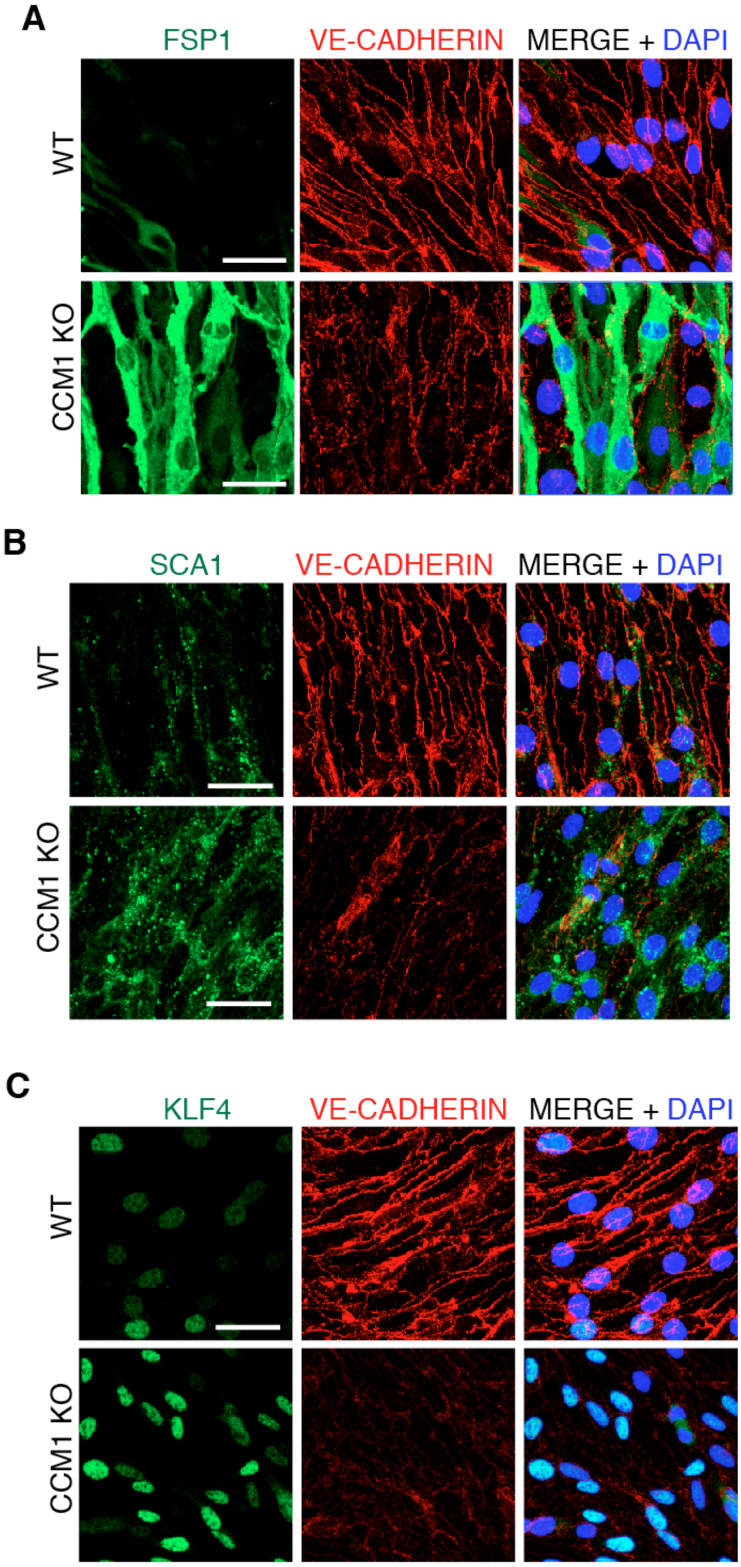
A
FSP1
VE-CADHERIN
MERGE + DAPI
WT
CCM1 KO
B
SCA1
VE-CADHERIN
MERGE + DAPI
WT
CCM1 KO
C
KLF4
VE-CADHERIN
MERGE + DAPI
WT
CCM1 KO

**Figure 17 - Co-expression of VE-CADHERIN and representative EndMT markers in CCM1 KO ECs.** A) Confocal analysis of VE-CADHERIN (red) and FSP1 (green) in cultured lung derived WT and CCM1 KO ECs. B) Confocal microscopy of VE-CADHERIN (red) and SCA1 (green) in the cell lines reported in A. C) Immunofluorescence of VE-CADHERIN (red) and KLF4 (green) in the cell lines reported in A. These data are representative of three independent observations. Scale bar: 30 μm

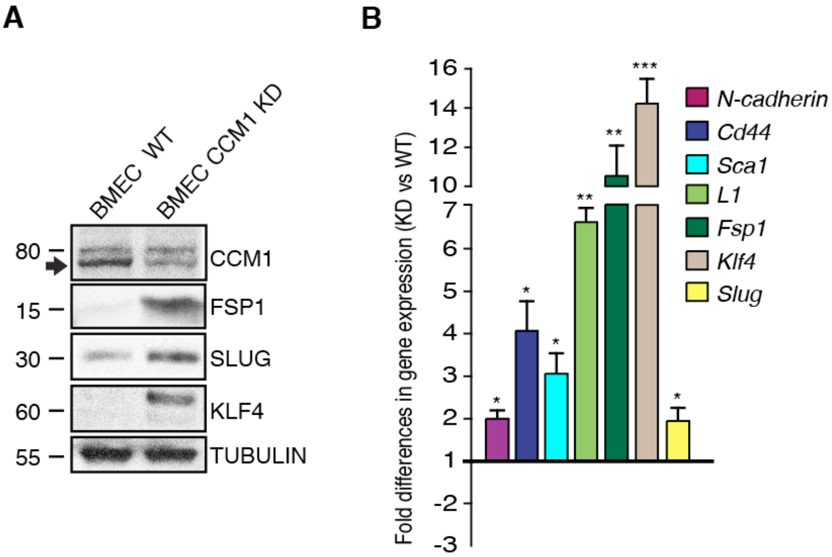

**Figure 18 - Endothelial *Ccm1* gene ablation induces a mesenchymal and stem cell-like phenotype in *vitro* in brain derived ECs (BMECs).**

A) WB of CCM1 and mesenchymal/stem cell markers in WT and CCM1 KD BMECs. Tubulin was the loading control. B) qRT-PCR analysis of several mesenchymal and stem cell expression in WT and CCM1 knocked-down (KD) BMECs. Means ± SD from three independent experiments. Fold changes are relative to WT BMECs *P<0.05; **P<0.01; ***P <0.001.

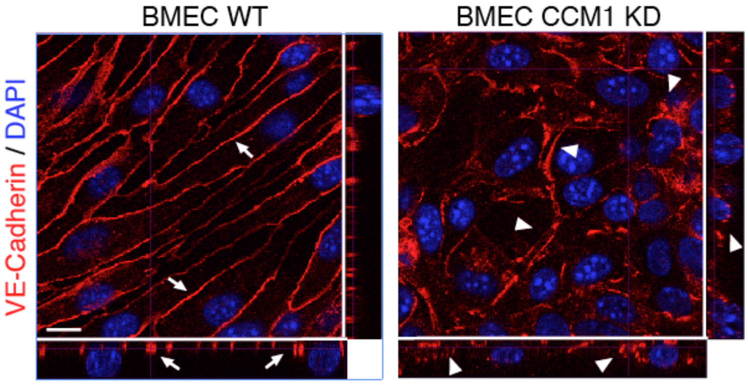

**Figure 19 - Alteration of VE-CADHERIN localization in CCM1 KO BMECs.**

Confocal microscopy analysis of VE-CADHERIN in WT and CCM1 KD BMECs. Arrows: normal VE-CADHERIN localisation at cell-to-cell junctions. Arrowheads: altered VE-cadherin distribution. DAPI visualizes nuclei. Scale bar: 10 µm.

Cell-transition to a mesenchymal phenotype is usually accompanied by increased proliferation, enhanced migratory capacity and invasiveness [114]. Consistently we found that the *Ccm1* gene ablation caused a significant enhancement of EC proliferation both *in vitro* and *in vivo* at the level of vascular lesion, as determined by the staining of the proliferation-associated nuclear protein Ki-67 [283] (Figure 20 A-C). In addition, to test migratory capacity of WT and CCM1 KO ECs, we performed a spheroid assay. A certain number of ECs seeded in a methylcellulose-based medium collagen matrix were allowed to form a 3D spheroid. These spheroids were then transferred in a collagen matrix and stimulated with pro-angiogenic factors such as VEGFA and FGF-2. In line with previous observations obtained in different experimental settings [105], CCM1 KO ECs showed a greater invasive/sprouting capacity in response to VEGF-A/FGF-2 (Figure 21).

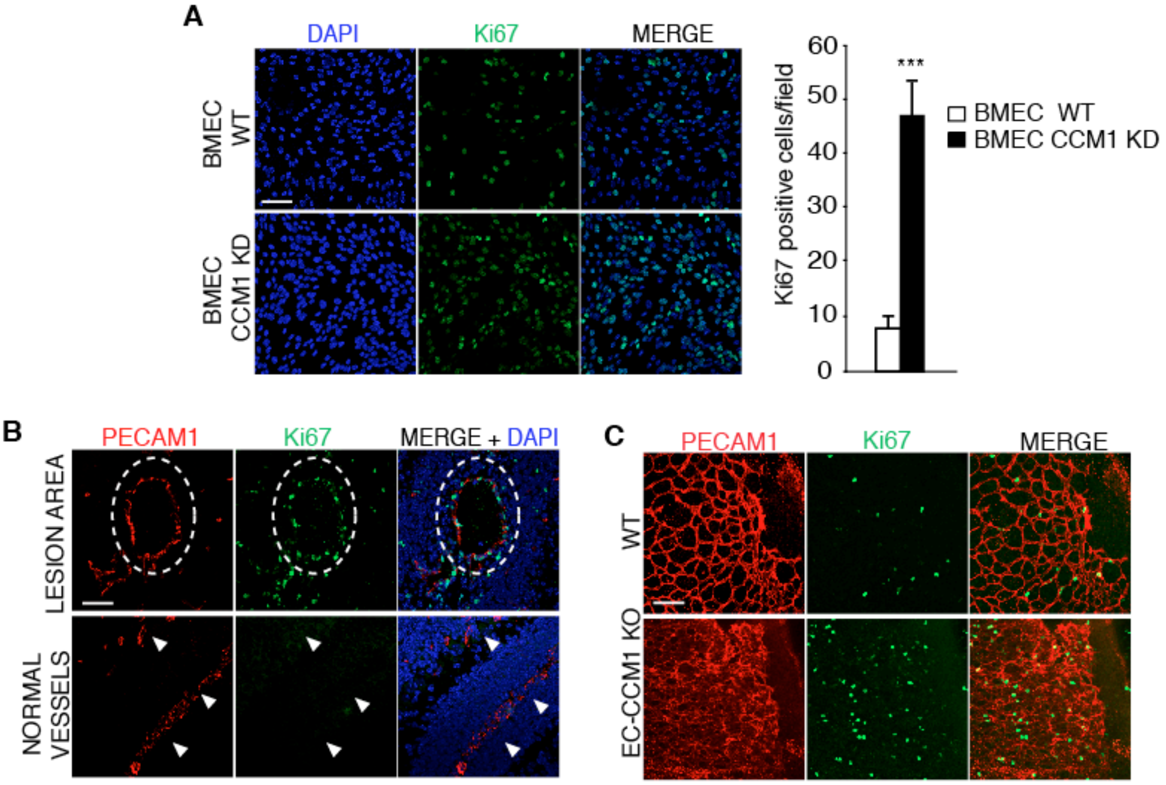
A
DAPI
Ki67
MERGE
BMEC WT
BMEC CCM1 KD
Ki67 positive cells/field
0
10
20
30
40
50
60
***
☐ BMEC WT
■ BMEC CCM1 KD
B
PECAM1
Ki67
MERGE + DAPI
LESION AREA
NORMAL VESSELS
C
PECAM1
Ki67
MERGE
WT
EC-CCM1 KO

**Figure 20 - *Ccm1* gene ablation increases cell proliferation *in vitro* and *in vivo*.**

A) Proliferation of WT and CCM1 KD BMECs was evaluated using Ki-67 staining (green). A representative image was shown. The number of Ki-67 positive cells for each analysed field was indicated in the chart (n=8 fields were analyzed for each cell type). Means ± SD from three independent experiments. ***P<0.001. B-C)

EC proliferation in brain sections (B) and retinas (C) of WT and EC-CCM1 KO mice (P13) analysed by Ki-67 staining. The dotted area showed a vascular lesion formed by proliferating ECs, while arrowheads indicated very limited mitosis in normal brain vessels (PECAM1 staining marks ECs, red; Ki-67, green). Scale bars: 50 μm

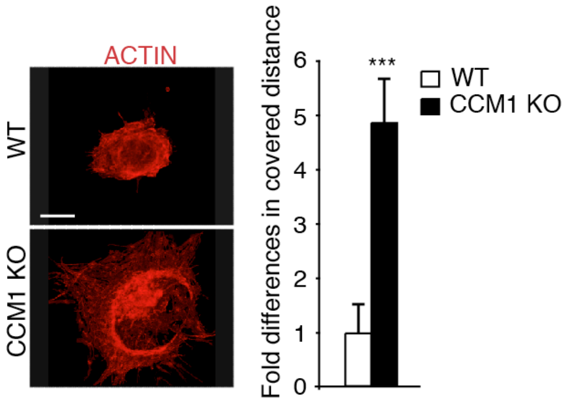

**Figure 21 -** ***Ccm1*** **null ECs shows increased cell migration** ***in vitro*****.**

WT and CCM1 KO lung EC migration in a 3D collagen-based matrix system visualized by actin staining (red). Quantification of the covered migration distance has been represented as fold difference relative wo WT ECs. Data represent the means ± SD from three independent experiments. ***P<0.001. Scale bars: 100 μm.

## 6.4 Activation of the TGF-β signalling contributes to EndMT in CCM1 null ECs

TGF-β/BMP signalling pathway has been suggested as major inducer of EndMT in several physiological and pathological conditions [284]. We therefore investigated whether the EndMT switch observed in CCM1 deficient endothelium was due to an alteration of this signalling pathway. Upon ligand binding, a heterotetrameric complex of type I and II receptors phosphorylates the cytosolic mediator SMADs that, in turn, translocate into the nucleus to regulate the transcription of specific target genes in complex with several transcription factors [126]. As shown in Figure 22 A, both SMAD1/5/8 and SMAD3 phosphorylation was enhanced in CCM1 null ECs. Moreover, in agreement with a possible increased transcriptional activity, immuno-staining revealed a stronger nuclear localization of both pSMAD1 and pSMAD3 in CCM1 KO compared to WT ECs (Figure 22 B).

To investigate the involvement of the activated TGF-β/BMP pathway in the EndMT occurring in CCM1 null ECs, we treated WT and CCM1 KO ECs for 4 days with LY-364947, a selective ATP-competitive of Transforming Growth Factor-β Type I receptor kinase (TβRI ALK5) [285]. The inhibitor abrogated the increased SMAD1 and 3 phosphorylation observed in CCM1-null ECs (Figure 23 A). Most importantly, LY-364947 treatment of CCM1 KO ECs restored in part the normal EC phenotype by significantly decreasing the expression of thr EndMT related transcripts *Fsp1*, *Klf4*, *Cd44*, *Id1* while up-regulating *Claudin5* (Figure 24). Furthermore, we found that LY-364947 inhibited the abnormal proliferation of CCM1 KO ECs (Figure 25).

Overall these results showed that *in vitro* loss of *Ccm1* led to a hyperactivation of TGF-β/BMP signalling that, in turn, was responsible for the EndMT phenotype observed in CCM1 KO ECs.

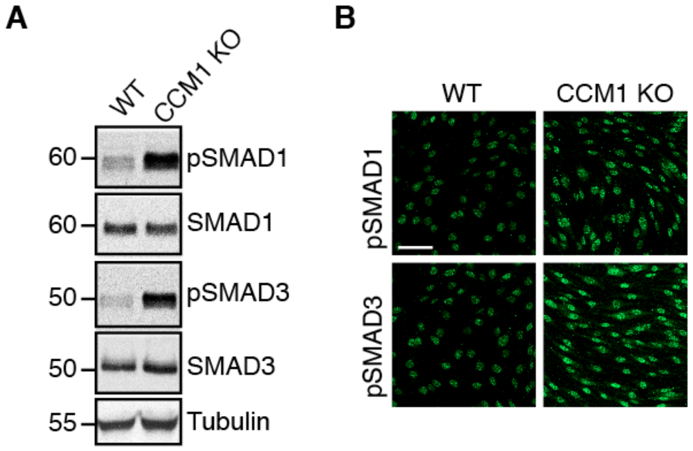
A
B
WT
CCM1 KO
60
pSMAD1
60
SMAD1
50
pSMAD3
50
SMAD3
55
Tubulin
WT
CCM1 KO
pSMAD1
pSMAD3

**Figure 22 - Loss of *Ccm1* induces TGF-b/BMP signalling activation in ECs.**

A) WB analysis of SMAD1/5/8 and SMAD3 phosphorylation and total amount in WT and CCM1 KO ECs. Tubulin was used as loading control. WB results are representative of three independent observations. B) Immunofluorescence analysis of pSMAD1 and pSMAD3 in WT and CCM1 KO lung derived ECs. Images are representative of three independent experiments. Scale bar: 50 µm.

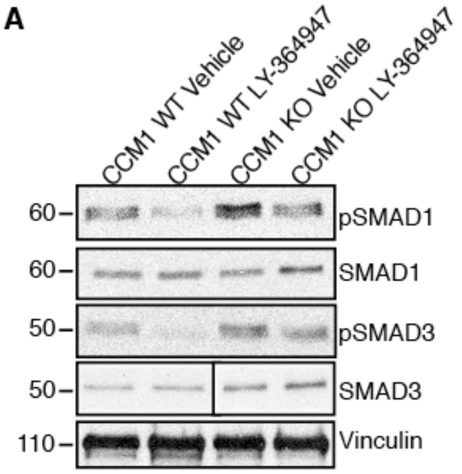
A
CCM1 WT Vehicle
CCM1 WT LY-364947
CCM1 KO Vehicle
CCM1 KO LY-364947
60
pSMAD1
60
SMAD1
50
pSMAD3
50
SMAD3
110
Vinculin

**Figure 23 - The ALK5 inhibitor LY-364947 effectively inhibits SMAD signalling activation in CCM1 KO ECs.**

WB analysis of pSMADs after LY-364947-mediated TGF-β pathway inhibition. Vinculin was used as loading control. Images are representative of three independent experiments.

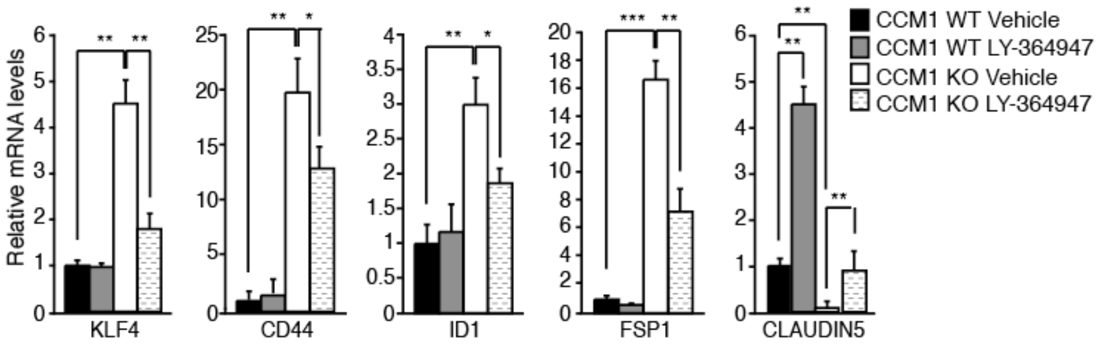

**Figure 24 - *Ccm1* deletion induces EndMT via TGF-b/BMP signalling activation.**

qRT-PCR analysis of the effect of the treatment of LY-364947 on the expression of *Klf4*, *Claudin-5*, *Cd44*, *Id1* and *Fsp1* in WT and CCM1 KO ECs. Data represent the means ± SD from three independent experiments. *P<0.05; **P<0.01; ***P<0.001.

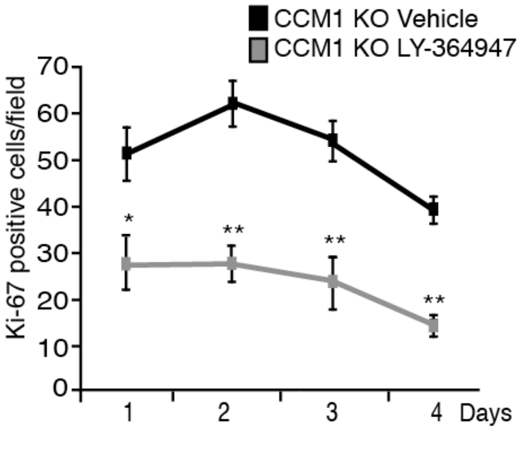

**Figure 25 - Inhibition of TGFβ/BMP signalling decreases the proliferation rate of CCM1 KO ECs.**

Proliferation of vehicle- or LY-364947-treated CCM1 KO ECs quantified by counting Ki-67-positive cells (n=8 fields for each treatment). Data are mean ± SD from three independent experiments. *P<0.05; **P<0.01.

### 6.5 TGF-β/BMP signalling and EndMT are critical events for development and progression of CCM lesions

To investigate the role of the activation of TGF-β/BMP signalling in the appearance and progression of CCM pathology, we tried to inhibit this pathway *in vivo*. To this purpose WT and EC-CCM1 KO pups were treated daily with LY-364947 two days after tamoxifen injection (performed at P1) and then sacrified at P13 to evaluate the number/size of vascular lesions together with the inhibition of pSMAD-depedent signalling. Pilot experiments using doses of this inhibitor reported in literature to be active *in vivo* (5mg/kg or 10 mg/kg) revealed only a partial inhibition of the TGF-β/BMP signalling that was accompanied by a mild reduction in lesion burden of EC-CCM1 KO mice (Figure 26 A, right panel). Therefore in order to achieve a more robust inhibition of TGF-β/BMP signalling we decided to combine the treatment of LY-364947 with SB-431542, another inhibitor of pSMAD signalling reported to be very effective *in vivo* [293]. The animals were subjected to a daily treatment with 10mg/Kg of LY-364947 plus 10mg/kg of SB-431542 two days after tamoxifen injection (performed at P1). As expected, vehicle-treated mice presented at P13 large and frequent cerebellar lesions, with associated diffuse hemorrhagic zones. In contrast, LY-364947/SB-431542-treated pups showed a macroscopic reduction in the number and extension of the lesions and associated hemorrhage (Figure 26 A). Since CCM lesions are higly permeable [286], we tested also the effect of TGF-β/BMP pathway inhibition on vascular permeability by injecting IP fluorescent cadaverine two hours before mouse sacrifice at P13 [287]. As reported in Figure 26 B, *Ccm1* depletion resulted in marked cadaverine extravasation that was almost abrogated by LY-364947/SB-431542 treatment, thus suggesting that inhibition of the TGF-β/BMP pathway not only reduced number and size of lesions, but also restored a normal BBB function by strongly decreasing the marked brain vascular leakage observed in EC-CCM1 KO mice. To test whether LY-364947/SB-431542 treatment was able to effectively inhibit TGF-β/BMP signalling dependent EndMT *in vivo*, we analyzed the phosphorylation state of SMAD proteins and the expression of some representative EndMT/stem cell markers by immuno-staining. As shown in Figure 27 (A-C), SMAD3 phosphorylation was markedly downregulated in LY-364947/SB-431542-treated EC-CCM1 KO pups as well as KLF4 and ID1 expression.

Taken together these data showed that pharmacological inhibition of TGF-β/BMP signalling pathway was able to reduce lesion burden and EndMT *in vivo* in *Ccm1* null mice.

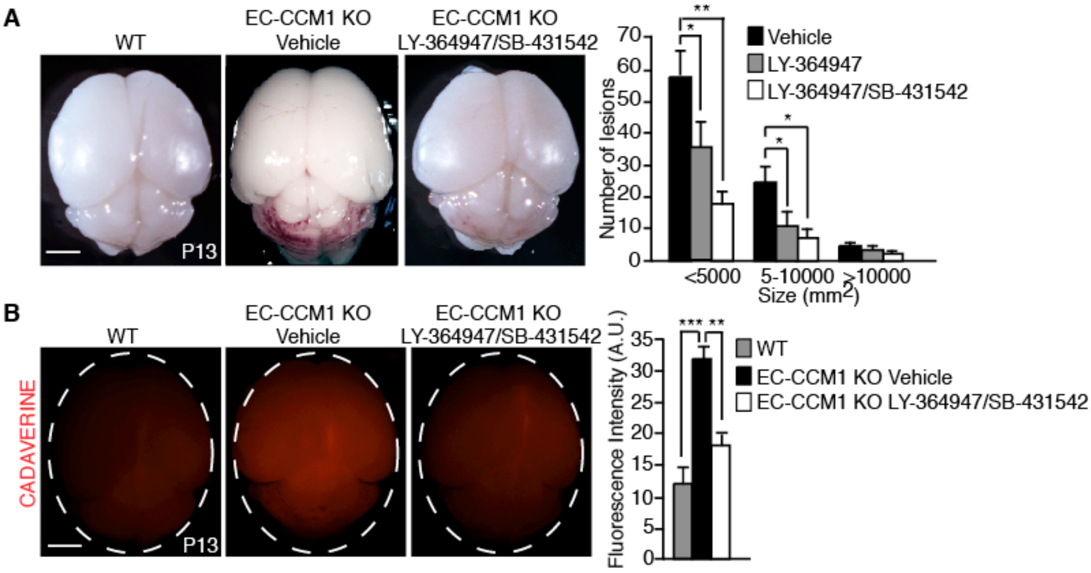

**Figure 26 - TGF-b/BMP signalling inhibition reduces number and size of lesions and vessel leakage in CCM1 null mice.**

A) Representative images of either WT or EC-CCM1 KO vehicle-treated and LY-364947/SB-431542-treated mouse brains after dissection (left panels) and quantification of number and size of lesions (right panel) (n = 5 in each group from three different litters). B) Whole brains photographed after fluorescent cadaverine injection of mice treated ad reported in A (left panels) and quantification of the recovered fluorescence (right). Data are mean ± SD from three independent experiments. *P<0.05; **P<0.01; ***P<0.001. Scale bar: 500 μm.

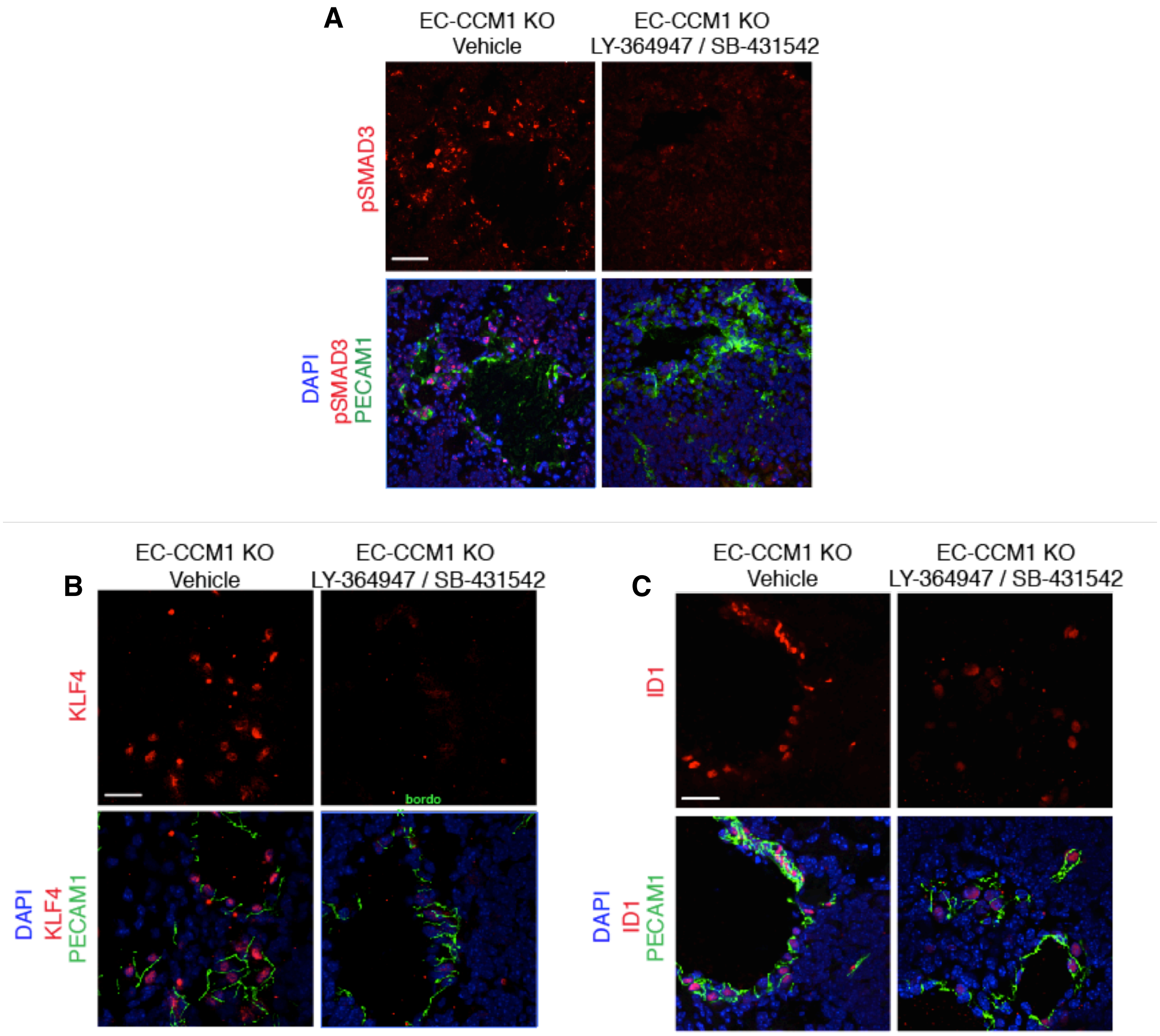
A
EC-CCM1 KO
Vehicle
EC-CCM1 KO
LY-364947 / SB-431542
pSMAD3
DAPI
pSMAD3
PECAM1
B
EC-CCM1 KO
Vehicle
EC-CCM1 KO
LY-364947 / SB-431542
KLF4
bordo
DAPI
KLF4
PECAM1
C
EC-CCM1 KO
Vehicle
EC-CCM1 KO
LY-364947 / SB-431542
ID1
DAPI
ID1
PECAM1

**Figure 27 - TGF-β/BMP signalling inhibition reduces the mesenchymal phenotype of ECs lining CCM lesions *in vivo*.**

(A-C) Confocal analysis of pSMAD3, KLF4 and ID1 in the cavernomas of vehicle- and LY-364947/SB-431542-treated EC-CCM1 KO mice. (PECAM1 identifies ECs, green; KLF4, ID1, pSmad3 red; DAPI visualized nuclei, blue). Images are representative of three independent experiments. Scale bars: 50 µm (A) 30 µm (B, C).

## 6.6 Autocrine production of BMP6 in CCM1 null ECs induces pSMAD signalling activation and EndMT

In order to understand the molecular mechanism through which loss of CCM1 induced TGF-β/BMP signalling and EndMT, we investigated whether ablation of CCM1 could modulate the expression of TGF-β/BMP superfamily ligands, receptors and other critical components of this signalling pathway (such as the common partner SMAD4 or the known negative regulators such as SMURFs). Among all the genes examined only *Bmp6* ligand was significantly increased after CCM1 ablation in cultured ECs (Figure 28 A, B). Interestingly *Bmp6* upregulation was confirmed also *in vivo* in EC-CCM1 KO mice in comparison to WT animals as verified by qRT-PCR analysis performed on RNA extracts of PECAM1 positive freshly isolated brain ECs (Figure 28 C). BMPs are secreted proteins that, upon binding to their receptors, signal through both autocrine and paracrine mechanisms by phosphorylating SMADs [289]. Since BMPs have been associated with EMT [290], we hypothesized that the increased amount *Bmp6* could be responsible of TGF-β/BMP signalling activation and EndMT in CCM1 null ECs. In agreement with this hypothesis the treatment of WT ECs with recombinant BMP6 resulted in an increased SMADs phosphorylation (Figure 29) together with a significant induction of mesenchymal and stem cell markers and a reduction of claudin5 expression (Figure 30). In order to prove that increased SMAD phosphorylation and EndMT marker upregulation in CCM1 KO ECs were BMP6-dependent, we performed siRNA mediated knockdown of *Bmp6 in vitro*. Interestigly, *Bmp6* silencing resulted in decreased phosphorylation state of both SMAD1 and SMAD3 proteins, with a concomitant reduction of the mesenchymal/stem cell markers upregulated in the absence of CCM1 (Figure 31).

Altogether our data suggested that loss of CCM1 increased *Bmp6* expression that, in turn, strongly contributed to the observed EndMT.

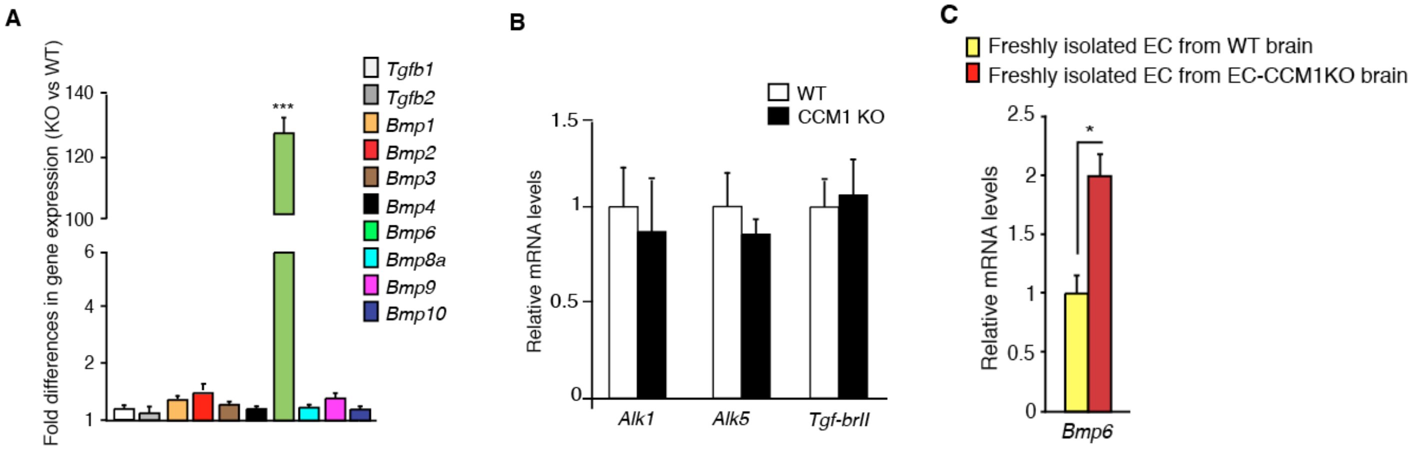

**Figure 28 - *Bmp6* expression is upregulated upon loss of *Ccm1 in vitro* and *in vivo***

A) TGFb/BMP superfamily ligand gene expression profile in WT and CCM1 KO ECs (fold changes in CCM1 KO versus WT). Data are mean ± SD from three independent experiments. B) qRT-PCR analysis of *Alk1*, *Alk5* and *Tgf-brII* in WT and CCM1 KO ECs. Means ± SD from three independent experiments. C) qRT–PCR analysis of *Bmp6* in freshly isolated brain ECs from WT and EC-CCM1 KO mice. Data are mean ± SD from three independent observations. $^{*}P< 0.05$;$^{**}P< 0.01$; $^{***}P< 0.001$.

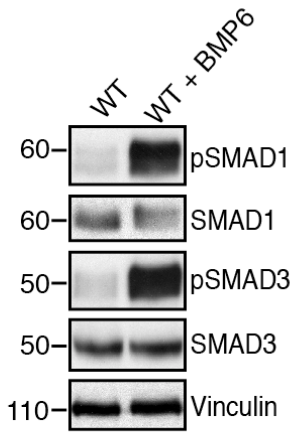

**Figure 29 - BMP6 stimulation induces SMAD phosphorylation in WT ECs.**

WB analysis of SMAD1 and SMAD3 phosphorylation upon 4 hours of treatment of WT ECs with 100ng/ml of recombinant BMP6. Vinculin was the loading control. Images are representative of three independent observations.

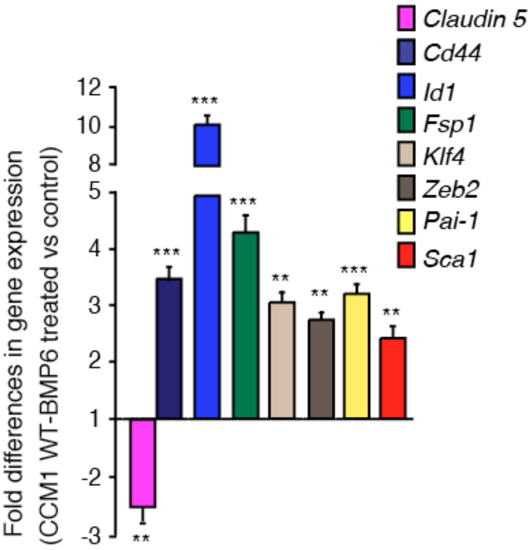

**Figure 30- BMP6-mediated upregulation of mesenchymal and stem-cell makers in WT ECs.**

qRT-PCR analysis of mesenchymal and stem-cell markers upon 96 hours of recombinant BMP6 stimulation. Fold changes in gene expression in BMP6-treated versus control. Data are mean ± SD from three independent experiments. *P <0.05;**P<0.01; ***P<0.001.

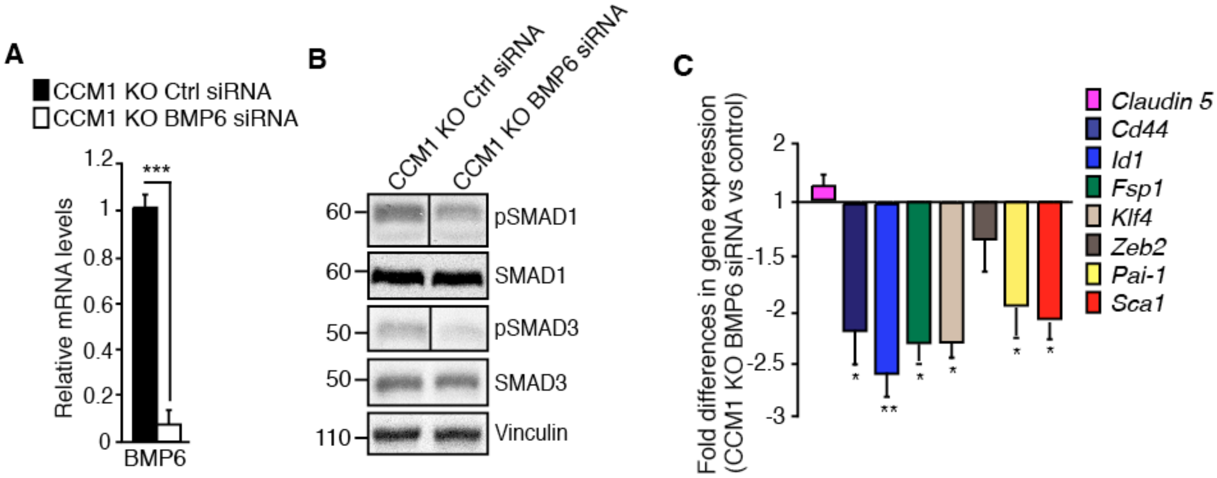

**Figure 31 - *Ccm1* deletion induces TGFb/BMP signalling activation and EndMT via BMP6 upregulation.**

A) *Bmp6* relative mRNA levels in both *Bmp6* and control (ctrl) short interfering RNA siRNA-treated CCM1 KO ECs. Data are mean ± SD from three independent experiments. B) WB analysis of SMAD phosphorylation in *Bmp6* and control (ctrl) short interfering RNA (siRNA)-treated CCM1 KO ECs. Vinculin was the loading control. WB data are representative of three experiments. C) qRT-PCR of EndMT markers in *Bmp6* and control siRNA-treated CCM1 KO ECs. Fold change in *Bmp6* siRNA versus control. Data are mean ± SD from three independent experiments. *P <0.05;**P<0.01; ***P<0.001.

### 6.7 KLF4 expression is increased in murine models of CCM disease and in CCM patients

In order to identify upstream regulators of *Bmp6* expression and TGFβ/BMP signalling activation we performed a global gene expression analysis of CCM1 KO BMECs in comparison to WT using the Affymetrix chip platform. When ranked according to fold change, the transcription factor KLF4 emerged as one of the most significantly upregulated gene upon *Ccm1* gene recombination (Appendix Table 1). As reported above KLF4 was the only analyzed EndMT marker poorly expressed in brain vessels of WT mice (Figure 15 I), while strongly upregulated not only in ECs lining the cavernae of any size but also in peri-lesion vessels that still did not show any abnormal phenotype at the time of the analysis (Figure 15 H). This preliminary observation led us to hypothesize KLF4 up-regulation upon loss of *Ccm1* as an event preceding the formation of vascular lesions, thus suggesting KLF4 as a good candidate for the induction of both TGFβ/BMP activation and EndMT. Further characterization of KLF4 expression *in vivo* revealed that KLF4 was poorly expressed in the retinal vessels of WT mice, while its expression was strongly increased in lesion and peri-lesion vessels located both at the centre and at the periphery of the retina vasculature in EC-CCM1 KO mice (Figure 32). *Klf4* upregulation was an early event during CCM pathogenesis since it appeared at P3, soon after *Ccm1* gene recombination, in freshly isolated ECs from EC-CCM1 KO brains compared to WT brain ECs and it remained high during the disease progression (Figure 33). The increase in KLF4 and its pattern of expression *in vivo* in ECs lining the lesions as well as in pseudonormal peri-lesion vessels were further confirmed in tamoxifen-inducible endothelial-specific *Ccm2* (EC-CCM2 KO) and *Ccm3* (EC-CCM3 KO) loss-of-function mice [69, 92] (Figure 34). Consistently, *in vitro* siRNA mediated knockdown of any one of the three *Ccm* genes in cultured ECs resulted in *Klf4* upregulation (Figure 35). Interestingly, the increase in KLF4 was observed also in cultured human brain ECs (hCMEC/D3) upon *Ccm1* silencing (Figure 36) and, most importantly, immunohistochemical analysis of tissue biopsies of

CCM1 familial and sporadic patients confirmed the increase of KLF4 nuclear signal in ECs lining the cavernomas in comparison to normal peri-lesion vessels used as internal control (Figure 37).

Taken together, these data showed that KLF4 upregulation is an hallmark of murine models of CCM disease as well as of the human pathology. KLF4 expression was already increased at early stages during the development and progression of the disease and is detectable also in pseudo-normal peri lesion vessels, thus prompting us to investigate a possible causal role of KLF4 during CCM pathogenesis.

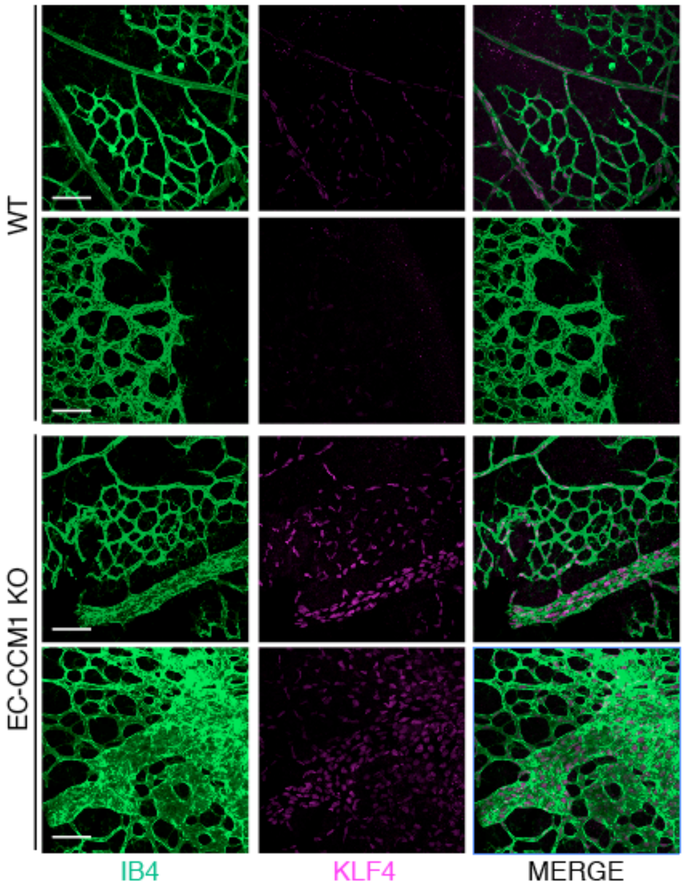

**Figure 32 - KLF4 expression is increased in the retina of EC-CCM1 KO mice.**

KLF4 staining (magenta) in WT and EC-CCM1 KO mouse retinas at P7. ECs are marked by IB4 (green). Data are representative of three independent observations (n = 4 for each genotype from 2 different litters). Scale bars: 50 μm.

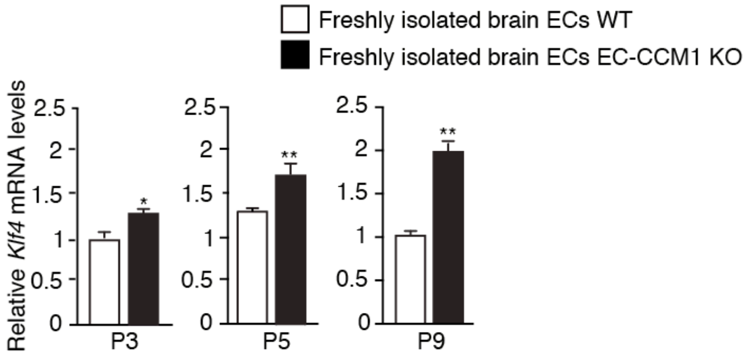

**Figure 33 - *Klf4* is upregulated at an early stage of CCM disease progression *in vivo*.**

qRT-PCR analysis of *Klf4* at different times (P3, P5 and P9) during disease progression after tamoxifen-induced *Ccm1* recombination in freshly isolated brain ECs derived from WT and EC-CCM1 KO pups. Data are mean ± SD (n=3 in each group). Fold changes are relative to WT animals. * P<0.05, **P<0.01

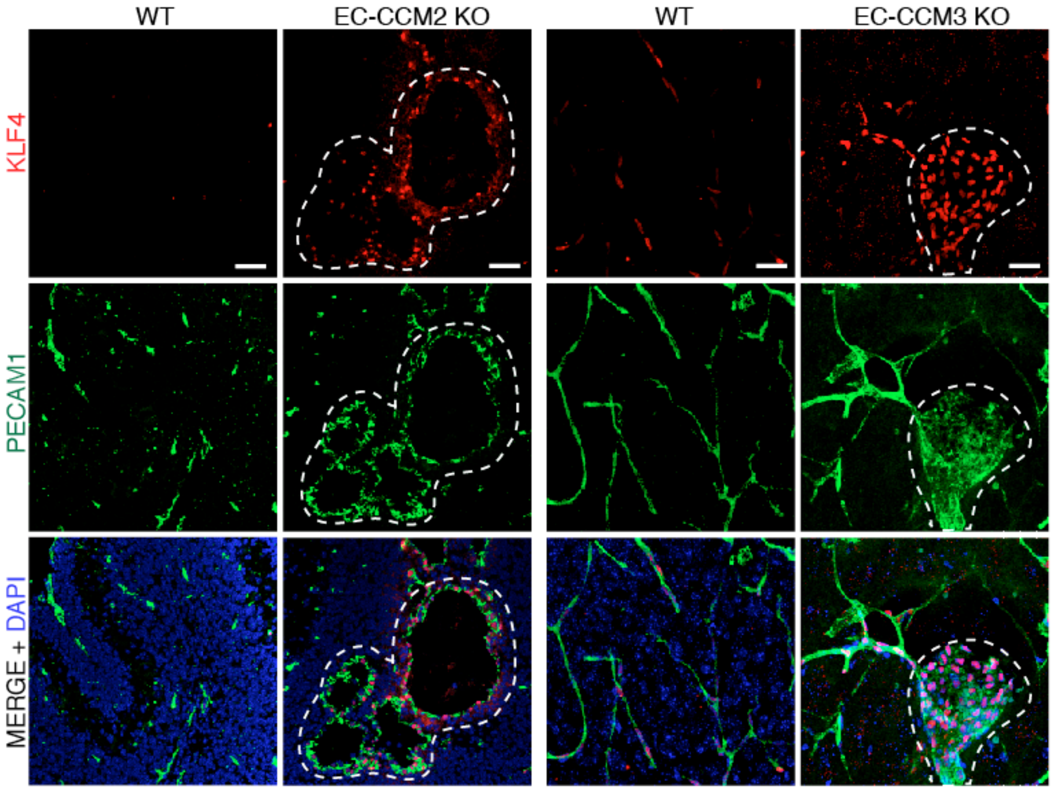

**Figure 34 - Endothelial-specific ablation of either *Ccm2* or *Ccm3* induces KLF4 upregulation in the brain vasculature.**

Representative immunostaining of KLF4 (red) in combination with PECAM1 (green, to identify ECs) in brain sections of EC-CCM2 KO, EC-CCM3 KO mice and their relative WT controls (one out of three performed). Cell nuclei are visualized with DAPI; dotted area highlights lesion area. Scale bars: 50µm.

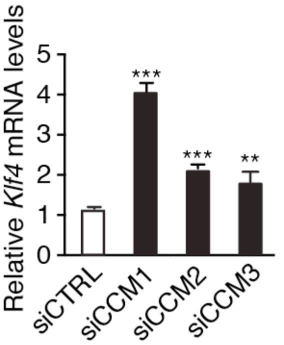

**Figure 35 - Silencing of any of the three *Ccm* genes leads to *Klf4* upregulation *in vitro*.**

qRT-PCR analysis of *Klf4* in lung derived WT ECs transfected with either siRNA directed to anyone of the three *Ccm* genes or control siRNA (siCTRL). Data are presented as mean ± SD (n=3). Results are shown as fold changes relative to control siRNA treated ECs. **P<0.01; ***P<0.001.

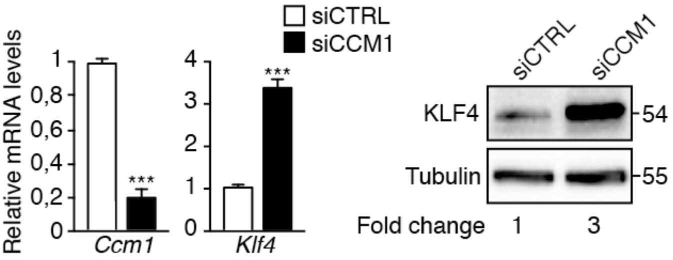

**Figure 36 - KLF4 upregulation upon *Ccm1* silencing is conserved in brain ECs of human origin.**

Left panel: *Ccm1* and *Klf4* relative mRNA levels in *Ccm1* (siCCM1) and control (siCTRL) siRNA-treated hCMEC/D3. The result was shown as fold changes in gene expression in siCCM1-treated versus control. Data are presented as mean ± SD (n=3). ***P<0.001. Right panel: WB analysis of KLF4 amount in both siCCM1- and siCTRL-treated hCMEC/D3. Tubulin was used as loading control. KLF4 normalized over tubulin was quantified by densitometry scan. These data are representative of three independent observations.

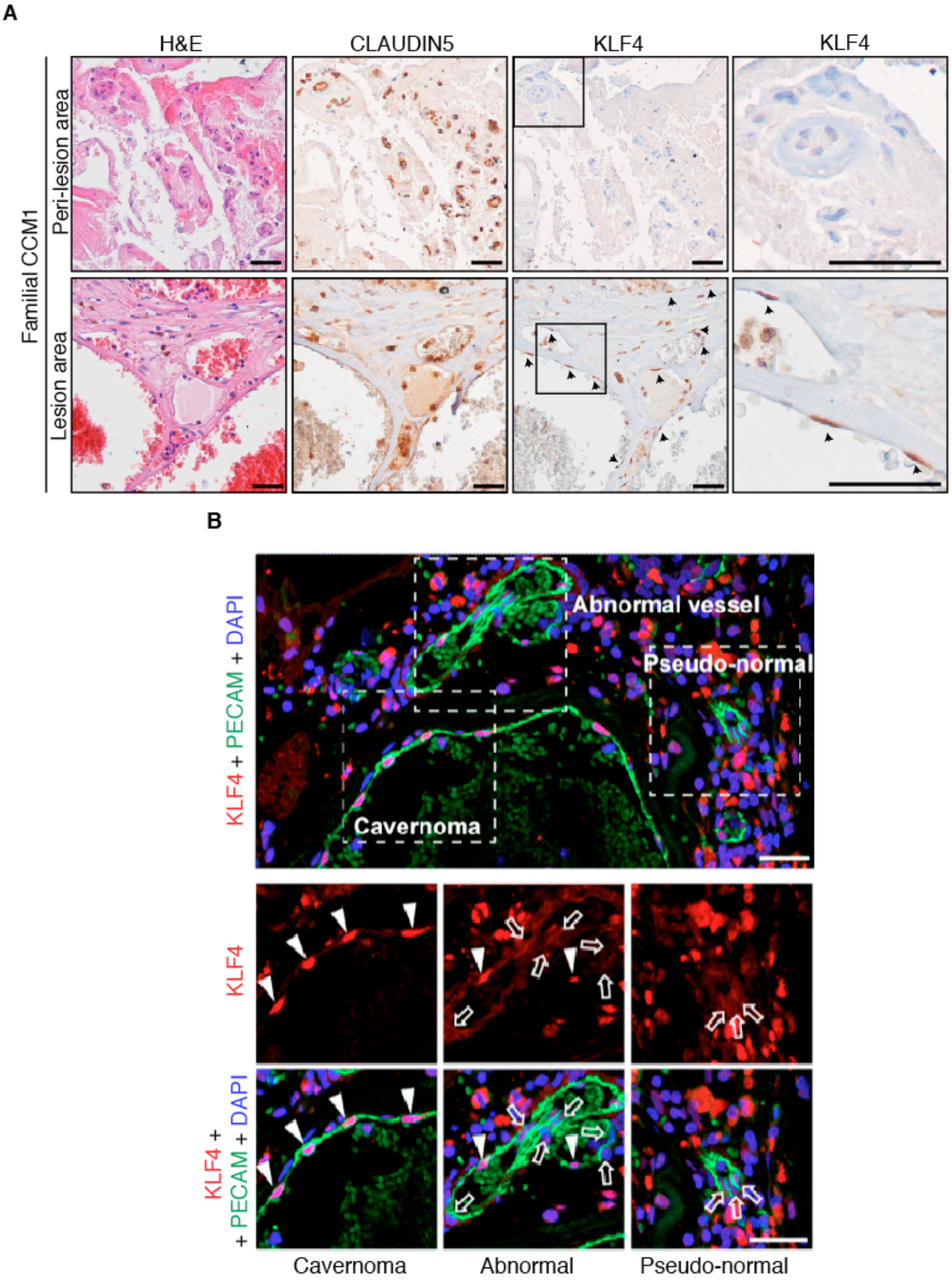
A
H&E
CLAUDIN5
KLF4
KLF4
Familial CCM1
Peri-lesion area
Lesion area
B
KLF4 + PECAM + DAPI
Abnormal vessel
Pseudo-normal
Cavernoma
KLF4
KLF4 + PECAM + DAPI
Cavernoma
Abnormal
Pseudo-normal

**Figure 37 - The increase of KLF4 in ECs lining the cavernomas is observed in familial and sporadic CCM patients.**

A) Immunohistochemical analysis performed on serial sections of brain tissue derived from a familial CCM1 patient. Hematoxilin and Eosin (left panels), CLAUDIN5 (central panels) and KLF4 (right panels) stainings were performed in brain lesion and normal peri-lesion vessels as control brain tissue. Higher magnification images of KLF4 staining of the boxed regions are shown. CLAUDIN5 identifies ECs and arrowheads mark endothelial KLF4 positive nuclei. Scale bar: 100 µm. These data are representative of three independent observations. B) Immunofluorescence analysis of KLF4 expression (red) on sections of brain tissue derived from a sporadic CCM patient. Arrowheads indicate KLF4 positive EC nuclei; arrows highlight KLF4-

negative EC nuclei. Images are representantive of three independent observations. Single staining for KLF4 of boxed areas is shown on the right. PECAM1 (green) marks endothelial cells. DAPI visualises cell nuclei. Arrows identify peri-lesion pseudo-normal vessels. Scale bar: 30 μm.

### 6.8 KLF4 is a causative factor for the development and progression of CCM lesions

In order to study the role of KLF4 in the development of CCM malformations, we generated both endothelial-specific tamoxifen-inducible *Ccm1* and *Klf4* double loss of function mice (EC-CCM1 KO KLF4 KO) and *Ccm1* loss of function mice heterozygous for *Klf4* (EC-CCM1 KO KLF4 HET) [219, 260, 291]. As previously described, the newborn mice were tamoxifen-injected at P1 to induce expression of Cre-recombinase and endothelial-specific gene ablation. The pups were analyzed within two weeks upon gene recombination. *Ccm1* deletion was comparable in freshly isolated brain ECs derived from EC-CCM1 KO, EC-CCM1 KO KLF4 HET and EC-CCM1 KO KLF4 KO animals at P12 (Figure 38). *Klf4* expression was almost completely abrogated in the double KO pups as verified by qRT-PCR (Figure 38) and immunofluorescence (Figure 39 B). EC-CCM1 KO KLF4 KO mice showed a macroscopic reduction in the number, size and extension of the CCM vascular malformations in the cerebellum (Figure 39 A-C). Quantification of the number of cavernomas of any size revealed a 70% reduction in EC-CCM1 KO KLF4 KO in comparison to EC-CCM1 mice (Figure 39 C). Very interestingly, abrogation of *Klf4* also reduced by 75% mouse mortality observed in *Ccm1* deficient pups (Figure 40). Notably, in EC-CCM1 KO KLF4 HET mice *Klf4* expression was almost comparable to WT mice as assessed by qRT-PCR while immunofluorescence analysis revealed that endothelial cells lining vascular lesions of EC-CCM1 KO KLF4 HET mice showed a marked KLF4 positivity comparable to the one observed in EC-CCM1 KO mice (Figure 38 and Figure 39 B). EC-CCM1 KO KLF4 HET animals display a milder phenotype characterized by both a partial reduction in lesion burden (that anyway lacked a proper quantification) and a 33% increase in overall mice survival, thus suggesting that the effect of KLF4 activity was gene dosage dependent (Figure 39 A-B and Figure 40).

Since EC-CCM1 KO animals developed vascular malformations also at the periphery of the retinal vascular plexus [69, 291] (Figure 13 A and B), we then analyze the morphology of the retinal vessels by isolectin B4 staining upon *Klf4* gene deletion. Loss of either one or both *Klf4* alleles significantly reduced both the area and the vascular density at the front of malformed *Ccm1* deficient retinal vessels (Figure 41 C and D), while the advancing of the vasculature across the vitreal surface (vascular progression) was not modified by the absence of KLF4 (Figure 41 E). To date no studies in literature analyzed the retinal vascular plexus upon endothelial-specific *Klf4* gene deletion. To this purpose we generated inducible endothelial-specific KLF4 KO (EC-KLF4 KO) mice by crossing tamoxifen-inducible *Cdh5(PAC)*-CreERT2 and *Klf4* floxed/floxed transgenic mice. The newborn mice were tamoxifen-injected at P1 and then analyzed at P6, a stage during which endothelial cells are actively expanding across the superficial layer of the retina [292]. As shown in Figure 42, abrogation of *Klf4* expression *per se* did not significantly alter the vasculature in term of vascular progression, number of branching points and tip cells at the leading edge of the plexus.

In conclusion, our data indicate that KLF4 was strongly required for the development and progression of brain and retina cavernomas in the absence of *Ccm1*.

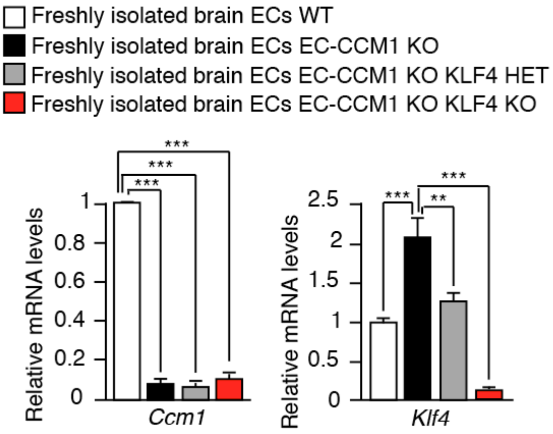

**Figure 38 - Recombination efficiency of *Ccm1* and *Klf4* in the brain vasculature of EC-CCM1 KO, EC-CCM1 KO KLF4 HET and EC-CCM1 KO KLF4 KO mice.**

qRT-PCR of both *Ccm1* and *Klf4* performed in freshly isolated brain ECs derived by WT, EC-CCM1 KO, EC-CCM1 KO KLF4 HET and EC-CCM1 KO KLF4 KO pups at P12. Data are mean ± SD (n=3 for each genotype). Fold difference in gene expression are relative to WT mice. *P<0.05; ** P<0.01; ***P<0.001.

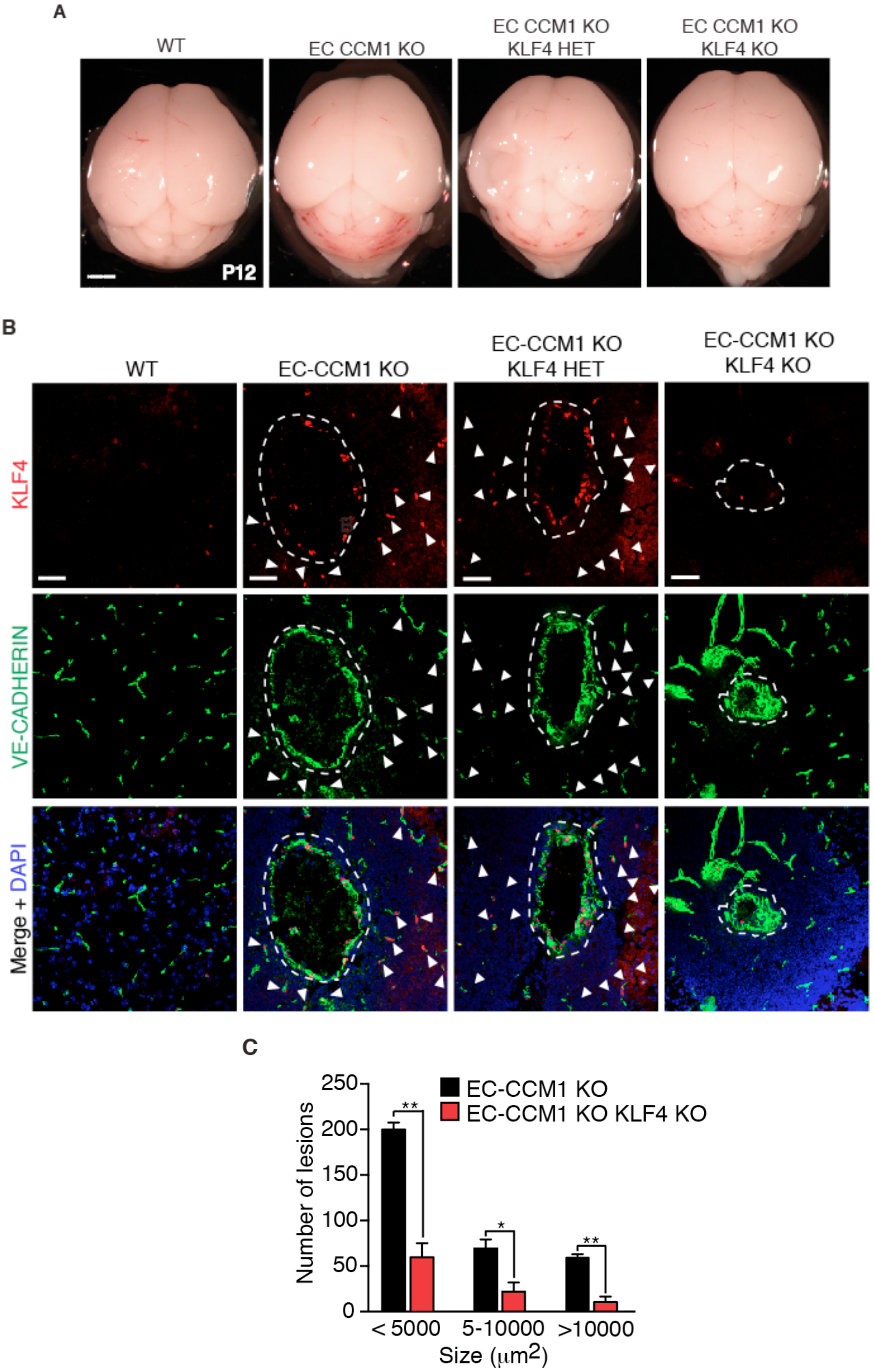
A
WT
EC CCM1 KO
EC CCM1 KO KLF4 HET
EC CCM1 KO KLF4 KO
P12
B
WT
EC-CCM1 KO
EC-CCM1 KO KLF4 HET
EC-CCM1 KO KLF4 KO
KLF4
VE-CADHERIN
Merge + DAPI
C
Number of lesions
250
200
150
100
50
0
EC-CCM1 KO
EC-CCM1 KO KLF4 KO
**
*
**
< 5000
5-10000
>10000
Size (μm2)

**Figure 39 - KLF4 is determinant for CCM development and progression *in vivo*.**

A) Representative images of WT, EC-CCM1 KO, EC-CCM1 KO KLF4 HET and EC-CCM1 KO KLF4 KO mouse brains at P12 (n=5 for each genotype). Scale bar: 500 μm. B) Representative confocal analysis of VE-CADHERIN (green) and KLF4 (red) in vascular lesions (dotted area) and pseudo-normal cerebellar vessels (white arrowheads) of WT, EC-CCM1 KO, EC-CCM1 KO KLF4 HET and EC-CCM1 KO KLF4 KO (n=4 in each group). VE-CADHERIN identifies ECs; DAPI visualizes nuclei. Scale bar: 50 µm. C) Quantification of number and size of vascular lesions in the cerebellum of both EC-CCM1 KO and EC-CCM1 KO KLF4 KO mice at P12. Columns represent means ± SD (n=4 for each genotype from 2 litters). *P<0.05; ** P<0.01.

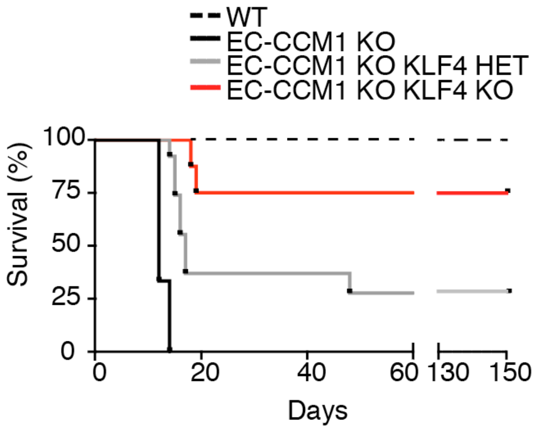

**Figure 40 - Loss of *Klf4* stringly increases survival in *Ccm1* null mice.**

Kaplan–Meier survival curve of WT, EC-CCM1 KO, EC-CCM1 KO KLF4 HET and EC-CCM1 KO KLF4 KO mice (n=8 for each group). P<0.001.

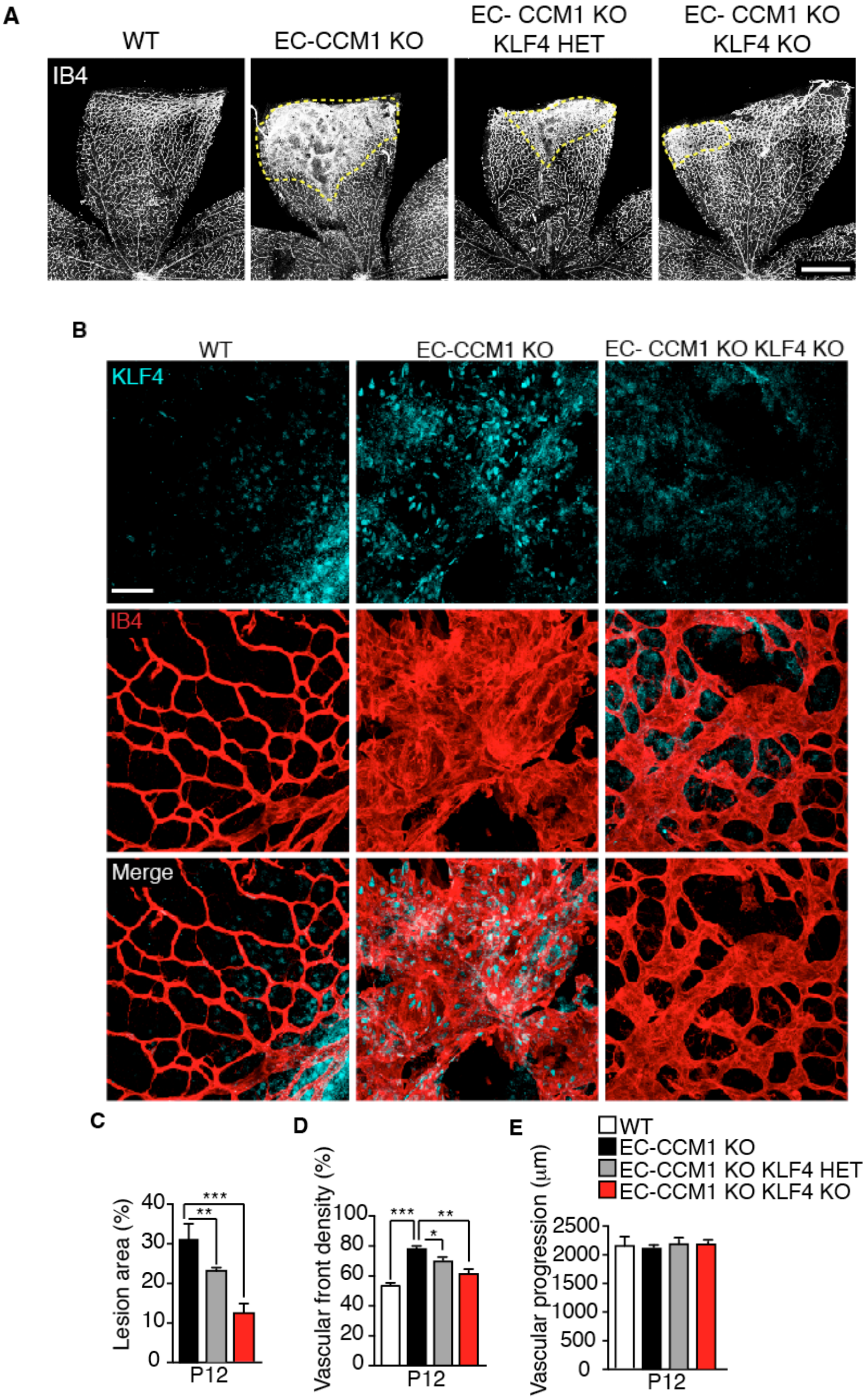
A
WT
EC-CCM1 KO
EC- CCM1 KO KLF4 HET
EC- CCM1 KO KLF4 KO
IB4
B
WT
EC-CCM1 KO
EC- CCM1 KO KLF4 KO
KLF4
IB4
Merge
C
Lesion area (%)
40
30
20
10
0
***
**
P12
D
Vascular front density (%)
100
80
60
40
20
0
***
**
*
P12
E
Vascular progression (µm)
2500
2000
1500
1000
500
0
P12
☐ WT
■ EC-CCM1 KO
▨ EC-CCM1 KO KLF4 HET
🟥 EC-CCM1 KO KLF4 KO

**Figure 41 - *Klf4* is critical for cavernoma development in the retina in the absence of *Ccm1*.**

A) Isolectin B4 staining (IB4, used to identify vasculature) on WT, EC-CCM1 KO, EC-CCM1 KO KLF4 HET and EC-CCM1 KO KLF4 KO retinae at P12. Dotted area highligths macroscopic differences in the extension of CCM lesion area between EC-CCM1 KO, EC-CCM1 KO KLF4 HET and EC-CCM1 KO KLF4 KO mice. Images are representative of 5 mice for each genotype. B) Representative immunostaining (one out of three performed) for KLF4 (light blue) in the retinae of WT, EC-CCM1 KO and EC-CCM1 KO KLF4 KO mice. Vasculature at the periphery of the retina is shown after isolectin B4 staining (red). C-E) Quantification of several vascular parameters in retinae from WT, EC-CCM1 KO, EC-CCM1 KO KLF4 HET and EC-CCM1 KO KLF4 KO mice at P12. Data are mean ± SD (n=5 for each genotype from 3 different litters). C) Percentage of retinal area covered by vascular lesions. D) Vascular front density at the leading edge of the plexus. E) Average distance covered by the growing vessels measured as vascular progression. Scale bar: 500 μm (A), 60 μm (B).$^{**}P<0.01$, $^{***}P<0.001$

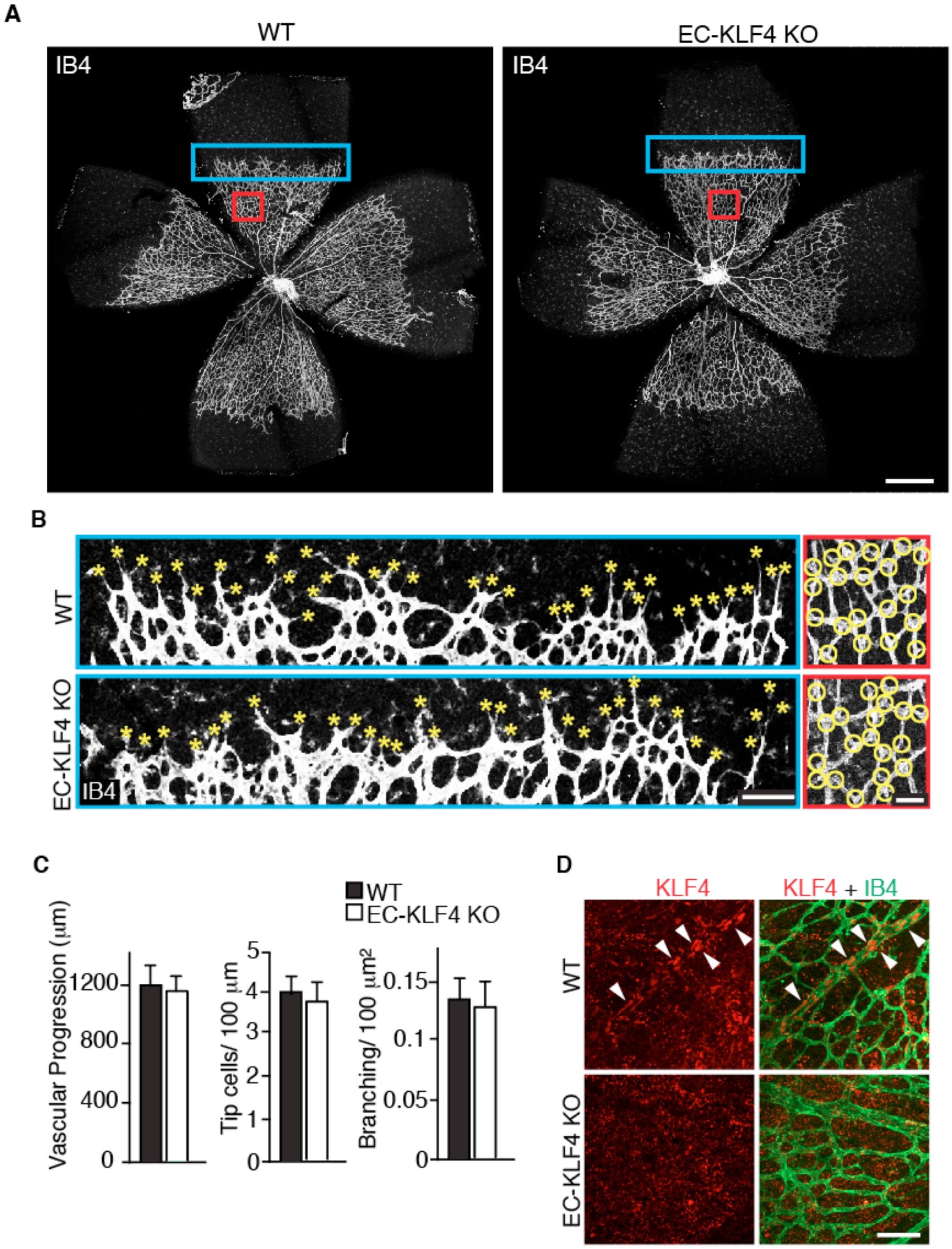
A
WT
EC-KLF4 KO
IB4
IB4
B
WT
EC-KLF4 KO
IB4
C
WT
EC-KLF4 KO
Vascular Progression (μm)
1200
800
400
0
Tip cells/ 100 μm
5
4
3
2
1
0
Branching/ 100 μm2
0.15
0.1
0.05
0
D
KLF4
KLF4 + IB4
WT
EC-KLF4 KO

**Figure 42 - The vasculature of the retina is not altered in the absence of KLF4.**

A) Isolectin B4 staining (IB4, used to identify vasculature) on WT and EC-KLF4 KO retinae at P6. Images are representative of 5 mice for each genotype. Scale bar: 300 μm. B-C) Quantification of several vascular parameters (vascular progression, number of tip cells and branching points) in the retinae from WT and EC-KLF4 KO mice at P6. Data are mean ± SD (n=5 for each genotype from 3 different litters). B) Higher magnification pictures of the blue and red boxed areas shown in A and used as representative images for quantification of both number of tip cells (indicated by yellow asterisks) and branching points (indicated by yellow circles) in the retinal vasculature of WT and EC-KLF4 KO animals. Scale bars: 30 μm (blue boxes) and 20 μm (red boxes). C) Quantification of the average distance covered by the growing vessels measured as vascular progression (left panel), number of tip cells in 100 μm at the leading edge of the plexus (middle panel) and number of branchings in 100 $\mu m^2$ area (right panel). D) Representative immunostaining (one out of three performed) for KLF4 (red) in the retinae of WT and EC-KLF4 KO mice to show gene ablation. Vasculature of the retina is stained with IB4 (green). Scale bar: 40 μm.

## 6.9 KLF4 induces EndMT in CCM1 null ECs *in vitro*

Endothelial-specific deletion of *Ccm1* gene induces EndMT switch in ECs lining the cavernomas [291]. To investigate whether KLF4 had a key role in this process we stably transduced lung derived WT and CCM1 KO ECs with either a lentiviral vector expressing a short hairpin RNA directed to *Klf4* (shKLF4) or with a lentiviral vector expressing a non-targeting shRNA as control (shCTRL). As depicted in Figure 43, we achieved a 65% knockdown, restoring *Klf4* mRNA and protein level similar to WT ECs (Figure 43 A and B). *Klf4* silencing strongly attenuates the expression of mesenchymal and stem cell markers upregulated in CCM1 KO ECs (Figure 43 A and B), but it was ineffective in restoring the expression of the endothelial junction molecules *VE-Cadherin* and *Claudin5* (Figure 43 A and B).

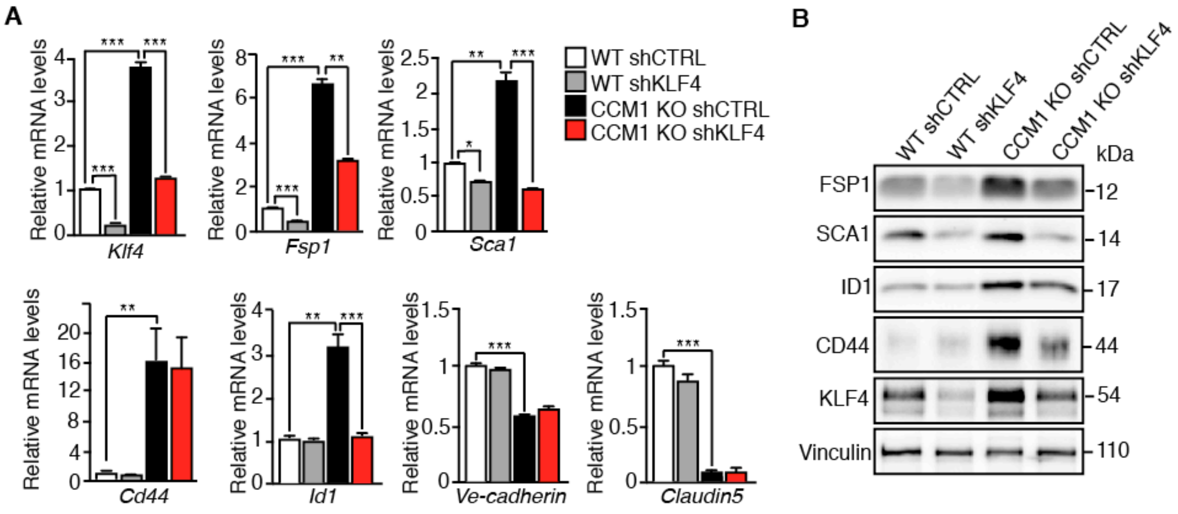

**Figure 43 - *Klf4* silencing inhibits EndMT marker expression in CCM1 KO lung derived ECs.**

A-B) WT and CCM1 KO ECs were lentiviral transduced with shRNA directed to either *Klf4* (shKLF4) or control sequence (shCTRL). A) qRT-PCR of mesenchymal (*Fsp1, Id1*), stem cell-like (*Sca1*) and endothelial markers (*VE-cadherin* and *Claudin5*) in WT shCTRL, WT shKLF4, CCM1 KO shCTRL and CCM1 KO shKLF4 ECs. Data are mean ± SD (n=3). Fold difference in gene expression are relative to WT shCTRL ECs. $*P<0.05$; $**P<0.01$; $***P<0.001$ B) WB of EndMT markers in WT shCTRL, WT shKLF4, CCM1 KO shCTRL and CCM1 KO shKLF4 ECs. Vinculin was the loading control. These data are representative of three independent observations.

As previously mentioned cell-transition to a mesenchymal phenotype in CCM1 KO ECs is accompanied by increased proliferation and migratory capacity [105, 291]. Interestingly we found that *Klf4* down-regulation in cultured CCM1 KO ECs inhibited ECs proliferation (Figure 44) and migration (Figure 45). Interestingly, in line with what previously reported by Hale et al. [232], *Klf4* silencing impairs proliferation also in WT ECs (Figure 44).

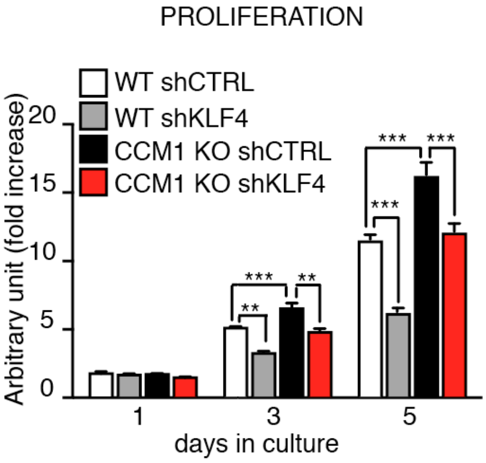

**Figure 44 - Klf4 silencing decreases the proliferation rate of both lung derived WT and CCM1 KO ECs.**

Proliferation rate of WT shCTRL, WTshKLF4, CCM1 KO shCTRL and CCM1 KO shKLF4 ECs cultured for 5 days. Columns represent mean ± SD (n=8). *P<0.05, **P<0.01, ***P<0.001

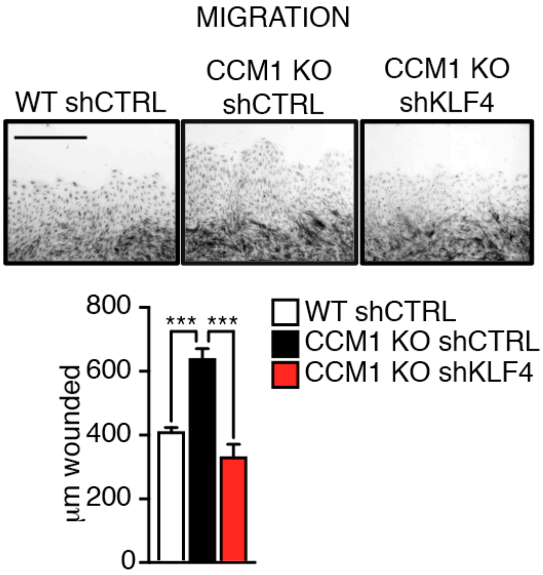

**Figure 45 - KLF4 silencing affects lung derived CCM1 KO ECs migration.**

Migration rate, measured in a wound assay, of WT shCTRL, CCM1 KO shCTRL and CCM1 KO shKLF4 ECs. Mean ± SD is graphed (n=6). Scale bar: 500 µm*P< 0.05, **P<0.01,***P<0.001

To further confirm these data in a more reliable cellular model and to understand whether loss of *Klf4* expression was able to prevent the EndMT process in CCM1 null ECs, we concomitantly deleted *Ccm1* and *Klf4* expression in primary brain derived ECs. Cells were isolated from brain of WT, *Ccm1* floxed/floxed and double *Ccm1-Klf4* floxed/floxed mice and treated with TAT Cre-recombinase *in vitro* to induce recombination of LoxP-site flanked genes (Figure 46 and 47). *Ccm1* deletion was comparable between CCM1 KO and CCM1-KLF4 KO BMECs (Figure 46 A) while, as expected, KLF4 expression was increased in CCM1 KO BMECs and almost abrogated in the double CCM1-KLF4 KO BMECs. Loss of KLF4 prevented the increased expression of mesenchymal and stem cell markers observed in the absence of *Ccm1* as verified by qRT-PCR (Figure 46 A), WB (Figure 46 B) and immunofluorescence analysis (Figure 46 C). Also in this experimental, VE-CADHERIN organization at junctions was not affected by KLF4 depletion (Figure 47), thus suggesting that KLF4 was not involved in junctional disorganization observed in CCM1 null ECs.

To investigate whether KLF4 is sufficient to promote EndMT we infected WT ECs in culture with a lentiviral vector expressing *Klf4* (LentiKLF4) or an empty vector (Mock) as control, achieving a 3-fold *Klf4* induction (Figure 48), a level of upregulation comparable to that observed in CCM1 KO ECs. KLF4 upregulation in WT ECs increased EndMT markers at both mRNA (Figure 48, left panel) and protein level (Figure 48, right panel), whereas it did not affect the expression of the endothelial junction molecules as *VE-cadherin* and *Claudin5* (Figure 48, left panel), confirming that KLF4 did not seem to be involved in junction organization.

Taken together, loss and gain of function approaches showed that KLF4 was necessary to induce EndMT in CCM1 null ECs *in vitro*.

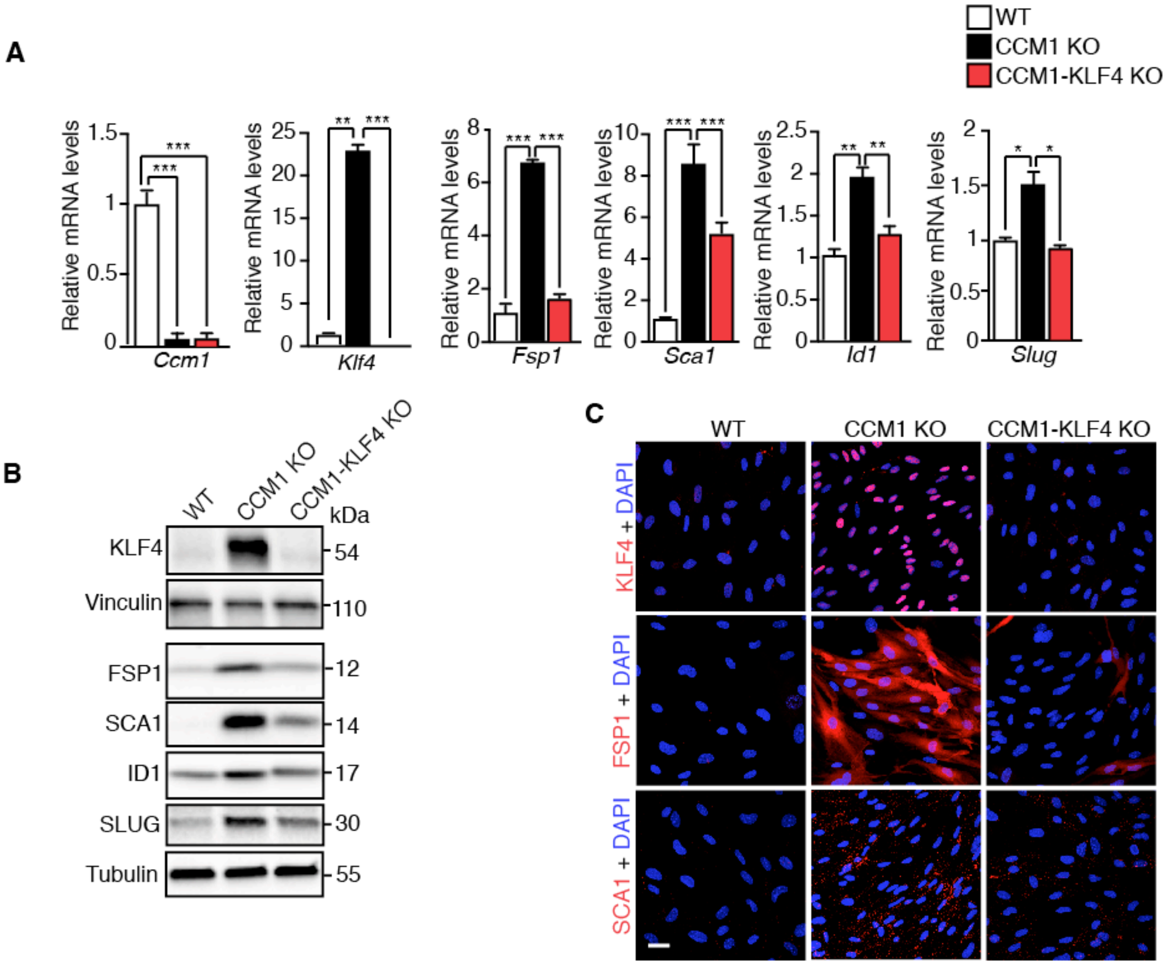

**Figure 46 - Loss of KLF4 prevents the EndMT switch induced by the loss of *Ccm1* in BMECs.**

A) qRT-PCR of *Ccm1*, *Klf4* and several EndMT markers after *in vitro* TAT-Cre recombinase treatment of BMECs from WT, *Ccm*1 floxed/floxed and *Ccm1-Klf4* floxed/floxed mice to originate cultured WT, CCM1 KO and CCM1-KLF4 KO primary brain ECs, respectively. Data are presented as mean ± SD (n=3). Fold changes are relative to WT BMECs. B) WB of KLF4 and EndMT markers in WT, CCM1 KO and CCM1-KLF4 KO BMECs. Tubulin was the loading control. These data are representative of three independent observations. C) Representative confocal analysis (out of three performed) of KLF4, FSP1 and SCA1 (red) in WT, CCM1 KO and CCM1-KLF4 KO BMECs obtained as in A. DAPI visualizes nuclei. Scale bar: 30 µm. *P< 0.05, **P<0.01, ***P<0.001

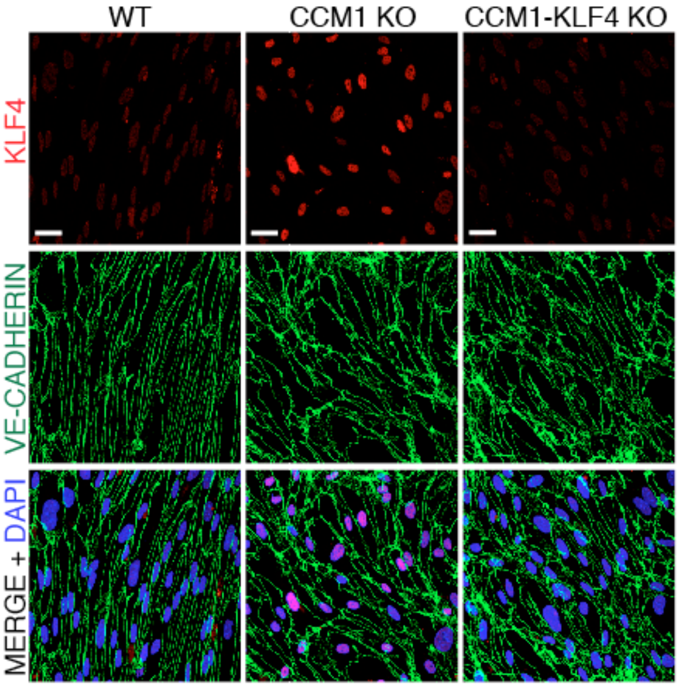

**Figure 47 - *Klf4* gene ablation did not restore the proper VE-CADHERIN localization at the cell-to-cell contacts.**

Representative confocal analysis (out of three performed) of KLF4 (red) and VE-CADHERIN (green) in WT, CCM1 KO and CCM1-KLF4 KO primary brain ECs obtained as in A. DAPI visualizes nuclei. Scale bar: 30 μm.

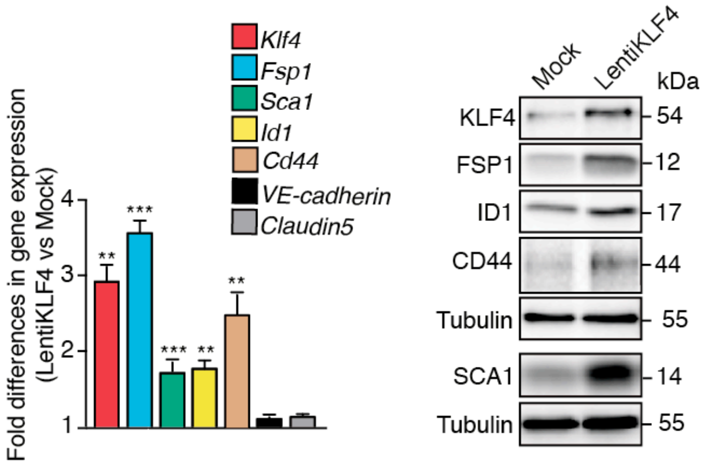

**Figure 48 - KLF4 overexpression induces EndMT marker expression in WT ECs.**

Cultured lung derived WT ECs were lentiviral transduced with a full length murine *Klf4* (LentiKLF4) or empty vector (Mock). qRT-PCR (left panel) and WB (right panel) of EndMT markers in Mock and LentiKLF4 ECs. qRT-PCR data are mean ± SD (n=3) and the fold changes are relative to Mock ECs. WB results are representative of three independent observations. Tubulin was the loading control. *P<0.05, **P<0.01, ***P<0.001

### 6.10 KLF4 induces EndMT in CCM1 null ECs *in vivo* in a context dependent manner

To investigate whether the absence of KLF4 was able to prevent EndMT switch ongoing in the absence of CCM1 *in vivo* [291], we analyzed the expression of a number of mesenchymal and stem-cell markers both in normal cerebellar vessels of WT mice and vascular lesions of EC-CCM1 KO and EC-CCM1 KO KLF4 KO animals. Unlike EC-CCM1 KO mice, immunofluorescence analysis revealed that EC-CCM1 KO KLF4 KO animals developed a limited number of vascular lesions, which were smaller in size and weakly positive for the expression of FSP1, SCA1 and ID1 (Figure 49). A strong reduction in EndMT marker expression was also confirmed *ex vivo* in freshly isolated brain derived ECs from EC-CCM1 KO KLF4 KO mice compared to EC-CCM1 KO (Figure 50 A). Moreover qRT-PCR analysis of freshly isolated brain ECs from EC-KLF4 KO and WT mice showed that abrogation of *Klf4* expression *per se* resulted in reduction of both *Sca1* and *Id1* expression, thus suggesting that KLF4 could modulate the transcription of some of EndMT markers *in vivo* also in normal conditions when *Ccm1* is not deleted (Figure 50 B). A residual amount of EndMT expression in the few small lesions developed in EC-CCM1 KO KLF4 KO mice mice might be ascribable to an incomplete KLF4 recombination. Notably, preliminary immunofluorescence analysis revealed that ECs positive for EndMT markers staining still retained KLF4 (Figure 51 A and B). In this regard, to understand whether KLF4 incomplete recombination is responsible for the development of lesions in EC-CCM1 KO KLF4 KO, it would be important in the future to quantify how many lesions in EC-CCM1 KO KLF4 KO mice still retain *Klf4* expression.

Intriguingly, the role of KLF4 as inducer of EndMT appears strongly cell-context dependent. CCM malformations at the periphery of the retina vasculature are restricted to veins and the surrounding capillaries [69, 92, 291] . By measuring KLF4 intensity in retinal endothelial cell nuclei we observed that KLF4 amount was higher in veins than arteries in both WT and EC-CCM1 KO mice and was further increased at the level of lesion area (Figure 52 A-C). To test whether a higher KLF4 expression correlated with an increased amount of EndMT markers, we performed immunofluorescence staining also for ID1, FSP1 and SCA1 in retinae of WT and EC-CCM1 KO mice at P12. Accordingly, ID1 expression pattern in the retina correlated with KLF4 one (Figure 52 A, B and D), while FSP1 and SCA1 staining did not work properly in retina samples. However this analysis, even if partial, suggested that higher levels of KLF4 in veins may explain the venous origin of the cavernomas.

Moreover, in order to understand the role of KLF4 in the brain vasculature specificity of the disease, we compared freshly isolated endothelial cells derived from brain, lung, heart and spleen of WT and EC-CCM1 KO after gene recombination. In the absence of CCM1, KLF4 expression was almost equally increased in ECs of different origins while among all the EndMT markers analysed only *Sca1* expression was increased also in spleen and in lung of EC-CCM1 KO mice, even if not at comparable levels to brain microvasculature. Since a full EndMT marker upregulation was detected only in brain ECs (Figure 53), it is likely that KLF4 upregulation may require a specific environment in order to induce the acquisition of a mesenchymal phenotype.

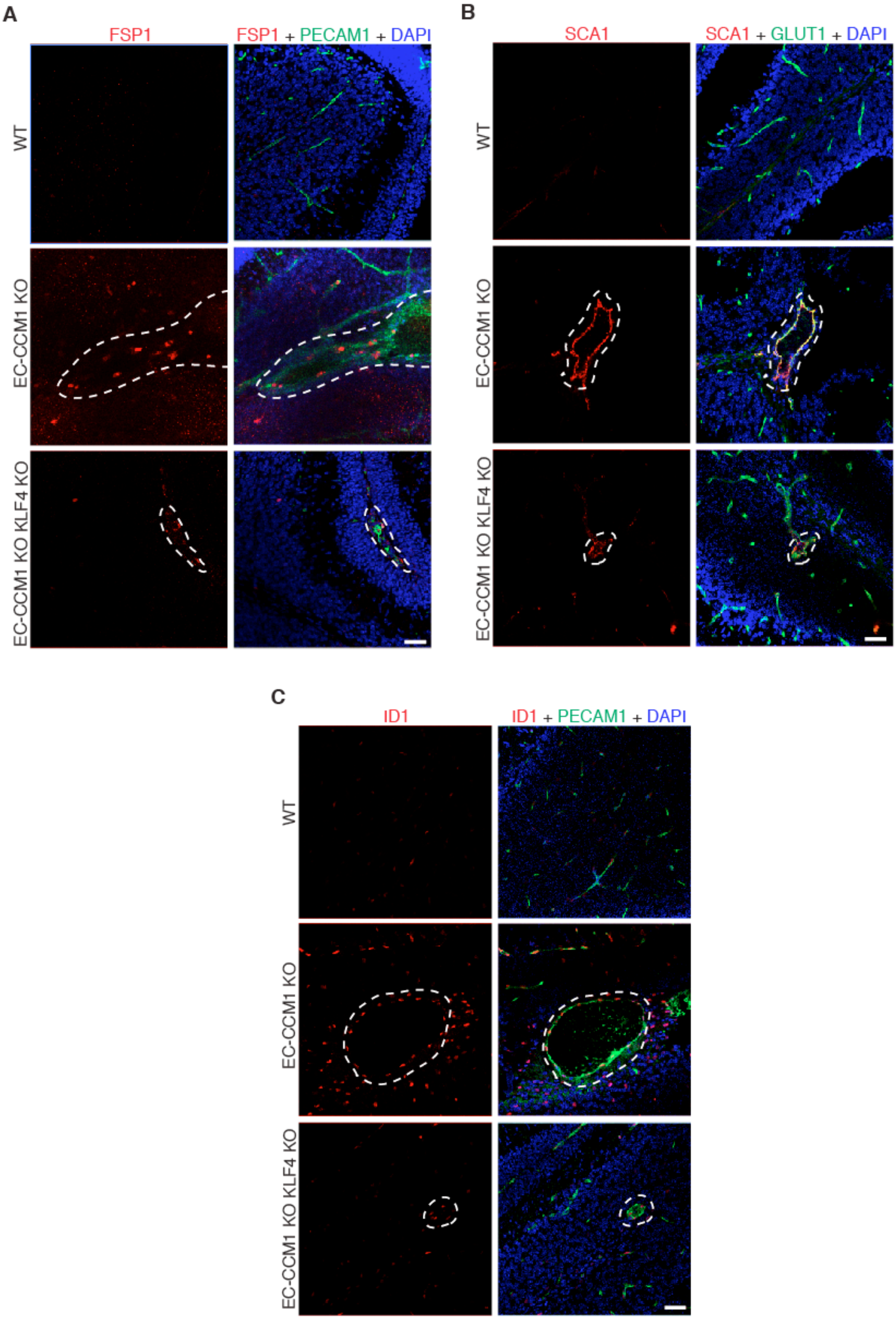
A
FSP1
FSP1 + PECAM1 + DAPI
WT
EC-CCM1 KO
EC-CCM1 KO KLF4 KO
B
SCA1
SCA1 + GLUT1 + DAPI
WT
EC-CCM1 KO
EC-CCM1 KO KLF4 KO
C
ID1
ID1 + PECAM1 + DAPI
WT
EC-CCM1 KO
EC-CCM1 KO KLF4 KO

**Figure 49 - EndMT marker expression is reduced in ECs lining the cavernomas in the absence of *Klf4*.** A) Representative confocal analysis of PECAM1 (green) and FSP1 (red) in normal cerebellar vessels of WT mice and vascular lesions (dotted area) of both EC-CCM1 KO and EC-CCM1 KO KLF4 KO mice (n=4 in each group). PECAM1 identifies ECs; DAPI marks nuclei. B) Representative confocal analysis of GLUT1 (green) and SCA1 (red) in normal cerebellar vessels of WT mice and vascular lesions (dotted area) of both

EC-CCM1 KO and EC-CCM1 KO KLF4 KO mice (n=4 in each group). GLUT1 identifies ECs; DAPI marks nuclei. C) Representative confocal analysis of PECAM (green) and ID1 (red) in normal cerebellar vessels of WT mice and vascular lesions (dotted area) of both EC-CCM1 KO and EC-CCM1 KO KLF4 KO mice. PECAM1 identifies ECs; DAPI visualizes nuclei. Scale bars: 50 µm (B, C, D).

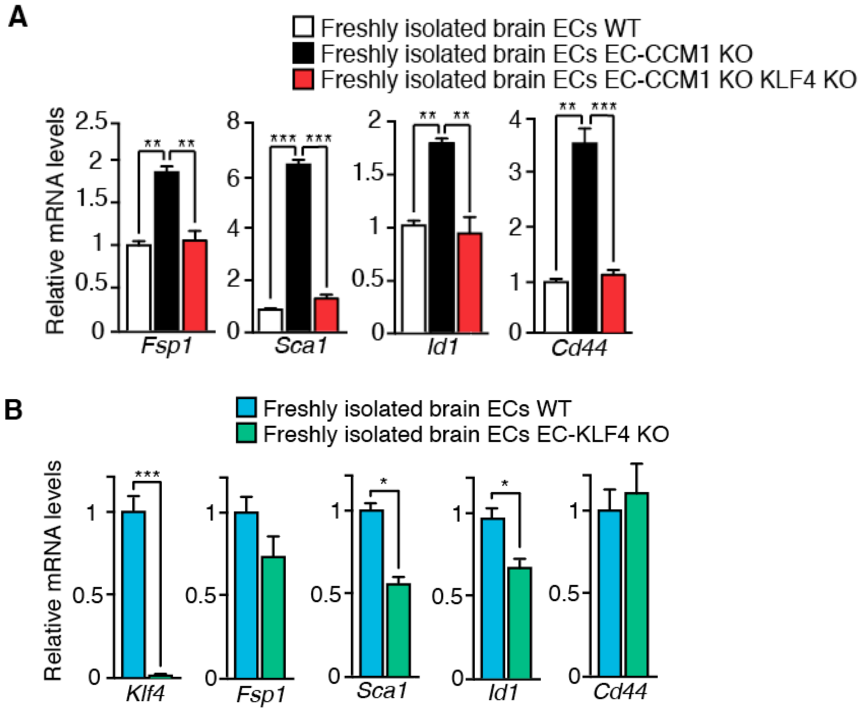

**Figure 50 - EndMT markers gene expression analysis in freshly isolated brain ECs from mice WT or null for *Ccm1*, *Klf4* or both genes**

A) qRT-PCR of some EndMT markers in freshly isolated brain ECs from WT, EC-CCM1 KO and EC-CCM1 KO KLF4 KO mice analyzed at P12. Fold changes are relative to WT animals. Data are mean ± SD (n=3 for each genotype). ** $P < 0.01$, ***$P<0.001$. B) qRT-PCR of some EndMT markers in freshly isolated brain ECs from WT and EC-KLF4 KO mice analyzed at P12. Fold changes are relative to WT animals. Data are mean ± SD (n=3 for each genotype). * $P < 0.05$

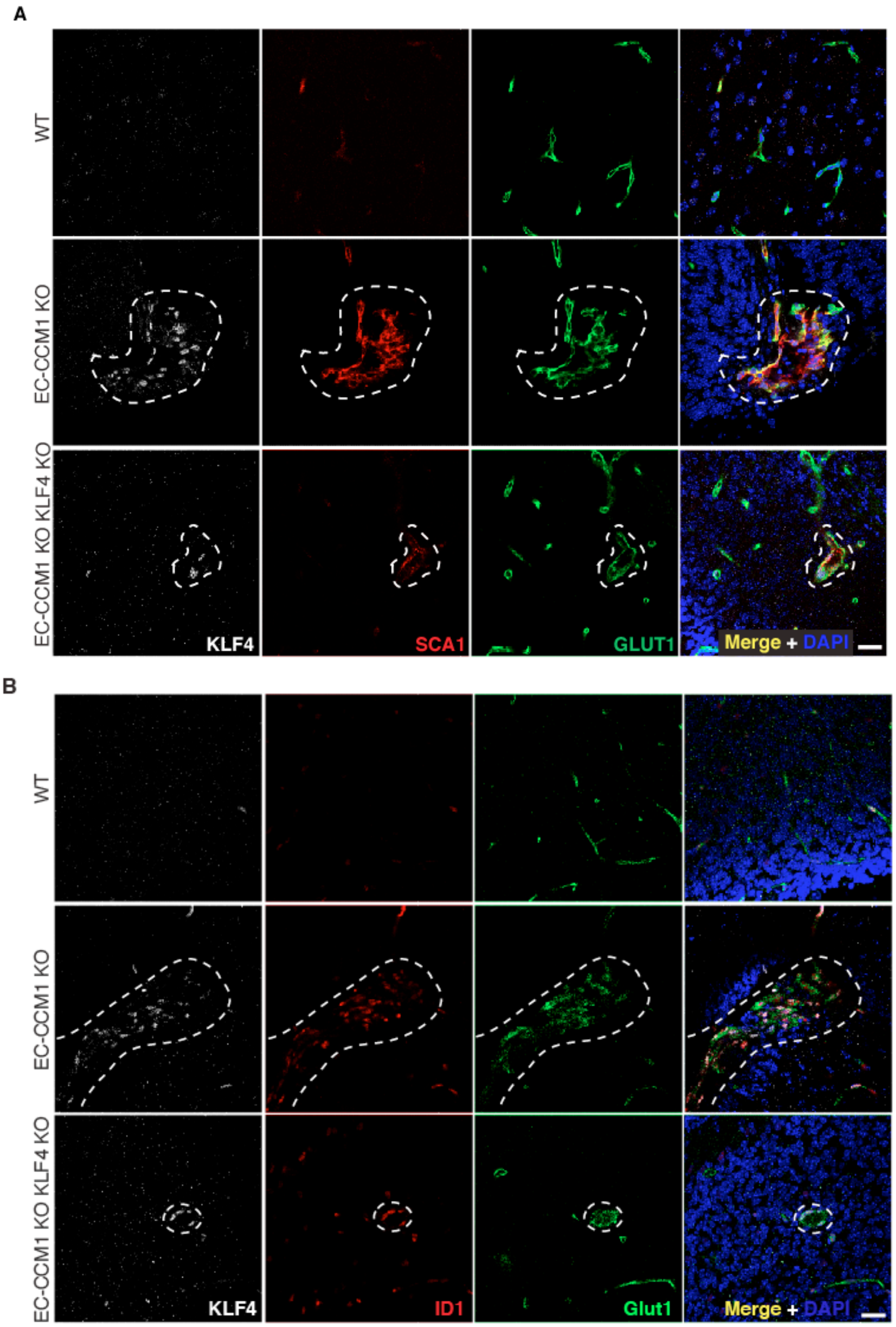
A
WT
EC-CCM1 KO
EC-CCM1 KO KLF4 KO
KLF4
SCA1
GLUT1
Merge + DAPI
B
WT
EC-CCM1 KO
EC-CCM1 KO KLF4 KO
KLF4
ID1
Glut1
Merge + DAPI

**Figure 51 - Incomplete Klf4 gene recombination in ECs lining the vascular lesions of EC-CCM1 KO KLF4 KO mice.**

A) Representative confocal analysis of KLF4 (white), SCA1 (red) and GLUT1 (green) in normal cerebellar vessels of WT mice and vascular lesions (dotted area) of both EC-CCM1 KO and EC-CCM1 KO KLF4 KO mice at p12 (n=4 for each genotype). B) Representative confocal analysis of KLF4 (white), ID1 (red) and GLUT1 (green) in normal cerebellar vessels of WT mice and vascular lesions (dotted area) of both EC-

CCM1 KO and EC-CCM1 KO KLF4 KO mice at p12 (n=4 for each genotype). GLUT1 marks endothelial cells while DAPI visualized nuclei. Scale bar: 20μm

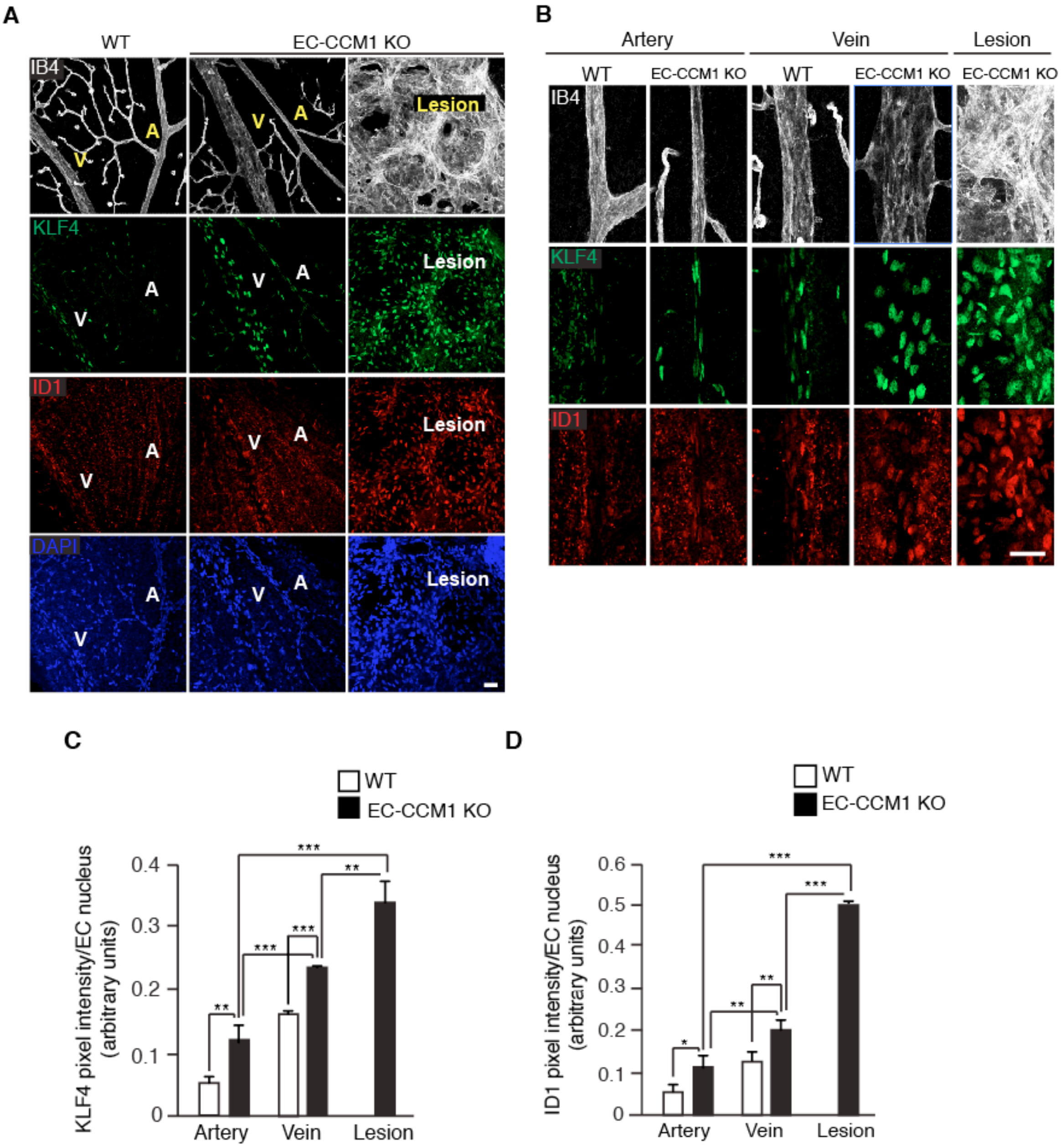
A
WT
EC-CCM1 KO
IB4
KLF4
ID1
DAPI
A
V
Lesion
B
Artery
Vein
Lesion
WT
EC-CCM1 KO
WT
EC-CCM1 KO
EC-CCM1 KO
IB4
KLF4
ID1
C
WT
EC-CCM1 KO
KLF4 pixel intensity/EC nucleus (arbitrary units)
0.4
0.3
0.2
0.1
0
***
**
***
***
**
Artery
Vein
Lesion
D
WT
EC-CCM1 KO
ID1 pixel intensity/EC nucleus (arbitrary units)
0.6
0.5
0.4
0.3
0.2
0.1
0
***
***
**
**
*
Artery
Vein
Lesion

**Figure 52 - KLF4 amount is higher in veins than in arteries of the retinal vasculature in both WT and EC-CCM1 KO mice.**

A) Confocal analysis of isolectin B4 (IB4, white), KLF4 (green) and ID1 (red) in the retinae of WT and EC-CCM1 KO mice at p12. A:artery; V:vein. IB4 identifies the vasculature; DAPI visualizes nuclei. Images are representative of three mice for each genotype. Scale bar: 30 μm. B) Higher magnification images of IB4 (white), KLF4 (green) and ID1 (red) in artery, vein and lesion of WT and EC-CCM1 KO mice retinae at p12.

Scale bar: 30 μm. C) Quantification of the KLF4 pixel intensity per endothelial nucleus in retinal arteries, veins and lesions of WT and EC-CCM1 KO mice. Co-localization highlighter plug in of Image J has been used to identify KLF4 positive pixels co-localizing with DAPI (to exclude background). Mean intensity of co-localizing pixel per field has been calculated through Image J and normalized on the number of endothelial nuclei. Three different fields for three different samples for each group (arteries, veins and lesions) have been analysed. D) Quantification of the ID1 pixel intensity per endothelial nucleus in retinal arteries, veins and lesion of WT and EC-CCM1 KO mice performed as described in C. *P<0.05, **P<0.01, ***P<0.001

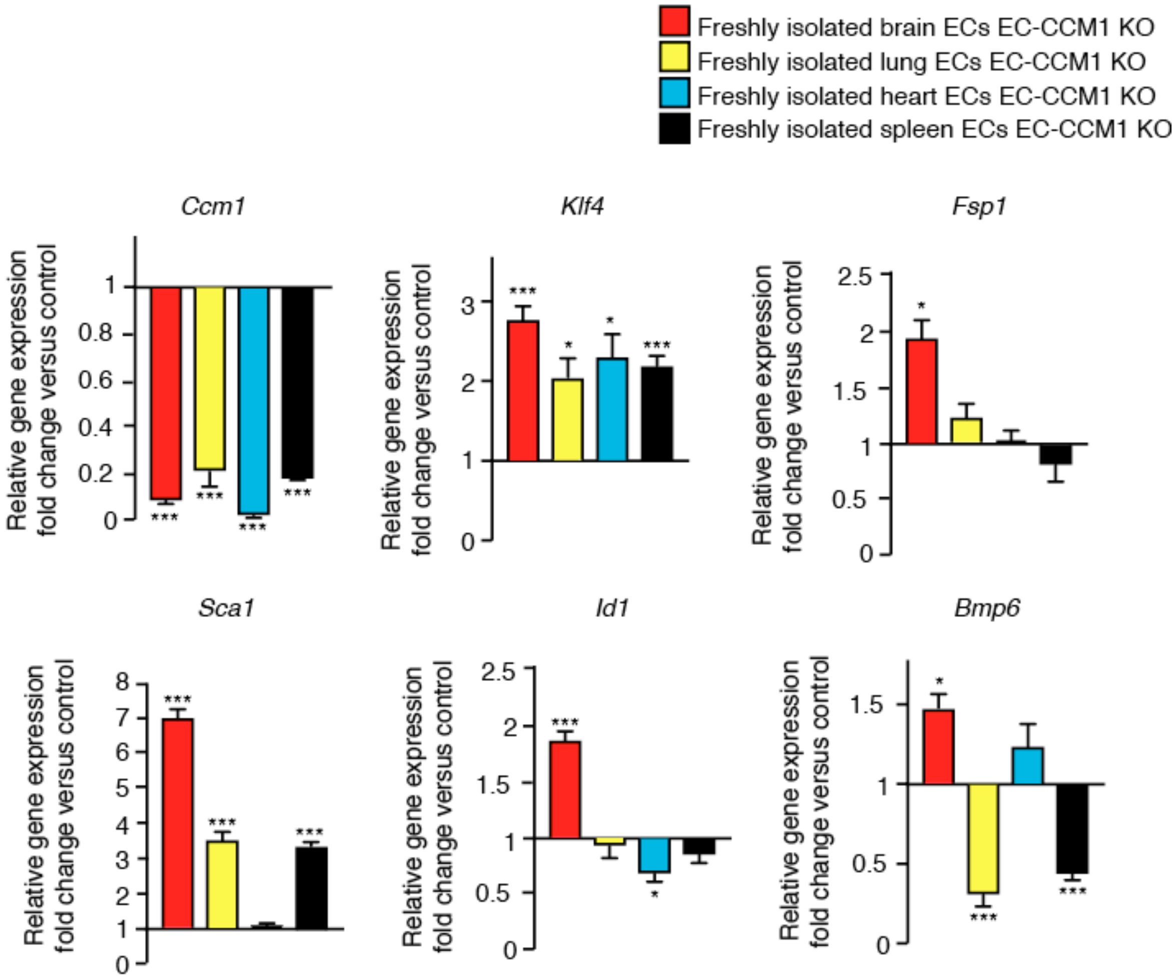

**Figure 53 - EndMT occurs specifically in the brain vasculature of EC-CCM1 KO mice.**

qRT-PCR analysis of *Ccm1*, *Klf4*, *Fsp1, Sca1, Id1* and *Bmp6* in freshly isolated ECs from brain, lung, heart and spleen of WT and EC-CCM1 KO mice at P12. Fold changes are relative to matched WT animals. Data are expressed as fold change versus control WT animals and are means ± SD from at least three mice for group. The SD of values obtained in control mice did not exceed 10% of the mean. *P<0.05, **P<0.01, ***P<0.001

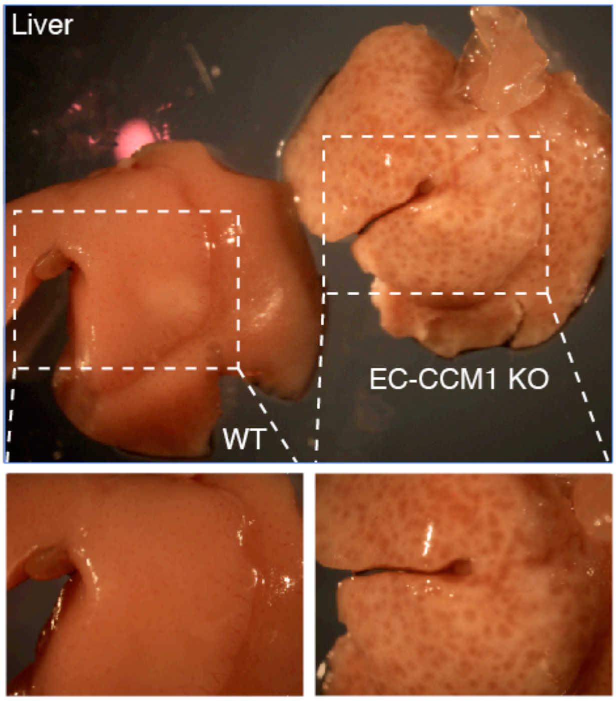

**Figure 54 - Phenotype of livers in EC-CCM1 KO mice.**

Representative images of WT and EC-CCM1 KO mouse livers at P12 (n=3 for each genotype).

To note, while harvesting different organs to perform fresh EC isolation in EC-CCM1 KO pups, we observed that all the organs appeared macroscopically normal with the exception of the liver which showed a pale colour with diffuse red spots on the surface (Figure 54). As liver angiomas were reported to be found in a low percentage of familial CCM patients [293], further experiments will be directed in the future to analyse this phenotype in CCM mouse model.

Taken together, these results showed that KLF4 upregulation was critical to promote the EndMT switch induced by CCM1 abrogation in *vivo*. However, the strength of this effect was context dependent being observed preferentially in the brain microvasculature.

### 6.11 KLF4 regulates BMP6-mediated signalling

TGF-β/BMP pathway is a major inducer of EndMT in CCM1 KO ECs [119]. Upon loss of CCM1, endogenous *Bmp6* up-regulation in ECs leads to an increased SMAD phosphorylation resulting in EndMT marker acquisition [291]. We therefore asked whether KLF4 could promote the EndMT switch observed in CCM1 KO ECs by modulating TGF-β/BMP signalling. As shown in Figure 55, *Klf4* silencing decreased *Bmp6* expression together with a significant reduction in phosphorylated SMAD1 (pSMAD1) (Figure 56), that, as expected are strongly increased in CCM1 KO ECs shCTRL. The same data was confirmed in BMECs since *Bmp6* amount was reduced in CCM1-KLF4 KO in comparison to CCM1 KO ECs (Figure 57). Interestingly, immunohistochemical analysis of brain tissues confirmed BMP6 reduction *in vivo* in ECs lining the cavernomas of double EC-CCM1 KO KLF4 KO mice compared to EC-CCM1 KO animals (Figure 58).

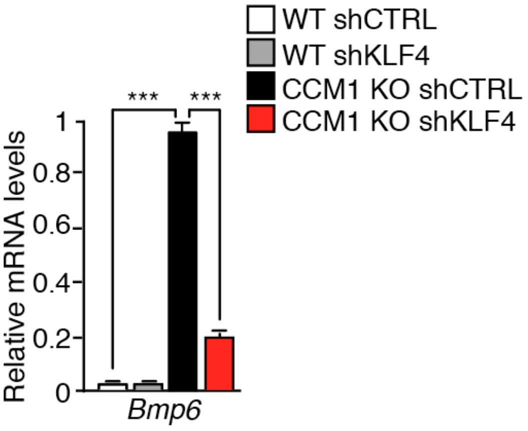

**Figure 55 - *Klf4* silencing decreases *Bmp6* expression in CCM1 KO lung ECs.**

qRT-PCR of *Bmp6* expression in WT shCTRL, WT shKLF4, CCM1 KO shCTRL and CCM1 KO shKLF4 cultured ECs. Data represent the mean ± SD (n=3). Fold changes are relative to CCM1 KO shCTRL ECs. ***P<0.001

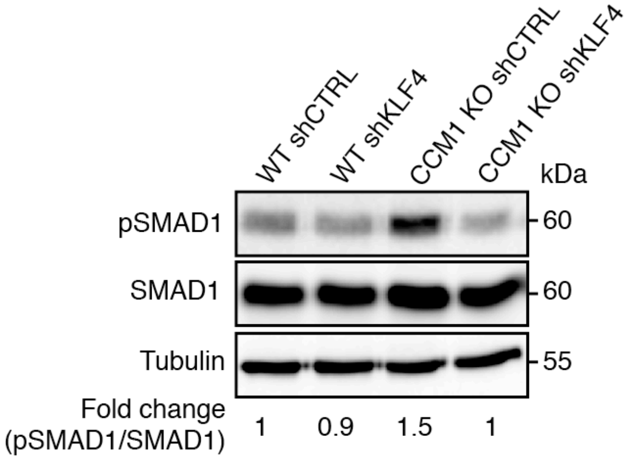
WT shCTRL
WT shKLF4
CCM1 KO shCTRL
CCM1 KO shKLF4
kDa
pSMAD1
60
SMAD1
60
Tubulin
55
Fold change (pSMAD1/SMAD1)
1
0.9
1.5
1

**Figure 56 - *Klf4* silencing decreases SMAD1 phosphorylation in CCM1 KO lung ECs.**

WB of pSMAD1 and SMAD1 in WT shCTRL, WT shKLF4, CCM1 KO shCTRL and CCM1 KO shKLF4 ECs. pSMAD1/SMAD1 ratio normalized over tubulin was quantified by densitometry scan. These data are representative of three independent observations.

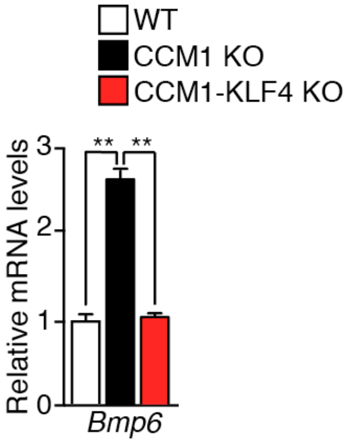

**Figure 57 - *Klf4* increases *Bmp6* in CCM1 KO BMECs.**

qRT-PCR of *Bmp6* in WT, CCM1 KO and CCM1-KLF4 KO BMECs. Data are mean ± SD (n=3). Fold changes are relative to WT ECs. **P<0.01,

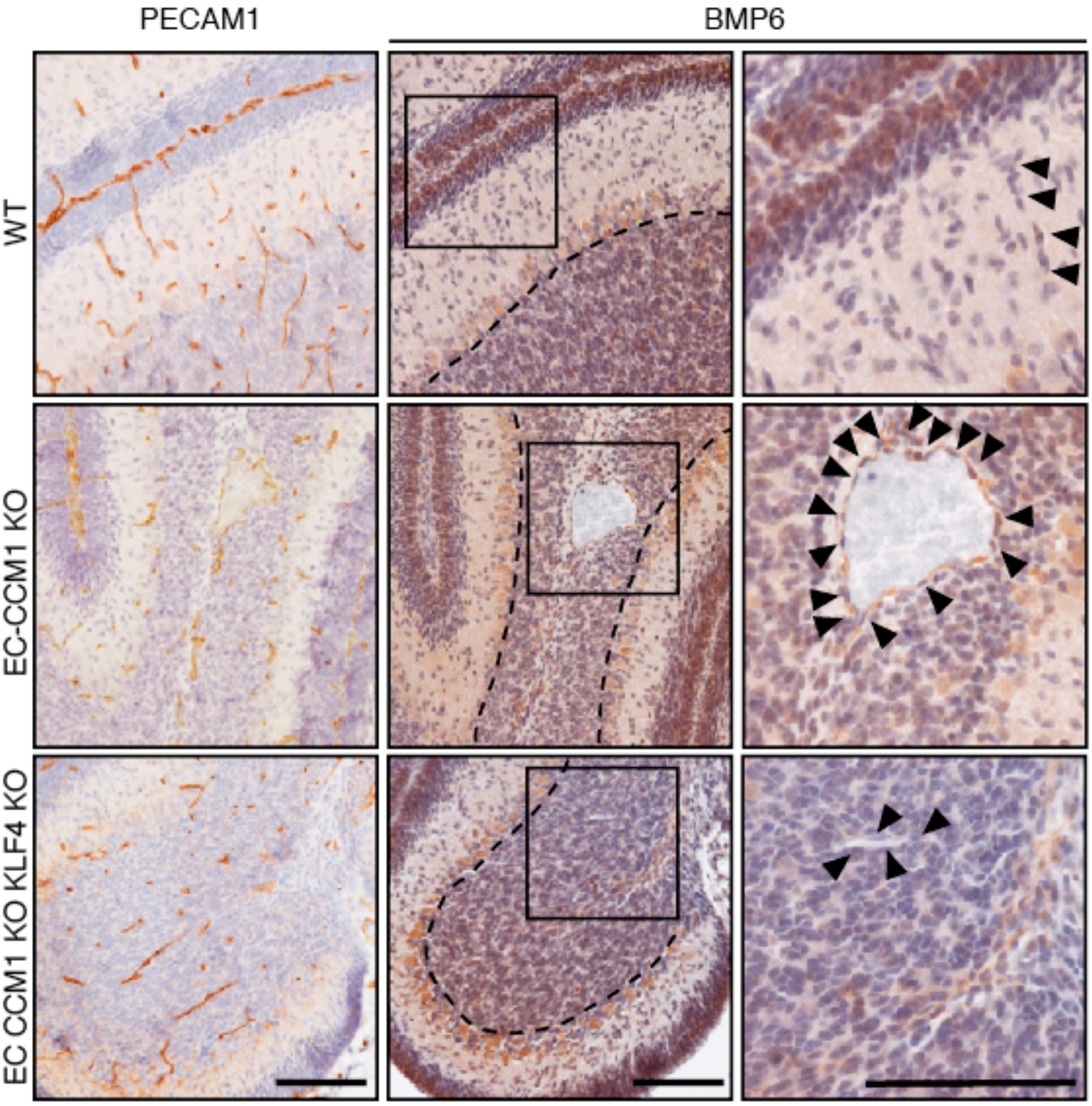

**Figure 58 - Loss of endothelial *Klf4* decreases BMP6 amount *in vivo* in ECs lining the cavernomas in EC-CCM1 KO mice.**

Immunohistochemical analysis of PECAM1 (left panels) and BMP6 (central panels) performed on serial sections of cerebellum derived from WT, EC-CCM1 KO and EC-CCM1 KO KLF4 KO mice at P12. Higher magnification images of the boxed regions are shown in the right panels. Black arrowheads mark ECs, dotted area indicates the Purkinje cell layer used as positive control of the staining. Scale bar: 100 µm. These data are representative of three independent observations (n=3 for each genotype).

To understand whether *Bmp6* is a direct transcriptional target of KLF4, we performed chromatin immunoprecipitation assay (ChIP). Eight putative KLF4 binding sites were identified within the murine *Bmp6* promoter region at -5.0KB and +1.0 KB from the transcription start site (tss). As depicted in Figure 59, KLF4 binding was enriched at the selected sites on *Bmp6* promoter in CCM1 KO ECs but not in WT cells, thus suggesting *Bmp6* as a KLF4 target gene in ECs. To demonstrate that the binding of KLF4 to *Bmp6* promoter is functionally active, we generated a *Bmp6* reporter construct by cloning the promoter region enriched in KLF4 binding sites upstream of the Luciferase cDNA of the PGL3 basic cloning vector (Figure 60). A transcriptional reporter assay was performed by co-transfecting the *Bmp6* reporter construct together with an expression plasmid of a full length KLF4 or a mutant KLF4 lacking the DNA-binding zinc finger domains (KLF4 ΔZnF). We found that KLF4 induced *Bmp6* promoter activity and this effect was reduced when KLF4 binding to DNA was altered (Figure 60), thus suggesting that KLF4 actively regulated *Bmp6* transcription.

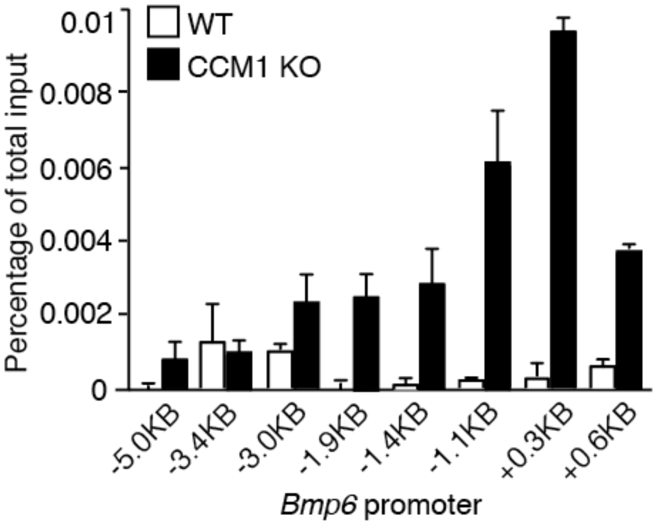

**Figure 59 - KLF4 binds *Bmp6* promoter in CCM1 null ECs.**

ChIP analysis of KLF4 binding to *Bmp6* promoter. Putative KLF4 binding sites identified by MatInspector are indicated. The levels of DNA are normalized to input. Columns are mean ±SD of triplicates from a representative experiment out of three.

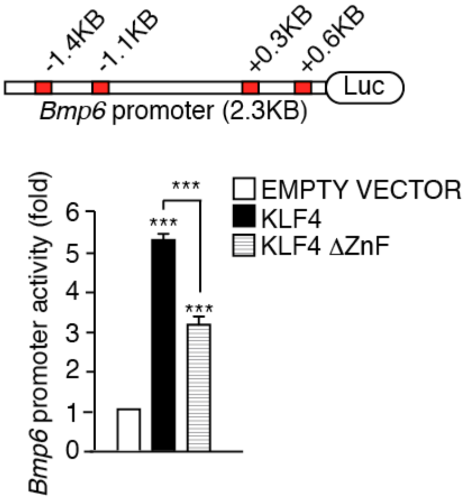

**Figure 60 - KLF4 regulates *Bmp6* promoter activity.**

Transcriptional reporter assay performed in HEK-293 cells transfected with *Bmp6* reporter plasmid together with an empty vector, a full lenght KLF4 or a mutant KLF4 lacking the DNA binding zinc finger domain (KLF4 DZnF). Red boxes in the picture indicate KLF4 binding sites validated by ChIP. Fold change in the *Bmp6* promoter activity are relative to empty vector transfected cells. Data are mean ± SD (n=3). ***P<0.001

Furthermore, we confirmed the same results through a gain of function approach. Both *Bmp6* mRNA (Figure 61) and pSMAD1 amount (Figure 62) were upregulated in KLF4 overexpressing ECs (LENTIKLF4) in comparison to empty vector transduced cells (MOCK). Similarly ChIP analysis revealed enriched KLF4 binding to selected putative sites within *Bmp6* promoter region in LENTIKLF4 ECs (Figure 63). To prove that increased SMAD1 phosphorylation and EndMT marker up-regulation were BMP6-dependent, we infected Mock and LENTIKLF4 ECs with a lentiviral vector expressing a short hairpin directed to *Bmp6* (shBMP6) or a control sequence (shCTRL) (Figure 64). Stable *Bmp6* silencing prevented the increase of both pSMAD1 (Figure 65 A) and EndMT markers induced by KLF4 in LentiKLF4 ECs (Figure 65 B).

Overall our results demonstrate that KLF4 was able to promote *Bmp6* expression that, in turn, contributed to the EndMT program of CCM1 null ECs.

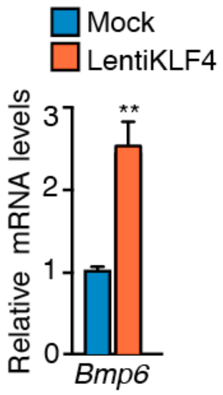

**Figure 61 - KLF4 overexpression in WT ECs upregulates *Bmp6*.**

qRT-PCR of *Bmp6* in Mock and LentiKLF4 cultured ECs. Data are mean ± SD (n=3). Fold changes are relative to Mock ECs. **P<0.01

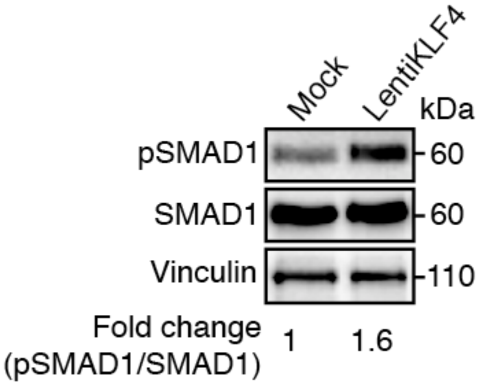
Mock
LentiKLF4
kDa
pSMAD1
-60
SMAD1
-60
Vinculin
-110
Fold change (pSMAD1/SMAD1)
1
1.6

**Figure 62 - KLF4 overexpression in WT ECs increases SMAD1 phosphorylation.**

WB analysis of pSMAD1 and SMAD1 in Mock and LentiKLF4 ECs. Vinculin was used as loading control. pSMAD1/SMAD1 ratio normalized over vinculin was quantified by densitometry scan. These data are representative of three independent experiments.

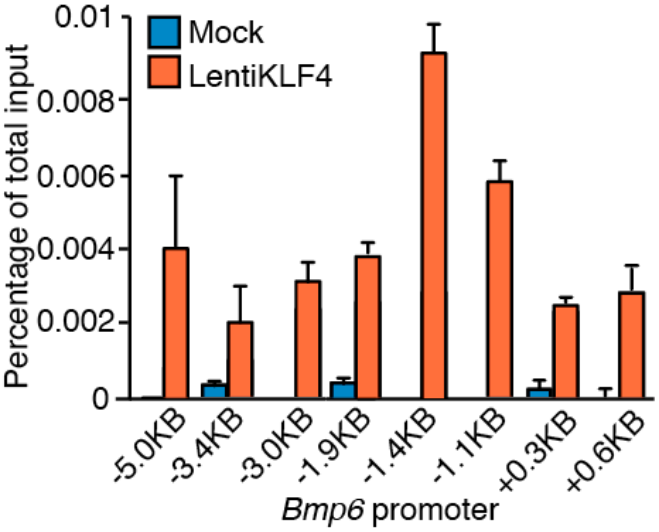

**Figure 63 - KLF4 binds *Bmp6* promoter in KLF4 overexpressing cells.**

ChIP of KLF4 interaction with *Bmp6* promoter in Mock and LentiKLF4 ECs. Putative KLF4 binding sites identified by MatInspector are indicated. The levels of DNA are normalized to input. Columns are mean ±SD of triplicates from a representative experiment out of three.

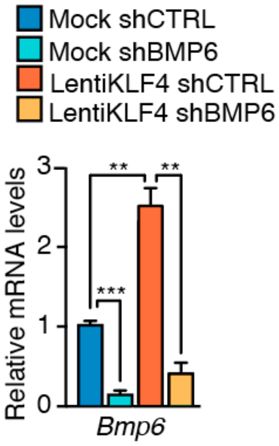

**Figure 64 - Knockdown efficiency of *Bmp6* in Mock and LentiKLF4 ECs transduced with a lentiviral vector expressing a shRNA directed to *Bmp6*.**

Mock and LentiKLF4 cultured ECs were lentiviral transduced with shRNA directed to either *Bmp6* (shBMP6) or control sequence (shCTRL). qRT-PCR analysis of *Bmp6* in Mock shCTRL, Mock shBMP6, LentiKLF4 shCTRL and LentiKLF4 shBMP6 ECs. qRT-PCR data represent the mean ± SD (n=3) and the fold changes are relative to Mock shCTRL ECs. ***P<0.001, **P<0.01

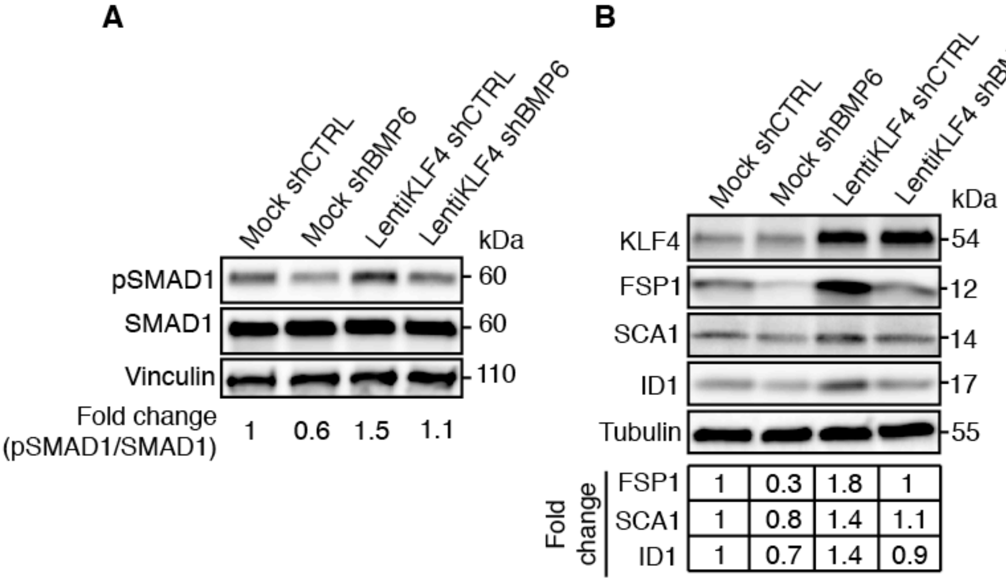
A
Mock shCTRL
Mock shBMP6
LentiKLF4 shCTRL
LentiKLF4 shBMP6
kDa
pSMAD1
- 60
SMAD1
- 60
Vinculin
- 110
Fold change (pSMAD1/SMAD1)
1
0.6
1.5
1.1
B
Mock shCTRL
Mock shBMP6
LentiKLF4 shCTRL
LentiKLF4 shBMP6
kDa
KLF4
-54
FSP1
-12
SCA1
-14
ID1
-17
Tubulin
-55
Fold change
FSP1 1 0.3 1.8 1
SCA1 1 0.8 1.4 1.1
ID1 1 0.7 1.4 0.9

**Figure 65 - Silencing of *Bmp6* in KLF4 overexpressing ECs decreases SMAD phosphorylation and EndMT marker expression.**

Mock and LentiKLF4 ECs were lentiviral transduced with shRNA directed to either *Bmp6* (shBMP6) or control sequence (shCTRL). A) WB of pSMAD1 and SMAD1 in Mock shCTRL, Mock shBMP6, LentiKLF4 shCTRL and LentiKLF4 shBMP6 ECs. Vinculin was used as loading control. pSMAD1/SMAD1 ratio normalized over vinculin was quantified by densitometry scan.. These WB data are representative of three independent observations. B) WB analysis of EndMT markers in Mock shCTRL, Mock shBMP6, LentiKLF4 shCTRL and LentiKLF4 shBMP6 ECs. Tubulin was the loading control. FSP1, SCA1 and ID1 fold changes were normalized over tubulin and quantified by densitometry scan. These WB data are representative of three independent observations.

### 6.12 KLF4 directly regulates the expression of some EndMT markers

We then investigated whether KLF4-induced EndMT was fully dependent on the upregulation of BMP6 or whether KLF4 could also have an independent and direct effect on EndMT marker expression. To this purpose we isolated ECs from lungs of KLF4 floxed/floxed mice, we immortalized them PmT antigen and then we recombined the gene through a treatment with TAT-Cre *in vitro* (Figure 66). WT and KLF4 KO ECs were stimulated with 100ng/ml of recombinant BMP6 for 96 hours and a number of representative mesenchymal and stem-cells markers were analyzed. Although the induction of SMAD1 phosphorylation was comparable in both cell type (Figure 67), BMP6-induced expression of *Fsp1* and *Sca1*, but not *Id1*, was reduced in the absence of KLF4 (Figure 68), thus suggesting a direct contribution of KLF4 to the upregulation of some EndMT markers. Consistently with this hypothesis several consensus sequences for KLF4 were identified in the promoter region of murine *Fsp1*, *Sca1* and *Id1*. ChIP analysis revealed KLF4 binding to both *Fsp1* (Figure 69 A) and *Sca1* promoters (Figure 69 B), with the binding occuring mainly in the regions located at +0.1KB and +0.7 KB (*Fsp1*) and -0.1 KB and +0.4KB (*Sca1*) from the tss, respectively. Conversely KLF4 binding to *Id1* promoter was barely detectable, suggesting that Id1, a *bona fide* BMP6 target gene [294] was not directly regulated by KLF4 (Figure 69 C). Moreover, both *Fsp1* and *Sca1* transcriptional reporters (generated by cloning the promoter regions enriched in KLF4 binding sites validated by ChIP upstream of the Luciferase cDNA into the PGL3 basic vector) were strongly induced by KLF4 in a DNA-binding dependent manner (Figure 70 A and B). Interestingly, regions bound by KLF4 in the *Fsp1* and *Sca1* promoters are surrounded by canonical SMAD binding elements. SMADs bind weakly to the promoter of target genes [295] and through the association with KLF4 this binding could be reinforced.

In conclusion, our results demonstrated that Klf4, besides modulating TGFb/BMP signalling pathway, could also regulate EndMT marker expression by directly binding to promoter regions of specific EndMT markers.

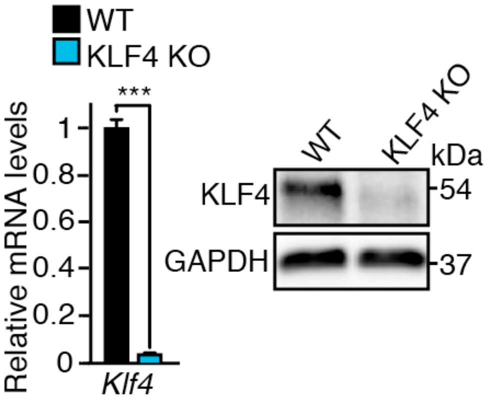

**Figure 66 - Establishment of lung derived endothelial cell line KO for KLF4.**

A) qRT-PCR (left panel) and WB (right panel) analysis of KLF4 in cultured lung WT and KLF4 KO ECs. qRT-PCR data represent the mean ± SD (n=3) and the fold changes are relative to WT ECs. A two-tailed unpaired *t*-test was performed. $^{***}$P<0.001. GAPDH was the loading control in WB. These WB data are representative of three independent observations.

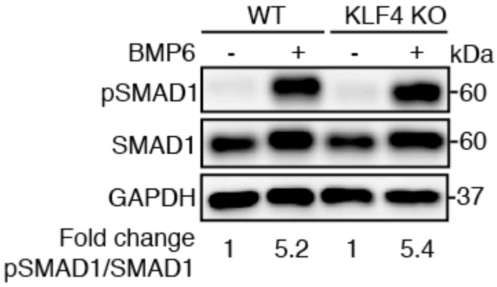

**Figure 67 - Loss of KLF4 does not affect SMAD1 phosphorylation upon BMP6 stimulation.**

WB analysis of pSMAD1 and SMAD1 in WT and KLF4 KO ECs left untreated or treated with recombinant BMP6 for 4 h. GAPDH was the loading control in WB. pSMAD1/SMAD1 ratio normalized over GAPDH was quantified by densitometry scan. These data are representative of three independent observations.

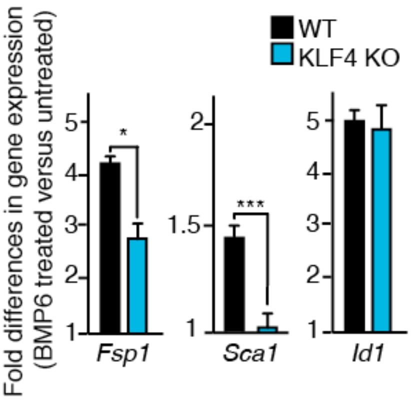

**Figure 68 - BMP6-dependent *Fsp1* and *Sca1* induction is strongly reduced in KLF4 KO lung ECs.**

qRT-PCR of *Fsp1*, *Sca1* and *Id1* in WT and KLF4 KO ECs stimulated with BMP6 for 96 h. qRT-PCR data are mean ± SD (n=3). Fold changes in gene expression in BMP6-treated versus untreated ECs. $^{*}P<0.05$, $^{***}P<0.001$

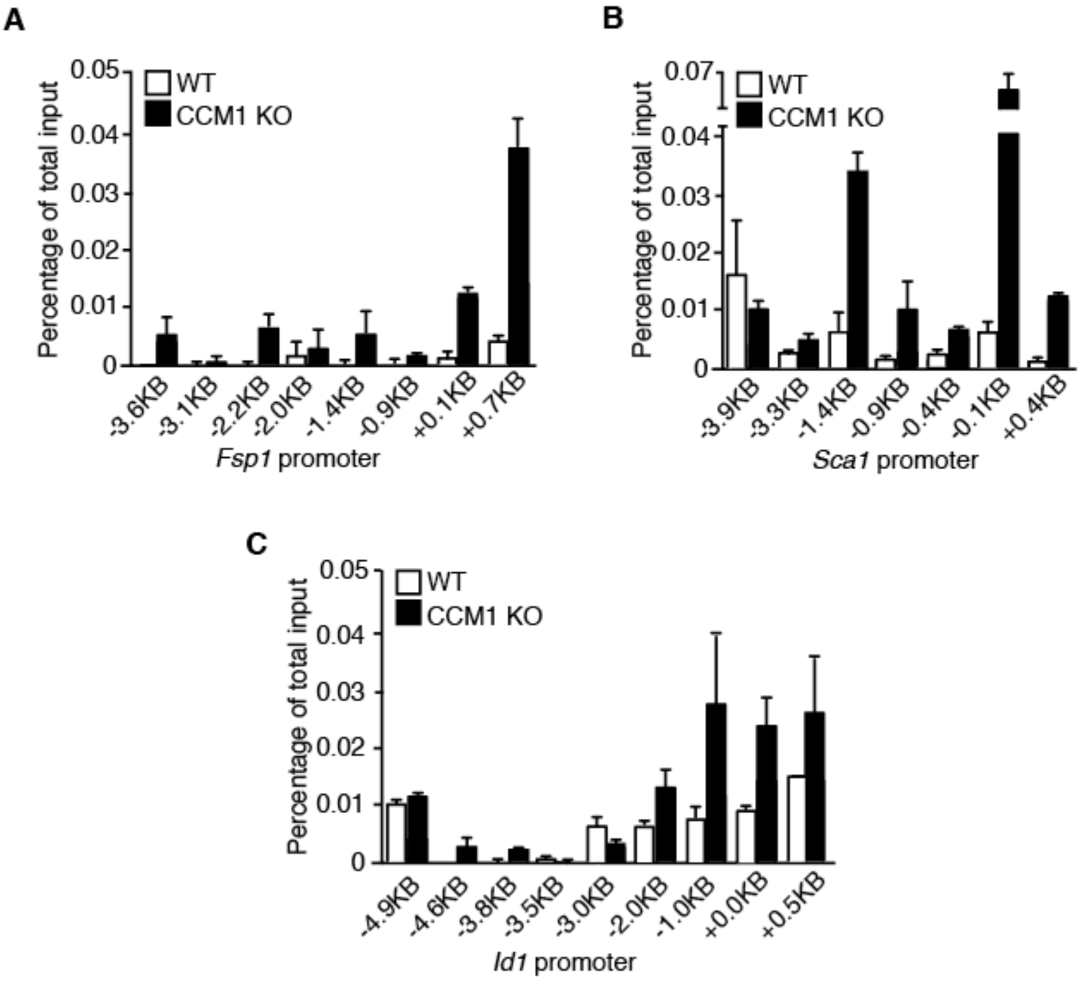

**Figure 69 - KLF4 directly binds to promoter regions of specific EndMT markers.**

ChIP analysis of KLF4 binding to the promoters of *Fsp1*(A), *Sca1*(B) and *Id1*(C) in WT and CCM1 KO ECs. The positions of the putative KLF4 binding sites identified with MatInspector in the promoters of the genes analysed were indicated. The levels of DNA were normalized to input. Columns are mean ± SD of triplicates from a representative experiment out of three performed.

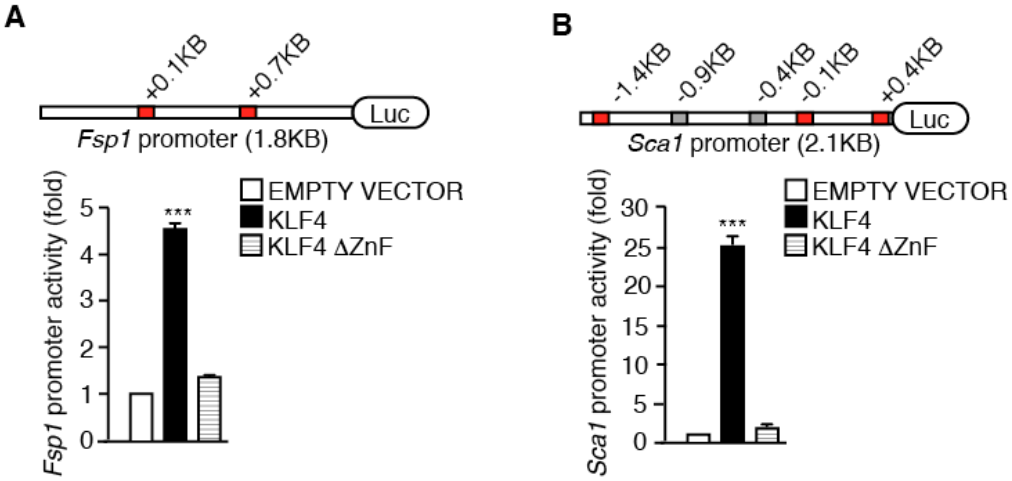

**Figure 70 - KLF4 increases promoter activity of specific EndMT markers.**

Transcriptional reporter assays performed in HEK-293 cells transfected with either *Fsp1* (A) or *Sca1* (B) reporter plasmid together with an empty vector, full lenght KLF4 or KLF4 DZnF. In the pictures: red boxes indicate KLF4 binding sites validated by ChIP, while grey boxes indicate KLF4 binding sites not validated by ChIP. Fold change in the promoter activity are relative to empty vector transfected cells. Data are mean ± SD (n=3). $^{***}$P<0.001

### 6.13 KLF2 expression is dispensable for EndMT transition in CCM1 null ECs

KLF2, another member of KLF family that shares a high level of structural and functional homology with KLF4, was recently reported to be increased upon loss of *Ccm* genes [107, 296]. KLF2 was found to play a causative role in the cardiac abnormalities observed in the absence of CCM in both mouse and zebrafish embryos since it was responsible for both digestion of the cardiac jelly [296] and excessive angiogenesis [107]. Moreover *in vitro* and *in vivo* studies showed that loss of KLF2 resulted in an increase of KLF4 and *viceversa* thus raising the possibility that these factors may compensate one another [228, 297]. KLF2 was found to be present in the list of the most upregulated transcripts that we obtained by Affimetrix analysis (Appendix Table1) performed to compare the gene expression profile of WT and CCM1 KO BMECs. In order to validate microarray data we first evaluated *Klf2* expression *ex vivo* in freshly isolated PECAM+ brain ECs derived from WT, EC-CCM1 KO and double EC-CCM1 KO KLF4 KO mice (Figure 71 A and B). *Klf2* was found to be upregulated in the absence of *Ccm1* in EC-CCM1 KO compared to WT matched controls. However *Klf4* depletion did not alter *Klf2* expression levels either in EC-CCM1 KO KLF4 KO or in EC-KLF4 KO mice (Figure 71), thus suggesting a non redundant role of these two transcription factors in CCM1 null ECs *ex vivo*. To further confirm these data *in vitro* we evaluated *Klf2* expression in WT. CCM1 KO and double CCM1-KLF4 KO BMECs. As shown in Figure 72, *Klf2* was found to be induced in the absence of *Ccm1* and its expression was not further increased upon *Klf4* ablation in CCM1-KLF4 double KO BMECs and did not apparently compensate for the lack of Klf4 in inducing EndMT (Figure 37) .

In conclusion, even if the relative contribution of KLF2 to CCM brain disease remains an open issue that requires future studies, our data might suggest that KLF2 upregulation is apparently dispensable for the EndMT phenotype observed in the absence of *Ccm1*.

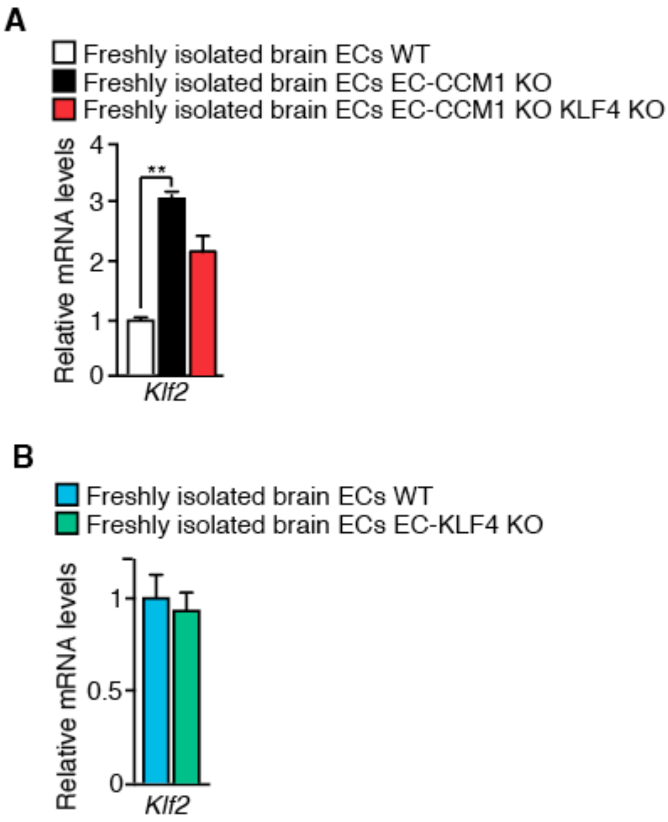

**Figure 71 - Loss of *Klf4* does not affect *Klf2* expression in ECs in *vivo*.**

A) qRT-PCR of *Klf2* in freshly isolated brain ECs from WT, EC-CCM1 KO and EC-CCM1 KO KLF4 KO mice analyzed at P12. Fold changes are relative to WT animals. Data are mean ± SD (n=3). ** P<0.01, B) qRT-PCR of *Klf2* in freshly isolated brain ECs from WT and EC-KLF4 KO mice analyzed at P12. Fold changes are relative to WT animals. Data are mean ± SD (n=3).

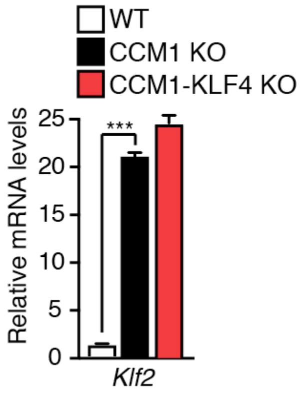

**Figure 72 - Loss of *Ccm1* induces *Klf2* upregulation *in vitro* in BMECs.**

qRT-PCR of *Klf2* after *in vitro* TAT-Cre recombinase treatment of primary brain ECs derived from WT, *Ccm1* floxed/floxed and *Ccm1-Klf4* floxed/floxed mice to originate cultured WT, CCM1 KO and CCM1-KLF4 KO brain ECs, respectively. Data are presented as mean ± SD (n=3). Fold changes were relative to WT brain ECs. ***P<0.001

### 6.14 Erk5 activation mediates KLF4 upregulation and KLF4-dependent EndMT in the absence of *Ccm1*

We then moved to investigate the molecular mechanism through which loss of *Ccm* lead to *Klf4* upregulation. Previous studies extensively reported that ERK5 phosphorylation and activation promotes *Klf2* and *Klf4* transcription upon shear stress in ECs [226, 298, 299]. As both *Klf2* and *Klf4* were concomitantly upregulated upon loss of *Ccm1,* we hypothesized that ERK5 could be involved in the regulation of *Klf4* expression also in our experimental models. We found that ERK5 phosphorylation was increased in freshly isolated brain ECs of EC-CCM1 KO mice in comparison to matched controls (Figure 73). Accordingly, ERK5 phosphorylation was higher in cultured BMECs upon *Ccm1* ablation and was not further modified by KLF4 depletion (Figure 74). To investigate whether ERK5 activation was responsible for the upregulation of both KLF4 and EndMT marker expression in the absence of CCM1, we transfected WT ECs with siRNAs directed to *Erk5* and *Ccm1*. The downregulation of ERK5 strongly prevented KLF4 upregulation in *Ccm1* silenced ECs (Figure 75). Similarly, the treatment of WT and CCM1 KO ECs for 72 hours with 5 μm of XMD8-92, a specific ATP-competitive for ERK5 kinase [259, 299], strongly decreased ERK5 phosphorylation and KLF4 overexpression together with an inhibition of *Bmp6* upregulation, SMAD1 phosphorylation and EndMT marker acquisition in CCM1 null ECs (Figure 76 A-D). Comparable data where obtained when XMD8-92 treatment was performed in WT and CCM1 KO BMECs (Figure 77).

Myocyte enhanced (MEF) family of transcription factors are the best characterized downstream targets of ERK5 and were previously reported to be directly involved in the regulation of *Klf2* and *Klf4* expression in ECs [255, 256, 300, 301]. To investigate a possible role of MEF2 transcription factors in KLF4 upregulation in the absence of CCM1 we silenced anyone of *Mef2a*, *Mef2c* and *Mef2d* in WT and CCM1 KO ECs. Both *Mef2a* and *Mef2c* knockdown in CCM1 KO ECs led to a partial but significant decrease in *Klf4* expression (Figure 78 A and B) while *Mef2d* silencing did not affected KLF4 upregulation at all

(Figure 78 C).

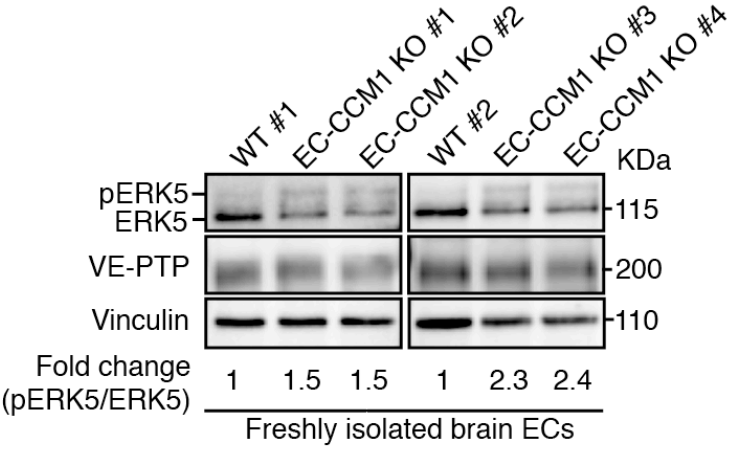
WT #1
EC-CCM1 KO #1
EC-CCM1 KO #2
WT #2
EC-CCM1 KO #3
EC-CCM1 KO #4
KDa
pERK5
ERK5
115
VE-PTP
200
Vinculin
110
Fold change (pERK5/ERK5)
1
1.5
1.5
1
2.3
2.4
Freshly isolated brain ECs

**Figure 73 - Loss of *Ccm1* induce Erk5 phosphorylation in ECs *in vivo*.**

A) WB analysis of phoshorylated ERK5 (pERK5) and total ERK5 in freshly isolated brain ECs from WT (n=2) and EC-CCM1 KO (n=4) mice from 2 different litters at P12. VE-PTP measured the endothelial content and vinculin was the loading control. pERK5/ERK5 ratio normalized over vinculin and VE-PTP was quantified by densitometry scan.

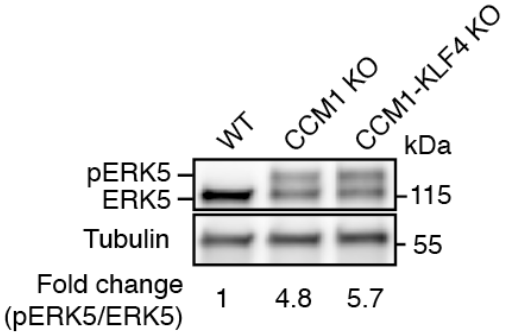
WT
CCM1 KO
CCM1-KLF4 KO
kDa
pERK5
ERK5
115
Tubulin
55
Fold change (pERK5/ERK5)
1
4.8
5.7

**Figure 74 - Erk5 phosphorylation is increased upon loss of *Ccm1* in BMECs *in vitro*.**

A) WB analysis of pERK5 and ERK5 protein levels after *in vitro* TAT-Cre recombinase treatment of primary brain ECs derived from WT, *Ccm1* floxed/floxed and *Ccm1-Klf4* floxed/floxed mice to originate cultured WT, CCM1 KO and CCM1-KLF4 KO BMECs. pERK5/ERK5 ratio normalized over the loading control tubulin was indicated. This WB data is representative of three independent experiments.

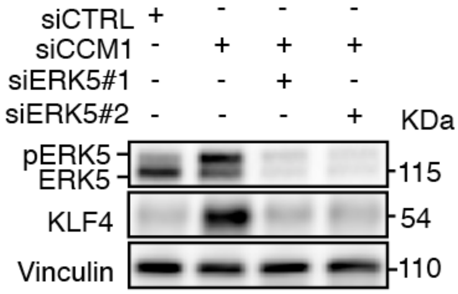

**Figure 75 - Erk5 activitation is responsible for KLF4 upregulation upon *Ccm1* silencing *in vitro.***

WB analysis of pERK5, ERK5 and KLF4 protein leves in cultured lung derived WT ECs either *Ccm1* (siCCM1) or control (siCTRL) siRNA-treated alone or in combination with two siRNA targeting *Erk5* (siERK5#1,2). pERK5/ERK5 ratio normalized over  the loading control vinculin was indicated. This WB data is representative of three independent experiments.

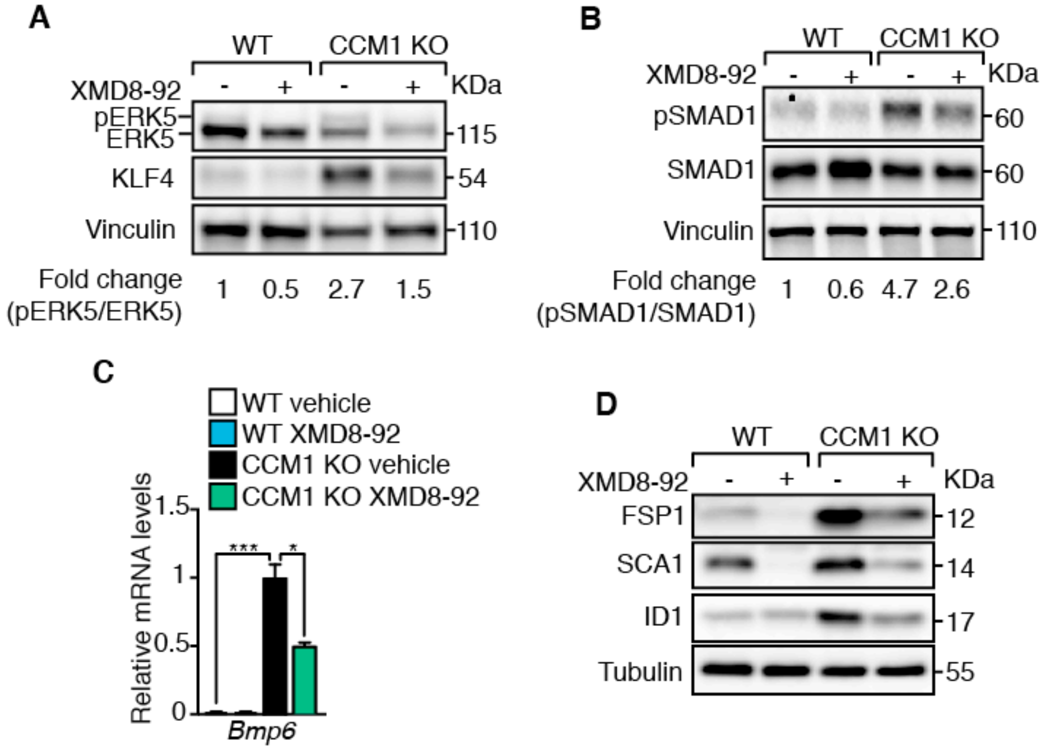

**Figure 76 - In the absence of *Ccm1* increased ERK5 phosphorylation is responsible for KLF4 upregulation, *Bmp6*-dependent SMAD signalling and KLF4-dependent EndMT *in vitro* in CCM1 KO ECs.**

A-D) Treatment of WT and CCM1 KO ECs with either 5 μM of XMD8-92 or the vehicle for 72 hours. A) WB analysis of pERK5, ERK5 and KLF4. pERK5/ERK5 ratio was quantified over  the loading control vinculin. B) Evaluation of pSMAD1 and SMAD1 protein levels by immunoblot analysis. pSMAD1/SMAD1 ratio normalized over the loading control vinculin was shown. C) qRT-PCR of *Bmp6*. The data represent the mean ± SD (n=3). Fold changes are relative to vehicle-treated CCM1 KO ECs. $^{**}$P<0.001, $^{*}$P<0.01. D) Representative WB analysis of EndMT markers expression. Tubulin was used as loading control. All WB data presented in this figure are representative of three independent experiments.

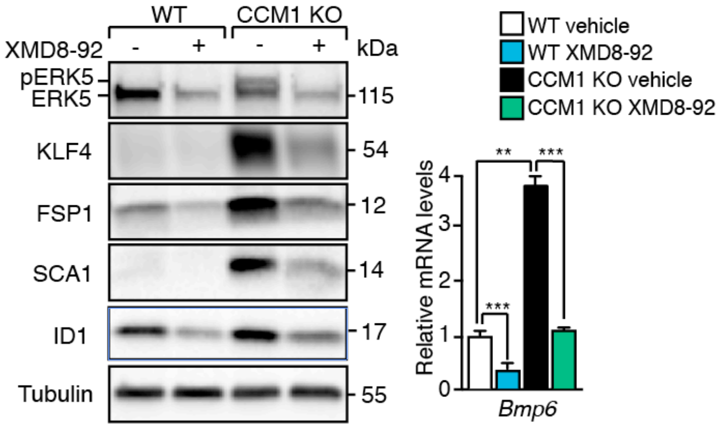

**Figure 77 - In the absence of *Ccm1* increased ERK5 phosphorylation is responsible for KLF4 upregulation, *Bmp6* overexpression and KLF4-dependent EndMT *in vitro* in CCM1 null BMECs.**

Treatment of WT and CCM1 KO BMECs with either 5 µM of XMD8-92 or the vehicle for 72 hours. Left panel: WB analysis of pERK5, ERK5, KLF4, FSP1, SCA1, ID1. Tubulin was the loading control. These WB data are representative of three independent experiments. Right panel: qRT-PCR of *Bmp6*. Data are shown as mean ± SD (n=3) and fold changes are relative to vehicle-treated WT ECs. $^{***}$P<0.001, *$^{*}$P<0.01

It has been reported in literature that MEF transcription factors show functional redundancy and can compensate one another [301]. To exclude the possibility that the partial KLF4 downregulation that we observed upon the single knockdown of any of *Mef2a*, *Mef2c* and *Mef2d* was due to a functional compensation of the other MEF family members, we performed a simultaneous triple knockdown of *Mef2a*, *Mef2c* and *Mef2d*. The combined silencing of all the three members of this family of transcription factors resulted in a decreased expression of *Klf4* in CCM1 KO ECs (Figure 79) that, however, was comparable to that obtained upon *Mef2a* or *Mef2c* single knockdown. Thus, it is coincevable that either other ERK5-downstream transcription factors or ERK5 alone [243] could be involved in KLF4 upregulation upon loss of *Ccm* genes.

Interestingly, to identify ERK5-mediated KLF4 upregulation and KLF4-dependent EndMT as common molecular nodes in CCM, we analyzed ERK5 activation, KLF4 amount and EndMT marker expression in lung-derived WT, CCM2 KO or CCM3 KO ECs obtained as previously described for CCM1 null ECs. More in detail, ECs from the lung of WT, *Ccm2* and *Ccm3* floxed/floxed mice were isolated, immortalyzed and then *in vitro* treated with TAT-cre recombinase to induce gene ablation. Notably, we found that in ECs null for either *Ccm2* or *Ccm3* ERK5 phosphorylation was increased (Figure 80 A and 81 A, respectively). Furthermore the treatment of both CCM2 KO and CCM3 KO ECs with 5µm of XMD8-92 for 3 days strongly inhibited KLF4 overexpression and EndMT marker upregulation (Figure 80 B and 81 B, respectively).

Taken toghether these results showed that ERK5-MEF2A/C signalling axis is a common molecular node responsible for KLF4 upregulation and KLF4-dependent EndMT in ECs null for any of the three *Ccm* genes.

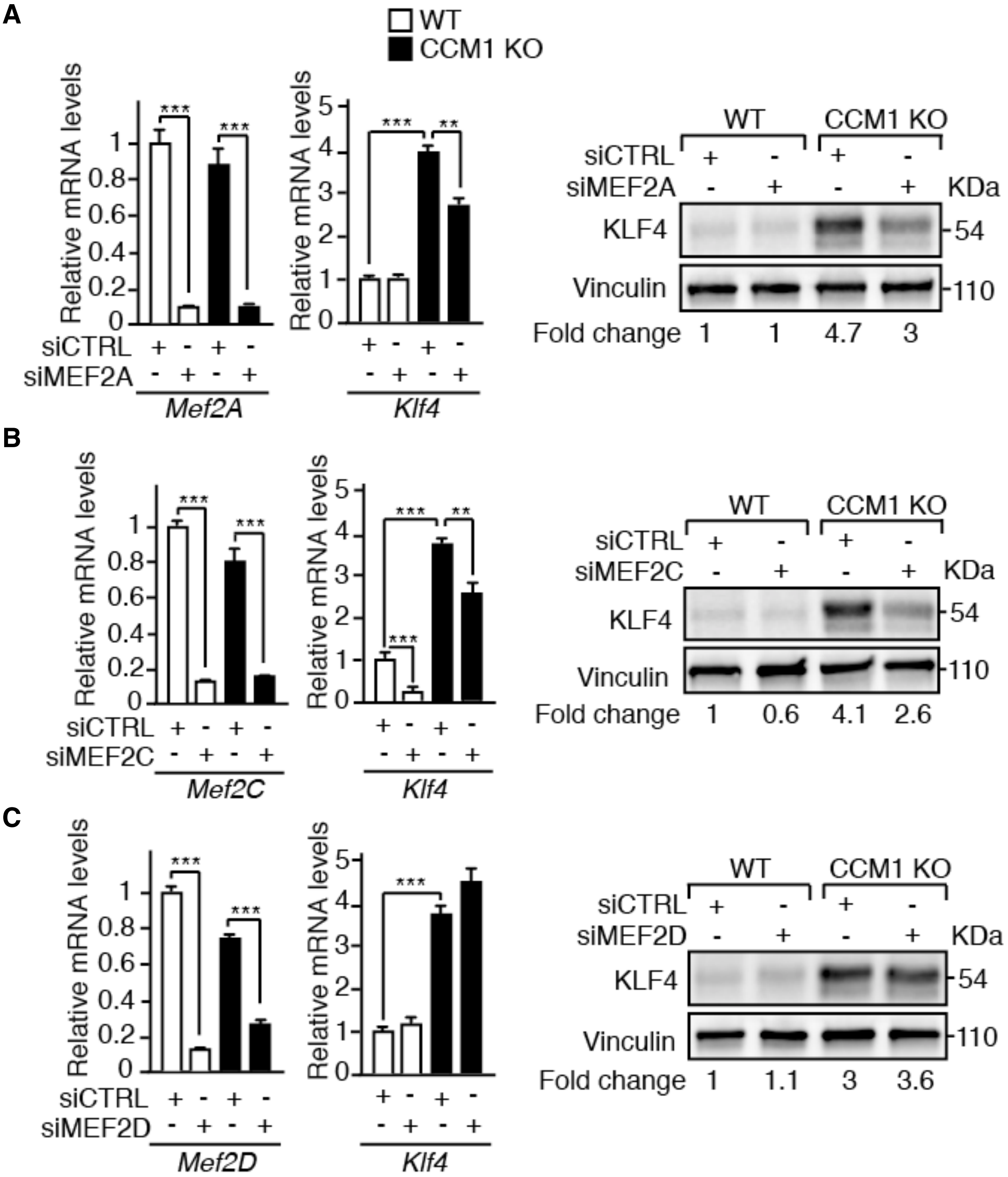

**Figure 78 - Mef2A and Mef2C contribute to KLF4 upregulation in CCM1 KO ECs.**

A) qRT-PCR analysis of *Klf4* and *Mef2A* (left panel) and WB analysis of KLF4 (right panel) in WT and CCM1 KO ECs treated with either control siRNA (siCTRL) or siRNA directed to *Mef2A*. qRT-PCR data represent the mean ± SD (n=3) and the fold changes are relative to WT siCTRL ECs. B) qRT-PCR analysis of *Klf4* and *Mef2C* (left panel) and WB analysis of KLF4 (right panel) in WT and CCM1 KO lECs treated with either control siRNA (siCTRL) or siRNA directed to *Mef2C*. qRT-PCR data represent the mean ± SD (n=3) and the fold changes are relative to WT siCTRL ECs. C) qRT-PCR analysis of *Klf4* and *Mef2D* (left panel) and WB analysis of KLF4 (right panel) in WT and CCM1 KO ECs treated with either control siRNA (siCTRL) or siRNA directed to *Mef2D*. qRT-PCR data represent the mean ± SD (n=3) and the fold changes are relative to WT siCTRL ECs.

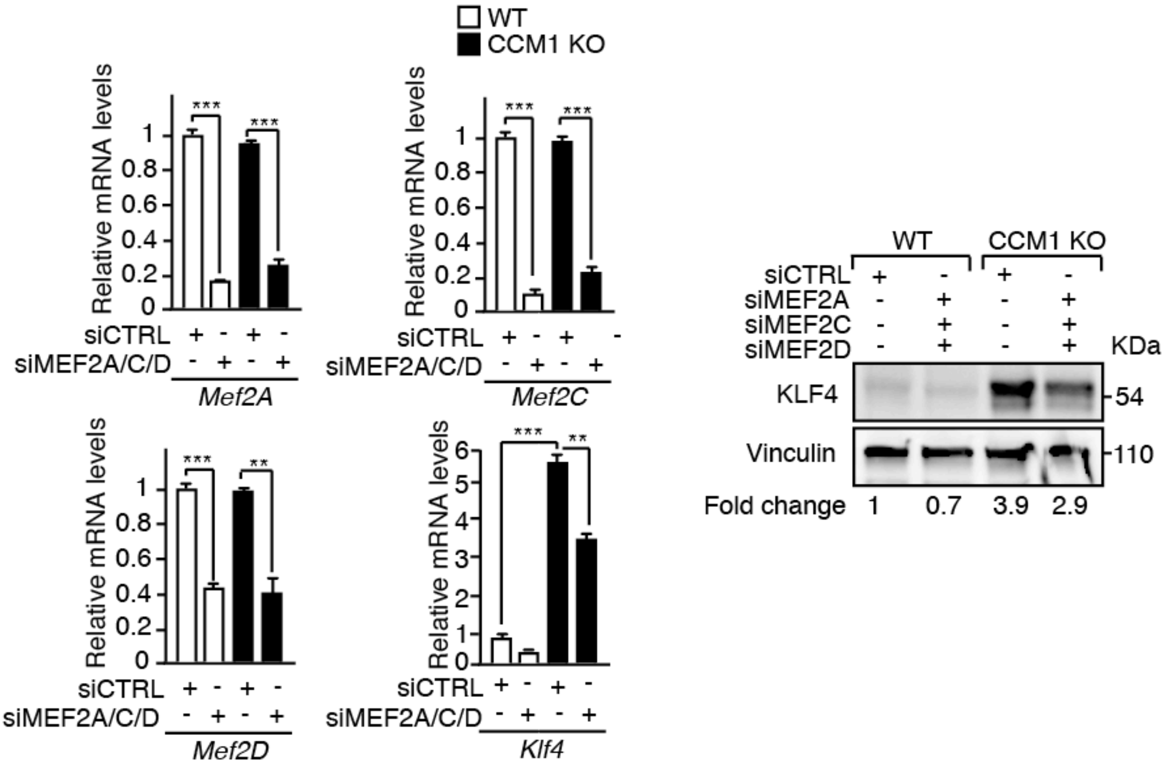

**Figure 79 - Combined silencing of *Mef2A*, *Mef2C* and *Mef2D* leads to partial downregulation of *Klf4* expression in CCM1 KO ECs.**

A) Left panels: qRT-PCR analysis of *Mef2A, Mef2C, Mef2D* and *Klf4* in WT and CCM1 KO lECs treated with either control siRNA (siCTRL) or a combination of siRNA directed to *Mef2A, Mef2C* and *Mef2D.* qRT-PCR data represent the mean ± SD (n=3) and the fold changes are relative to WT siCTRL ECs. Right panel: WB analysis of KLF4 (right panel) in WT and CCM1 KO ECs treated with either control siRNA (siCTRL) or siRNA directed to *Mef2A, Mef2C, Mef2D*. Vinculin was the loading control. These WB data are representative of three independent experiments. **P<0.01, ***P<0.001

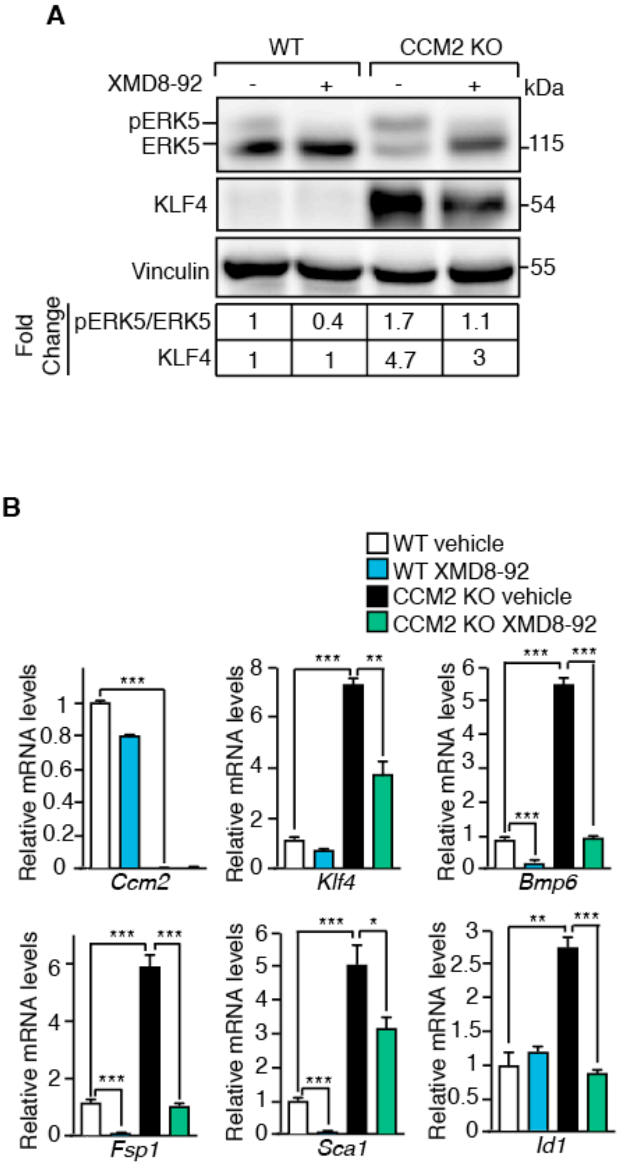

**Figure 80 - ERK5 activation in CCM2 null ECs is responsible for KLF4 upregulation and increased EndMT marker expression.**

A) WB analysis of pERK5, ERK5 and KLF4 in lung derived WT and CCM2 KO ECs treated with XMD8-92 or vehicle for 72 h. Both pERK5/ERK5 ratio and KLF4 amount normalized over vinculin, the loading control, were quantified by densitometry scan. These data are representative of three independent experiments. B) qRT-PCR of *Ccm2, Klf4, Bmp6* and some EndMT markers in WT and CCM2 KO ECs treated as in A. qRT-PCR results are shown as mean ± SD (n=3) and fold changes are relative to vehicle-treated WT ECs. *P<0.05, **P<0.01, ***P<0.001

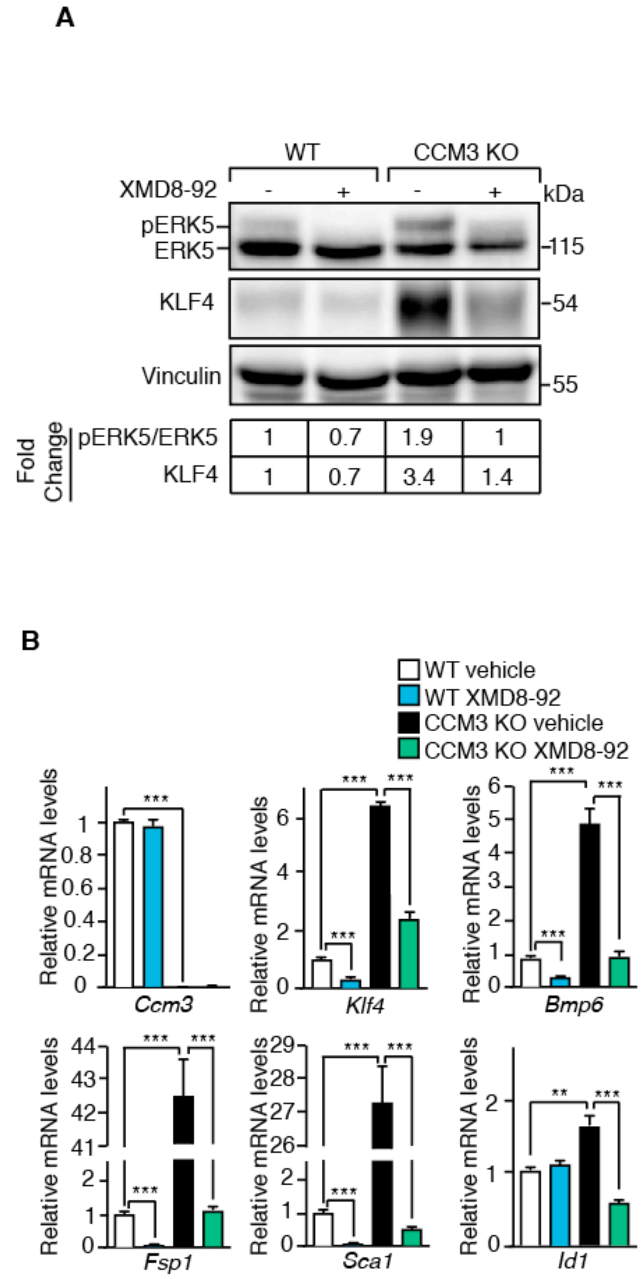

**Figure 81 - ERK5 activation in CCM3 null ECs is responsible for KLF4 upregulation and increased EndMT marker expression.**

A) WB analysis of pERK5, ERK5 and KLF4 in lung derived WT and CCM3 KO ECs treated with XMD8-92 or vehicle for 72 h. Both pERK5/ERK5 ratio and KLF4 amount normalized over vinculin, the loading control, were quantified by densitometry scan. These data are representative of three independent experiments. B) qRT-PCR of *Ccm3, Klf4, Bmp6* and some EndMT markers in WT and CCM3 KO ECs treated as in A. qRT-PCR results are shown as mean ± SD (n=3) and fold changes are relative to vehicle-treated WT ECs. **P<0.01, ***P<0.001

### 6.15 Mekk3-Mek5-dependent signalling cascade promotes ERK5 activation and KLF4 upregulation in CCM1 KO ECs

The final goal of this study was to clarify the signalling cascade through which the disruption of CCM complex promotes ERK5 activation and ERK5-dependent KLF4 upregulation. In order to clarify this molecular step we referred to previous publications in which the MAP3K MEKK3 was identified as a CCM2 and CCM1 binding partner [296, 302]. Active MEKK3 phosphorylates the MAP2K MEK5 that, in turn, directly activates ERK5 [303, 304]. We therefore explored the possibility that the lack of CCM might increase *Klf4* expression through the MEKK3-MEK5-ERK5 signalling axis. To this purpose we silenced *Mekk3* in WT and CCM1 KO ECs using two different siRNA. Even if MEKK3 levels were reduced in CCM1 KO ECs, a further *Mekk3* knockdown strongly reduced ERK5 phosphorylation in the absence of CCM1 (Figure 82). Interestingly, this effect was accompanied by the inhibition of *Klf4* mRNA (Figure 82) and protein (Figure 83) upregulation. These results strongly correlated with *Mekk3* downregulation efficiency that we obtained with the two different siRNA, thus supporting the idea that *Mekk3* activity is fundamental for activation of the ERK5-dependent KLF4 regulation.

Then, to evaluate if MEK5 could be the molecular link between MEKK3 and ERK5, we silenced *Mek5* in WT and CCM1 KO ECs. Knockdown of *Mek5* led to a decrease in ERK5 phosphorylation (Figure 84) and KLF4 upregulation (Figure 84 and 85) observed in CCM1 KO ECs. Accordingly, the treatment of WT and CCM1 KO ECs with BIX-02189, a specific MEK5 inhibitor [258], resulted in the loss of ERK5 activation (Figure 86) and KLF4 upregulation in CCM1 KO ECs (Figure 86 and Figure 87).

Thus, *Ccm1* gene ablation resulted in increased MEKK3-MEK5-dependent ERK5 phosphorylation responsible for KLF4 upregulation and KLF4-dependent EndMT. These data suggest that future pharmacological approaches targeting the MEKK3-MEK5-ERK5-KLF4 signalling could be very promising for the treatment of CCM.

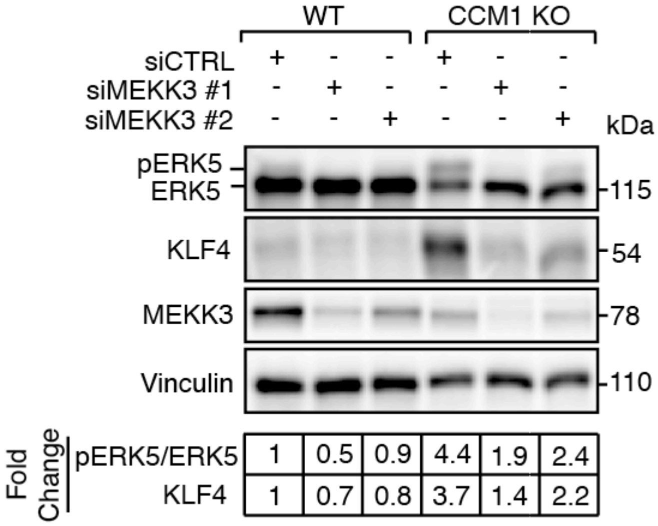
WT
CCM1 KO
siCTRL + - - + - -
siMEKK3 #1 - + - - + -
siMEKK3 #2 - - + - - +
kDa
pERK5
ERK5
115
KLF4
54
MEKK3
78
Vinculin
110
Fold Change
pERK5/ERK5 1 0.5 0.9 4.4 1.9 2.4
KLF4 1 0.7 0.8 3.7 1.4 2.2

**Figure 82 - MEKK3 activity is required for ERK5-mediated KLF4 upregulation.**

WB analysis of pERK5, ERK5, KLF4 and MEKK3 in WT and CCM1 KO lung ECs treated with either two different siRNAs against *Mekk3* (siMEKK3 #1 and siMEKK3 #2) or a control sequence (siCTRL). Both pERK5/ERK5 ratio and KLF4 amount normalized over vinculin were quantified by densitometry scan. These WB data are representative of three independent experiments.

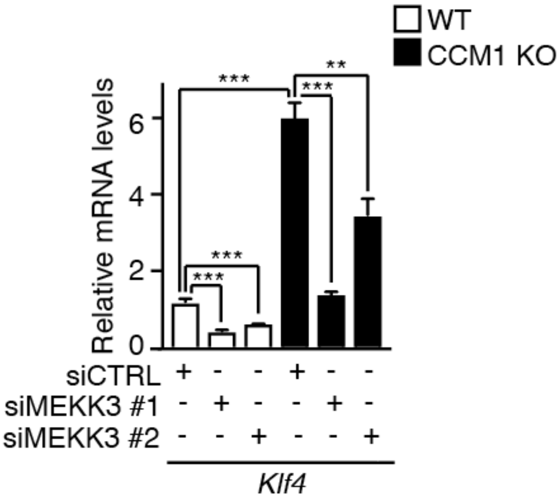

**Figure 83 - *Mekk3* silencing inhibits KLF4 upregulation in CCM1 KO ECs.**

qRT-PCR of *Klf4* in WT and CCM1 KO lung ECs treated with two different siRNAs directed to *Mekk3* (siMEKK3 #1 and siMEKK3 #2) or a control sequence (siCTRL). qRT-PCR results are shown as mean ± SD (n=3) and fold changes are relative to siCTRL-treated WT ECs. **P<0.01, ***P<0.001

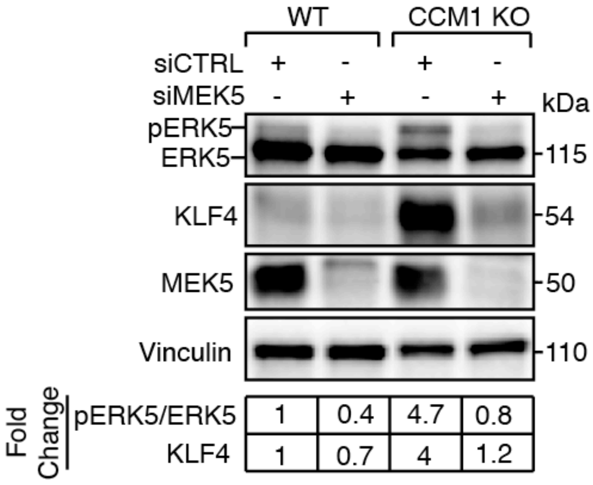
WT
CCM1 KO
siCTRL + - + -
siMEK5 - + - +
kDa
pERK5
ERK5
115
KLF4
54
MEK5
50
Vinculin
110
Fold Change
pERK5/ERK5 1 0.4 4.7 0.8
KLF4 1 0.7 4 1.2

**Figure 84 - MEK5 activity is required for ERK5-mediated KLF4 upregulation.**

WB analysis of pERK5, ERK5, MEK5 and KLF4 in WT and CCM1 KO lung ECs treated with either a siRNA against *Mek5* or a control sequence (siCTRL). Quantification of pERK5/ERK5 and KLF4 protein levels over vinculin were performed. These WB data are representative of three independent experiments.

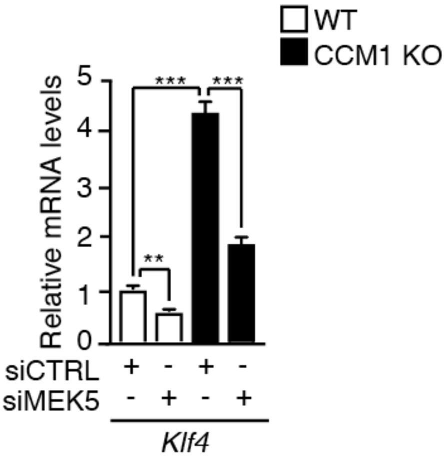

**Figure 85 - *Mek5* silencing decreases *Klf4* mRNA levels in CCM1 KO ECs.**

qRT-PCR of *Klf4* in WT and CCM1 KO lung ECs treated with either siMEK5 or siCTRL. qRT-PCR results are shown as mean ± SD (n=3). Fold changes are relative to siCTRL treated WT ECs. $^{**}P<0.01$, $^{***}P<0.001$

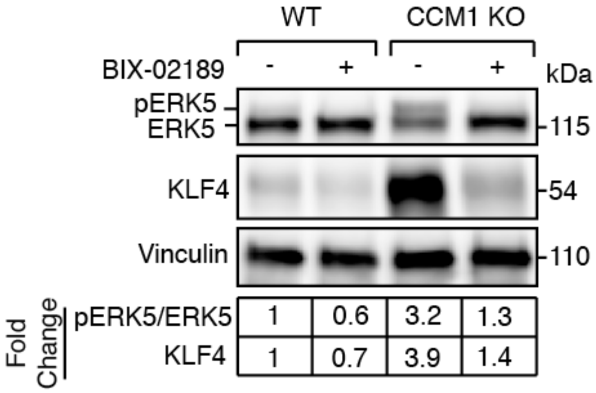
WT
CCM1 KO
BIX-02189
-
+
-
+
kDa
pERK5
ERK5
-115
KLF4
-54
Vinculin
-110
Fold Change
pERK5/ERK5
1
0.6
3.2
1.3
KLF4
1
0.7
3.9
1.4

**Figure 86 - Chemical inhibition of MEK5 activity is required for ERK5-mediated KLF4 upregulation.**

WB analysis of pERK5, ERK5, and KLF4 in WT and CCM1 KO lung ECs treated with 10 μM of BIX-02189 or vehicle for 48 hours. pERK5/ERK5 and KLF4 protein quantification over vinculin were shown. These WB data are representative of three independent experiments.

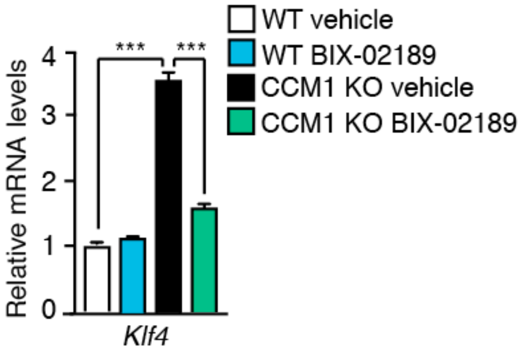

**Figure 87 - Chemical MEK5 inhibition decreases *Klf4* mRNA levels in CCM1 KO ECs.**

qRT-PCR of *Klf4* in WT and CCM1 KO lung ECs after 48 hours of treatment with 10 μM of BIX-02189 or vehicle. Fold changes are relative to vehicle treated WT ECs. qRT-PCR results are shown as mean ± SD (n=3). $***P<0.001$

# DISCUSSION

In the present study we introduced the concept that CCM lesions are formed by ECs undergoing EndMT transition. In the attempt to understand the molecular mechanisms through which loss of *Ccm* genes led to the high susceptibility of ECs to acquire a mesenchymal/stem cell-like phenotype, we identified the transcription factor KLF4 as a master regulator of EndMT ongoing in *Ccm* null ECs. KLF4 promoted an endogenous production of *Bmp6* in ECs that, in turn, activated the TGF-β/BMP signalling pathway. *Klf4* genetic inactivation as well as the pharmacological TGF-β/BMP pathway inhibition blocked the development and progression of CCM vascular lesions. Importantly, loss of *Klf4* almost abolished the 100% mortality observed in EC-CCM1 KO mice due to brain hemorrhage.

## 7.1 Development of a new mouse model of CCM disease

We developed a relevant mouse model for CCM disease with a complete penetrance and a rapid progression of the disease useful to study in detail the signalling pathways involved in the etiology of CCM disease. Endothelial cell-specific deletion of the *Ccm1* gene at P1 in mice resulted in the development of several vascular lesions within the CNS and in retina that faithfully phenocopied the human malformations. Thus, vascular lesions presented a mulberry-like structure composed of dilated vessels with multiple lumens, hemosiderin accumulation and a marked inflammatory reaction due to immune cell infiltration. In the area of the cavernomas the neurovascular unit was compromised due to an impaired endothelial/astrocyte interaction and pericyte coverage and the architecture of the endothelial junctions was strongly affected. The lesions had a venous origin and the number and size of malformations did not regress but, instead, increased with time. Finally, the morphology of the malformations was similar in the three strains of mutants (*Ccm1*, *Ccm*2 or *Ccm3* loss-of-function mice), with the phenotype of mice with *Ccm3* deficiency being the most severe [69, 92, 291]. All these alterations were previously described in human CCM. Although every mouse model had always limitations and it would be unrealistic to assume that they could reproduce in all details what occurs in human patients, our murine CCM model was quite close to the human disease. The rapid onset of the disease in this model makes it suitable for deciphering the molecular mechanisms involved in the different phases of development of the disease and for the study of future therapeutic agents. This was particularly important since, so far, no pharmacological therapy is available for CCM patients.

## 7.2 Molecular mechanisms associated to CCM disease: KLF4 upregulation and KLF4-dependent EndMT

The process of EndMT occurring in several physiological and pathological conditions is characterized by multiple EC functional changes that include altered junction organisation, loss of cell polarity, increased cell proliferation and migratory capacity and finally modifications in the cytoskeleton and in the ECM organization [114, 278]. Thus, the EndMT switch could explain most of the previously reported changes in phenotype of CCM null ECs [69, 88, 100, 103]. Here we demonstrated that the increased *Klf4* expression promoted most of the cellular phenotypic transitions associated to EndMT in the absence of *Ccm1*. In agreement, inhibition of KLF4 in CCM null ECs resulted in decreased expression of mesenchymal and stem-cell markers together with a relevant inhibition of cell proliferation and migration while a correct junction organization was not restored. In this regard KLF4 has been reported to maintain the endothelial barrier integrity by regulating the expression of important endothelial junction molecules *in vitro* [227, 229, 230]. In our cellular models neither KLF4 depletion nor KLF4 overexpression seemed to affect *VE-cadherin* or *Claudin5* expression and localization, thus suggesting that junction dismantiling described in the absence of *Ccm1* is KLF4 independent and other molecular mechanisms altered upon loss of *Ccm1* could cause modifications in endothelial cell-to-cell junction organization.

The mechanism of action of KLF4 in inducing CCM malformations is complex and here we defined some of the molecular steps involved (Figure 88). *Klf4* expression increased soon after *Ccm* ablation and it remained high in ECs lining CCM lesions and pseudo normal peri-lesion vessels. KLF4 induction led to a strong endogenous production of BMP6 in CCM null ECs. This growth factor was able to activate the TGF-β/BMP signalling pathway and to induce the EndMT switch [291]. In agreement, chemical inhibition of the TGF-β/BMP signalling prevented the EndMT switch in CCM1 null ECs and the appearance of CCM lesions *in vivo* [291]. Besides modulating *Bmp6* expression and TGF-β/BMP pathway activation, KLF4 binds to the promoters of some EndMT markers (*Sca1* and *Fsp1*) and directly promotes their transcription. Intriguingly, the promoter regions of these representantive mesenchymal and stem-cell markers with a higher KLF4 binding affinity were surrounded by putative SMAD binding sites. Since pSMADs bind weakly to their target gene promoters [295] it could be possible that their DNA binding is reinforced through the association with KLF4, adding a further level of regulation of SMAD activity by KLF4 [305]. *Viceversa*, we found that TGF-β/BMP signalling pathway was able to regulate *Klf4* expression. Stimulation of ECs with different TGF-β/BMP family ligands induces KLF4 upregulation [306, 307]. Moreover treatment with TGF-β/BMP pathway inhibitors as well as *Bmp6* silencing decreased KLF4 expression in CCM1 null ECs both *in vitro* and *in vivo* [291], thus suggesting that TGF-β/BMP pathway, once activated, could sustain *Klf4* expression in a positive feedback loop.

KLF4 could regulate the expression of other genes whose activity is potentially relevant for both EndMT dependent or independent CCM development and progression. Among a large number of genes that were differentialy expressed upon loss of *Ccm1* in our Affimetrix analysis performed using mRNA extracts derived from WT and CCM1 KO BMECs, we focused our attention on *Lrg1*, *Edn1* and *Ednrb*. The leucine-rich alpha-2-

glycoprotein 1 (*Lrg1*) is an angiogenic molecule that is able to promote TβRII-ALK1-SMAD1/5/8 signalling pathway in ECs by binding to the accessory receptor ENG [308]. Since *Lrg1* expression increased upon loss of *Ccm1* in the Affimetrix analysis, we performed preliminary experiments in order to validate this data. Silencing of any one of the three *Ccm* genes in lung WT ECs (Appendix Figure 1 A) as well as loss of *Ccm1* in primary brain ECs (Appendix Figure 1 B) led to *Lrg1* upregulation. Interestingly loss of *Klf4* abolished *Lrg1* upregulation in the absence of *Ccm1* both *in vitro* and *in vivo* (Appendix Figure 1B and C), thus suggesting *Lrg1* as a putative KLF4 target gene. Since *Lrg1* is a modulator of TGF-β signalling pathway [308], we will investigate the role of this molecule during EndMT and CCM lesion development.

Both *Edn1* and *Ednrb* expression has been previously linked to KLF4 transcriptional activity [224]. EDN1 fulfills complex fuctions in vascular biology, including cellular proliferation, apoptosis and angiogenesis [309]. EDN1 has a dual role in blood vessels: 1) it induces potent and long lasting vasoconstrinction by binding to the endothelin receptor A (*Ednra*), a receptor expressed specifically in SMCs; 2) it promotes vasodilation by binding EDNRB on ECs and inducing nitric oxide (NO) synthesis. Endothelial KLF4 modulates the EDN-dependent pathway by repressing *Edn1* expression and increasing *Ednrb* transcription [224]. In line with these data, qRT-PCR analysis in primary brain ECs *in vitro* revealed that *Edn1* was reduced while *Ednrb* was strongly increased in CCM1 KO BMECs compared to WT (Appendix Figure 1D). Moreover, loss of *klf4* increased *Edn1* levels while it abolished *Ednrb* upregulation in the absence of *Ccm1* (Appendix Figure 1D). Since abnormal vessel dilation is a hallmark of CCM vascular malformations, future studies will be directed to evaluate the relevance of EDN-dependent signalling dysregulation in CCM disease.

Thus, since we report that KLF4 is a master regulator of EndMT in CCM, a tempting idea is to understand whether KLF4 could play a role also in tumor EndMT. ECs are prominent component of tumor microenvironment and during cancer progression they can undergo EndMT. Recent studies showed that a significant number of cancer-associated fibroblasts (CAFs) derive from ECs undergoing EndMT [118, 310]. CAFs are key component of the tumor stroma that facilitate tumor growth and metastasis by modifying tumor microenvironment [118, 310]. Moreover, as EndMT leads to the loss of a correct function and organization of the endothelium, a number of other processes involved in tumor progression can be affected. For instance, by weakening endothelial barrier function, EndMT has been reported to enable metastatic dissemination by facilitating tumor cell intra and extravasation [311] As TGF-β/BMP signalling pathway has been suggested as major inducer of EndMT [284] in several physiological and pathological conditions including cancer [118], it would be of particular interest to understand whether KLF4 might act as a critical molecular effector of TGF-β/BMP signalling in the induction of EndMT during tumorigenesis.

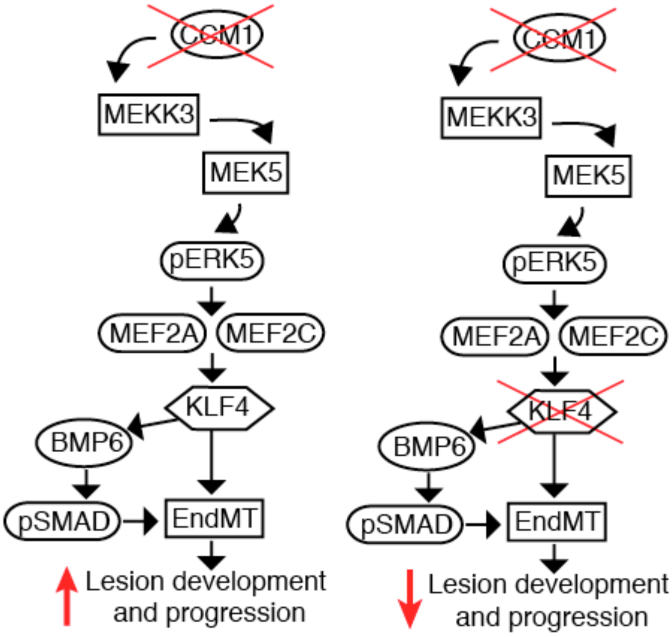
CCM1
MEKK3
MEK5
pERK5
MEF2A
MEF2C
KLF4
BMP6
pSMAD
EndMT
Lesion development and progression
CCM1
MEKK3
MEK5
pERK5
MEF2A
MEF2C
KLF4
BMP6
pSMAD
EndMT
Lesion development and progression

**Figure 88 - Schematic model of KLF4 activity and regulation during CCM pathogenesis.**

Loss of *Ccm1* led to MEKK3-MEK5-dependent ERK5 phosphorylation that, in turn, induced a strong upregulation of *Klf4* expression in brain ECs. The resulting increased KLF4 transcriptional activity was responsible for the EndMT switch observed in CCM1 null ECs, since it was able to: i) promote *Bmp6* expression and consequent SMAD signalling activation; ii) drive the transcription of a number of EndMT markers involved in CCM pathogenesis. *In vivo Klf4* genetic inactivation blocked the development and progression of cavernomas.

## 7.3 MEKK3-MEK5-ERK5 signalling pathways induce KLF4 expression in Ccm null ECs

In the present study we also investigated the mechanism through which loss of *Ccm* genes leads to an increased *Klf4* expression with the final aim of identifying new targets for future pharmacological therapies. Laminar flow through ERK5 activation is a well-known inducer of *Klf4* expression and activity [226, 236]. CCM complex disruption in the endocardium modulates the MEKK3-MEK5-ERK5 axis to upregulate *Klf4* and *Klf2* expression resulting in mid-gestation heart failure [296]. MEKK3, identified as a CCM2 binding partner in the osmosensing complex [302], activates MEK5 that, in turn, through ERK5 dual phosphorylation, induces transcription factors MEF2A, MEF2C and MEF2D to regulate their target genes [303, 304]. In agreement with these reports we found that MEKK3-MEK5 axis promoted ERK5 activation upon loss of *Ccm1* and the inhibition of ERK5 prevented KLF4 upregulation and EndMT induction in cultured CCM1 KO ECs (Figure 88), thus supporting the concept that ERK5 is a key regulator of *Klf4* expression after CCM complex disruption. Importantly, ERK5-dependent KLF4 upregulation is induced by inactivation of any one of the three *Ccm* genes consistent with the comparable phenotype observed in patients. Phosphorylated ERK5 promoted *Klf4* expression largely through MEF2A and MEF2C transcriptional activity. However, since a complete KLF4 downregulation was not observed when these two transcription factors were silenced, either ERK5 alone or other ERK5-downstream transcription factors could be responsible for KLF4 upregulation [241].

A marked increase in ERK5 activity and *Klf4* expression in CCM null ECs was described in the absence of flow, thus suggesting that CCM complex distruption could mimic a condition of permanent flow. In line with this hypothesis Jilkova et al demonstrated that *Ccm* depletion led ECs to acquire an elongated “shear stress-like” phenotype even in the absence of flow [312]. Since differentially from the arteries the venous capillary bed, in which CCM specifically arises, is characterized by low shear stress, a molecular condition that mimics a sustained flow could explain the venous manifestation of the disease. Moreover CCM complex is necessary for maintaining β1 integrin in a low activation state *in vitro* in condition of low blood flow [312]. In the absence of *Ccm* genes β1 integrin is hyperactivated by flow and could be responsible for the vessel dilation observed in CCM [312]. Thus CCMs appeared as mechanotrasducers able to modulate the EC response to different conditions of blood flow.

### 7.4 Possible crosstalk between KLF4 and other signalling pathway involved in CCM

Several recent pubblications unveiled that beyond KLF4-dependent signalling other pathways may contribute to CCM [92, 96, 112, 313, 314].

*Ccm* genes deletion promoted β-catenin nuclear translocation and transcriptional signaling [92, 101]. The activation of β-catenin-mediated transcription is a very early event in lesion formation in EC-CCM3 KO mice and is critical for the acquisition of a mesenchymal phenotype in ECs lining the cavernomas [92]. Accordingly, inhibition of β-catenin signalling in CCM3 null ECs both by using a dominant-negative mutant of TCF4 (dnTCF4) or by a treatment with Sulindac, a nonsteroidal anti-inflammatory drug reported to switch off β-catenin signalling, resulted in strong reduction in the number and size of lesions as well as associated EndMT [92]. A possible link between β-catenin and KLF4 emerged from this study [92]. β-catenin signalling inhibition reduced KLF4 upregulation in CCM3 null ECs both *in vitro* and *in vivo* thus suggesting a possible contribution of β-catenin transcriptional activity to the increase of *Klf4* expression at least in the absence of *Ccm3* [92]. β-catenin signalling was found to be increased also in CCM1 KO ECs opening the possibility of a β-catenin-dependent KLF4 upregulation as a common molecular node upon loss-of-function of any of the three *Ccm* genes. Since we demonstrated that ERK5 activity is critical for KLF4 upregulation in CCM null ECs, future studies will be directed to evaluate a possible crosstalk between β-catenin and the MEKK3-MEK5-ERK5 signalling cascade. Differentially to what we observed upon *Klf4* silencing in CCM1 null ECs, β-catenin signalling inhibition was able, at least in part, to restore a proper junction organization in CCM3 KO ECs. Thus, β-catenin could promote multiple features of the EndMT switch through both KLF4-dependent and independent mechanisms.

CCM1 deficiency promoted also RhoA activation [88, 96] and Rho-dependent cytoskeletal rearrangements. Pharmacological inhibition of the Rho effector ROCK through Fasudil reduced stress fibers *in vitro* in CCM null ECs and decreased the number and size of vascular lesions in *vivo* [91]. Since Rho activation has been reported to occurr during TGF-β-dependent EMT [315, 316], we hypothesized that KLF4-depedent TGF-β/BMP pathway activation could result in RhoA-dependent cytoskeletal rearrangements and increased endothelial permeability observed in CCM.

A recent report claimed that defective autophagy could play a role during CCM pathogenesis [317]. Loss of *Ccm1* induced mTOR hyperactivation that, in turn, was important for the EndMT transition [317]. The inhibition of mTOR activity with rapamycin or Torin1 reduced the expression of some mesenchymal markers (such as *Cd44* and *Id1*) and increased the levels of junctional molecules such as VE-cadherin and Pecam1 *in vitro*, thus suggesting mTOR inhibitor, which are currently used in several clinical trials, as a promising therapy for CCM [317]. Since KLF4 has been reported to control autophagy in cardiomyocite [318] and in ECs (M.Jain personal communication), future studies will evaluate a possible relantioship between KLF4 and *Ccm* defective autophagy.

### 7.5 KLF4 context-dependent functions: a possible explanation for the brain specificity of the CCM disease

KLF4 fulfills pleiotropic functions in EC biology. It is widely considered a vascular protective factor due to its ability to activate specific transcriptional programs with anti-inflammatory, anti-coagulant and anti-oxidant roles in the endothelium [224, 227, 228]. However, recent publications have associated KLF4 also to endothelial pathologies, since it can promote sprouting angiogenesis by regulating the Notch signalling pathway and it is upregulated in several pathological conditions [225, 319, 320].

A context-dependent function of KLF4 could explain its protective versus pathogenic role in different type of vessels. While it confers vascular protection to atherothrombosis and pulmonary arterial hypertension when is upregulated in arteries [224, 228], it could play a causative role in the development of venous-derived CCM cavernomas [69, 291]. Albeit we still do not know the molecular basis of these discrepancies, it is conceivable that the interaction with cell-specific transcription factors or differences in kinetics and levels of expression may modulate the response of ECs to KLF4. In this direction, it is noticeable that the levels of KLF4 are higher in retinal veins than in arteries in both physiological condition and upon *Ccm1* deletion. Since KLF4 can differentially regulate EC gene expression also through coactivator competition by interacting with/sequestering p300 acetylase [215, 228], different cell-type specific and context-dependent function KLF4 could be placed in a central position in promoting either vascular health or disease.

A large debate on CCM is related to the tissue specificity of the pathology. The lesions develop mainly in CNS vasculature although the gene was inactivated in all ECs [69, 92, 291]. In this regard a comparable increase in KLF4 induced in ECs of different organs by loss of *Ccm1* resulted in a full EndMT switch only in brain ECs. These data support the idea of a KLF4-dependent specific activation of brain ECs to undergo EndMT. The difference between the endothelium of the brain in comparison to other organs is due to the surrounding environment that strongly influences EC function. ECs of the brain vasculature are enwrapped by pericyte, astrocytic end feet processes and neuronal synapses and the correct crosstalk between these multiple components has been found to be necessary for proper formation and function of BBB. This type of interaction is unique for the brain vessels and may explain why in other organs the appearance of vascular malformations is much less frequent.

### 7.6 KLF4 constitutes a novel target for a future pharmacological therapy for the treatment of CCM

Pharmacological treatment limiting CCM disease progression is dearly needed as available therapy is limited to surgical lesion eradication. Loss of *Klf4 in vivo* prevented the onset and progression of vascular lesion and almost abolished mouse mortality due to brain hemorrhage in EC-CCM1 KO mice. Since the upregulation in KLF4 observed in our murine model of CCM was confirmed both in familial and sporadic CCM patients, the use of inhibitors of KLF4 could constitute a common strategy for the treatment of the familial and sporadic forms of the disease. Sporadic patients, at variance with the familial ones, got a diagnosis frequently at late phases of the disease when established vascular lesion are already symptomatic. Thus, the treatment of these patients with KLF4 inhibitors will require further studies on the effects of KLF4 inhibition at later stages of the CCM disease.

Transcription factors are considered, in general, “undruggable agents”. Indeed, KLF4 is a member of the large family of Kruppel-like factors that are highly homologous sharing a triple zinc finger DNA-binding domain [182]. The functions of the KLF family members can be exclusive or in some cases overlapping and redundant, compensating for one another and this might impair the efficacy of a possible therapy based on specific chemical compounds [198]. An alternative approach could be the use of inhibitor of the MEKK3-MEK5-ERK5 axis responsible for the upregulation of KLF4 upon loss of anyone of the *Ccm* genes. Since the specific ERK5 inhibitor XMD8-92 was very effective in reducing KLF4-dependent EndMT in cultured CCM1 KO ECs and was previously used *in vivo* [259], we are going to test its efficacy in preventing lesion development and progression in EC-CCM1 KO mice. However, widespread inhibition of ERK5 kinase could lead to severe side effects since ERK5 activity was reported to be critical for endothelial cell physiology by preventing apoptosis, regulating tumor angiogenesis and mediating EC response to shear stress [241, 243]. The use of KLF4 or ERK5 inhibitors bound to nano-particles targeting specifically CCM vascular lesions may represent a more safe therapeutic approach.

In the immediate future a high throughput screening of small molecule libraries will be performed in collaboration with the Uppsala University to identify new componds able to inhibit the MEK5-ERK5-KLF4 signalling axis. They will be tested *in vivo* in our mouse model for their efficacy in preventing, arresting or even reverting the growth of CCM lesions.

A targeted therapy with KLF4 inhibitors could anyway promote inflammation in vascular lesions. A robust infiltration of immune cells in human CCM specimens had been reported in literature [272]. In agreement, vascular lesions in EC-CCM1 KO mice were infiltrated by CD11b and CD3 positive cells and showed an increased expression of cell adhesion molecules (CAMs) such as ICAM1 and VCAM1 [282]. KLF4 was described as a modulator of EC inflammation by its ability to inhibit NF-kB activity and the expression of pro-adhesive (such as *Vcam1*) and pro-thrombotic genes (such as *Pai-1*) [227, 228]. Since inflammatory cytokines produced by immune cell infiltrated in CCM could act in synergism with TGF-β/BMP signalling to promote EndMT [278], targeting KLF4 expression in an established CCM lesion with an inflammatory reaction ongoing could lead to unexpected side effects.

### 7.7 KLF2 and KLF4 do not have overlapping roles in CCM

Two different research groups recently reported a causative role for KLF2 in the cardiac phenotype observed in the absence of CCM in both mouse and zebrafish embryos [107, 296].

In these studies KLF2 was responsible for both digestion of the cardiac jelly [296] and increased angiogenesis [107]. In our CCM disease model we found that *Klf2* was upregulated in freshly isolated brain derived CCM1 null ECs or in cultured CCM1 KO BMECs supporting the idea of a possible cooperation between KLF2 and KLF4. However, although these two transcription factors have many common targets, they still exhibit specificity due to individual differences in their affinities for jointly regulated promoters. The lack of a fully overlapping biological role of KLF2 and KLF4 is also demonstrated by the different phenotype of the respective null mice. While *Klf2* null mice exhibit abnormal blood vessel formation resulting in embryonic hemorrhage and death [321], *Klf4* null mice die within one day after birth due to loss of skin barrier function [218]. The relative contribution of KLF2 to the development of CCM remains an open question and requires future studies, since *Klf2* was not further upregulated upon *Klf4* ablation in our CCM model and apparently did not compensate for the lack of KLF4 in inducing EndMT.

### 7.8 Concluding remarks

In conclusion, this study highlights the importance of KLF4 transcriptional activity for the onset and development of CCM pathology and identifies novel potential pharmacological targets to prevent the progression of this so far incurable disease.

# APPENDIX

| List of upregulated genes (threshold =1.2, P<0.05) | | |
|---|---|---|
| **Gene name** | **Fold change** | **Gene ID** |
| SERPINB9B | 3,324091282 | 10404439 |
| KLF4 | 3,148817186 | 10513008 |
| STMN2 | 3,131122603 | 10490818 |
| FBLN2 | 3,034081838 | 10540085 |
| EDNRB | 2,951564768 | 10422164 |
| DLL1 | 2,941944438 | 10448034 |
| KLF2 | 2,790241509 | 10572800 |
| LMCD1 | 2,610977454 | 10540523 |
| NEURL2 | 2,556606278 | 10489566 |
| NPNT | 2,450489559 | 10502240 |
| PLTP | 2,426118469 | 10489569 |
| F5 | 2,404721801 | 10351224 |
| LRG1 | 2,396352264 | 10451953 |
| CYP1B1 | 2,375432151 | 10453057 |
| FNDC1 | 2,329047398 | 10447649 |
| RAMP3 | 2,321472193 | 10374197 |
| LTBP4 | 2,298734744 | 10561212 |
| TNFSF18 | 2,294468499 | 10351099 |
| CMKLR1 | 2,260794718 | 10532711 |
| FAM20A | 2,24657932 | 10392464 |
| PGLYRP1 | 2,193401621 | 10550509 |
| FAM107A | 2,101296871 | 10417561 |
| NMNAT2 | 1,992120616 | 10350697 |
| CEACAM1 | 1,930902074 | 10561008 |
| KCNB1 | 1,9282004 | 10489872 |
| PTHLH | 1,926136571 | 10549388 |
| JAM2 | 1,904576187 | 10436666 |
| CD55 | 1,900916287 | 10357488 |
| RTP3 | 1,880380989 | 10597273 |

| | | |
|---|---|---|
| LSR | 1,875324167 | 10562181 |
| SERPINB1A | 1,865516344 | 10408557 |
| ADAMTS5 | 1,85637735 | 10440534 |
| SNCG | 1,840400814 | 10418921 |
| SLCO2A1 | 1,838692212 | 10588263 |
| FAM189A2 | 1,83422421 | 10466735 |
| TSC22D3 | 1,823784159 | 10606989 |
| FMO1 | 1,818948883 | 10359571 |
| FAM55D | 1,80884025 | 10585068 |
| OLFML2A | 1,803982071 | 10471882 |
| DHRS3 | 1,77509963 | 10510129 |
| LBP | 1,769553034 | 10478048 |
| SELP | 1,765736419 | 10351206 |
| GBP4 | 1,757384653 | 10531987 |
| NR4A1 | 1,739273725 | 10427035 |
| ITGB4 | 1,706050084 | 10382713 |
| CD14 | 1,701638995 | 10458382 |
| NOV | 1,700778188 | 10424119 |
| NQO1 | 1,687818767 | 10581538 |
| MGLL | 1,687052652 | 10539894 |
| LFNG | 1,67692132 | 10527012 |
| TRPV4 | 1,667625109 | 10532839 |
| GPR1 | 1,66470899 | 10355109 |
| 1700020C07RIK | 1,664512841 | 10489562 |
| PMP22 | 1,662783111 | 10376950 |
| C430048L16RIK | 1,65900703 | 10503359 |
| 2310046K01RIK | 1,656725977 | 10477052 |
| PPAP2B | 1,645972235 | 10506488 |
| CLIC5 | 1,644865933 | 10445347 |
| CXX1A | 1,644672122 | 10604633 |
| SERPINB8 | 1,636189673 | 10349174 |
| EGFL8 | 1,634330772 | 10450212 |
| PKN3 | 1,630613653 | 10470913 |
| CADM3 | 1,624944 | 10360349 |

| | | |
|---|---|---|
| CXX1A | 1,62113024 | 10604637 |
| TSPAN7 | 1,61505131 | 10598626 |
| TINAGL1 | 1,603417361 | 10516735 |
| ATP2B4 | 1,599099822 | 10357833 |
| CYSLTR1 | 1,593092459 | 10606355 |
| 2200002K05RIK | 1,574550468 | 10583291 |
| CBFA2T3 | 1,572309247 | 10582429 |
| CRIP1 | 1,570365083 | 10399005 |
| CAR7 | 1,570256237 | 10574480 |
| AFAP1L2 | 1,562065555 | 10468668 |
| XDH | 1,55413303 | 10452815 |
| CKB | 1,552189822 | 10402708 |
| RASSF1 | 1,54975483 | 10596671 |
| RET | 1,547581084 | 10547227 |
| RIPPLY3 | 1,532572156 | 10437073 |
| ATP2A3 | 1,52136888 | 10378216 |
| SCGB3A1 | 1,521295065 | 10375608 |
| GPRC5A | 1,520673048 | 10542335 |
| P2RY2 | 1,519292869 | 10565962 |
| ANPEP | 1,513758436 | 10564818 |
| L1CAM | 1,510148057 | 10605113 |
| DISP2 | 1,508751285 | 10474814 |
| APLNR | 1,50703717 | 10473444 |
| PNKD | 1,501214365 | 10347310 |
| NR4A2 | 1,494424487 | 10482772 |
| KLF10 | 1,483546349 | 10428302 |
| ARF2 | 1,481737616 | 10381744 |
| ZFP341 | 1,476503729 | 10488802 |
| SCD1 | 1,451430005 | 10467979 |
| CBFA2T3 | 1,448595702 | 10582427 |
| CDC42EP2 | 1,438385119 | 10465278 |
| SLC9A3R2 | 1,434452305 | 10448676 |
| PLVAP | 1,430956683 | 10579525 |
| FMO2 | 1,427311276 | 10359582 |

| | | |
|---|---|---|
| 4930578C19RIK | 1,422225275 | 10603796 |
| ADAMTS1 | 1,422077411 | 10440522 |
| SLC46A3 | 1,421717672 | 10535841 |
| RAMP2 | 1,420550382 | 10381298 |
| MS4A6D | 1,419079092 | 10466210 |
| TRIL | 1,418641444 | 10544837 |
| CAPN5 | 1,415493378 | 10565689 |
| APOD | 1,409564993 | 10439009 |
| SLCO1A4 | 1,409545452 | 10548996 |
| LY6C2 | 1,405662262 | 10429573 |
| DOK4 | 1,404464346 | 10580782 |
| PDLIM1 | 1,402163903 | 10467420 |
| MAL | 1,401940382 | 10487441 |
| EZR | 1,397332155 | 10447602 |
| NRGN | 1,396852802 | 10592330 |
| JAG2 | 1,3934971 | 10402808 |
| SLCO2B1 | 1,389436594 | 10565819 |
| SPA17 | 1,387103077 | 10592336 |
| CAR5B | 1,383545414 | 10607738 |
| EMP2 | 1,375923252 | 10437639 |
| TMEM44 | 1,371885427 | 10438942 |
| ACER3 | 1,366130212 | 10565712 |
| CD97 | 1,3649991 | 10580033 |
| CST6 | 1,363712949 | 10464999 |
| DNAJA1 | 1,359668546 | 10503995 |
| 2210411K11RIK | 1,359404685 | 10559673 |
| WFDC1 | 1,357121606 | 10575917 |
| PBK | 1,353547015 | 10416037 |
| LCN2 | 1,349355042 | 10481627 |
| S1PR4 | 1,347415686 | 10371217 |
| LEPREL1 | 1,345059506 | 10438753 |
| ANKRD37 | 1,344155456 | 10578515 |
| FAM78B | 1,338034208 | 10351400 |
| MN1 | 1,330718116 | 10524327 |

| | | |
|---|---|---|
| ZFYVE9 | 1,328750284 | 10515028 |
| MYBL1 | 1,327806574 | 10353010 |
| STC1 | 1,327121079 | 10416181 |
| UPP1 | 1,32317144 | 10374236 |
| ID1 | 1,32317144 | 10477169 |
| ZFP697 | 1,322447088 | 10494655 |
| AQP11 | 1,321146084 | 10565627 |
| NRM | 1,318218936 | 10444927 |
| ABI3 | 1,317739321 | 10390186 |
| NCOA3 | 1,312374985 | 10478718 |
| NT5E | 1,310897605 | 10587639 |
| LY6C1 | 1,308940937 | 10429568 |
| THBD | 1,300304944 | 10488378 |
| RFK | 1,299989526 | 10461898 |
| PODXL | 1,295447007 | 10543791 |
| PROM1 | 1,294751294 | 10529824 |
| AI836003 | 1,29463463 | 10426581 |
| KLF7 | 1,294369932 | 10355141 |
| MUSTN1 | 1,293697215 | 10413609 |
| HSPH1 | 1,292751519 | 10535904 |
| PIK3R6 | 1,289221363 | 10377286 |
| TEAD4 | 1,28403542 | 10548146 |
| KCTD12 | 1,283021192 | 10422059 |
| BAIAP2L1 | 1,282598833 | 10535559 |
| APOLD1 | 1,281781187 | 10542319 |
| BANP | 1,27980588 | 10576073 |
| ALS2CL | 1,275882082 | 10589654 |
| IDH1 | 1,275444392 | 10355214 |
| GBP6 | 1,27525875 | 10531994 |
| KIF23 | 1,273721618 | 10594251 |
| PAQR5 | 1,272962571 | 10594277 |
| STARD8 | 1,272327437 | 10600921 |
| FAM20C | 1,272274524 | 10526853 |
| BC020535 | 1,271428207 | 10477237 |

| | | |
|---|---|---|
| NUSAP1 | 1,269864884 | 10474984 |
| CALCRL | 1,269666854 | 10484371 |
| 8430408G22RIK | 1,269037763 | 10541071 |
| NSG1 | 1,26791673 | 10529656 |
| PIR | 1,267161142 | 10603087 |
| CHORDC1 | 1,266318226 | 10583347 |
| DGKA | 1,262820862 | 10373542 |
| SH3BGRL2 | 1,261967713 | 10587503 |
| SDPR | 1,261464844 | 10346164 |
| NEK7 | 1,259804614 | 10358259 |
| SHE | 1,256272992 | 10493604 |
| GJA1 | 1,256229453 | 10363173 |
| PLAUR | 1,254258748 | 10550906 |
| KRAS | 1,253589499 | 10549256 |
| KIF11 | 1,253298444 | 10462796 |
| HLX | 1,25103747 | 10360834 |
| CDC25B | 1,248707001 | 10476252 |
| E2F8 | 1,248503616 | 10563780 |
| 2810417H13RIK | 1,244770694 | 10586448 |
| RNF125 | 1,243951295 | 10454198 |
| ADAMTS4 | 1,243882318 | 10351551 |
| OXA1L | 1,240180405 | 10419744 |
| HIST1H1B | 1,239974112 | 10408081 |
| GPR182 | 1,239565924 | 10373325 |
| STK10 | 1,23741978 | 10375083 |
| RYBP | 1,237346876 | 10546706 |
| NOS3 | 1,236061049 | 10520126 |
| MEST | 1,234121983 | 10537062 |
| EMP3 | 1,233920973 | 10563441 |
| SLC16A3 | 1,232984788 | 10383502 |
| KANK3 | 1,232681428 | 10444028 |
| CDA | 1,232126174 | 10517609 |
| RNF167 | 1,228616787 | 10377927 |
| BST1 | 1,225945632 | 10521667 |

| | | |
|---|---|---|
| AZIN1 | 1,224455209 | 10428310 |
| 2610034B18RIK | 1,222229324 | 10564849 |
| ADAMTS9 | 1,221623737 | 10546432 |
| GPR31C | 1,219787638 | 10447647 |
| RACGAP1 | 1,219141008 | 10432511 |
| EBP | 1,218756573 | 10603485 |
| HIST1H1A | 1,218570736 | 10404069 |
| ENTPD1 | 1,21828359 | 10463070 |
| SERPINB6B | 1,218156929 | 10404422 |
| DPAGT1 | 1,217777025 | 10584700 |
| DHRS7 | 1,217363487 | 10400941 |
| PPDPF | 1,216089997 | 10599576 |
| HES1 | 1,215955136 | 10434925 |
| PDGFA | 1,215529578 | 10535043 |
| AVPI1 | 1,214607346 | 10467739 |
| TEK | 1,214531577 | 10505954 |
| PALMD | 1,213732084 | 10501734 |
| LAYN | 1,212849046 | 10593449 |
| ACY3 | 1,212630488 | 10460263 |
| MMP15 | 1,212382556 | 10574350 |
| GPR146 | 1,211861645 | 10526943 |
| FUCA2 | 1,209214346 | 10361790 |
| ADAMTS9 | 1,209029964 | 10546450 |
| CASKIN2 | 1,208338782 | 10392998 |
| MARVELD1 | 1,206476655 | 10463224 |
| PPP1R11 | 1,206351222 | 10450814 |
| AURKB | 1,205348224 | 10377405 |
| 3110001D03RIK | 1,205264679 | 10513952 |
| C2CD2L | 1,203720131 | 10592802 |
| ERI1 | 1,203290515 | 10578193 |
| PIK3R3 | 1,202010918 | 10507273 |

**Appendix Table 1- List of upregulated genes in CCM1 KO BMECs obtained by Affymetrix analysis and ranked according to the fold change.**

| **List of down regulated genes threshold =1.2, P<0.05** | | |
|---|---|---|
| **Gene name** | **Fold change** | **Gene ID** |
| FAM163A | 2,220246717 | 10359113 |
| STFA1 | 1,875376162 | 10435501 |
| ZFP462 | 1,748848117 | 10505073 |
| CCL2 | 1,673246504 | 10379511 |
| KDM4D | 1,651824026 | 10590915 |
| SELE | 1,597720445 | 10351182 |
| IRG1 | 1,576510742 | 10416837 |
| ANKRD1 | 1,56004214 | 10467191 |
| EPHA7 | 1,535533514 | 10503659 |
| CCRN4L | 1,532758069 | 10491915 |
| PRSS23 | 1,527407486 | 10554814 |
| CLDN1 | 1,523025398 | 10438769 |
| CCL5 | 1,515811125 | 10389207 |
| THY1 | 1,48728899 | 10584628 |
| ARRDC4 | 1,45031874 | 10564507 |
| SNORD49B | 1,42795449 | 10376885 |
| MYL9 | 1,423167036 | 10477920 |
| ADAMTS7 | 1,419098765 | 10587748 |
| ACPP | 1,417235983 | 10596303 |
| TGFB2 | 1,398325279 | 10360920 |
| ITGAV | 1,396001024 | 10473281 |
| F2RL2 | 1,3950579 | 10406736 |
| GPX3 | 1,3823903 | 10376201 |
| SRPX2 | 1,38148031 | 10601659 |
| CSF1 | 1,377115915 | 10501164 |
| HMCN1 | 1,351615687 | 10358577 |
| ZIC3 | 1,351503268 | 10599812 |
| PLXDC2 | 1,347051492 | 10469457 |
| APCDD1 | 1,346206754 | 10456184 |
| ST5 | 1,344551486 | 10566767 |
| SNCA | 1,338191884 | 10545086 |
| ARHGAP28 | 1,337677185 | 10452613 |

| | | |
|---|---|---|
| GNAS | 1,335675916 | 10490203 |
| ICAM1 | 1,327627115 | 10583519 |
| LCP2 | 1,326293436 | 10375145 |
| RASSF2 | 1,323905365 | 10487894 |
| TAGLN | 1,321553655 | 10593123 |
| BC046404 | 1,317958552 | 10386916 |
| MT2 | 1,314077169 | 10574023 |
| VCAM1 | 1,313166636 | 10501608 |
| GM8979 | 1,312848098 | 10566578 |
| CHGA | 1,307005308 | 10397882 |
| LPAR4 | 1,306493548 | 10601412 |
| TNS3 | 1,305972936 | 10384233 |
| NFKBIE | 1,302149415 | 10445412 |
| H2-Q6 | 1,295626606 | 10444824 |
| JAG1 | 1,291815468 | 10488060 |
| ESM1 | 1,287604925 | 10407281 |
| PHF15 | 1,285567177 | 10385747 |
| KCNQ4 | 1,284133327 | 10515960 |
| RCAN2 | 1,281732322 | 10445325 |
| PTGS2 | 1,281470262 | 10350516 |
| GM8979 | 1,280493562 | 10566571 |
| KRIT1 | 1,27832529 | 10519392 |
| SLC39A4 | 1,277811475 | 10430006 |
| RND1 | 1,273809909 | 10432236 |
| EDN1 | 1,272927277 | 10404783 |
| RND3 | 1,26779809 | 10482500 |
| SERPINE1 | 1,265142594 | 10534667 |
| NCKAP5L | 1,263381192 | 10432473 |
| GADD45B | 1,261683458 | 10364950 |
| ITIH5 | 1,261591635 | 10469151 |
| RGS16 | 1,255620075 | 10350733 |
| ISM1 | 1,253858894 | 10476560 |
| ENC1 | 1,25078602 | 10406817 |
| RIPK2 | 1,250720999 | 10511703 |

| | | |
|---|---|---|
| ODC1 | 1,250668984 | 10394770 |
| 2610008E11RIK | 1,250582297 | 10370544 |
| HSPG2 | 1,24971576 | 10509280 |
| SLC40A1 | 1,23876283 | 10354374 |
| GNAI1 | 1,235508555 | 10528227 |
| F2R | 1,232296994 | 10411229 |
| HIVEP1 | 1,227267722 | 10404774 |
| COL15A1 | 1,222004841 | 10504775 |
| LAMB1 | 1,221327405 | 10395163 |
| VWA1 | 1,219212839 | 10519196 |
| ERN1 | 1,219128332 | 10392183 |
| VWF | 1,218748126 | 10541910 |
| TCFEC | 1,218490497 | 10543239 |
| ODC1 | 1,218241368 | 10582295 |
| NLRC5 | 1,217295984 | 10574100 |
| MEOX1 | 1,216330256 | 10391504 |
| NUAK1 | 1,215550642 | 10371379 |
| GVIN1 | 1,213774149 | 10566574 |
| WBP5 | 1,208904265 | 10601854 |
| TBC1D1 | 1,208736687 | 10522024 |
| TXNDC5 | 1,206142195 | 10408741 |
| HBEGF | 1,202427575 | 10458340 |
| ENPP2 | 1,202194229 | 10428619 |

**Appendix Table 2 - List of downregulated genes in CCM1 KO BMECs obtained by Affymetrix analysis and ranked according to the fold change.**

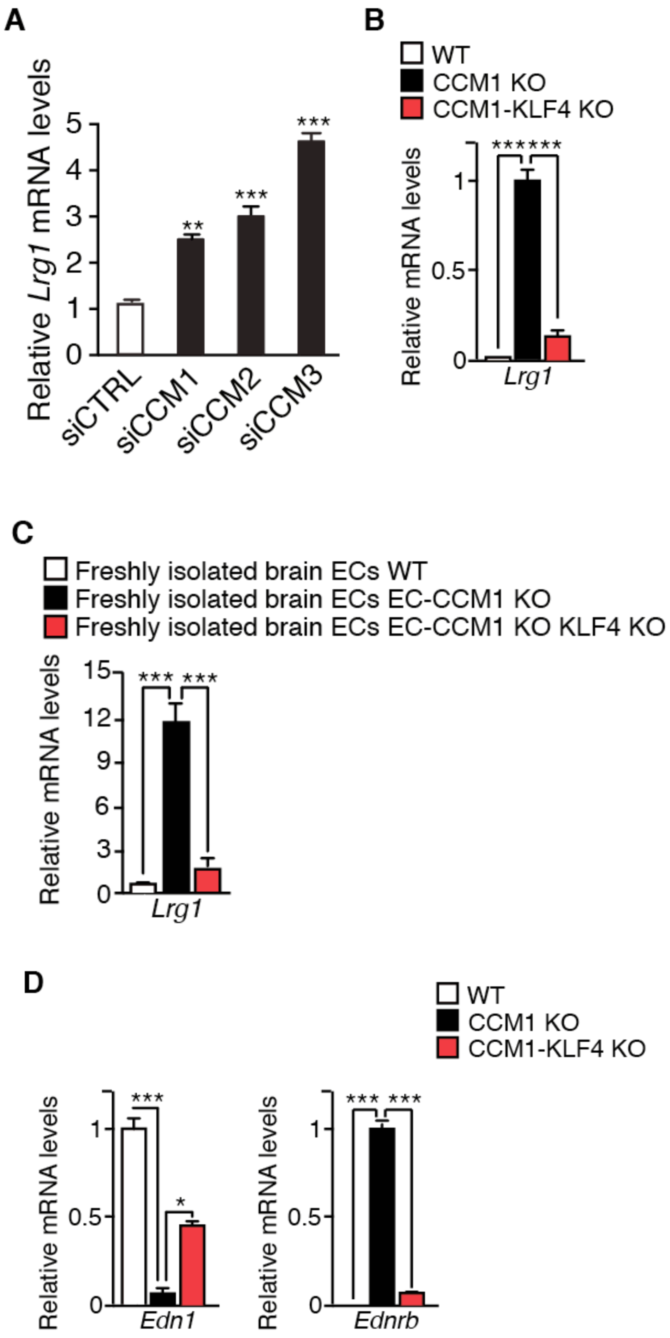

**Appendix Figure 1 – Analysis of *Lrg1*, *Edn1* and *Ednrb* expression in WT, CCM1 KO and CCM1-KLF4 BMECs KO.**

A) qRT-PCR of *Lrg1* upon silencing of anyone of the three *Ccm* genes in lung WT ECs. Data are mean ± SD (n=3) and fold changes are relative to siCTRL-treated WT ECs. B) qRT-PCR of *Lrg1* in WT, CCM1 KO and CCM1-KLF4 KO BMECs. Data are mean ± SD (n=3) and fold changes are relative to WT BMECs C) qRT-PCR of *Lrg1* in freshly isolated ECs from WT, EC-CCM1 KO and EC- CCM1 KO KLF4 KO. qRT-PCR results are shown as mean ± SD (n=3) and are relative to WT freschly isolated ECs  D) qRT-PCR of *Edn1* and *Ednrb* in WT, CCM1 KO and CCM1-KLF4 KO BMECs. Data are mean ± SD (n=3) and fold changes are relative to to WT BMECs. *P<0.05, ** P<0.01, ***P<0.001.

# REFERENCES

1. Dvorak, A. M., Kohn, S., Morgan, E. S., Fox, P., Nagy, J. A., & Dvorak, H. F. (1996). The vesiculo-vacuolar organelle (VVO): a distinct endothelial cell structure that provides a transcellular pathway for macromolecular extravasation. *Journal of leukocyte biology*, *59*(1), 100-115.
2. Stevens, T., Garcia, J. G., Shasby, D. M., Bhattacharya, J., & Malik, A. B. (2000). Mechanisms regulating endothelial cell barrier function. *American Journal of Physiology-Lung Cellular and Molecular Physiology*, *279*(3), L419-L422.
3. Dejana, E., Bazzoni, G., & Lampugnani, M. G. (1999). The role of endothelial cell-to-cell junctions in vascular morphogenesis. *Thromb Haemost*, *82*(2), 755-761.
4. Bazzoni, G., & Dejana, E. (2004). Endothelial cell-to-cell junctions: molecular organization and role in vascular homeostasis. *Physiological reviews*, *84*(3), 869-901.
5. Ikenouchi, J., Umeda, K., Tsukita, S., Furuse, M., & Tsukita, S. (2007). Requirement of ZO-1 for the formation of belt-like adherens junctions during epithelial cell polarization. *The Journal of cell biology*, *176*(6), 779-786.
6. Taddei, A., Giampietro, C., Conti, A., Orsenigo, F., Breviario, F., Pirazzoli, V., ... & Dejana, E. (2008). Endothelial adherens junctions control tight junctions by VE-cadherin-mediated upregulation of claudin-5. *Nature cell biology*, *10*(8), 923-934.
7. Wolburg, H., & Lippoldt, A. (2002). Tight junctions of the blood–brain barrier: development, composition and regulation. *Vascular pharmacology*, *38*(6), 323-337.
8. Dejana, E., Orsenigo, F., & Lampugnani, M. G. (2008). The role of adherens junctions and VE-cadherin in the control of vascular permeability. *Journal of cell science*, *121*(13), 2115-2122.
9. Engelhardt, B. (2003). Development of the blood-brain barrier. *Cell and tissue research*, *314*(1), 119-129.
10. Lampugnani, M. G., Resnati, M., Raiteri, M., Pigott, R., Pisacane, A., Houen, G., ... & Dejana, E. (1992). A novel endothelial-specific membrane protein is a marker of cell-cell contacts. *The Journal of cell biology*, *118*(6), 1511-1522.
11. Navarro, P., Ruco, L., & Dejana, E. (1998). Differential localization of VE-and N-cadherins in human endothelial cells: VE-cadherin competes with N-cadherin for junctional localization. *The Journal of cell biology*, *140*(6), 1475-1484.
12. Giampietro, C., Taddei, A., Corada, M., Sarra-Ferraris, G. M., Alcalay, M., Cavallaro, U., ... & Dejana, E. (2012). Overlapping and divergent signaling pathways of N-cadherin and VE-cadherin in endothelial cells. *Blood*, *119*(9), 2159-2170.
13. Carmeliet, P., Lampugnani, M. G., Moons, L., Breviario, F., Compernolle, V., Bono, F., ... & Dejana, E. (1999). Targeted deficiency or cytosolic truncation of the VE-cadherin gene in mice impairs VEGF-mediated endothelial survival and angiogenesis. *Cell*, *98*(2), 147-157.
14. Luo, Y., & Radice, G. L. (2005). N-cadherin acts upstream of VE-cadherin in controlling vascular morphogenesis. *The Journal of cell biology*, *169*(1), 29-34.
15. Dejana, E., Tournier-Lasserve, E., & Weinstein, B. M. (2009). The control of vascular integrity by endothelial cell junctions: molecular basis and pathological implications. *Developmental cell*, *16*(2), 209-221.
16. Nyqvist, D., Giampietro, C., & Dejana, E. (2008). Deciphering the functional role of endothelial junctions by using in vivo models. *EMBO reports*, *9*(8), 742-747.
17. Yamada, S., Pokutta, S., Drees, F., Weis, W. I., & Nelson, W. J. (2005). Deconstructing the cadherin-catenin-actin complex. *Cell*, *123*(5), 889-901.
18. Lampugnani, M. G., Zanetti, A., Breviario, F., Balconi, G., Orsenigo, F., Corada, M., ... & Dejana, E. (2002). VE-cadherin regulates endothelial actin activating Rac

and increasing membrane association of Tiam. *Molecular biology of the cell*, *13*(4), 1175-1189.

19. Wimmer, R., Cseh, B., Maier, B., Scherrer, K., & Baccarini, M. (2012). Angiogenic sprouting requires the fine tuning of endothelial cell cohesion by the Raf-1/Rok-α complex. *Developmental cell*, *22*(1), 158-171.
20. Lampugnani, M. G., Orsenigo, F., Gagliani, M. C., Tacchetti, C., & Dejana, E. (2006). Vascular endothelial cadherin controls VEGFR-2 internalization and signaling from intracellular compartments. *The Journal of cell biology*, *174*(4), 593-604.
21. Rudini, N., Felici, A., Giampietro, C., Lampugnani, M., Corada, M., Swirsding, K., ... & Dejana, E. (2008). VE-cadherin is a critical endothelial regulator of TGF-β signalling. *The EMBO journal*, *27*(7), 993-1004.
22. Hou, W. H., Liu, I. H., Tsai, C. C., Johnson, F. E., Huang, S. S., & San Huang, J. (2011). CRSBP-1/LYVE-1 ligands disrupt lymphatic intercellular adhesion by inducing tyrosine phosphorylation and internalization of VE-cadherin. *Journal of cell science*, *124*(8), 1231-1244.
23. Andriopoulou, P., Navarro, P., Zanetti, A., Lampugnani, M. G., & Dejana, E. (1999). Histamine induces tyrosine phosphorylation of endothelial cell-to-cell adherens junctions. *Arteriosclerosis, thrombosis, and vascular biology*, *19*(10), 2286-2297.
24. Esser, S., Lampugnani, M. G., Corada, M., Dejana, E., & Risau, W. (1998). Vascular endothelial growth factor induces VE-cadherin tyrosine phosphorylation in endothelial cells. *Journal of cell science*, *111*(13), 1853-1865.
25. Orsenigo, F., Giampietro, C., Ferrari, A., Corada, M., Galaup, A., Sigismund, S., ... & Dejana, E. (2012). Phosphorylation of VE-cadherin is modulated by haemodynamic forces and contributes to the regulation of vascular permeability in vivo. *Nature communications*, *3*, 1208.
26. Angelini, D. J., Hyun, S. W., Grigoryev, D. N., Garg, P., Gong, P., Singh, I. S., ... & Goldblum, S. E. (2006). TNF-α increases tyrosine phosphorylation of vascular endothelial cadherin and opens the paracellular pathway through fyn activation in human lung endothelia. *American Journal of Physiology-Lung Cellular and Molecular Physiology*, *291*(6), L1232-L1245.
27. Hudry-Clergeon, H., Stengel, D., Ninio, E., & Vilgrain, I. (2005). Platelet-activating factor increases VE-cadherin tyrosine phosphorylation in mouse endothelial cells and its association with the PtdIns3′-kinase. *The FASEB journal*, *19*(6), 512-520.
28. Weis, S., Shintani, S., Weber, A., Kirchmair, R., Wood, M., Cravens, A., ... & Cheresh, D. (2004). Src blockade stabilizes a Flk/cadherin complex, reducing edema and tissue injury following myocardial infarction. *Journal of Clinical Investigation*, *113*(6), 885.
29. Nawroth, R., Poell, G., Ranft, A., Kloep, S., Samulowitz, U., Fachinger, G., ... & Vestweber, D. (2002). VE-PTP and VE-cadherin ectodomains interact to facilitate regulation of phosphorylation and cell contacts. *The EMBO journal*, *21*(18), 4885-4895.
30. Lampugnani, M. G., Zanetti, A., Corada, M., Takahashi, T., Balconi, G., Breviario, F., ... & Dejana, E. (2003). Contact inhibition of VEGF-induced proliferation requires vascular endothelial cadherin, β-catenin, and the phosphatase DEP-1/CD148. *The Journal of cell biology*, *161*(4), 793-804.
31. Sui, X. F., Kiser, T. D., Hyun, S. W., Angelini, D. J., Del Vecchio, R. L., Young, B. A., ... & Goldblum, S. E. (2005). Receptor protein tyrosine phosphatase μ regulates the paracellular pathway in human lung microvascular endothelia. *The American journal of pathology*, *166*(4), 1247-1258.

32. Ukropec, J. A., Hollinger, M. K., Salva, S. M., & Woolkalis, M. J. (2000). SHP2 association with VE-cadherin complexes in human endothelial cells is regulated by thrombin. *Journal of Biological Chemistry*, *275*(8), 5983-5986.
33. Gavard, J., & Gutkind, J. S. (2006). VEGF controls endothelial-cell permeability by promoting the β-arrestin-dependent endocytosis of VE-cadherin. *Nature cell biology*, *8*(11), 1223-1234.
34. Hermant, B., Bibert, S., Concord, E., Dublet, B., Weidenhaupt, M., Vernet, T., & Gulino-Debrac, D. (2003). Identification of proteases involved in the proteolysis of vascular endothelium cadherin during neutrophil transmigration. *Journal of Biological Chemistry*, *278*(16), 14002-14012.
35. Furuse, M. (2010). Molecular basis of the core structure of tight junctions. *Cold Spring Harbor perspectives in biology*, *2*(1), a002907.
36. Steed, E., Balda, M. S., & Matter, K. (2010). Dynamics and functions of tight junctions. *Trends in cell biology*, *20*(3), 142-149.
37. Morita, K., Sasaki, H., Furuse, M., & Tsukita, S. (1999). Endothelial Claudin Claudin-5/Tmvcf Constitutes Tight Junction Strands in Endothelial Cells. *The Journal of cell biology*, *147*(1), 185-194.
38. Ebnet, K., Suzuki, A., Ohno, S., & Vestweber, D. (2004). Junctional adhesion molecules (JAMs): more molecules with dual functions?. *Journal of Cell Science*, *117*(1), 19-29.
39. Ebnet, K., Suzuki, A., Horikoshi, Y., Hirose, T., zu Brickwedde, M. K. M., Ohno, S., & Vestweber, D. (2001). The cell polarity protein ASIP/PAR-3 directly associates with junctional adhesion molecule (JAM). *The EMBO journal*, *20*(14), 3738-3748.
40. Lamagna, C., Hodivala-Dilke, K. M., Imhof, B. A., & Aurrand-Lions, M. (2005). Antibody against junctional adhesion molecule-C inhibits angiogenesis and tumor growth. *Cancer Research*, *65*(13), 5703-5710.
41. Katsuno, T., Umeda, K., Matsui, T., Hata, M., Tamura, A., Itoh, M., ... & Tsukita, S. (2008). Deficiency of zonula occludens-1 causes embryonic lethal phenotype associated with defected yolk sac angiogenesis and apoptosis of embryonic cells. *Molecular biology of the cell*, *19*(6), 2465-2475.
42. Gottardi, C. J., Arpin, M., Fanning, A. S., & Louvard, D. (1996). The junction-associated protein, zonula occludens-1, localizes to the nucleus before the maturation and during the remodeling of cell-cell contacts. *Proceedings of the National Academy of Sciences*, *93*(20), 10779-10784.
43. Traweger, A., Lehner, C., Farkas, A., Krizbai, I. A., Tempfer, H., Klement, E., ... & Bauer, H. (2008). Nuclear Zonula occludens-2 alters gene expression and junctional stability in epithelial and endothelial cells. *Differentiation*, *76*(1), 99-106.
44. McCrea, P. D., Gu, D., & Balda, M. S. (2009). Junctional music that the nucleus hears: cell–cell contact signaling and the modulation of gene activity. *Cold Spring Harbor perspectives in biology*, *1*(4), a002923.
45. Balda, M. S., Garrett, M. D., & Matter, K. (2003). The ZO-1–associated Y-box factor ZONAB regulates epithelial cell proliferation and cell density. *The Journal of cell biology*, *160*(3), 423-432.
46. Aird, W. C. (2007). Phenotypic heterogeneity of the endothelium I. Structure, function, and mechanisms. *Circulation research*, *100*(2), 158-173.
47. Atkins, G. B., Jain, M. K., & Hamik, A. (2011). Endothelial Differentiation Molecular Mechanisms of Specification and Heterogeneity. *Arteriosclerosis, thrombosis, and vascular biology*, *31*(7), 1476-1484.
48. Clementi, F. R. A. N. C. E. S. C. O., & Palade, G. E. (1969). Intestinal capillaries I. Permeability to peroxidase and ferritin. *The Journal of cell biology*, *41*(1), 33-58.
49. Wisse, E. An electron microscopic study of the fenestrated endothelial lining of rat

liver sinusoids. *Journal of ultrastructure research* **31**, 125-150 (1970).

50. Warren, M. S., Zerangue, N., Woodford, K., Roberts, L. M., Tate, E. H., Feng, B., ... & Koller, K. J. (2009). Comparative gene expression profiles of ABC transporters in brain microvessel endothelial cells and brain in five species including human. *Pharmacological research*, *59*(6), 404-413.
51. Aird, W. C. (2006). Mechanisms of endothelial cell heterogeneity in health and disease. *Circulation research*, *98*(2), 159-162.
52. Augustin, H. G., Kozian, D. H., & Johnson, R. C. (1994). Differentiation of endothelial cells: analysis of the constitutive and activated endothelial cell phenotypes. *Bioessays*, *16*(12), 901-906.
53. Engelhardt, B., & Sorokin, L. (2009, November). The blood–brain and the blood–cerebrospinal fluid barriers: function and dysfunction. In *Seminars in immunopathology* (Vol. 31, No. 4, pp. 497-511). Springer-Verlag.
54. Paolinelli, R., Corada, M., Orsenigo, F., & Dejana, E. (2011). The molecular basis of the blood brain barrier differentiation and maintenance. Is it still a mystery?. *Pharmacological Research*, *63*(3), 165-171.
55. Abbott, N. J., Patabendige, A. A., Dolman, D. E., Yusof, S. R., & Begley, D. J. (2010). Structure and function of the blood–brain barrier. *Neurobiology of disease*, *37*(1), 13-25.
56. Obermeier, B., Daneman, R., & Ransohoff, R. M. (2013). Development, maintenance and disruption of the blood-brain barrier. *Nature medicine*, *19*(12), 1584-1596.
57. Daneman, R., & Prat, A. (2015). The Blood–Brain Barrier. *Cold Spring Harbor perspectives in biology*, *7*(1), a020412.
58. Nitta, T., Hata, M., Gotoh, S., Seo, Y., Sasaki, H., Hashimoto, N., ... & Tsukita, S. (2003). Size-selective loosening of the blood-brain barrier in claudin-5–deficient mice. *The Journal of cell biology*, *161*(3), 653-660.
59. Saitou, M., Furuse, M., Sasaki, H., Schulzke, J. D., Fromm, M., Takano, H., ... & Tsukita, S. (2000). Complex phenotype of mice lacking occludin, a component of tight junction strands. *Molecular biology of the cell*, *11*(12), 4131-4142.
60. Ha, S. N., Hochman, J., & Sheridan, R. P. (2007). Mini review on molecular modeling of P-glycoprotein (Pgp). *Current topics in medicinal chemistry*, *7*(15), 1525-1529.
61. Oldendorf, W. H., Cornford, M. E., & Brown, W. J. (1977). The large apparent work capability of the blood-brain barrier: A study of the mitochondrial content of capillary endothelial cells in brain and other tissues of the rat. *Annals of neurology*, *1*(5), 409-417.
62. Zlokovic, B. V. (2008). The blood-brain barrier in health and chronic neurodegenerative disorders. *Neuron*, *57*(2), 178-201.
63. Daneman, R., Zhou, L., Agalliu, D., Cahoy, J. D., Kaushal, A., & Barres, B. A. (2010). The mouse blood-brain barrier transcriptome: a new resource for understanding the development and function of brain endothelial cells. *PloS one*, *5*(10), e13741-e13741.
64. Shue, E. H., Carson-Walter, E. B., Liu, Y., Winans, B. N., Ali, Z. S., Chen, J., & Walter, K. A. (2008). Plasmalemmal vesicle associated protein-1 (PV-1) is a marker of blood-brain barrier disruption in rodent models. *BMC neuroscience*, *9*(1), 29.
65. Keuschnigg, J., Henttinen, T., Auvinen, K., Karikoski, M., Salmi, M., & Jalkanen, S. (2009). The prototype endothelial marker PAL-E is a leukocyte trafficking molecule. *Blood*, *114*(2), 478-484.
66. Huang, J., Upadhyay, U. M., & Tamargo, R. J. (2006). Inflammation in stroke and focal cerebral ischemia. *Surgical neurology*, *66*(3), 232-245.
67. Davies, P. F., Civelek, M., Fang, Y., Guerraty, M. A., & Passerini, A. G. (2010,

April). Endothelial heterogeneity associated with regional athero-susceptibility and adaptation to disturbed blood flow in vivo. In *Seminars in thrombosis and hemostasis* (Vol. 36, No. 3). NIH Public Access.

68. Cavalcanti, D. D., Kalani, M. Y. S., Martirosyan, N. L., Eales, J., Spetzler, R. F., & Preul, M. C. (2012). Cerebral cavernous malformations: from genes to proteins to disease: Clinical article. *Journal of neurosurgery*, *116*(1), 122-132.
69. Boulday, G., Rudini, N., Maddaluno, L., Blécon, A., Arnould, M., Gaudric, A., ... & Tournier-Lasserve, E. (2011). Developmental timing of CCM2 loss influences cerebral cavernous malformations in mice. *The Journal of experimental medicine*, *208*(9), 1835-1847.
70. Clatterbuck, R. E., Eberhart, C. G., Crain, B. J., & Rigamonti, D. (2001). Ultrastructural and immunocytochemical evidence that an incompetent blood-brain barrier is related to the pathophysiology of cavernous malformations. *Journal of Neurology, Neurosurgery & Psychiatry*, *71*(2), 188-192.
71. Batra, S., Lin, D., Recinos, P. F., Zhang, J., & Rigamonti, D. (2009). Cavernous malformations: natural history, diagnosis and treatment. *Nature Reviews Neurology*, *5*(12), 659-670.
72. Rigamonti, D., Hadley, M. N., Drayer, B. P., Johnson, P. C., Hoenig-Rigamonti, K., Knight, J. T., & Spetzler, R. F. (1988). Cerebral cavernous malformations. *New England Journal of Medicine*, *319*(6), 343-347.
73. Labauge, P., Denier, C., Bergametti, F., & Tournier-Lasserve, E. (2007). Genetics of cavernous angiomas. *The Lancet Neurology*, *6*(3), 237-244.
74. Riant, F., Bergametti, F., Ayrignac, X., Boulday, G., & Tournier-Lasserve, E. (2010). Recent insights into cerebral cavernous malformations: the molecular genetics of CCM. *FEBS journal*, *277*(5), 1070-1075.
75. Verlaan, D. J., Roussel, J., Laurent, S. B., Elger, C. E., Siegel, A. M., & Rouleau, G. A. (2005). CCM3 mutations are uncommon in cerebral cavernous malformations. *Neurology*, *65*(12), 1982-1983.
76. Gianfrancesco, F., Esposito, T., Penco, S., Maglione, V., Liquori, C. L., Patrosso, M. C., ... & Squitieri, F. (2008). ZPLD1 gene is disrupted in a patient with balanced translocation that exhibits cerebral cavernous malformations. *Neuroscience*, *155*(2), 345-349.
77. Shenkar, R., Shi, C., Rebeiz, T., Stockton, R. A., McDonald, D. A., Mikati, A. G., ... & Awad, I. A. (2014). Exceptional aggressiveness of cerebral cavernous malformation disease associated with PDCD10 mutations. *Genetics in Medicine*, *17*(3), 188-196.
78. Bacigaluppi, S., Retta, S. F., Pileggi, S., Fontanella, M., Goitre, L., Tassi, L., ... & Penco, S. (2013). Genetic and cellular basis of cerebral cavernous malformations: implications for clinical management. *Clinical genetics*, *83*(1), 7-14.
79. Akers, A. L., Johnson, E., Steinberg, G. K., Zabramski, J. M., & Marchuk, D. A. (2009). Biallelic somatic and germline mutations in cerebral cavernous malformations (CCMs): evidence for a two-hit mechanism of CCM pathogenesis. *Human molecular genetics*, *18*(5), 919-930.
80. Chan, A. C., Li, D. Y., Berg, M. J., & Whitehead, K. J. (2010). Recent insights into cerebral cavernous malformations: animal models of CCM and the human phenotype. *FEBS journal*, *277*(5), 1076-1083.
81. Gore, A. V., Lampugnani, M. G., Dye, L., Dejana, E., & Weinstein, B. M. (2008). Combinatorial interaction between CCM pathway genes precipitates hemorrhagic stroke. *Disease models & mechanisms*, *1*(4-5), 275-281.
82. Mably, J. D., Chuang, L. P., Serluca, F. C., Mohideen, M. A. P., Chen, J. N., & Fishman, M. C. (2006). Santa and valentine pattern concentric growth of cardiac myocardium in the zebrafish. *Development*, *133*(16), 3139-3146.
83. Zheng, X., Xu, C., Di Lorenzo, A., Kleaveland, B., Zou, Z., Seiler, C., ... & Kahn,

M. L. (2010). CCM3 signaling through sterile 20–like kinases plays an essential role during zebrafish cardiovascular development and cerebral cavernous malformations. *The Journal of clinical investigation*, *120*(8), 2795.

84. Hogan, B. M., Bussmann, J., Wolburg, H., & Schulte-Merker, S. (2008). ccm1 cell autonomously regulates endothelial cellular morphogenesis and vascular tubulogenesis in zebrafish. *Human molecular genetics*, *17*(16), 2424-2432.
85. Kleaveland, B., Zheng, X., Liu, J. J., Blum, Y., Tung, J. J., Zou, Z., ... & Kahn, M. L. (2009). Regulation of cardiovascular development and integrity by the heart of glass–cerebral cavernous malformation protein pathway. *Nature medicine*, *15*(2), 169-176.
86. Mably, J. D., Burns, C. G., Chen, J. N., Fishman, M. C., & Mohideen, M. A. P. (2003). Heart of glass regulates the concentric growth of the heart in zebrafish. *Current biology*, *13*(24), 2138-2147.
87. Zheng, X., Riant, F., Bergametti, F., Myers, C. D., Tang, A. T., Kleaveland, B., ... & Kahn, M. L. (2014). Cerebral Cavernous Malformations Arise Independent of the Heart of Glass Receptor. *Stroke*, *45*(5), 1505-1509.
88. Whitehead, K. J., Chan, A. C., Navankasattusas, S., Koh, W., London, N. R., Ling, J., ... & Li, D. Y. (2009). The cerebral cavernous malformation signaling pathway promotes vascular integrity via Rho GTPases. *Nature medicine*, *15*(2), 177-184.
89. He, Y., Zhang, H., Yu, L., Gunel, M., Boggon, T. J., Chen, H., & Min, W. (2010). Cerebral cavernous malformation gene CCM3 is critical for vascular development by regulating VEGFR2 signaling. *Science signaling*, *3*(116), ra26.
90. Plummer, N. W., Gallione, C. J., Srinivasan, S., Zawistowski, J. S., Louis, D. N., & Marchuk, D. A. (2004). Loss of p53 sensitizes mice with a mutation in Ccm1 (KRIT1) to development of cerebral vascular malformations. *The American journal of pathology*, *165*(5), 1509-1518.
91. McDonald, D. A., Shenkar, R., Shi, C., Stockton, R. A., Akers, A. L., Kucherlapati, M. H., ... & Marchuk, D. A. (2011). A novel mouse model of cerebral cavernous malformations based on the two-hit mutation hypothesis recapitulates the human disease. *Human molecular genetics*, *20*(2), 211-222.
92. Bravi, L., Rudini, N., Cuttano, R., Giampietro, C., Maddaluno, L., Ferrarini, L., ... & Lampugnani, M. G. (2015). Sulindac metabolites decrease cerebrovascular malformations in CCM3-knockout mice. *Proceedings of the National Academy of Sciences*, *112*(27), 8421-8426.
93. Louvi, A., Chen, L., Two, A. M., Zhang, H., Min, W., & Günel, M. (2011). Loss of cerebral cavernous malformation 3 (Ccm3) in neuroglia leads to CCM and vascular pathology. *Proceedings of the National Academy of Sciences*, *108*(9), 3737-3742.
94. Hilder, T. L., Malone, M. H., Bencharit, S., Colicelli, J., Haystead, T. A., Johnson, G. L., & Wu, C. C. (2007). Proteomic identification of the cerebral cavernous malformation signaling complex. *Journal of proteome research*, *6*(11), 4343-4355.
95. Li, X., Zhang, R., Zhang, H., He, Y., Ji, W., Min, W., & Boggon, T. J. (2010). Crystal structure of CCM3, a cerebral cavernous malformation protein critical for vascular integrity. *Journal of Biological Chemistry*, *285*(31), 24099-24107.
96. Stockton, R. A., Shenkar, R., Awad, I. A., & Ginsberg, M. H. (2010). Cerebral cavernous malformations proteins inhibit Rho kinase to stabilize vascular integrity. *The Journal of experimental medicine*, *207*(4), 881-896.
97. Fisher, O. S., & Boggon, T. J. (2014). Signaling pathways and the cerebral cavernous malformations proteins: lessons from structural biology. *Cellular and Molecular Life Sciences*, *71*(10), 1881-1892.
98. Crose, L. E., Hilder, T. L., Sciaky, N., & Johnson, G. L. (2009). Cerebral cavernous malformation 2 protein promotes smad ubiquitin regulatory factor 1-mediated RhoA degradation in endothelial cells. *Journal of Biological Chemistry*, *284*(20), 13301-13305.

99. Fidalgo, M., Guerrero, A., Fraile, M., Iglesias, C., Pombo, C. M., & Zalvide, J. (2012). Adaptor protein cerebral cavernous malformation 3 (CCM3) mediates phosphorylation of the cytoskeletal proteins ezrin/radixin/moesin by mammalian Ste20-4 to protect cells from oxidative stress. *Journal of Biological Chemistry*, *287*(14), 11556-11565.
100. Glading, A., Han, J., Stockton, R. A., & Ginsberg, M. H. (2007). KRIT-1/CCM1 is a Rap1 effector that regulates endothelial cell–cell junctions. *The Journal of cell biology*, *179*(2), 247-254.

101. Glading, A. J., & Ginsberg, M. H. (2010). Rap1 and its effector KRIT1/CCM1 regulate β-catenin signaling. *Disease models & mechanisms*, *3*(1-2), 73-83.
102. Iden, S., Rehder, D., August, B., Suzuki, A., Wolburg-Buchholz, K., Wolburg, H., ... & Ebnet, K. (2006). A distinct PAR complex associates physically with VE-cadherin in vertebrate endothelial cells. *EMBO reports*, *7*(12), 1239-1246.
103. Lampugnani, M. G., Orsenigo, F., Rudini, N., Maddaluno, L., Boulday, G., Chapon, F., & Dejana, E. (2010). CCM1 regulates vascular-lumen organization by inducing endothelial polarity. *Journal of cell science*, *123*(7), 1073-1080.
104. Fidalgo, M., Fraile, M., Pires, A., Force, T., Pombo, C., & Zalvide, J. (2010). CCM3/PDCD10 stabilizes GCKIII proteins to promote Golgi assembly and cell orientation. *Journal of cell science*, *123*(8), 1274-1284.
105. Wüstehube, J., Bartol, A., Liebler, S. S., Brütsch, R., Zhu, Y., Felbor, U., ... & Fischer, A. (2010). Cerebral cavernous malformation protein CCM1 inhibits sprouting angiogenesis by activating DELTA-NOTCH signaling. *Proceedings of the National Academy of Sciences*, *107*(28), 12640-12645.
106. Zawistowski, J. S., Stalheim, L., Uhlik, M. T., Abell, A. N., Ancrile, B. B., Johnson, G. L., & Marchuk, D. A. (2005). CCM1 and CCM2 protein interactions in cell signaling: implications for cerebral cavernous malformations pathogenesis. *Human molecular genetics*, *14*(17), 2521-2531.
107. Renz, M., Otten, C., Faurobert, E., Rudolph, F., Zhu, Y., Boulday, G., ... & Abdelilah-Seyfried, S. (2015). Regulation of β1 Integrin-Klf2-Mediated Angiogenesis by CCM Proteins. *Developmental cell*, *32*(2), 181-190.
108. Yoruk, B., Gillers, B. S., Chi, N. C., & Scott, I. C. (2012). Ccm3 functions in a manner distinct from Ccm1 and Ccm2 in a zebrafish model of CCM vascular disease. *Developmental biology*, *362*(2), 121-131.
109. Morrison, L., & Akers, A. (2011). Cerebral cavernous malformation, familial.
110. Mouchtouris, N., Chalouhi, N., Chitale, A., Starke, R. M., Tjoumakaris, S. I., Rosenwasser, R. H., & Jabbour, P. M. (2015). Management of cerebral cavernous malformations: From diagnosis to treatment. *The Scientific World Journal*, *2015*.
111. Li, D. Y., & Whitehead, K. J. (2010). Evaluating strategies for the treatment of cerebral cavernous malformations. *Stroke*, *41*(10 suppl 1), S92-S94.
112. Gibson, C. C., Zhu, W., Davis, C. T., Bowman-Kirigin, J. A., Chan, A. C., Ling, J., ... & Li, D. Y. (2015). Strategy for identifying repurposed drugs for the treatment of cerebral cavernous malformation. *Circulation*, *131*(3), 289-299.
113. McDonald, D. A., Shi, C., Shenkar, R., Stockton, R. A., Liu, F., Ginsberg, M. H., ... & Awad, I. A. (2012). Fasudil decreases lesion burden in a murine model of cerebral cavernous malformation disease. *Stroke*, *43*(2), 571-574.
114. Kalluri, R., & Weinberg, R. A. (2009). The basics of epithelial-mesenchymal transition. *The Journal of clinical investigation*, *119*(6), 1420.
115. Markwald, R. R., Fitzharris, T. P., & Manasek, F. J. (1977). Structural development of endocardial cushions. *American Journal of Anatomy*, *148*(1), 85-119.
116. Eisenberg, L. M., & Markwald, R. R. (1995). Molecular regulation of atrioventricular valvuloseptal morphogenesis. *Circulation research*, *77*(1), 1-6.
117. Armstrong, E. J., & Bischoff, J. (2004). Heart valve development endothelial cell

signaling and differentiation. *Circulation research*, *95*(5), 459-470.

118. Zeisberg, E. M., Potenta, S., Xie, L., Zeisberg, M., & Kalluri, R. (2007). Discovery of endothelial to mesenchymal transition as a source for carcinoma-associated fibroblasts. *Cancer research*, *67*(21), 10123-10128.
119. Zeisberg, E. M., Tarnavski, O., Zeisberg, M., Dorfman, A. L., McMullen, J. R., Gustafsson, E., ... & Kalluri, R. (2007). Endothelial-to-mesenchymal transition contributes to cardiac fibrosis. *Nature medicine*, *13*(8), 952-961.
120. Rastaldi, M. P. (2006). Epithelial-mesenchymal transition and its implications for the development of renal tubulointerstitial fibrosis. *Journal of nephrology*, *19*(4), 407.
121. Zeisberg, E. M., Potenta, S. E., Sugimoto, H., Zeisberg, M., & Kalluri, R. (2008). Fibroblasts in kidney fibrosis emerge via endothelial-to-mesenchymal transition. *Journal of the American Society of Nephrology*, *19*(12), 2282-2287.
122. Piera-Velazquez, S., Li, Z., & Jimenez, S. A. (2011). Role of endothelial-mesenchymal transition (EndoMT) in the pathogenesis of fibrotic disorders. *The American journal of pathology*, *179*(3), 1074-1080.
123. Thiery, J. P., & Sleeman, J. P. (2006). Complex networks orchestrate epithelial–mesenchymal transitions. *Nature reviews Molecular cell biology*, *7*(2), 131-142.
124. Kalluri, R., & Neilson, E. G. (2003). Epithelial-mesenchymal transition and its implications for fibrosis. *Journal of Clinical Investigation*, *112*(12), 1776.
125. Gonzalez, D. M., & Medici, D. (2014). Signaling mechanisms of the epithelial-mesenchymal transition. *Science signaling*, *7*(344), re8.
126. van Meeteren, L. A., & Ten Dijke, P. (2012). Regulation of endothelial cell plasticity by TGF-β. *Cell and tissue research*, *347*(1), 177-186.
127. Galat, A. (2011). Common structural traits for cystine knot domain of the TGFβ superfamily of proteins and three-fingered ectodomain of their cellular receptors. *Cellular and Molecular Life Sciences*, *68*(20), 3437-3451.
128. Shi, Y., & Massagué, J. (2003). Mechanisms of TGF-β signaling from cell membrane to the nucleus. *Cell*, *113*(6), 685-700.
129. ten Dijke, P., & Arthur, H. M. (2007). Extracellular control of TGFβ signalling in vascular development and disease. *Nature reviews Molecular cell biology*, *8*(11), 857-869.
130. Moustakas, A., & Heldin, C. H. (2009). The regulation of TGFβ signal transduction. *Development*, *136*(22), 3699-3714.
131. Ross, S., & Hill, C. S. (2008). How the Smads regulate transcription. *The international journal of biochemistry & cell biology*, *40*(3), 383-408.
132. Makkar, P., Metpally, R. P. R., Sangadala, S., & Reddy, B. V. B. (2009). Modeling and analysis of MH1 domain of Smads and their interaction with promoter DNA sequence motif. *Journal of Molecular Graphics and Modelling*, *27*(7), 803-812.
133. Heldin, C. H., Miyazono, K., & Ten Dijke, P. (1997). TGF-β signalling from cell membrane to nucleus through SMAD proteins. *Nature*, *390*(6659), 465-471.
134. Goumans, M. J., Valdimarsdottir, G., Itoh, S., Rosendahl, A., Sideras, P., & ten Dijke, P. (2002). Balancing the activation state of the endothelium via two distinct TGF-β type I receptors. *The EMBO journal*, *21*(7), 1743-1753.
135. Itoh, S., & ten Dijke, P. (2007). Negative regulation of TGF-β receptor/Smad signal transduction. *Current opinion in cell biology*, *19*(2), 176-184.
136. Nakao, A., Afrakhte, M., Morn, A., Nakayama, T., Christian, J. L., Heuchel, R., ... & ten Dijke, P. (1997). Identification of Smad7, a TGFβ-inducible antagonist of TGF-β signalling. *Nature*, *389*(6651), 631-635.
137. Kavsak, P., Rasmussen, R. K., Causing, C. G., Bonni, S., Zhu, H., Thomsen, G. H., & Wrana, J. L. (2000). Smad7 binds to Smurf2 to form an E3 ubiquitin ligase that targets the TGFβ receptor for degradation. *Molecular cell*, *6*(6), 1365-1375
138. Dennler, S., Itoh, S., Vivien, D., ten Dijke, P., Huet, S., & Gauthier, J. M. (1998). Direct binding of Smad3 and Smad4 to critical TGFβ-inducible elements in the

promoter of human plasminogen activator inhibitor-type 1 gene. *The EMBO journal*, *17*(11), 3091-3100.

139. Jonk, L. J., Itoh, S., Heldin, C. H., ten Dijke, P., & Kruijer, W. (1998). Identification and functional characterization of a Smad binding element (SBE) in the JunB promoter that acts as a transforming growth factor-β, activin, and bone morphogenetic protein-inducible enhancer. *Journal of Biological Chemistry*, *273*(33), 21145-21152.
140. Gomis, R. R., Alarcón, C., He, W., Wang, Q., Seoane, J., Lash, A., & Massagué, J. (2006). A FoxO–Smad synexpression group in human keratinocytes. *Proceedings of the National Academy of Sciences*, *103*(34), 12747-12752.
141. Verrecchia, F., Vindevoghel, L., Lechleider, R. J., Uitto, J., Roberts, A. B., & Mauviel, A. (2001). Smad3/AP-1 interactions control transcriptional responses to TGF-beta in a promoter-specific manner. *Oncogene*, *20*(26), 3332-3340.
142. Selvamurugan, N., Kwok, S., & Partridge, N. C. (2004). Smad3 interacts with JunB and Cbfa1/Runx2 for transforming growth factor-β1-stimulated collagenase-3 expression in human breast cancer cells. *Journal of Biological Chemistry*, *279*(26), 27764-27773.
143. López-Rovira, T., Chalaux, E., Rosa, J. L., Bartrons, R., & Ventura, F. (2000). Interaction and Functional Cooperation of NF-κB with Smads TRANSCRIPTIONAL REGULATION OF THE junBPROMOTER. *Journal of Biological Chemistry*, *275*(37), 28937-28946.
144. López-Rovira, T., Chalaux, E., Massagué, J., Rosa, J. L., & Ventura, F. (2002). Direct Binding of Smad1 and Smad4 to Two Distinct Motifs Mediates Bone Morphogenetic Protein-specific Transcriptional Activation ofId1 Gene. *Journal of Biological Chemistry*, *277*(5), 3176-3185.
145. Brugger, S. M., Merrill, A. E., Torres-Vazquez, J., Wu, N., Ting, M. C., Cho, J. Y. M., ... & Maxson, R. (2004). A phylogenetically conserved cis-regulatory module in the Msx2 promoter is sufficient for BMP-dependent transcription in murine and Drosophila embryos. *Development*, *131*(20), 5153-5165.
146. López-Casillas, F., Wrana, J. L., & Massagué, J. (1993). Betaglycan presents ligand to the TGFβ signaling receptor. *Cell*, *73*(7), 1435-1444.
147. Sankar, S., Mahooti-Brooks, N., Centrella, M., McCarthy, T. L., & Madri, J. A. (1995). Expression of transforming growth factor type III receptor in vascular endothelial cells increases their responsiveness to transforming growth factor β2. *Journal of Biological Chemistry*, *270*(22), 13567-13572.
148. Lebrin, F., Goumans, M. J., Jonker, L., Carvalho, R. L., Valdimarsdottir, G., Thorikay, M., ... & ten Dijke, P. (2004). Endoglin promotes endothelial cell proliferation and TGF-β/ALK1 signal transduction. *The EMBO journal*, *23*(20), 4018-4028.
149. Kirkbride, K. C., Townsend, T. A., Bruinsma, M. W., Barnett, J. V., & Blobe, G. C. (2008). Bone morphogenetic proteins signal through the transforming growth factor-β type III receptor. *Journal of Biological Chemistry*, *283*(12), 7628-7637.
150. Zhang, Y. E. (2009). Non-Smad pathways in TGF-β signaling. *Cell research*, *19*(1), 128-139.
151. Pardali, E., Goumans, M. J., & ten Dijke, P. (2010). Signaling by members of the TGF-β family in vascular morphogenesis and disease. *Trends in cell biology*, *20*(9), 556-567.
152. A van Meeteren, L., Goumans, M. J., & ten Dijke, P. (2011). TGF-β receptor signaling pathways in angiogenesis; emerging targets for anti-angiogenesis therapy. *Current pharmaceutical biotechnology*, *12*(12), 2108-2120.3
153. Oh, S. P., Seki, T., Goss, K. A., Imamura, T., Yi, Y., Donahoe, P. K., ... & Li, E. (2000). Activin receptor-like kinase 1 modulates transforming growth factor-β1

signaling in the regulation of angiogenesis. *Proceedings of the National Academy of Sciences*, *97*(6), 2626-2631.

154. Lebrin, F., Deckers, M., Bertolino, P., & ten Dijke, P. (2005). TGF-β receptor function in the endothelium. *Cardiovascular research*, *65*(3), 599-608
155. Muñoz-Félix, J. M., González-Núñez, M., & López-Novoa, J. M. (2013). ALK1-Smad1/5 signaling pathway in fibrosis development: friend or foe?. *Cytokine & growth factor reviews*, *24*(6), 523-537.
156. Watabe, T., Nishihara, A., Mishima, K., Yamashita, J., Shimizu, K., Miyazawa, K., ... & Miyazono, K. (2003). TGF-β receptor kinase inhibitor enhances growth and integrity of embryonic stem cell–derived endothelial cells. *The Journal of cell biology*, *163*(6), 1303-1311.
157. Noel, A., Maillard, C., Rocks, N., Jost, M., Chabottaux, V., Sounni, N. E., ... & Foidart, J. M. (2004). Membrane associated proteases and their inhibitors in tumour angiogenesis. *Journal of clinical pathology*, *57*(6), 577-584.
158. Goumans, M. J., Valdimarsdottir, G., Itoh, S., Lebrin, F., Larsson, J., Mummery, C., ... & ten Dijke, P. (2003). Activin receptor-like kinase (ALK) 1 is an antagonistic mediator of lateral TGFβ/ALK5 signaling. *Molecular cell*, *12*(4), 817-828.3
159. Miyazono, K., & Miyazawa, K. (2002). Id: a target of BMP signaling. *Science signaling*, *2002*(151), pe40-pe40.
160. David, L., Feige, J. J., & Bailly, S. (2009). Emerging role of bone morphogenetic proteins in angiogenesis. *Cytokine & growth factor reviews*, *20*(3), 203-212.
161. Pardali, E., & Ten Dijke, P. (2012). TGFβ signaling and cardiovascular diseases. *International journal of biological sciences*, *8*(2), 195.
162. Valdimarsdottir, G., Goumans, M. J., Rosendahl, A., Brugman, M., Itoh, S., Lebrin, F., ... & Ten Dijke, P. (2002). Stimulation of Id1 expression by bone morphogenetic protein is sufficient and necessary for bone morphogenetic protein–induced activation of endothelial cells. *Circulation*, *106*(17), 2263-2270.
163. Suzuki, Y., Ohga, N., Morishita, Y., Hida, K., Miyazono, K., & Watabe, T. (2010). BMP-9 induces proliferation of multiple types of endothelial cells in vitro and in vivo. *Journal of cell science*, *123*(10), 1684-1692.
164. Itoh, F., Itoh, S., Goumans, M. J., Valdimarsdottir, G., Iso, T., Dotto, G. P., ... & ten Dijke, P. (2004). Synergy and antagonism between Notch and BMP receptor signaling pathways in endothelial cells. *The EMBO journal*, *23*(3), 541-551.
165. Moya, I. M., Umans, L., Maas, E., Pereira, P. N., Beets, K., Francis, A., ... & Zwijsen, A. (2012). Stalk cell phenotype depends on integration of Notch and Smad1/5 signaling cascades. *Developmental cell*, *22*(3), 501-514.
166. Rivera-Feliciano, J., & Tabin, C. J. (2006). Bmp2 instructs cardiac progenitors to form the heart-valve-inducing field. *Developmental biology*, *295*(2), 580-588.
167. Camenisch, T. D., Molin, D. G., Person, A., Runyan, R. B., Gittenberger-de Groot, A. C., McDonald, J. A., & Klewer, S. E. (2002). Temporal and distinct TGFβ ligand requirements during mouse and avian endocardial cushion morphogenesis. *Developmental biology*, *248*(1), 170-181.
168. Bartram, U., Molin, D. G., Wisse, L. J., Mohamad, A., Sanford, L. P., Doetschman, T., ... & Gittenberger-de Groot, A. C. (2001). Double-outlet right ventricle and overriding tricuspid valve reflect disturbances of looping, myocardialization, endocardial cushion differentiation, and apoptosis in TGF-β2–knockout mice. *Circulation*, *103*(22), 2745-2752.
169. Liebner, S., Cattelino, A., Gallini, R., Rudini, N., Iurlaro, M., Piccolo, S., & Dejana, E. (2004). β-catenin is required for endothelial-mesenchymal transformation during heart cushion development in the mouse. *The Journal of cell biology*, *166*(3), 359-367.

170. Niessen, K., Fu, Y., Chang, L., Hoodless, P. A., McFadden, D., & Karsan, A. (2008). Slug is a direct Notch target required for initiation of cardiac cushion cellularization. *The Journal of cell biology*, *182*(2), 315-325.
171. Mueller, M. M., & Fusenig, N. E. (2004). Friends or foes—bipolar effects of the tumour stroma in cancer. *Nature Reviews Cancer*, *4*(11), 839-849.
172. Kalluri, R., & Zeisberg, M. (2006). Fibroblasts in cancer. *Nature Reviews Cancer*, *6*(5), 392-401.
173. Medici, D., Shore, E. M., Lounev, V. Y., Kaplan, F. S., Kalluri, R., & Olsen, B. R. (2010). Conversion of vascular endothelial cells into multipotent stem-like cells. *Nature medicine*, *16*(12), 1400-1406.
174. Lounev, V. Y., Ramachandran, R., Wosczyna, M. N., Yamamoto, M., Maidment, A. D., Shore, E. M., ... & Kaplan, F. S. (2009). Identification of progenitor cells that contribute to heterotopic skeletogenesis. *The Journal of Bone & Joint Surgery*, *91*(3), 652-663.
175. Tabas, I., García-Cardeña, G., & Owens, G. K. (2015). Recent insights into the cellular biology of atherosclerosis. *The Journal of cell biology*, *209*(1), 13-22.
176. Hahn, C., & Schwartz, M. A. (2009). Mechanotransduction in vascular physiology and atherogenesis. *Nature reviews Molecular cell biology*, *10*(1), 53-62.
177. Libby, P., Lichtman, A. H., & Hansson, G. K. (2013). Immune effector mechanisms implicated in atherosclerosis: from mice to humans. *Immunity*, *38*(6), 1092-1104.
178. Chen, P. Y., Qin, L., Baeyens, N., Li, G., Afolabi, T., Budatha, M., ... & Simons, M. (2015). Endothelial-to-mesenchymal transition drives atherosclerosis progression. *The Journal of Clinical Investigation*, *125*(12), 0-0.
179. Chen, P. Y., Qin, L., Barnes, C., Charisse, K., Yi, T., Zhang, X., ... & Simons, M. (2012). FGF regulates TGF-β signaling and endothelial-to-mesenchymal transition via control of let-7 miRNA expression. *Cell reports*, *2*(6), 1684-1696.
180. Feaver, R. E., Gelfand, B. D., Wang, C., Schwartz, M. A., & Blackman, B. R. (2010). Atheroprone hemodynamics regulate fibronectin deposition to create positive feedback that sustains endothelial inflammation. *Circulation research*, *106*(11), 1703-1711.
181. Rohwedder, I., Montanez, E., Beckmann, K., Bengtsson, E., Dunér, P., Nilsson, J., ... & Fässler, R. (2012). Plasma fibronectin deficiency impedes atherosclerosis progression and fibrous cap formation. *EMBO molecular medicine*, *4*(7), 564-576.
182. McConnell, B. B., & Yang, V. W. (2010). Mammalian Krüppel-like factors in health and diseases. *Physiological reviews*, *90*(4), 1337-1381.
183. Schuh, R., Aicher, W., Gaul, U., Côte, S., Preiss, A., Maier, D., ... & Jäckle, H. (1986). A conserved family of nuclear proteins containing structural elements of the finger protein encoded by Krüppel, a Drosophila segmentation gene. *Cell*, *47*(6), 1025-1032.
184. Miller, I. J., & Bieker, J. J. (1993). A novel, erythroid cell-specific murine transcription factor that binds to the CACCC element and is related to the Krüppel family of nuclear proteins. *Molecular and cellular biology*, *13*(5), 2776-2786.
185. Pearson, R., Fleetwood, J., Eaton, S., Crossley, M., & Bao, S. (2008). Krüppel-like transcription factors: a functional family. *The international journal of biochemistry & cell biology*, *40*(10), 1996-2001.
186. Suske, G., Bruford, E., & Philipsen, S. (2005). Mammalian SP/KLF transcription factors: bring in the family. *Genomics*, *85*(5), 551-556.
187. Presnell, J. S., Schnitzler, C. E., & Browne, W. E. (2015). KLF/SP transcription factor family evolution: expansion, diversification, and innovation in eukaryotes. *Genome biology and evolution*, *7*(8), 2289-2309.
188. Kaczynski, J., Cook, T., & Urrutia, R. (2003). Sp1-and Kruppel-like transcription factors. *Genome Biol*, *4*(2), 206.

189. Nagai, R., Friedman, S. L., & Kasuga, M. (2009). *The biology of Krüppel-like Factors* (pp. 226-229). Springer.
190. Dang, D. T., Pevsner, J., & Yang, V. W. (2000). The biology of the mammalian Krüppel-like family of transcription factors. *The international journal of biochemistry & cell biology*, *32*(11), 1103-1121.
191. Camacho-Vanegas, O., Till, J., Miranda-Lorenzo, I., Ozturk, B., Camacho, S. C., & Martignetti, J. A. (2013). Shaking the family tree: identification of novel and biologically active alternatively spliced isoforms across the KLF family of transcription factors. *The FASEB Journal*, *27*(2), 432-436.
192. Turner, J., & Crossley, M. (1998). Cloning and characterization of mCtBP2, a co-repressor that associates with basic Krüppel-like factor and other mammalian transcriptional regulators. *The EMBO journal*, *17*(17), 5129-5140.
193. van Vliet, J., Turner, J., & Crossley, M. (2000). Human Krüppel-like factor 8: a CACCC-box binding protein that associates with CtBP and represses transcription. *Nucleic acids research*, *28*(9), 1955-1962.
194. Chinnadurai, G. (2007). Transcriptional regulation by C-terminal binding proteins. *The international journal of biochemistry & cell biology*, *39*(9), 1593-1607.
195. Sewalt, R. G., Gunster, M. J., van der Vlag, J., Satijn, D. P., & Otte, A. P. (1999). C-Terminal binding protein is a transcriptional repressor that interacts with a specific class of vertebrate Polycomb proteins. *Molecular and cellular biology*, *19*(1), 777-787.
196. Knoepfler, P. S., & Eisenman, R. N. (1999). Sin meets NuRD and other tails of repression. *Cell*, *99*(5), 447-450.
197. Pei, J., & Grishin, N. V. (2013). A new family of predicted Krüppel-like factor genes and pseudogenes in placental mammals.
198. Tetreault, M. P., Yang, Y., & Katz, J. P. (2013). Kruppel-like factors in cancer. *Nature Reviews Cancer*, *13*(10), 701-713.
199. Rowland, B. D., Bernards, R., & Peeper, D. S. (2005). The KLF4 tumour suppressor is a transcriptional repressor of p53 that acts as a context-dependent oncogene. *Nature cell biology*, *7*(11), 1074-1082.
200. Rowland, B. D., Bernards, R., & Peeper, D. S. (2005). The KLF4 tumour suppressor is a transcriptional repressor of p53 that acts as a context-dependent oncogene. *Nature cell biology*, *7*(11), 1074-1082.
201. Shields, J. M., Christy, R. J., & Yang, V. W. (1996). Identification and characterization of a gene encoding a gut-enriched Krüppel-like factor expressed during growth arrest. *Journal of Biological Chemistry*, *271*(33), 20009-20017.
202. Yet, S. F., McA'Nulty, M. M., Folta, S. C., Yen, H. W., Yoshizumi, M., Hsieh, C. M., ... & Lee, M. E. (1998). Human EZF, a Krüppel-like zinc finger protein, is expressed in vascular endothelial cells and contains transcriptional activation and repression domains. *Journal of Biological Chemistry*, *273*(2), 1026-1031.
203. Panigada, M., Porcellini, S., Sutti, F., Doneda, L., Pozzoli, O., Consalez, G. G., ... & Grassi, F. (1999). GKLF in thymus epithelium as a developmentally regulated element of thymocyte-stroma cross-talk. *Mechanisms of development*, *81*(1), 103-113.
204. Chiambaretta, F., De Graeve, F., Turet, G., Marceau, G., Gain, P., Dastugue, B., ... & Sapin, V. (2004). Cell and tissue specific expression of human Kruppel-like transcription factors in human ocular surface. *Mol Vis*, *10*, 901-909.
205. Cullingford, T. E., Butler, M. J., Marshall, A. K., Sugden, P. H., & Clerk, A. (2008). Differential regulation of Krüppel-like factor family transcription factor expression in neonatal rat cardiac myocytes: effects of endothelin-1, oxidative stress and cytokines. *Biochimica et Biophysica Acta (BBA)-Molecular Cell Research*, *1783*(6), 1229-1236.

206. Godmann, M., Kromberg, I., Mayer, J., & Behr, R. (2005). The mouse Krüppel-like Factor 4 (Klf4) gene: Four functional polyadenylation sites which are used in a cell-specific manner as revealed by testicular transcript analysis and multiple processed pseudogenes. *Gene*, *361*, 149-156.

207. Evans, P. M., Zhang, W., Chen, X., Yang, J., Bhakat, K. K., & Liu, C. (2007). Krüppel-like factor 4 is acetylated by p300 and regulates gene transcription via modulation of histone acetylation. *Journal of Biological Chemistry*, *282*(47), 33994-34002.

208. Dang, D. T., Zhao, W., Mahatan, C. S., Geiman, D. E., & Yang, V. W. (2002). Opposing effects of Krüppel-like factor 4 (gut-enriched Krüppel-like factor) and Krüppel-like factor 5 (intestinal-enriched Krüppel-like factor) on the promoter of the Krüppel-like factor 4 gene. *Nucleic acids research*, *30*(13), 2736-2741.

209. Chen, X., Xu, H., Yuan, P., Fang, F., Huss, M., Vega, V. B., ... & Ng, H. H. (2008). Integration of external signaling pathways with the core transcriptional network in embryonic stem cells. *Cell*, *133*(6), 1106-1117.

210. Shields, J. M., & Yang, V. W. (1998). Identification of the DNA sequence that interacts with the gut-enriched Krüppel-like factor. *Nucleic acids research*, *26*(3), 796-802.

211. Liu, Y., Olanrewaju, Y. O., Zheng, Y., Hashimoto, H., Blumenthal, R. M., Zhang, X., & Cheng, X. (2014). Structural basis for Klf4 recognition of methylated DNA. *Nucleic acids research*, *42*(8), 4859-4867.

212. Vangapandu, H., & Ai, W. (2009). Kruppel like factor 4 (KLF4): a transcription factor with diverse context-dependent functions. *Gene Ther Mol Biol*, *13*, 194-203.

213. Shields, J. M., & Yang, V. W. (1997). Two potent nuclear localization signals in the gut-enriched Krüppel-like factor define a subfamily of closely related Krüppel proteins. *Journal of Biological Chemistry*, *272*(29), 18504-18507.

214. Feinberg, M. W., Cao, Z., Wara, A. K., Lebedeva, M. A., SenBanerjee, S., & Jain, M. K. (2005). Kruppel-like factor 4 is a mediator of proinflammatory signaling in macrophages. *Journal of Biological Chemistry*, *280*(46), 38247-38258.

215. Evans, P. M., Chen, X., Zhang, W., & Liu, C. (2010). KLF4 interacts with β-catenin/TCF4 and blocks p300/CBP recruitment by β-catenin. *Molecular and cellular biology*, *30*(2), 372-381.

216. Noti, J. D., Johnson, A. K., & Dillon, J. D. (2005). The leukocyte integrin gene CD11d is repressed by gut-enriched Kruppel-like factor 4 in myeloid cells. *Journal of Biological Chemistry*, *280*(5), 3449-3457.

217. Ehlermann, J., Pfisterer, P., & Schorle, H. (2003). Dynamic expression of Krüppel-like factor 4 (Klf4), a target of transcription factor AP-2α during murine mid-embryogenesis. *The Anatomical Record Part A: Discoveries in Molecular, Cellular, and Evolutionary Biology*, *273*(2), 677-680.

218. Segre, J. A., Bauer, C., & Fuchs, E. (1999). Klf4 is a transcription factor required for establishing the barrier function of the skin. *Nature genetics*, *22*(4), 356-360.

219. Katz, J. P., Perreault, N., Goldstein, B. G., Actman, L., McNally, S. R., Silberg, D. G., ... & Kaestner, K. H. (2005). Loss of Klf4 in mice causes altered proliferation and differentiation and precancerous changes in the adult stomach. *Gastroenterology*, *128*(4), 935-945.

220. Swamynathan, S. K., Katz, J. P., Kaestner, K. H., Ashery-Padan, R., Crawford, M. A., & Piatigorsky, J. (2007). Conditional deletion of the mouse Klf4 gene results in corneal epithelial fragility, stromal edema, and loss of conjunctival goblet cells. *Molecular and cellular biology*, *27*(1), 182-194.

221. Takahashi, K., Tanabe, K., Ohnuki, M., Narita, M., Ichisaka, T., Tomoda, K., & Yamanaka, S. (2007). Induction of pluripotent stem cells from adult human fibroblasts by defined factors. *cell*, *131*(5), 861-872.

222. Atkins, G. B., & Jain, M. K. (2007). Role of Krüppel-like transcription factors in endothelial biology. *Circulation Research*, *100*(12), 1686-1695.

223. Cowan, C. E., Kohler, E. E., Dugan, T. A., Mirza, M. K., Malik, A. B., & Wary, K. K. (2010). Krüppel-like factor-4 transcriptionally regulates VE-cadherin expression and endothelial barrier function. *Circulation research*, *107*(8), 959-966.

224. Shatat, M. A., Tian, H., Zhang, R., Tandon, G., Hale, A., Fritz, J. S., ... & Hamik, A. (2014). Endothelial Krüppel-like factor 4 modulates pulmonary arterial hypertension. *American journal of respiratory cell and molecular biology*, *50*(3), 647-653.

225. Hale, A. T., Tian, H., Anih, E., Recio, F. O., Shatat, M. A., Johnson, T., ... & Hamik, A. (2014). Endothelial Krüppel-like Factor 4 Regulates Angiogenesis and the Notch Signaling Pathway. *Journal of Biological Chemistry*, *289*(17), 12016-12028.

226. Ohnesorge, N., Viemann, D., Schmidt, N., Czymai, T., Spiering, D., Schmolke, M., ... & Schmidt, M. (2010). Erk5 activation elicits a vasoprotective endothelial phenotype via induction of Krüppel-like Factor 4 (KLF4). *Journal of Biological Chemistry*, *285*(34), 26199-26210.

227. Hamik, A., Lin, Z., Kumar, A., Balcells, M., Sinha, S., Katz, J., ... & Jain, M. K. (2007). Kruppel-like factor 4 regulates endothelial inflammation. *Journal of Biological Chemistry*, *282*(18), 13769-13779.

228. Zhou, G., Hamik, A., Nayak, L., Tian, H., Shi, H., Lu, Y., ... & Jain, M. K. (2012). Endothelial Kruppel-like factor 4 protects against atherothrombosis in mice. *The Journal of clinical investigation*, *122*(12), 4727.

229. Ma, J., Wang, P., Liu, Y., Zhao, L., Li, Z., & Xue, Y. (2014). Krüppel-Like Factor 4 Regulates Blood-Tumor Barrier Permeability via ZO-1, Occludin and Claudin-5. *Journal of cellular physiology*, *229*(7), 916-926.

230. Zhao, Y. Y., Zhao, L. N., Wang, P., Miao, Y. S., Liu, Y. H., Wang, Z. H., ... & Xue, Y. X. (2015). Overexpression of miR-18a negatively regulates myocyte enhancer factor 2D to increase the permeability of the blood–tumor barrier via Krüppel-like factor 4-mediated downregulation of zonula occluden-1, claudin-5, and occludin. *Journal of neuroscience research*.

231. Palmer, R. M., Ferrige, A. G., & Moncada, S. (1987). Nitric oxide release accounts for the biological activity of endothelium-derived relaxing factor.

232. Farber, H. W., & Loscalzo, J. (2004). Pulmonary arterial hypertension. *New England Journal of Medicine*, *351*(16), 1655-1665.

233. Sheikh, A. Q., Misra, A., Rosas, I. O., Adams, R. H., & Greif, D. M. (2015). Smooth muscle cell progenitors are primed to muscularize in pulmonary hypertension. *Science translational medicine*, *7*(308), 308ra159-308ra159.

234. Wang, Y., Yang, C., Gu, Q., Sims, M., Gu, W., Pfeffer, L. M., & Yue, J. (2015). KLF4 Promotes Angiogenesis by Activating VEGF Signaling in Human Retinal Microvascular Endothelial Cells. *PloS one*, *10*(6), e0130341.

235. Zheng, X., Li, A., Zhao, L., Zhou, T., Shen, Q., Cui, Q., & Qin, X. (2013). Key role of microRNA-15a in the KLF4 suppressions of proliferation and angiogenesis in endothelial and vascular smooth muscle cells. *Biochemical and biophysical research communications*, *437*(4), 625-631.

236. Clark, P. R., Jensen, T. J., Kluger, M. S., Morelock, M., Hanidu, A., Qi, Z., ... & Pober, J. S. (2011). MEK5 is activated by shear stress, activates ERK5 and induces KLF4 to modulate TNF responses in human dermal microvascular endothelial cells. *Microcirculation*, *18*(2), 102-117.

237. Zhou, G., Bao, Z. Q., & Dixon, J. E. (1995). Components of a new human protein kinase signal transduction pathway. *Journal of Biological Chemistry*, *270*(21), 12665-12669.

238. Lee, J. D., Ulevitch, R. J., & Han, J. H. (1995). Primary structure of BMK1: a new mammalian map kinase. *Biochemical and biophysical research communications*, *213*(2), 715-724.

239. Yan, C., Luo, H., Lee, J. D., Abe, J. I., & Berk, B. C. (2001). Molecular cloning of mouse ERK5/BMK1 splice variants and characterization of ERK5 functional domains. *Journal of Biological Chemistry*, *276*(14), 10870-10878.
240. Mody, N., CAMPBELL, D., Morrice, N., Peggie, M., & Cohen, P. (2003). An analysis of the phosphorylation and activation of extracellular-signal-regulated protein kinase 5 (ERK5) by mitogen-activated protein kinase kinase 5 (MKK5) in vitro. *Biochem. J*, *372*, 567-575.
241. Nithianandarajah-Jones, G. N., Wilm, B., Goldring, C. E., Müller, J., & Cross, M. J. (2012). ERK5: structure, regulation and function. *Cellular signalling*, *24*(11), 2187-2196.
242. Nishimoto, S., & Nishida, E. (2006). MAPK signalling: ERK5 versus ERK1/2. *EMBO reports*, *7*(8), 782-786.
243. Nithianandarajah-Jones, G. N., Wilm, B., Goldring, C. E., Mueller, J., & Cross, M. J. (2014). The role of ERK5 in endothelial cell function. *Biochemical Society transactions*, *42*(6), 1584-1589.
244. Chao, T. H., Hayashi, M., Tapping, R. I., Kato, Y., & Lee, J. D. (1999). MEKK3 directly regulates MEK5 activity as part of the big mitogen-activated protein kinase 1 (BMK1) signaling pathway. *Journal of Biological Chemistry*, *274*(51), 36035-36038.
245. Sun, W., Kesavan, K., Schaefer, B. C., Garrington, T. P., Ware, M., Johnson, N. L., ... & Johnson, G. L. (2001). MEKK2 associates with the adapter protein Lad/RIBP and regulates the MEK5-BMK1/ERK5 pathway. *Journal of Biological Chemistry*, *276*(7), 5093-5100.
246. Morimoto, H., Kondoh, K., Nishimoto, S., Terasawa, K., & Nishida, E. (2007). Activation of a C-terminal transcriptional activation domain of ERK5 by autophosphorylation. *Journal of Biological Chemistry*, *282*(49), 35449-35456
247. Wang, X., & Tournier, C. (2006). Regulation of cellular functions by the ERK5 signalling pathway. *Cellular signalling*, *18*(6), 753-760.
248. Hayashi, M., & Lee, J. D. (2004). Role of the BMK1/ERK5 signaling pathway: lessons from knockout mice. *Journal of Molecular Medicine*, *82*(12), 800-808.
249. Regan, C. P., Li, W., Boucher, D. M., Spatz, S., Su, M. S., & Kuida, K. (2002). Erk5 null mice display multiple extraembryonic vascular and embryonic cardiovascular defects. *Proceedings of the National Academy of Sciences*, *99*(14), 9248-9253.
250. Yan, L., Carr, J., Ashby, P. R., Murry-Tait, V., Thompson, C., & Arthur, J. S. C. (2003). Knockout of ERK5 causes multiple defects in placental and embryonic development. *BMC developmental biology*, *3*(1), 11.
251. Hayashi, M., Kim, S. W., Imanaka-Yoshida, K., Yoshida, T., Abel, E. D., Eliceiri, B., ... & Lee, J. D. (2004). Targeted deletion of BMK1/ERK5 in adult mice perturbs vascular integrity and leads to endothelial failure. *Journal of Clinical Investigation*, *113*(8), 1138.
252. Wang, X., Merritt, A. J., Seyfried, J., Guo, C., Papadakis, E. S., Finegan, K. G., ... & Tournier, C. (2005). Targeted deletion of mek5 causes early embryonic death and defects in the extracellular signal-regulated kinase 5/myocyte enhancer factor 2 cell survival pathway. *Molecular and Cellular Biology*, *25*(1), 336-345.
253. Yang, J., Boerm, M., McCarty, M., Bucana, C., Fidler, I. J., Yuan, Z. J., & Su, B. (2000). Mekk3 is essential for early embryonic cardiovascular development. *Nature genetics*, *24*(3), 309-313.
254. Roberts, O. L., Holmes, K., Müller, J., Cross, D. A., & Cross, M. J. (2010). ERK5 is required for VEGF-mediated survival and tubular morphogenesis of primary human microvascular endothelial cells. *Journal of cell science*, *123*(18), 3189-3200.
255. Parmar, K. M., Larman, H. B., Dai, G., Zhang, Y., Wang, E. T., Moorthy, S. N., ... & García-Cardeña, G. (2006). Integration of flow-dependent endothelial phenotypes by Kruppel-like factor 2. *Journal of Clinical Investigation*, *116*(1), 4

256. Villarreal, G., Zhang, Y., Larman, H. B., Gracia-Sancho, J., Koo, A., & García-Cardeña, G. (2010). Defining the regulation of KLF4 expression and its downstream transcriptional targets in vascular endothelial cells. *Biochemical and biophysical research communications*, *391*(1), 984-989.
257. Hayashi, M., Fearns, C., Eliceiri, B., Yang, Y., & Lee, J. D. (2005). Big mitogen-activated protein kinase 1/extracellular signal-regulated kinase 5 signaling pathway is essential for tumor-associated angiogenesis. *Cancer research*, *65*(17), 7699-7706.
258. Tatake, R. J., O'Neill, M. M., Kennedy, C. A., Wayne, A. L., Jakes, S., Wu, D., ... & Snow, R. J. (2008). Identification of pharmacological inhibitors of the MEK5/ERK5 pathway. *Biochemical and biophysical research communications*, *377*(1), 120-125.
259. Yang, Q., Deng, X., Lu, B., Cameron, M., Fearns, C., Patricelli, M. P., ... & Lee, J. D. (2010). Pharmacological inhibition of BMK1 suppresses tumor growth through promyelocytic leukemia protein. *Cancer cell*, *18*(3), 258-267.
260. Wang, Y., Nakayama, M., Pitulescu, M. E., Schmidt, T. S., Bochenek, M. L., Sakakibara, A., ... & Adams, R. H. (2010). Ephrin-B2 controls VEGF-induced angiogenesis and lymphangiogenesis. *Nature*, *465*(7297), 483-486.
261. Liebner, S., Corada, M., Bangsow, T., Babbage, J., Taddei, A., Czupalla, C. J., ... & Dejana, E. (2008). Wnt/β-catenin signaling controls development of the blood–brain barrier. *The Journal of cell biology*, *183*(3), 409-417.
262. Cattelino, A., Liebner, S., Gallini, R., Zanetti, A., Balconi, G., Corsi, A., ... & Dejana, E. (2003). The conditional inactivation of the β-catenin gene in endothelial cells causes a defective vascular pattern and increased vascular fragility. *The Journal of cell biology*, *162*(6), 1111-1122.
263. Weksler, B. B., Subileau, E. A., Perriere, N., Charneau, P., Holloway, K., Leveque, M., ... & Couraud, P. O. (2005). Blood-brain barrier-specific properties of a human adult brain endothelial cell line. *The FASEB journal*, *19*(13), 1872-1874.

264. Taulli, R., Accornero, P., Follenzi, A., Mangano, T., Morotti, A., Scuoppo, C., ... & Ponzetto, C. (2005). RNAi technology and lentiviral delivery as a powerful tool to suppress Tpr-Met-mediated tumorigenesis. *Cancer gene therapy*, *12*(5), 456-463.
265. Spagnuolo, R., Corada, M., Orsenigo, F., Zanetta, L., Deuschle, U., Sandy, P., ... & Dejana, E. (2004). Gas1 is induced by VE-cadherin and vascular endothelial growth factor and inhibits endothelial cell apoptosis. *Blood*, *103*(8), 3005-3012.
266. Korff, T., KIMMINA, S., MARTINY-BARON, G. E. O. R. G., & AUGUSTIN, H. G. (2001). Blood vessel maturation in a 3-dimensional spheroidal coculture model: direct contact with smooth muscle cells regulates endothelial cell quiescence and abrogates VEGF responsiveness. *The FASEB Journal*, *15*(2), 447-457.
267. Cartharius, K., Frech, K., Grote, K., Klocke, B., Haltmeier, M., Klingenhoff, A., ... & Werner, T. (2005). MatInspector and beyond: promoter analysis based on transcription factor binding sites. *Bioinformatics*, *21*(13), 2933-2942.
268. Nakae, J., Kitamura, T., Kitamura, Y., Biggs, W. H., Arden, K. C., & Accili, D. (2003). The forkhead transcription factor Foxo1 regulates adipocyte differentiation. *Developmental cell*, *4*(1), 119-129.
269. Corada, M., Orsenigo, F., Morini, M. F., Pitulescu, M. E., Bhat, G., Nyqvist, D., ... & Dejana, E. (2013). Sox17 is indispensable for acquisition and maintenance of arterial identity. *Nature communications*, *4*.
270. Whitehead, K. J., Plummer, N. W., Adams, J. A., Marchuk, D. A., & Li, D. Y. (2004). Ccm1 is required for arterial morphogenesis: implications for the etiology of human cavernous malformations. *Development*, *131*(6), 1437-1448.
271. Soriano, P. (1999). Generalized lacZ expression with the ROSA26 Cre reporter strain. *Nature genetics*, *21*(1), 70-71.

272. Shenkar, R., Shi, C., Check, I. J., Lipton, H. L., & Awad, I. A. (2007). Concepts and hypotheses: inflammatory hypothesis in the pathogenesis of cerebral cavernous malformations. *Neurosurgery*, *61*(4), 693-703.
273. Reddy, S., Gorin, M. B., McCannel, T. A., Tsui, I., & Straatsma, B. R. (2010). Novel KRIT1/CCM1 mutation in a patient with retinal cavernous hemangioma and cerebral cavernous malformation. *Graefe's Archive for Clinical and Experimental Ophthalmology*, *248*(9), 1359-1361.
274. Corada, M., Nyqvist, D., Orsenigo, F., Caprini, A., Giampietro, C., Taketo, M. M., ... & Dejana, E. (2010). The Wnt/β-catenin pathway modulates vascular remodeling and specification by upregulating Dll4/Notch signaling. *Developmental cell*, *18*(6), 938-949.
275. Pitulescu, M. E., Schmidt, I., Benedito, R., & Adams, R. H. (2010). Inducible gene targeting in the neonatal vasculature and analysis of retinal angiogenesis in mice. *Nature protocols*, *5*(9), 1518-1534.
276. López-Novoa, J. M., & Nieto, M. A. (2009). Inflammation and EMT: an alliance towards organ fibrosis and cancer progression. *EMBO molecular medicine*, *1*(6-7), 303-314.
277. Mariotti, A., Perotti, A., Sessa, C., & Rüegg, C. (2007). N-cadherin as a therapeutic target in cancer.
278. Thiery, J. P., Acloque, H., Huang, R. Y., & Nieto, M. A. (2009). Epithelial-mesenchymal transitions in development and disease. *cell*, *139*(5), 871-890.
279. Li, Y., Yang, J., Luo, J. H., Dedhar, S., & Liu, Y. (2007). Tubular epithelial cell dedifferentiation is driven by the helix-loop-helix transcriptional inhibitor Id1. *Journal of the American Society of Nephrology*, *18*(2), 449-460.
280. Welm, B. E., Tepera, S. B., Venezia, T., Graubert, T. A., Rosen, J. M., & Goodell, M. A. (2002). Sca-1 pos cells in the mouse mammary gland represent an enriched progenitor cell population. *Developmental biology*, *245*(1), 42-56.
281. Stingl, J., Eirew, P., Ricketson, I., Shackleton, M., Vaillant, F., Choi, D., ... & Eaves, C. J. (2006). Purification and unique properties of mammary epithelial stem cells. *Nature*, *439*(7079), 993-997.
282. Shtutman, M., Levina, E., Ohouo, P., Baig, M., & Roninson, I. B. (2006). Cell adhesion molecule L1 disrupts E-cadherin-containing adherens junctions and increases scattering and motility of MCF7 breast carcinoma cells. *Cancer Research*, *66*(23), 11370-11380.
283. Gunia, S., Albrecht, K., Koch, S., Herrmann, T., Ecke, T., Loy, V., ... & May, M. (2008). Ki67 staining index and neuroendocrine differentiation aggravate adverse prognostic parameters in prostate cancer and are characterized by negligible inter-observer variability. *World journal of urology*, *26*(3), 243-250.
284. Nakajima, Y., Yamagishi, T., Hokari, S., & Nakamura, H. (2000). Mechanisms involved in valvuloseptal endocardial cushion formation in early cardiogenesis: Roles of transforming growth factor (TGF)-β and bone morphogenetic protein (BMP). *The Anatomical Record*, *258*(2), 119-127.
285. Gauger, K. J., Chenausky, K. L., Murray, M. E., & Schneider, S. S. (2011). SFRP1 reduction results in an increased sensitivity to TGF-β signaling. *BMC cancer*, *11*(1), 59.
286. Tanaka, H., Shinto, O., Yashiro, M., Yamazoe, S., Iwauchi, T., Muguruma, K., ... & Hirakawa, K. (2010). Transforming growth factor β signaling inhibitor, SB-431542, induces maturation of dendritic cells and enhances anti-tumor activity. *Oncology reports*, *24*(6), 1637-1643.
287. Yadla, S., Jabbour, P. M., Shenkar, R., Shi, C., Campbell, P. G., & Awad, I. A. (2010). Cerebral cavernous malformations as a disease of vascular permeability: from bench to bedside with caution. *Neurosurgical focus*, *29*(3), E4.

288. Armulik, A., Genové, G., Mäe, M., Nisancioglu, M. H., Wallgard, E., Niaudet, C., ... & Betsholtz, C. (2010). Pericytes regulate the blood-brain barrier. *Nature*, *468*(7323), 557-561.
289. Cai, J., Pardali, E., Sánchez-Duffhues, G., & ten Dijke, P. (2012). BMP signaling in vascular diseases. *FEBS letters*, *586*(14), 1993-2002.
290. McLean, K., Gong, Y., Choi, Y., Deng, N., Yang, K., Bai, S., ... & Buckanovich, R. J. (2011). Human ovarian carcinoma–associated mesenchymal stem cells regulate cancer stem cells and tumorigenesis via altered BMP production. *The Journal of clinical investigation*, *121*(8), 3206.
291. Maddaluno, L., Rudini, N., Cuttano, R., Bravi, L., Giampietro, C., Corada, M., ... & Dejana, E. (2013). EndMT contributes to the onset and progression of cerebral cavernous malformations. *Nature*, *498*(7455), 492-496.
292. Milde, F., Lauw, S., Koumoutsakos, P., & Iruela-Arispe, M. L. (2013). The mouse retina in 3D: quantification of vascular growth and remodeling. *Integrative Biology*, *5*(12), 1426-1438.
293. Drigo, P., Mammi, I., Battistella, P. A., Ricchieri, G., & Carollo, C. (1994). Familial cerebral, hepatic, and retinal cavernous angiomas: a new syndrome. *Child's Nervous System*, *10*(4), 205-209.
294. Korchynskyi, O., & ten Dijke, P. (2002). Identification and functional characterization of distinct critically important bone morphogenetic protein-specific response elements in the Id1 promoter. *Journal of Biological Chemistry*, *277*(7), 4883-4891.
295. Shi, Y., Wang, Y. F., Jayaraman, L., Yang, H., Massagué, J., & Pavletich, N. P. (1998). Crystal structure of a Smad MH1 domain bound to DNA: insights on DNA binding in TGF-β signaling. *Cell*, *94*(5), 585-594.
296. Zhou, Z., Rawnsley, D. R., Goddard, L. M., Pan, W., Cao, X. J., Jakus, Z., ... & Kahn, M. L. (2015). The Cerebral Cavernous Malformation Pathway Controls Cardiac Development via Regulation of Endocardial MEKK3 Signaling and KLF Expression. *Developmental cell*, *32*(2), 168-180.
297. Atkins, G. B., Wang, Y., Mahabeleshwar, G. H., Shi, H., Gao, H., Kawanami, D., ... & Jain, M. K. (2008). Hemizygous deficiency of Krüppel-like factor 2 augments experimental atherosclerosis. *Circulation research*, *103*(7), 690-693.
298. Dekker, R. J., van Soest, S., Fontijn, R. D., Salamanca, S., de Groot, P. G., VanBavel, E., ... & Horrevoets, A. J. (2002). Prolonged fluid shear stress induces a distinct set of endothelial cell genes, most specifically lung Krüppel-like factor (KLF2). *Blood*, *100*(5), 1689-1698.
299. Komaravolu, R. K., Adam, C., Moonen, J. R. A., Harmsen, M. C., Goebeler, M., & Schmidt, M. (2014). Erk5 inhibits endothelial migration via KLF2-dependent down-regulation of PAK1. *Cardiovascular research*, cvu236.
300. Young, A., Wu, W., Sun, W., Larman, H. B., Wang, N., Li, Y. S., ... & García-Cardeña, G. (2009). Flow activation of AMP-activated protein kinase in vascular endothelium leads to Krüppel-like factor 2 expression. *Arteriosclerosis, thrombosis, and vascular biology*, *29*(11), 1902-1908.
301. Maejima, T., Inoue, T., Kanki, Y., Kohro, T., Li, G., Ohta, Y., ... & Wada, Y. (2014). Direct Evidence for Pitavastatin Induced Chromatin Structure Change in the KLF4 Gene in Endothelial Cells.
302. Uhlik, M. T., Abell, A. N., Johnson, N. L., Sun, W., Cuevas, B. D., Lobel-Rice, K. E., ... & Johnson, G. L. (2003). Rac–MEKK3–MKK3 scaffolding for p38 MAPK activation during hyperosmotic shock. *Nature cell biology*, *5*(12), 1104-1110.
303. Kato, Y., Kravchenko, V. V., Tapping, R. I., Han, J., Ulevitch, R. J., & Lee, J. D. (1997). BMK1/ERK5 regulates serum-induced early gene expression through transcription factor MEF2C. *The EMBO journal*, *16*(23), 7054-7066.

304. Sohn, S. J., Li, D., Lee, L. K., & Winoto, A. (2005). Transcriptional regulation of tissue-specific genes by the ERK5 mitogen-activated protein kinase. *Molecular and cellular biology*, *25*(19), 8553-8566.
305. Li, H. X., Han, M., Bernier, M., Zheng, B., Sun, S. G., Su, M., ... & Wen, J. K. (2010). Krüppel-like factor 4 promotes differentiation by transforming growth factor-β receptor-mediated Smad and p38 MAPK signaling in vascular smooth muscle cells. *Journal of Biological Chemistry*, *285*(23), 17846-17856.
306. Morikawa, M., Koinuma, D., Tsutsumi, S., Vasilaki, E., Kanki, Y., Heldin, C. H., ... & Miyazono, K. (2011). ChIP-seq reveals cell type-specific binding patterns of BMP-specific Smads and a novel binding motif. *Nucleic acids research*, gkr572.
307. King, K. E., Iyemere, V. P., Weissberg, P. L., & Shanahan, C. M. (2003). Krüppel-like factor 4 (KLF4/GKLF) is a target of bone morphogenetic proteins and TGFβ in the regulation of vascular smooth muscle cell phenotype. *Journal of Biological Chemistry*.
308. Wang, X., Abraham, S., McKenzie, J. A., Jeffs, N., Swire, M., Tripathi, V. B., ... & Greenwood, J. (2013). LRG1 promotes angiogenesis by modulating endothelial TGF-[bgr] signalling. *Nature*, *499*(7458), 306-311.
309. Lüscher, T. F., & Barton, M. (2000). Endothelins and endothelin receptor antagonists therapeutic considerations for a novel class of cardiovascular drugs. *Circulation*, *102*(19), 2434-2440.
310. Kalluri, R., & Zeisberg, M. (2006). Fibroblasts in cancer. *Nature Reviews Cancer*, *6*(5), 392-401.
311. Anderberg, C., Cunha, S. I., Zhai, Z., Cortez, E., Pardali, E., Johnson, J. R., ... & Pietras, K. (2013). Deficiency for endoglin in tumor vasculature weakens the endothelial barrier to metastatic dissemination. *The Journal of experimental medicine*, *210*(3), 563-579.
312. Jilkova, Z. M., Lisowska, J., Manet, S., Verdier, C., Deplano, V., Geindreau, C., ... & Duperray, A. (2014). CCM proteins control endothelial β1 integrin dependent response to shear stress. *Biology open*, *3*(12), 1228-1235.
313. Faurobert, E., Rome, C., Lisowska, J., Manet-Dupé, S., Boulday, G., Malbouyres, M., ... & Albiges-Rizo, C. (2013). CCM1–ICAP-1 complex controls β1 integrin–dependent endothelial contractility and fibronectin remodeling. *The Journal of cell biology*, *202*(3), 545-561.
314. Goitre, L., Balzac, F., Degani, S., Degan, P., Marchi, S., Pinton, P., & Retta, S. F. (2010). KRIT1 regulates the homeostasis of intracellular reactive oxygen species. *PLoS One*, *5*(7), e11786.
315. Tavares, A. L. P., Mercado-Pimentel, M. E., Runyan, R. B., & Kitten, G. T. (2006). TGFβ-mediated RhoA expression is necessary for epithelial-mesenchymal transition in the embryonic chick heart. *Developmental dynamics*, *235*(6), 1589-1598.
316. Tsapara, A., Luthert, P., Greenwood, J., Hill, C. S., Matter, K., & Balda, M. S. (2010). The RhoA activator GEF-H1/Lfc is a transforming growth factor-β target gene and effector that regulates α-smooth muscle actin expression and cell migration. *Molecular biology of the cell*, *21*(6), 860-870.
317. Marchi, S., Corricelli, M., Trapani, E., Bravi, L., Pittaro, A., Delle Monache, S., ... & Pinton, P. (2015). Defective autophagy is a key feature of cerebral cavernous malformations. *EMBO molecular medicine*, e201505316.
318. Liao, X., Zhang, R., Lu, Y., Prosdocimo, D. A., Sangwung, P., Zhang, L., ... & Jain, M. K. (2015). Kruppel-like factor 4 is critical for transcriptional control of cardiac mitochondrial homeostasis. *The Journal of clinical investigation*, *125*(9), 3461-3476.
319. Magrini, E., Villa, A., Angiolini, F., Doni, A., Mazzarol, G., Rudini, N., ... & Cavallaro, U. (2014). Endothelial deficiency of L1 reduces tumor angiogenesis and promotes vessel normalization. *The Journal of clinical investigation*, *124*(10), 4335.

320. Chen, P. Y., Qin, L., Tellides, G., & Simons, M. (2014). Fibroblast growth factor receptor 1 is a key inhibitor of TGFβ signaling in the endothelium. *Science signaling*, *7*(344), ra90-ra90.

321. Kuo, C. T., Veselits, M. L., Barton, K. P., Lu, M. M., Clendenin, C., & Leiden, J. M. (1997). The LKLF transcription factor is required for normal tunica media formation and blood vessel stabilization during murine embryogenesis. *Genes & development*, *11*(22), 2996-3006.

# ACKNOWLEDGEMENTS

I still remember well when I got the e-mail from the SEMM examination board notifying me that I was accepted in SEMM's PhD Program and assigned to the research group of Prof. Elisabetta Dejana". It was something extraordinarily desired and exciting. Desired because the year before I failed to enter the same PhD program and I worked hard for one year in order to try again the exam; exciting because it was given to me the possibility to work on angiogenesis, the research topic of my interest since the beginning of my studies. For all of this reason I really took this long road like I was living a dream.

I want to thank my boss, Elisabetta Dejana, to give me the opportunity to work in her group and to be involved in a so fascinating research project. Working for her it makes you fell as you are always at the edge of a new scientific discovery.

A particular thank goes to Noemins "Etna" Rudini. She shared with me the every day lab life of these four years. Only we two (and our families) know how much efforts are beyond this project. Noemins, I am fully convinced that you are the PhD supervisor that every student would desire to have.

I would like to give special thanks to Braves and Maria Grazia who shared with me the same scientific topic and provided me technical help and critical inspiriring comments respectively.

I want to thank Monica Corada that since the first days of my PhD was always available to help me and to discuss with me.

I am grateful to Federica Pisati who supported me with her big expertise in immunohistochemistry and for being really always available for me.

I want to thank Prof. Mukesh Jain, Prof. Gary Owens and Prof. Martin Schwartz that provided me precious reagents and contributed to scientific discussion.

I acknowledge my PhD supervisors, Ralph Adams and Gioacchino Natoli, for their very important and helpful feedback during these years.

These fours years would have been too much boring without the presence of special friends such as Benzocita, Frikkio, Giannottins, Jean Peter, Mari, Padellata, Papo Gaio Giacchè and Recchioman. Besides helping me everyday in the labwork, I really spent special time with each of you.

I thank all the past and present members of the Vascular Biology Group, especially Gani, Cerri, il Caro Maderna, Cicilia and my PhD mates Butt, Valentina e Lara.

I deeply thank my parents that always support me and give me the possibility to pursue my dreams.

To Michela, all this would not make sense without you.